UNIVERSITI TEKNOLOGI MARA

ZINC OXIDE NANOPARTICLES MODIFIED BY EMPTY FRUIT BUNCH DERIVED CARBON DOTS FOR ENHANCED PHOTOCATALYTIC TETRACYCLINE REMOVAL

WAN NURAISHAH BINTI
WAN ISHAK

PhD

June 2026

UNIVERSITI TEKNOLOGI MARA

ZINC OXIDE NANOPARTICLES MODIFIED BY EMPTY FRUIT BUNCH DERIVED CARBON DOTS FOR ENHANCED PHOTOCATALYTIC TETRACYCLINE REMOVAL

WAN NURAISHAH BINTI WAN ISHAK

Thesis submitted in fulfilment
of the requirements for the degree of
Doctor of Philosophy
(Chemical Engineering)

Faculty of Chemical Engineering

June 2026

CONFIRMATION BY PANEL OF EXAMINERS

I certify that a Panel of Examiners has met on 29 April 2026 to conduct the final examination of Wan Nuraishah Binti Wan Ishak on her Doctor of Philosophy thesis entitled "Zinc Oxide Nanoparticles Modified By Empty Fruit Bunch Derived Carbon Dots For Enhanced Photocatalytic Tetracycline Removal" in accordance with Universiti Teknologi MARA Act 1976 (Akta 173). The Panel of Examiners recommends that the student be awarded the relevant degree. The Panel of Examiners was as follows:

Nurul Fadhilah Kamalul Aripin, PhD
Associate Professor
Faculty of Chemical Engineering
Universiti Teknologi MARA
(Chairman)

Azil Bahari Alias @ Ales, PhD
Associate Professor
Faculty of Chemical Engineering
Universiti Teknologi MARA
(Internal Examiner)

Mohd Azmier Ahmad, PhD
Associate Professor
Faculty of Chemical Engineering
Universiti Sains Malaysia
(External Examiner)

PROF DR HJH ZURAEDA IBRAHIM
Dean
Institute of Postgraduates Studies
Universiti Teknologi MARA

Date: 22 June 2026

AUTHOR'S DECLARATION

I declare that the work in this thesis was carried out in accordance with the regulations of Universiti Teknologi MARA. It is original and is the results of my own work, unless otherwise indicated or acknowledged as referenced work. This thesis has not been submitted to any other academic institution or non-academic institution for any degree or qualification.

I, hereby, acknowledge that I have been supplied with the Academic Rules and Regulations for Post Graduate, Universiti Teknologi MARA, regulating the conduct of my study and research.

Name of Student	:	Wan Nuraishah Bt Wan Ishak
Student ID. No.	:	2022288228
Programme	:	Doctor of Philosophy (Chemical Engineering) –EH950
Faculty	:	Chemical Engineering
Thesis Title	:	Zinc Oxide Nanoparticles Modified By Empty Fruit Bunch Derived Carbon Dots For Enhanced Photocatalytic Tetracycline Removal
Signature of Student	:	
Date	:	June 2026

ABSTRACT

The widespread occurrence of antibiotic residues in aquatic environments, particularly tetracycline (TC), presents a significant environmental concern due to their persistence and contribution to antibiotic resistance. Despite extensive research on photocatalytic nanomaterials, many reported systems remain limited by poor visible light utilization, rapid electron hole recombination, and reliance on non-sustainable or chemically derived modifiers, which constrain their practical application. In addition, the role of biomass derived carbon-based modifier in photocatalysis in photocatalytic electrochemical charge transfer mechanisms remains insufficiently understood, particularly regarding their influence on charge carrier generation, interfacial charge separation, electron transport pathways, and recombination suppression. To address these gaps, this study develops a zinc oxide/carbon dots (ZnO/CDs) nanocomposite synthesized via a hydrothermal method, where carbon dots are sustainably derived from oil palm empty fruit bunches, offering a green and cost-effective strategy. A series of ZnO/CDs nanocomposites with mass ratios of 2:1, 1:1, and 1:2 was systematically evaluated under varying tetracycline concentrations, catalyst dosages, and light sources. The ZnO/CDs (1:2) nanocomposite exhibited superior photocatalytic performance, achieving 96.17% degradation of 5 ppm TC under UV irradiation at a catalyst dosage of 1 g L^{-1}, where the variation is attributed to differences in pollutant concentration and irradiation energy. Kinetic analysis followed pseudo first order behaviour with a rate constant of 0.017 min^{-1} under optimal conditions. Structural characterization confirmed effective integration of spherical CDs (0.32 nm lattice spacing) with ZnO nanoparticles (0.26 nm), resulting in enhanced light absorption and interfacial charge transfer. Electrochemical impedance spectroscopy showed a reduction in charge transfer resistance from 1.8 kΩ to 0.6 kΩ, while cyclic voltammetry and transient photocurrent measurements confirmed improved charge mobility and separation efficiency. Mott–Schottky analysis indicated n-type semiconductor behaviour and suitable band alignment supporting a Z scheme charge transfer mechanism. Reactive species trapping experiments identified hydroxyl and superoxide radicals as the dominant active species. The ZnO/CDs nanocomposite demonstrated good stability, retaining 88% efficiency after five cycles. Overall, this study provides mechanistic insight into biomass derived carbon dots in photocatalytic systems and offers a sustainable approach for antibiotic removal while supporting waste valorization.

ACKNOWLEDGEMENT

Alhamdulillah, all praise to Allah SWT for granting me the strength, patience, and perseverance to complete this PhD journey.

First and foremost, I would like to express my deepest and most heartfelt gratitude to my main supervisor, Dr. Tan Huey Ling. Words cannot fully capture how much her support has meant to me. From the very beginning, she believed in my potential even when I doubted myself. Her unwavering encouragement, kind heart, and constant presence through both my highs and lows have made an indelible mark on my life. She was not only a mentor in research but also a pillar of emotional strength who uplifted me during the most challenging phases of this journey. Her patience, wisdom, and motherly care gave me the courage to move forward and never give up. I will always carry her guidance and kindness with me, not only as a researcher, but as a person. Thank you, Dr. Tan, for being more than a supervisor for being an inspiration and a source of strength. I am eternally grateful.

I would also like to extend my heartfelt appreciation to Dr. Lim Ying Pei, whose compassionate mentorship and thoughtful guidance have been a significant part of my academic growth. Her willingness to share her knowledge, provide constructive feedback, and offer consistent encouragement truly helped refine the direction of my work. Dr. Lim's professionalism and genuine support created a positive and enriching environment that greatly contributed to the success of this research. I am sincerely thankful for her patience, her trust in my abilities, and the motivation she provided throughout this journey.

My sincere thanks also go to Dr. Noor Fitrah Abu Bakar, for her valuable insights, encouragement, and guidance that supported me through each stage of my work. To all academic and technical staff at the Faculty of Chemical Engineering, Universiti Teknologi MARA, and to my fellow research colleagues, thank you for the shared knowledge, assistance, and encouragement that made this journey smoother and more meaningful.

Most importantly, I dedicate this achievement to my late beloved father. His love, sacrifices, and prayers were the foundation of my strength. Although he is no longer with me, his spirit and teachings have guided me every step of the way. I am also forever grateful to my dearest mother and family, whose endless love, patience, and unwavering support have been my anchor throughout this journey. This PhD journey has been one of growth, resilience, and faith and it would not have been possible without the unwavering presence of those who believed in me from the very beginning.

TABLE OF CONTENTS

LIST OF TABLES

LIST OF FIGURES

LIST OF SYMBOLS

Symbols

Co	Initial Concentration Of Pollutant (mgL-1)
Ct	Pollutant Concentration at Time t (mgL-1)
k	Apparent Reaction Rate Constant (min-1)
kapp	Apparent Pseudo-First-Order Rate Constant
KLH	Langmuir Adsorption Equilibrium Constant
ro	Initial Degradation Rate
α	Absorption Coefficient
hv	Photon Energy
Eg	Band Gap Energy
Rct	Charge Transfer Resistance
A	Absorption Constant
E	Energy Level

LIST OF ABBREVIATIONS

Abbreviations

TC	Tetracycline
CDs	Carbon dots
ZnO	Zinc Oxide
HOMO	Highest Occupied Molecular Orbital
LUMO	Lowest Unoccupied Molecular Orbital
CB	Conduction Band
VB	Valance Band
PCD	Photocatalytic Degradation
EIS	Electrochemical Impedance Spectroscopy
AOPs	Advanced Oxidation Process
PFO	Pseudo-First Order
PSO	Pseudo-Second Order
L-H	Langmuir-Hinshelwood
ROS	Reactive Oxygen Species

LIST OF NOMENCLATURE

Nomenclatures

i.e.	That Is
e.g.	For Example,
et al.	Others
Photocatalysis	Light-Activated Catalytic Degradation
Z-scheme	A Charge Transfer Mechanism Mimicking Photosynthesis
Heterojunction	Interface Between Two Semiconductors
Scavenger test	Test To Determine Active Species (e.g., •OH, H^+, $•O_2^-$)
Band gap	Energy Difference Between CB And VB
Surface area	Indicates Adsorption Capacity for Photocatalysis
Charge recombination	Loss Of Photogenerated Electrons and Holes
Photoluminescence	Light Emission due to Electron Transitions
Flat-band potential	Electrochemical Parameter to Assess Band Alignment
Langmuir-Hinshelwood model	Kinetic Model for Surface Reactions

CHAPTER 1
INTRODUCTION

1.1 Research Background

Water pollution caused by emerging contaminants, particularly antibiotics such as tetracycline, ciprofloxacin, amoxicillin, and sulfamethoxazole, has become a significant environmental issue worldwide (Fiaz et al., 2021). Among these contaminants, tetracycline (TC) is one of particular concern due to its widespread use in human medicine, veterinary practices, and agriculture (Gopal et al., 2020). TC is commonly selected as a model pollutant in photocatalytic studies due to its high global consumption, extensive environmental occurrence, and well documented resistance to conventional treatment processes (Bhuin et al., 2024). Due to its high chemical stability and low biodegradability, TC persists in aquatic ecosystems, posing serious ecological and human health risks (Xu et al., 2021). One of the most concerning consequences of TC contamination is the promotion of antimicrobial resistance (AMR), which the World Health Organization recognizes as a major global health threat (World Health Organization, 2024). The World Health Organization (WHO) data shown that there was high antibiotic resistance incidence in both high-income and low-income countries with the occurrence of up to 500,000 cases across 22 countries and has killed approximately 700,000 people per year globally. Additionally, global antibiotic consumption was estimated at 100 000 to 200 000 tons per year in 2002, corresponding to approximately 34.8 billion defined daily doses in 2015, which represented a 65% increase since 2000 (Wu et al., 2020).

The continuous increase in antibiotic usage has intensified the discharge of antibiotic residues into aquatic environments through municipal wastewater, hospital effluents, livestock waste, and agricultural runoff (Jin et al., 2022). Among various antibiotic classes, tetracycline was selected as the target pollutant in this study because it is extensively used in human medicine, veterinary treatment, and livestock production, resulting in its frequent detection in wastewater and surface water systems (Jin et al., 2022). The presence of TC in the environment is of particular concern because it is only partially metabolised, relatively persistent, and difficult to completely remove using conventional wastewater treatment processes (Kouhail et al., 2020). Residual TC

may inhibit beneficial microbial communities, disrupt aquatic ecological balance, and exert selective pressure that promotes the development and dissemination of antibiotic-resistant bacteria and antibiotic resistance genes. In addition, TC has strong chelating ability with metal ions and can interact with suspended particles, sludge, soil, and sediments, which complicates its environmental fate and removal. Therefore, TC was selected as a representative and challenging model antibiotic to evaluate the photocatalytic efficiency of the ZnO/CDs nanocomposite developed in this study (Wu et al., 2020).The uncontrolled presence of TC usage could affect living things and the environment and have a few negative effects, including enhanced bacterial drug resistance, genetic exchange, and bio-toxicity (Gopal et al., 2020). Therefore, the development of efficient and sustainable remediation strategies for tetracycline contaminated wastewater is urgently required (Jin et al., 2022).

Conventional wastewater treatment methods, including biodegradation, adsorption, and membrane filtration, have proven inadequate for completely removing tetracycline due of its resistance to biodegradation and high-water solubility (Zhang et al., 2022). Biodegradation is limited because tetracycline has antimicrobial properties that can inhibit microbial activity, resulting in incomplete degradation and possible persistence of transformation products (Hasham Firooz et al., 2024). Adsorption can reduce tetracycline concentration in water, but it mainly transfers the pollutant from the aqueous phase onto the adsorbent surface rather than destroying it (Arfoy et al., 2026). Similarly, membrane filtration can physically separate tetracycline from water, but it may generate concentrated reject streams and suffer from membrane fouling (Hasham Firooz et al., 2024). Therefore, these limitations indicate that conventional methods are insufficient when complete degradation or mineralization is required. In this context, photocatalysis has emerged as an effective and sustainable approach for degrading antibiotic pollutants. This advanced oxidation process involves generating highly reactive species, such as hydroxyl radicals (•OH) and superoxide anions ($\bullet O_2^-$), under light irradiation, which can efficiently break down complex organic molecules into harmless end products (Kouhail et al., 2020). Among various photocatalysts, zinc oxide (ZnO) stands out due to its high photosensitivity, chemical stability, non-toxicity, and low cost (Semeraro et al., 2020). However, ZnO nanoparticles faces two significant challenges: limited light absorption and rapid electron-hole recombination. ZnO has a wide bandgap of 3.27 eV, allowing it to absorb only UV light, which constitutes less than 5% of the solar spectrum, leading to low solar energy utilization (Ayu et al., 2023).

Additionally, the rapid recombination of photogenerated electron-hole pairs significantly reduces the efficiency of reactive species generation, thereby limiting its photocatalytic performance (Wan Ishak, et al., 2025). Addressing these limitations, various modification strategies have been explored, including doping with metals or non-metals, coupling with other semiconductors, and surface modification with carbon-based materials (Zhao et al., 2022). Among these, modifying pristine ZnO nanoparticles with carbon dots (CDs) has shown great promise due to the unique properties of CDs, such as tunable photoluminescence, broad light absorption, high electron mobility, and environmental friendliness (Karaca et al., 2023).

Carbon dots are zero-dimensional carbon-based nanomaterials with sizes below 10 nm, and their unique optical, electronic, and chemical properties are attributed to the quantum confinement effect and abundant surface functional groups (Khairol Anuar et al., 2021). When integrated with ZnO nanoparticles, CDs can enhance photocatalytic performance by broadening the light absorption range, facilitating charge separation and transfer, and promoting the generation of reactive oxygen species (ROS) (Ozyurt et al., 2023). However, most studies employ chemically synthesized CDs, which are often expensive, hazardous, and challenging to scale up (Zaman et al., 2024). In contrast, biomass-derived CDs offer a sustainable and eco-friendly alternative, supporting waste valorisation and circular economy principles. Among various biomass sources, oil palm empty fruit bunches (EFB) are particularly attractive due to their abundance, high carbon content, and low cost (Gong et al., 2023). Utilizing EFB not only reduces agricultural waste but also addresses environmental pollution. Malaysia, as one of the largest palm oil producers globally, generates approximately 20–25 million tonnes of EFB annually, contributing to a substantial lignocellulosic waste stream (Dolah et al., 2021). On a global scale, EFB production was estimated at around 80 million tonnes in 2018, highlighting its significant availability compared to other biomass resources (Dolah et al., 2021). This abundance, combined with its high carbon content, makes EFB a promising and sustainable precursor for carbon-based nanomaterial synthesis. From an economic perspective, the use of EFB as a carbon precursor may reduce material cost by utilizing an abundant agricultural waste stream instead of costly synthetic carbon sources. The detailed economic evaluation of the ZnO/CDs photocatalytic system is discussed in Section 4.8. Despite these advantages, the application of biomass-derived CDs, especially from EFB, in enhancing ZnO nanoparticles photocatalysis for TC degradation remains underexplored.

This study addresses the identified research gap by synthesizes and characterizes ZnO nanoparticles modified with biomass-derived CDs from oil palm EFB for enhanced photocatalytic degradation of tetracycline in aquatic systems. In addition to structural and optical characterization, this research integrates electrochemical techniques, including cyclic voltammetry (CV), electrochemical impedance spectroscopy (EIS), Mott-Schottky analysis, and transient photocurrent response, to gain deeper insights into charge transfer dynamics, electron-hole separation efficiency, and interfacial charge transport behaviour. These electrochemical analyses provide a fundamental understanding of how CDs influence the electronic properties of ZnO nanoparticles, thereby enhancing photocatalytic efficiency.

Although ZnO-based photocatalysts have been widely investigated for antibiotic degradation, most studies primarily focus on improving photocatalytic efficiency through structural modification or enhanced light absorption (Sendão et al., 2023; S. Wang et al., 2022). However, a critical limitation remains in the insufficient understanding of charge carrier dynamics, particularly in terms of interfacial charge transfer, carrier mobility, and recombination behaviour. This limitation is more pronounced in systems incorporating carbon dots, where the mechanistic role of CDs in electron mediation and charge separation is often inferred rather than experimentally validated. Furthermore, existing studies predominantly utilize chemically synthesized carbon dots, with limited attention given to biomass-derived alternatives that offer sustainability advantages. In particular, the integration of oil palm empty fruit bunch (EFB)-derived CDs with ZnO and their influence on interfacial electronic properties remain largely unexplored. This study addresses this limitation by systematically investigating the role of EFB-derived CDs in modifying the charge transfer behaviour of ZnO through comprehensive electrochemical analysis. Techniques including cyclic voltammetry, electrochemical impedance spectroscopy, Mott–Schottky analysis, and transient photocurrent measurements are employed to quantitatively evaluate charge separation efficiency, carrier transport, and interfacial resistance. This approach enables direct correlation between electronic properties and photocatalytic performance, providing mechanistic evidence beyond conventional efficiency-based evaluation. The findings contribute to a more rigorous understanding of biomass-derived carbon dots systems and establish a framework for the rational design of high-performance, sustainable photocatalysts for wastewater treatment applications.

1.2 Problem Statement

The widespread application of tetracycline in agriculture, aquaculture, and medical sectors has resulted in its persistent occurrence in aquatic environments due to its high chemical stability and limited biodegradability. In aquaculture systems, approximately 80% of the administered tetracycline is released into surrounding waters through uneaten feed or excretion, contributing substantially to antibiotic contamination, particularly in high-production countries such as Malaysia (Gopal et al., 2020). Malaysia, which ranks 15th globally in aquaculture production (Louros et al., 2021), faces significant challenges in managing antibiotic pollution. Environmental monitoring studies conducted in marine aquaculture farms in Peninsular Malaysia (ladang akuakultur marin di Semenanjung Malaysia) have reported the presence of tetracycline residues at concentrations ranging from below detection limits to 25.6 ng/L, confirming its persistence in local aquatic systems (Thiang et al., 2022). The environmental persistence of tetracycline exacerbates the global antimicrobial resistance (AMR) crisis, which is projected by the World Health Organization to cause up to 10 million deaths annually by 2050, underscoring the urgent need for effective and sustainable remediation strategies.

Photocatalysis offers a sustainable pathway for degrading recalcitrant antibiotics such as tetracycline by generating reactive oxygen species under light irradiation. Zinc oxide (ZnO) remains one of the most promising photocatalysts owing to its high photosensitivity, chemical robustness, and economic viability. However, its wide bandgap energy (≈3.37 eV) restricts photo response primarily to the ultraviolet region, which constitutes less than 5% of the solar spectrum, while the rapid recombination of photogenerated charge carriers further suppresses quantum efficiency. These intrinsic limitations result in poor solar utilization and limited degradation kinetics.

Recent research indicates that the incorporation of carbon dots (CDs) can significantly enhance ZnO's photocatalytic activity through interfacial charge transfer and heterojunction formation, which facilitate charge separation and extend optical absorption into the visible range (Mukherjee et al., 2021). Nevertheless, the majority of reported studies employ chemically synthesized CDs derived from costly and hazardous precursors, contradicting the sustainability goals of green nanotechnology. Biomass-derived CDs have emerged as an environmentally benign alternative, capable of

integrating photocatalytic enhancement with waste valorisation within a circular economy framework.

Among various biomass sources, oil palm empty fruit bunch (EFB) is particularly attractive due to its high fixed carbon content, abundance, and negligible cost in Malaysia's palm oil industry. Despite these advantages, systematic investigations on EFB-derived CDs integrated with ZnO for antibiotic degradation remain scarce. Therefore, this research aims to develop and mechanistically evaluate EFB-derived ZnO/CDs nanocomposites as an efficient and sustainable photocatalyst for tetracycline degradation. The study focuses on elucidating the structure property performance correlation, emphasizing charge carrier dynamics, band alignment, and photoelectrochemical behaviour to advance understanding of biomass-based photocatalytic systems for environmental remediation.

Furthermore, a comprehensive photoelectrochemical (PEC) evaluation will be conducted to elucidate the interfacial charge transfer and electronic structure of the ZnO/CDs composite system. Cyclic voltammetry (CV) will be employed to assess the redox behavior and charge transfer kinetics at the semiconductor electrolyte interface, providing insight into electron mobility and catalytic activity. Electrochemical impedance spectroscopy (EIS) will be used to quantify the charge transfer resistance and carrier lifetime, thereby evaluating the efficiency of interfacial charge separation within the heterojunction. Mott–Schottky (MS) measurements will further determine the semiconductor type, flat-band potential, and carrier density, which are essential parameters for understanding band alignment and charge transfer pathways under illumination.

The integration of these techniques allows a correlative interpretation of structural, optical, and electrochemical properties, offering a mechanistic understanding of how EFB-derived carbon dots influence the electronic behaviour of ZnO. This systematic approach not only clarifies the role of CDs in suppressing recombination and enhancing visible-light response but also provides a foundation for designing high-performance photocatalysts tailored for the degradation of persistent antibiotics. The outcomes of this study will therefore contribute to the advancement of sustainable wastewater treatment technologies, particularly for regions with intensive aquaculture activities where antibiotic contamination poses a persistent environmental threat.

1.3 Research Objectives

Objectives of the research are:

i. To investigate the effect of ZnO-to-CDs ratio (1:1,1:2,2:1) on the physicochemical properties, band alignment, and interfacial charge transfer behavior of ZnO/CDs nanocomposites.
ii. To determine the optimum photocatalytic performance of ZnO/CDs nanocomposites for tetracycline degradation under operational parameters of tetracycline concentration, catalyst dosage, light source, and reusability
iii. To determine the photocatalytic kinetics of tetracycline degradation using the Langmuir-Hinshelwood model
iv. To determine the photocatalytic degradation mechanism of tetracycline and charge transfer mechanism to validate the degradation pathway mechanism.

1.4 Research Question

i. What influence does the ZnO-to-CDs ratio have on the physicochemical, optical, and electrochemical properties of ZnO/CDs nanocomposites, and why does this ratio govern their band alignment and charge transfer efficiency?
ii. What electrochemical characteristics such as charge separation behavior, carrier lifetime, and flat-band potential explain the enhanced photocatalytic activity of ZnO/CDs nanocomposites, and why are these parameters critical for understanding their interfacial charge dynamics?
iii. What are the optimal operational conditions tetracycline concentration, catalyst dosage, light source, and reusability that maximize the photocatalytic performance of ZnO/CDs nanocomposites, and why do these parameters govern the overall degradation efficiency?
iv. What extent does the Langmuir–Hinshelwood model accurately represent the photocatalytic kinetics of ZnO/CDs nanocomposites for tetracycline degradation, and why is this kinetic interpretation significant for understanding reaction mechanisms?
v. What reactive oxygen species (ROS) predominantly drive the photocatalytic degradation of tetracycline, and why do these specific species and their

associated intermediate products determine the degradation pathway and mineralization efficiency?

1.5 Scope and Limitation of the Study

This study explores the integration of biomass-derived carbon dots with ZnO nanoparticles to develop an advanced photocatalyst for the efficient degradation of tetracycline in wastewater. The research focuses on the synthesis, characterization, and photocatalytic performance of ZnO/CDs nanocomposites, with an emphasis on optimizing their physicochemical properties to enhance photocatalytic activity.

The study also investigates the underlying charge transfer mechanisms using electrochemical analysis, as shown in Figure 1.1. The hydrothermal method is employed to synthesize CDs from empty fruit bunch (EFB) biomass. The study systematically varies the ZnO-to-CDs ratio (1:1, 1:2, and 2:1) to investigate its impact on photocatalytic efficiency. The photocatalytic activity of ZnO/CDs is evaluated by degrading TC in aqueous solutions under different experimental conditions. The effects of key operational parameters, including TC concentration (5–25 ppm), ZnO/CDs dosage (0.5–2.5 g/L), and light source (UV, visible, solar) in 180 min are examined. The degradation efficiency is quantified using UV-Vis spectrophotometry at 357 nm. The optimal photocatalytic conditions are further analysed using kinetic modeling, particularly the pseudo-first-order model, to determine the rate constant and half-life of TC degradation.

A comprehensive characterization of ZnO/CDs nanocomposites is conducted using advanced analytical techniques. The structural and morphological properties are examined via X-ray diffraction (XRD) and high-resolution transmission electron microscopy (HRTEM), while elemental composition and chemical states are determined using X-ray photoelectron spectroscopy (XPS). Fourier-transform infrared spectroscopy (FTIR) is used to analyze functional groups, and UV-Vis diffuse reflectance spectroscopy (UV-DRS) assesses optical properties, including bandgap energy. The specific surface area and porosity of the photocatalyst are measured using the Brunauer-Emmett-Teller (BET) method. Electrochemical studies, including cyclic voltammetry (CV), electrochemical impedance spectroscopy (EIS), transient photocurrent response, and Mott-Schottky analysis, provide insights into charge transfer dynamics, electron-hole separation efficiency, and band alignment.

Additionally, scavenger tests are performed to identify dominant reactive oxygen species (ROS) involved in the photocatalytic process, and liquid chromatography-mass spectrometry (LC-MS) is employed to determine degradation intermediates.

Despite the promising outcomes, several limitations should be acknowledged. The study is conducted at laboratory scale using synthetic tetracycline solutions, which may not fully represent the complexity of real wastewater matrices containing competing ions and organic matter. The photocatalytic performance is evaluated primarily for a single pollutant system, limiting direct applicability to multi contaminant environments. In addition, catalyst stability is assessed over five cycles only, and long-term durability remains unverified. Furthermore, the study does not include total organic carbon (TOC) analysis or toxicity assessment of degradation intermediates, which are essential to confirm complete mineralization and environmental safety.

1.6 Significance of study

This research presents a sustainable and innovative approach for the photocatalytic degradation of tetracycline in wastewater using ZnO nanoparticles integrated with biomass-derived carbon dots. The study is particularly significant in addressing environmental pollution by utilizing agricultural waste, specifically oil palm empty fruit bunch, as a precursor for CDs. This valorisation of waste not only reduces environmental burden but also aligns with green chemistry principles by promoting resource recovery and sustainability. The hydrothermal synthesis method employed in this study offers an energy-efficient and environmentally friendly route for producing CDs, which can serve as an effective co-catalyst in ZnO-based photocatalytic systems.

The integration of CDs with ZnO nanoparticles is expected to enhance the overall photocatalytic performance by improving charge separation, reducing electron-hole recombination, and extending the light absorption capability of ZnO from the UV to the visible light spectrum. These modifications enhance the efficiency of ZnO/CDs nanocomposites under solar and artificial light sources, making them more applicable for real-world wastewater treatment scenarios. The study further provides a comprehensive physicochemical characterization of the synthesized ZnO/CDs nanocomposites using advanced analytical techniques such as High-Resolution Transmission Electron Microscopy (HRTEM), X-ray Photoelectron Spectroscopy (XPS), X-ray Diffraction (XRD), Fourier Transform Infrared Spectroscopy (FTIR), and

UV-Vis spectrophotometry. These techniques enable a deeper understanding of the structural, optical, and electronic properties of the synthesized photocatalyst, ensuring its effectiveness and reproducibility in wastewater treatment applications.

Additionally, the study employs electrochemical analyses, including Mott-Schottky analysis, transient photocurrent measurements, and scavenger tests, to elucidate the charge transfer mechanisms and the role of reactive oxygen species (ROS) in the photodegradation process. Such mechanistic insights contribute to the fundamental understanding of the photocatalytic process, providing valuable information for the further optimization and design of next generation photocatalysts. The research also investigates key operational parameters affecting photocatalytic efficiency, such as catalyst dosage, TC concentration, and different light sources (UV, visible, and solar light), to determine the optimal conditions for maximum degradation efficiency. Furthermore, kinetic modeling using pseudo-first-order kinetics and Langmuir-Hinshelwood models is applied to evaluate the reaction rate and adsorption behaviour, contributing to the theoretical framework of heterogeneous photocatalysis.

Beyond laboratory-scale experimentation, this study has significant implications for real-world applications in wastewater treatment. The findings offer insights into the scalability and feasibility of ZnO/CDs-based photocatalysts for industrial wastewater treatment, addressing the growing concern of antibiotic contamination in water bodies. The research aligns with Sustainable Development Goal (SDG) #6 (Clean Water and Sanitation) by proposing a cost-effective, sustainable, and high-performance solution for water purification. By bridging the fields of nanotechnology, electrochemistry, and environmental science, this study provides a crucial step toward the development of advanced photocatalytic materials for sustainable and efficient wastewater treatment system.

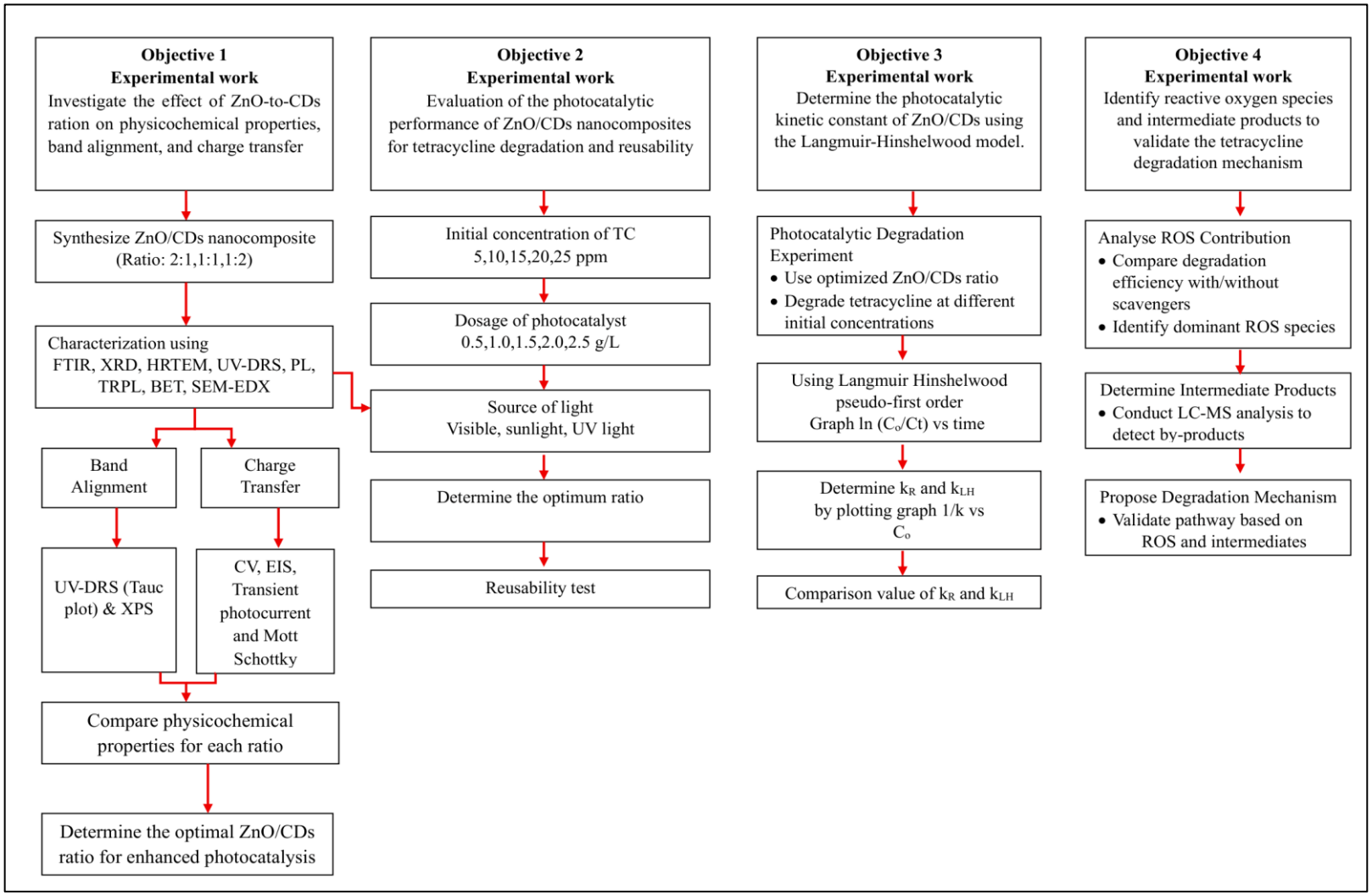

Figure 1.1 The Conceptual Framework Employed In This Research

CHAPTER 2
LITERATURE REVIEW

2.1 Introduction

The increasing presence of antibiotic pollutants in the environment has raised significant concerns due to their ecological persistence and potential human health impacts. Among various remediation strategies, photocatalysis has emerged as a promising approach for the degradation of recalcitrant antibiotics in wastewater due to its ability to generate highly reactive species for mineralization (Antos et al., 2024). In recent years, carbon dots have attracted considerable attention as functional nanomaterials owing to their tunable optical properties, high stability, and capability to enhance charge separation when integrated with semiconductor photocatalysts such as ZnO (Mohammadi et al., 2023). However, despite extensive research, several unresolved challenges remain in ZnO/CDs photocatalytic systems. The visible light response of ZnO is intrinsically limited by its wide band gap, while the contribution of CDs depends strongly on their surface states, functional groups, particle size, and loading ratio (Mohammadi et al., 2023). As a result, the visible light enhancement reported for ZnO/CDs composites is not always consistent across studies (Thiang et al., 2022). In addition, the exact role of CDs remains unclear because they may function as photosensitizers, electron acceptors, electron mediators, or recombination centres depending on the interfacial structure and CDs content (Thiang et al., 2022). Many studies have also proposed charge transfer mechanisms based mainly on degradation efficiency and optical characterization, without sufficient electrochemical or photoelectrochemical evidence to validate electron transport, interfacial resistance, and carrier separation (Thiang et al., 2022). Furthermore, the relationship between band alignment, reactive oxygen species formation, and degradation intermediates is often not fully established, resulting in incomplete mechanistic interpretation (Qurtulen et al., 2026). These limitations are more evident for biomass derived CDs, where systematic studies on ZnO/CDs charge transfer behaviour and practical photocatalytic performance remain limited (Qurtulen et al., 2026) .

This chapter critically reviews the current state of knowledge on antibiotic pollution, conventional and advanced treatment approaches, and the development of

carbon dots based photocatalysts (Qurtulen et al., 2026). Particular emphasis is placed on the synthesis, physicochemical properties, and functional roles of carbon dots in photocatalytic systems, as well as the mechanisms governing antibiotic degradation. This review establishes the scientific foundation and identifies key limitations that motivate the present study.

2.2 Antibiotic Pollutants in The Environment

The ubiquitous presence of antibiotic residues in the environment has emerged as a global environmental and public health concern. Antibiotics, as biologically active compounds, are extensively applied in human healthcare, veterinary medicine, and aquaculture to combat bacterial infections. Over the past decades, antibiotic usage has surged dramatically in response to increasing medical and agricultural demands. Between 2000 and 2015, global antibiotic consumption rose by approximately 65%, with 39% of this growth originating from low- and middle-income countries (Fiaz et al., 2021). In China, an estimated 180,000 metric tons of antibiotics are consumed annually for both human and agricultural purposes, significantly contributing to environmental contamination (Adeyemi et al., 2021; Fiaz et al., 2021). A considerable proportion of administered antibiotics is excreted unmetabolized, subsequently entering the environment through various anthropogenic sources. These include municipal wastewater, hospital effluents, landfill leachate, agricultural runoff, and aquaculture discharges (Gopal et al., 2020). Once released into aquatic environments, antibiotics can persist for long durations, interact with natural organic matter, and adsorb to sediments (Nikzad et al., 2024). These processes not only facilitate the bioaccumulation of antibiotics in aquatic organisms but also disrupt microbial communities, potentially altering nutrient cycles. More critically, the continuous release of antibiotics into the environment accelerates the emergence and proliferation of antibiotic resistance genes (ARGs) (Okab & Alwared, 2023). These genes can be horizontally transferred between environmental and pathogenic bacteria, posing severe threats to both ecological systems and human health. According to the World Health Organization (2024), antibiotic-resistant infections have been documented in 22 countries, contributing to approximately 700,000 deaths globally each year (World Health Organization, 2024).

Tetracyclines (TC) are among the most widely utilized antibiotics globally. As a broad-spectrum class, TC are known for their ability to inhibit bacterial protein

synthesis, thereby effectively treating a range of bacterial infections (Fiaz et al., 2021). These antibiotics are primarily derived from various Streptomyces species, with approximately twenty different tetracycline-based compounds having been introduced into the pharmaceutical market (Xu et al., 2021). Structurally, TC are characterized by a four-fused-ring naphthacene core, substituted with various functional groups including hydroxyl, keto, methyl, and dimethylamino moieties (Fiaz et al., 2021). The molecular structure of tetracycline plays a critical role in governing its adsorption behaviour and photocatalytic degradation pathways.

Tetracycline contains multiple functional groups, including hydroxyl (-OH), amide (-$CONH_2$), carbonyl (C=O), and dimethylamino (-$N(CH_3)_2$) moieties, which contribute to its strong interaction with catalyst surfaces (Gopal et al., 2020). These functional groups enable complexation with metal ions such as Zn^{2+} and facilitate adsorption onto photocatalyst surfaces through hydrogen bonding, electrostatic interactions, and surface complex formation (Thiang et al., 2022). The adsorption behaviour is highly pH-dependent, as tetracycline exists in cationic, zwitterionic, or anionic forms depending on solution conditions, which directly influences its affinity toward the photocatalyst surface (Chopra & Roberts, 2001).From a degradation perspective, the conjugated π-electron system within the tetracycline structure enhances its susceptibility to oxidative attack by reactive oxygen species such as hydroxyl radicals and superoxide radicals (Hao et al., 2024). Photocatalytic degradation typically proceeds through pathways including hydroxylation, demethylation, deamination, and ring opening reactions, primarily initiated at electron-rich functional groups such as the dimethylamino and phenolic sites (Hao et al., 2024). The presence of multiple reactive sites within the tetracycline molecule allows for stepwise degradation into intermediate compounds before eventual mineralization (Gopal et al., 2020). Therefore, the molecular structure of tetracycline not only governs its adsorption behaviour but also dictates the dominant degradation mechanisms and reaction pathways during photocatalytic treatment.

“Pharmacokinetic parameters, including the drug’s elimination rate (expressed as its half-life) and absorption properties further classify TC into three categories: oxytetracycline, chlortetracycline, and tetracycline itself, as illustrated in Figure 2.1, (Chopra & Roberts, 2001). Despite their clinical value, the overuse and mismanagement of TC have led to alarming environmental and health implications. A substantial fraction (ranging from 50% to 80%) of administered tetracycline is excreted in its

unmetabolized form, ultimately entering terrestrial and aquatic environments. Figure 2.2 schematically illustrates the major environmental dissemination pathways of tetracyclines, emphasizing their distribution through point sources (such as wastewater effluents) and non-point sources (such as agricultural runoff and manure leaching).

Tetracyclines exhibit notable environmental persistence due to their low biodegradability and resistance to photolytic and oxidative degradation under ambient conditions (Nikzad et al., 2024). Although their degradation may occur under extreme pH conditions, the resulting transformation products such as epimers, isoforms, and anhydro derivatives are often stable and potentially bioactive (Gopal et al., 2020). Furthermore, their low Henry's law constants (3.45×10^{-24} to 3.91×10^{-26} atm·m³/mol) indicates low volatility, further supporting their environmental stability and limited natural degradation (Gopal et al., 2020). Compared to other antibiotic classes such as fluoroquinolones, sulfonamides, and β-lactams, tetracyclines exhibit distinct environmental behaviour due to their strong chelation with metal ions, high affinity for sediments, and relatively low biodegradability (Antos et al., 2024). Fluoroquinolones tend to accumulate in sediments due to strong adsorption, whereas sulfonamides are more mobile and frequently detected in surface and groundwater systems (Antos et al., 2024). In contrast, tetracyclines demonstrate both persistence and partial adsorption behaviour, allowing them to remain in aqueous and solid phases simultaneously, which increases their environmental residence time and ecological impact.

Environmental monitoring studies have reported tetracycline concentrations typically ranging from ng/L to µg/L levels depending on the matrix (Antos et al., 2024). In surface waters, concentrations are commonly detected in the range of 10–500 ng/L, while higher levels up to several µg/L have been reported in wastewater effluents and aquaculture systems (Mohammadi et al., 2023). These concentration ranges confirm the widespread occurrence of tetracycline in aquatic environments and highlight its relevance as a model pollutant for photocatalytic degradation studies.

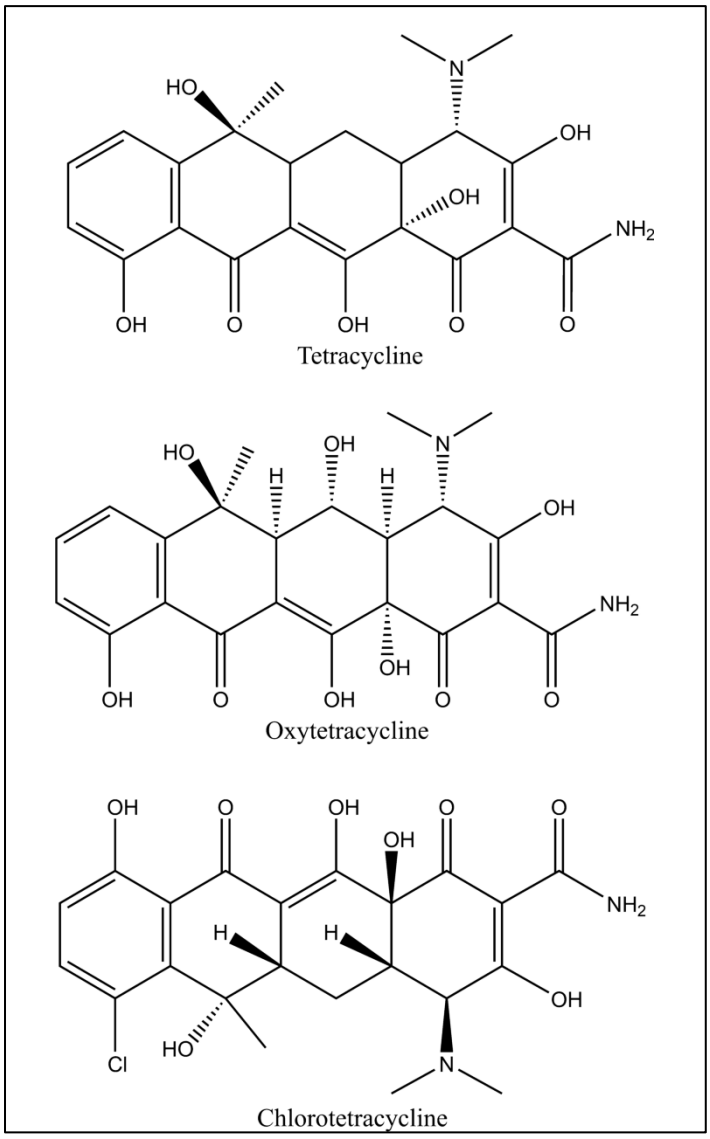

Figure 2.1 Chemical Structures Of Tetracycline, Oxytetracycline, And Chlortetracycline (Fiaz et al., 2021)

Conventional wastewater treatment processes, including activated sludge systems, membrane filtration, and ozonation, are commonly employed in municipal and industrial treatment facilities. However, these approaches are often insufficient for the complete removal of antibiotic contaminants such as tetracyclines (Nikzad et al., 2024). The inefficiency largely stems from the physicochemical properties of tetracycline compounds, particularly their strong chelating ability and high affinity for divalent metal ions such as Ca^{2+}, which leads to the formation of stable and persistent complexes (Fiaz et al., 2021). Consequently, residual tetracyclines are frequently detected in treated effluents, as well as in environmental matrices including surface water, groundwater, sediments, and sludge, highlighting the need for more advanced and

targeted removal strategies (Nikzad et al., 2024). These methods may result in the formation of toxic by-products and incomplete degradation, necessitating more advanced, environmentally friendly alternatives.

Given these concerns, advanced oxidation processes (AOPs), especially photocatalysis, have emerged as promising technologies for the complete mineralization of recalcitrant pollutants like tetracycline (Fang et al., 2022). Photocatalytic methods utilizing nanomaterials offer several advantages, including high degradation efficiency, operation under ambient conditions, and the potential for reusability. Therefore, the development of cost-effective, sustainable photocatalysts such as those derived from biomass waste represents a crucial step toward addressing the growing threat of antibiotic pollution and resistance in aquatic environments.

2.2.1 Sources and Pathways of Antibiotic Contamination

The increasing presence of antibiotics in the environment has raised significant concerns regarding their long-term ecological and public health impacts. Antibiotics enter environmental compartments through various pathways, including municipal wastewater, agricultural runoff, aquaculture discharges, and landfill leachates (Gopal et al., 2020). These pathways contribute to the accumulation of antibiotic residues in water bodies and soil, leading to the proliferation of antibiotic-resistant bacteria and potential threats to environmental and human health (Gopal et al., 2020). The primary sources, occurrence, and transport pathways of antibiotics into the ecosystem are presented in Figure 2.2.

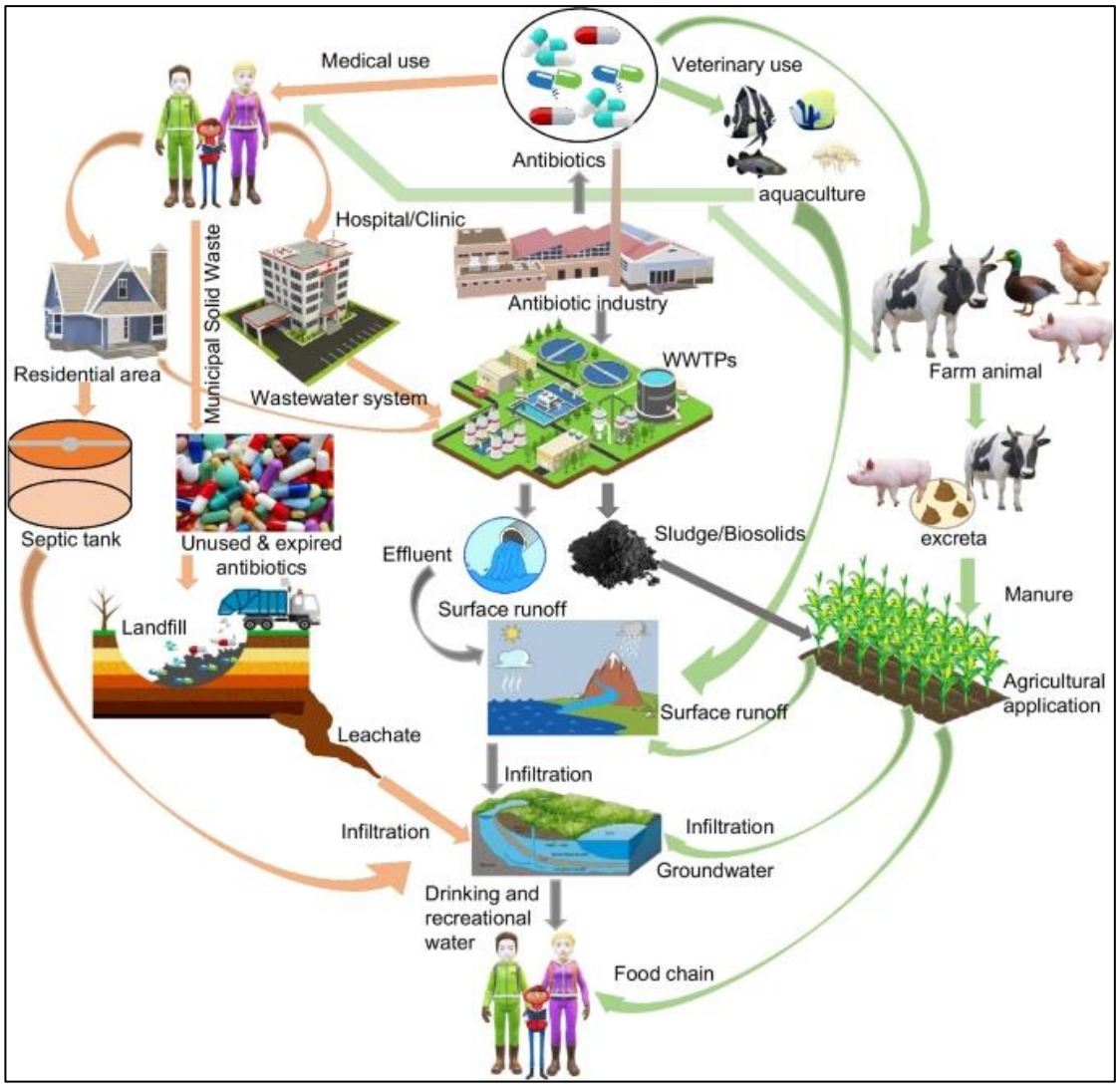

Figure 2.2 Possible Sources, Occurrence, And Fate Of Antibiotics In The Environment (Sonkar et al., 2024)

Among these, wastewater discharge from domestic, industrial, and healthcare facilities is a dominant source. A substantial fraction of administered antibiotics, typically 30–90%, is excreted unmetabolized through urine and feces (Hosny et al., 2022). These residues eventually reach municipal wastewater treatment plants, where conventional treatment processes are often insufficient to completely remove them. As a result, residual antibiotics persist in treated effluent and are subsequently released into surface water bodies, further exacerbating the risk of antibiotic resistance development (Jia et al., 2023). Hospital wastewater, in particular, has been reported to contain significantly higher concentrations of antibiotics, with levels reaching up to 100 μgL^{-1}, compared to approximately 1 μgL^{-1} detected in domestic wastewater (Gopal et al., 2020).

Agricultural activities and livestock farming also contribute significantly to environmental antibiotic contamination. In modern animal husbandry, antibiotics are widely used not only for therapeutic purposes but also as growth promoters and disease prevention agents. However, studies have shown that up to 80% of administered antibiotics are excreted by livestock in their original or partially metabolized forms (Kraemer et al., 2019). These antibiotic-contaminated animal manures are often applied as fertilizers, facilitating the infiltration of antibiotics into the soil and their subsequent migration to nearby water bodies via surface runoff. In China, for example, it has been estimated that approximately 180,000 tons of antibiotics are used annually in agriculture, highlighting the substantial contribution of this sector to environmental antibiotic pollution (Fiaz et al., 2021).

Another major contributor to antibiotic contamination is aquaculture, where antibiotics are directly introduced into aquatic environments to prevent and treat bacterial infections in fish and shrimp farming (Bai et al., 2022). Since a large proportion of these antibiotics are not absorbed by aquatic organisms, they are released into surrounding water bodies, leading to prolonged exposure and bioaccumulation in sediment (Bai et al., 2022). Studies have detected significant concentrations of tetracycline, sulfonamides, and fluoroquinolones in aquaculture wastewater, further supporting concerns that these environments serve as reservoirs for antibiotic-resistant bacteria (Oluwole & Olatunji, 2022) .

Additionally, landfill leachates and industrial discharges represent another critical pathway of antibiotic contamination (Gunjyal et al., 2023). Improper disposal of expired medications and pharmaceutical waste leads to the gradual leaching of antibiotics into groundwater and surface water systems. Industrial effluents, particularly from pharmaceutical manufacturing plants, have been reported to contain extremely high concentrations of antibiotic residues, sometimes exceeding environmental safety thresholds (Nyaaba et al., 2023). Due to their high stability and resistance to natural degradation processes, these contaminants persist in the environment for extended periods, further compounding the risks associated with antibiotic pollution (Nyaaba et al., 2023).

The persistence of antibiotics in various environmental compartments highlights the urgent need for effective mitigation strategies. Given that conventional wastewater treatment systems are often inadequate in completely removing antibiotics, advanced treatment technologies such as membrane filtration, advanced oxidation processes, and

adsorption techniques have been explored as potential solutions. Addressing these contamination pathways is critical to minimizing the ecological and human health risks associated with antibiotic pollution and preventing the further spread of antimicrobial resistance.

2.2.2 Limitations of Conventional Wastewater Treatment and the Need for Advanced Solutions

Traditional wastewater treatment plants (WWTPs) are not specifically designed to eliminate pharmaceutical contaminants such as antibiotics (Li et al., 2025). While primary and secondary treatment processes effectively remove suspended solids and biodegradable organic matter, compounds like tetracycline persist due to their stable molecular structures and resistance to biodegradation (Selvakumar et al., 2025).

Biological treatment methods, including activated sludge and biofilm reactors, exhibit limited efficiency in degrading antibiotics. Although certain bacteria can metabolize tetracycline, the degradation is often incomplete, resulting in transformation products that may retain antimicrobial activity (Gopal et al., 2020). Furthermore, the constant exposure of microbial communities in WWTPs to antibiotics can facilitate the emergence of antibiotic-resistant bacteria (ARB) and antibiotic resistance genes (ARGs), exacerbating the global resistance crisis.

Adsorption is a widely studied approach for removing antibiotics from water, with activated carbon, biochar, and clay minerals being commonly used adsorbents. These materials have high surface areas and strong affinity for tetracycline molecules, making them effective in removing the antibiotic from wastewater (Kraemer et al., 2019). However, adsorption only transfers tetracycline from one phase to another without degrading it, requiring additional treatment for the spent adsorbents. The regeneration of adsorption materials is often costly and energy-intensive, limiting large-scale applications.

Membrane-based filtration methods, such as reverse osmosis and nanofiltration, have demonstrated high removal efficiencies for tetracycline. These techniques rely on selective permeability to separate contaminants from water, effectively reducing antibiotic concentrations (Jia et al., 2023). Despite their effectiveness, membrane processes face challenges such as high operational costs, membrane fouling, and significant energy consumption. Additionally, concentrated tetracycline residues

accumulate in the reject stream, necessitating further disposal or treatment (X. Lu et al., 2023).

Ozonation involves the use of ozone (O_3) to oxidize tetracycline molecules, achieving high removal efficiencies. However, concerns regarding the formation of toxic byproducts and operational costs limit its widespread application (Fiaz et al., 2021). Similarly, the Fenton process, which generates hydroxyl radicals (•OH) through the reaction of hydrogen peroxide with iron salts, is effective but produces large amounts of sludge, requiring additional waste management (Sonkar et al., 2024). Due to these limitations, Advanced Oxidation Processes (AOPs) have garnered significant interest as they utilize highly reactive oxygen species (ROS) to achieve complete mineralization of pollutants.

A variety of semiconductor-based photocatalysts and their hybrid composites have been extensively developed to enhance the photodegradation efficiency of antibiotics and other recalcitrant pollutants. Titanium dioxide (TiO_2) remains the benchmark photocatalyst due to its high photochemical stability, strong oxidizing potential, and low toxicity. Nevertheless, its wide band gap (3.2 eV for anatase) restricts photoactivation predominantly to the ultraviolet region, which constitutes only a small fraction of the solar spectrum. To overcome this constraint, TiO_2 has been modified through noble-metal deposition (Ag, Au, Pt), non-metal doping (N, C, S), and coupling with carbonaceous materials such as graphene and carbon nanotubes to extend visible-light absorption and suppress charge recombination.

Bismuth-based photocatalysts, including $BiVO_4$, Bi_2WO_6, and Bi_2O_3, have gained considerable attention owing to their narrow band gaps and intrinsic internal electric fields that facilitate efficient charge separation (Wakjira et al., 2024). Similarly, tungsten oxide (WO_3) and cadmium sulfide (CdS) have demonstrated effective visible-light activity; however, WO_3 suffers from low conduction-band potential that limits reduction reactions, while CdS is prone to photo corrosion under prolonged irradiation (Murillo-Sierra et al., 2021). To address these limitations, composite architectures integrating multiple semiconductors or semiconductors–carbon frameworks have been proposed to achieve synergistic band alignment and efficient electron–hole migration pathways.

Recent advances have increasingly focused on hybrid systems combining traditional semiconductors with carbonaceous nanostructures such as carbon dots (CDs), graphene quantum dots (GQDs), and biochar derivatives. These carbon-based

materials serve dual functions as electron reservoirs and photosensitizers, broadening spectral response while promoting interfacial charge transfer (Wan Ishak, et al., 2025). Such strategies not only enhance photocatalytic performance but also align with green chemistry principles by enabling the use of biomass-derived precursors and low-energy synthesis routes.

Among AOPs, photocatalysis stands out as a promising, sustainable, and energy-efficient method for tetracycline degradation. Semiconductor photocatalysts like ZnO and TiO_2 show excellent photocatalytic activity under UV or visible light, enabling the mineralization of tetracycline into harmless byproducts (Fernández et al., 2019). However, a key limitation is the rapid recombination of photogenerated electron-hole pairs, which impedes efficiency.

To address this, composite materials such as ZnO decorated with biomass-derived carbon dots have been developed to enhance charge separation and prolong electron-hole lifetimes. These ZnO/CDs composites exhibit superior light harvesting, enhanced charge carrier mobility, and improved photocatalytic performance. The introduction of carbon dots, which act as electron acceptors and light sensitizers, further increases degradation efficiency while supporting environmental sustainability. Based on Table 2.1, several reported photocatalysts achieved moderate to high tetracycline removal efficiency; however, most systems are limited by UV dependence, complex composite design, absence of biomass derived carbon dots, limited sustainability emphasis, or insufficient long term stability evaluation. This supports the relevance of developing EFB derived ZnO/CDs nanocomposites as a greener photocatalytic system with improved charge transfer and photocatalytic performance.

The persistence of tetracycline in the environment and its contribution to antibiotic resistance and ecological harm underscore the urgent need for effective remediation technologies. While conventional methods offer partial solutions, photocatalysis especially with nanocomposite enhancements like ZnO/CDs presents a highly viable alternative. This innovative approach aligns with the goals of green chemistry and circular economy, offering a scalable pathway toward clean water solutions. Continued research into such advanced photocatalysts is essential to confront the growing threat of pharmaceutical pollution and safeguard global water resources.

Table 2.1
Comparative Summary Of Reported Photocatalytic Systems For Tetracycline Degradation

Catalyst or treatment system	**Target pollutant**	**Light source**	**Removal efficiency**	**Key limitation**	**Reference**
ZnO-modified $Y_2Ti_2O_7$	Tetracycline	UV light	76 %	No biomass derived CDs; limited green synthesis and sustainability focus	(Arfoy et al., 2026)
SDS modified ZnO nanophotocatalyst	Tetracycline	Visible light	49 %	Low efficiency; depends on TC sensitization and SDS surface complex formation; no biomass derived CDs	(K. Jia et al., 2022)
ZnO nanoparticles	Tetracycline	UV light	70.17 %	Moderate efficiency; UV dependent; rapid electron hole recombination; no CDs modification	(Wan Ishak, Tan, Abu Bakar, Lim, et al., 2025)
CQDs modified Bi_2MoO_6/CuS	Tetracycline	UV or visible light	78.25 %	Complex ternary system; not ZnO based; no biomass derived CDs; limited cycling stability	(D. Xu et al., 2024)
TiO_2/natural pyrite	Tetracycline	Visible light or solar light	84 %	No biomass derived CDs; mineral pyrite may introduce composition variability; limited long-term stability and real wastewater validation	(Hasham Firooz et al., 2024)

The comparison shows that reported photocatalytic systems can achieve moderate to high tetracycline degradation efficiency, but several limitations remain. Conventional ZnO based photocatalysts are low cost and easy to synthesize, but their activity is restricted by UV dependence and rapid electron hole recombination. Surface

modified ZnO systems can improve visible light response, but some rely on sensitization effects rather than intrinsic photocatalyst enhancement. More complex heterojunctions such as CQDs modified Bi_2MoO_6/CuS and TiO_2/natural pyrite show improved degradation performance, but their multi component structure, possible material variability, and limited long-term stability may restrict practical scalability. Most importantly, many reported systems do not integrate biomass derived CDs with detailed electrochemical validation of charge transfer behaviour. Therefore, the present EFB derived ZnO/CDs system addresses this research gap by combining sustainable carbon dot synthesis, photocatalytic performance enhancement, and mechanistic charge transfer evaluation.

2.3 Carbon dots: Structure, Synthesis, and Photocatalytic Properties

2.3.1 Structure and Composition of Carbon dots

Carbon dots (CDs) are a class of zero-dimensional carbon-based nanomaterials that exhibit remarkable physicochemical properties, rendering them highly attractive for a wide range of applications, including photocatalysis, bioimaging, drug delivery, and optoelectronic devices (Papaioannou et al., 2019; Tavan et al., 2025). CDs typically possess a quasi-spherical morphology with an average particle size of less than 10 nm (Liu et al., 2020). Their structural framework comprises a hybridized arrangement of sp^2 and sp^3 carbon atoms, which contributes to their distinct optical, electronic, and catalytic properties (Khairol Anuar et al., 2021; Zhang et al., 2022). The presence of oxygen and nitrogen containing functional groups on the surface of CDs significantly enhances their water dispersibility, chemical stability, and electron transfer efficiency, thereby improving their performance in photocatalytic applications (J. Liu et al., 2020).

Structurally, CDs exhibit a core-shell-like architecture, where the core consists of an amorphous or graphitic carbon framework, and the shell is enriched with a variety of functional groups, including hydroxyl (-OH), carboxyl (-COOH), and amine ($-NH_2$) moieties (Sun & Wang, 2023) as shown in Figure 2.3. These surface functional groups play a pivotal role in modulating the electronic properties of CDs by facilitating charge separation and transfer processes. Additionally, the presence of a π-conjugated system within the carbon framework enhances the mobility of charge carriers, enabling CDs to function as efficient electron acceptors or donors in photocatalytic systems (Chaudhary

et al., 2020; Papaioannou et al., 2019). The ability of CDs to modulate charge carrier dynamics makes them highly suitable for integration with semiconductor photocatalysts, thereby enhancing their overall photocatalytic performance (M. Wang & Liu, 2023).

In semiconductor CDs composite systems, the surface functional groups play a critical role in governing interfacial charge transfer processes. Functional groups such as hydroxyl, carboxyl, and amine moieties act as active interfacial sites that facilitate strong electronic coupling between CDs and semiconductor materials such as ZnO (Liu et al., 2020; Lu et al., 2025). These groups can form coordination bonds or surface complexes with metal ions (e.g. Zn^{2+}), creating efficient charge transfer pathways across the heterojunction interface (Hasanah et al., 2023). In addition, oxygen-containing groups introduce surface defect states or mid-gap energy levels, which can act as electron trapping sites, thereby suppressing electron–hole recombination and prolonging charge carrier lifetime (Hasanah et al., 2023; Hunge et al., 2022). Nitrogen-containing functional groups further enhance electron donating ability, improving electron mobility and promoting directional charge transfer from CDs to the semiconductor conduction band or vice versa, depending on band alignment (Hasanah et al., 2023). As a result, the presence and distribution of surface functional groups directly influence the efficiency of charge separation, interfacial electron transport, and overall photocatalytic performance of semiconductor CDs composites (Qurtulen et al., 2026).

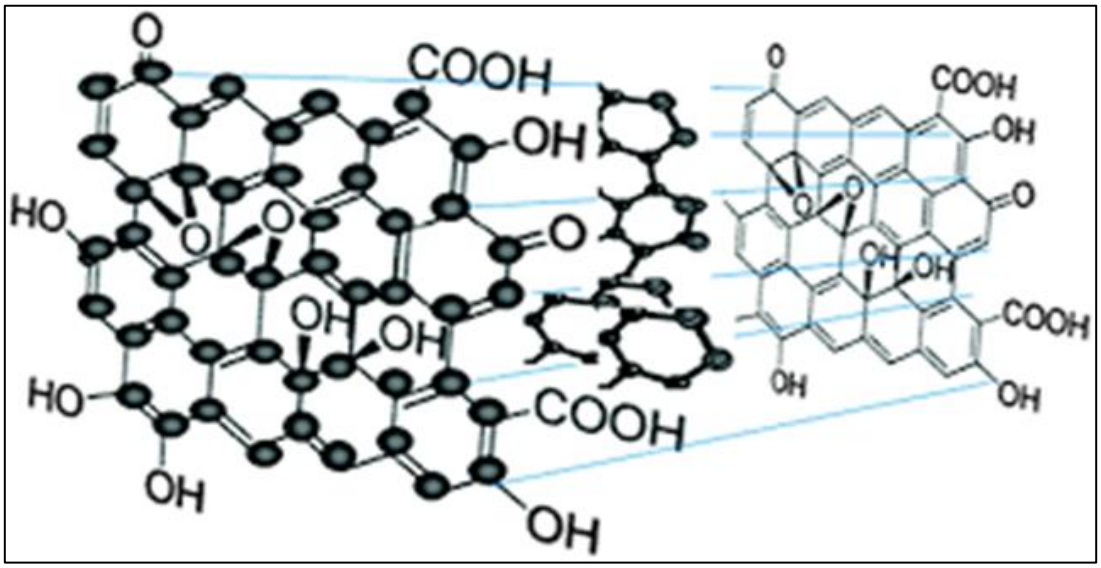

Figure 2.3 Structure Of Carbon Dots (Khairol Anuar et al., 2021).

2.3.2 Synthesis of Carbon dots

The synthesis of carbon dots can be broadly classified into top-down and bottom-up methodologies, as illustrated in Figure 2.4. Each approach offers distinct advantages in tailoring particle size, surface functionality, and optical properties.

2.3.2.1 Top-Down Synthesis

Top-down strategies involve the fragmentation of bulk carbon materials such as graphite, graphene oxide, and carbon nanotubes into nanoscale carbon domains. Common techniques include laser ablation, electrochemical oxidation, and chemical exfoliation (J. Liu et al., 2020) . For example, laser ablation utilizes high-energy pulsed laser irradiation in an inert or reactive medium to break down larger carbon structures into nanosized particles. Electrochemical oxidation, on the other hand, involves the anodic oxidation of graphite electrodes in an electrolyte solution, resulting in the formation of CDs with tunable surface functionalities (Zhang et al., 2022).

While these methods provide precise control over particle size and surface chemistry, they typically require sophisticated instrumentation, high energy consumption, and hazardous reagents (Khairol Anuar et al., 2021). Such limitations hinder their scalability and environmental sustainability, particularly in the context of synthesizing biomass-derived CDs. Therefore, alternative routes that are more energy-efficient, cost-effective, and environmentally benign are preferable for large-scale applications.

2.3.2.2 Bottom-Up Synthesis

Bottom-up approaches rely on molecular self-assembly and the carbonization of small organic molecules to synthesize carbon dots. Common techniques include hydrothermal and solvothermal synthesis, microwave-assisted processing, and pyrolysis (Berdimurodov et al., 2023). Among these, hydrothermal synthesis has emerged as a cost-effective and environmentally benign method suitable for large-scale production. This process involves the thermal treatment of carbon-rich precursors such as citric acid, glucose, or biomass-derived materials under controlled temperature and

pressure in a sealed autoclave (Nazatul Akmal Nazibudin et al., 2023). The thermal decomposition and subsequent reorganization of these precursors result in nanoscale carbon structures with tunable optical and surface characteristics (Nammahachak et al., 2022). The formation pathway illustrated in Figure 2.4 highlights the sequential transformation of biomass precursors into functionalized carbon dots, where each stage plays a critical role in determining the structural and photocatalytic properties of the final material.

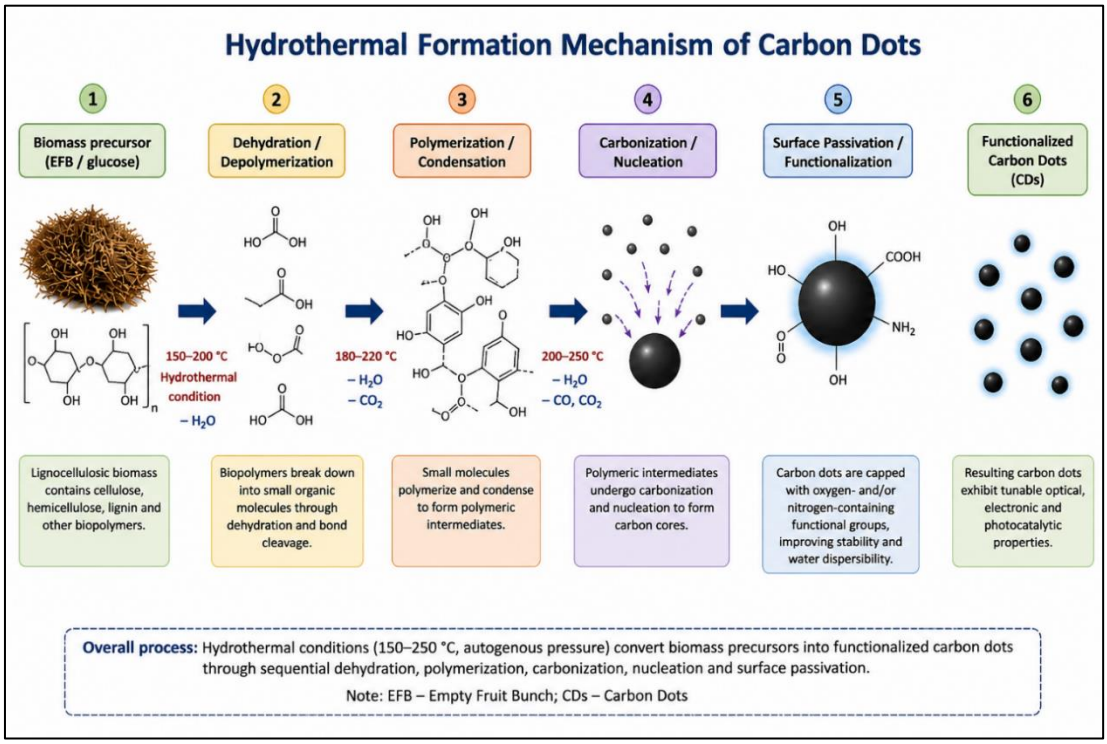

Figure 2.4 Schematic Representation Of Carbon Dot Formation Via Hydrothermal Synthesis, Illustrating Dehydration, Polymerization, Carbonization, Nucleation, And Surface Passivation Processes.

The physicochemical properties of the resulting CDs such as particle size, surface functional groups, and photoluminescence behaviour are strongly influenced by the choice of precursor and reaction parameters. Additionally, heteroatom doping (e.g., nitrogen, sulfur, phosphorus) can be achieved through dopant-containing feedstocks, enabling modulation of the electronic band structure and enhancement of photocatalytic activity (Sun & Wang, 2023). Various synthesis techniques have been reported for carbon dots production, differing in precursor type, reaction conditions, and resulting properties. Table 2.1 summarizes representative examples of CDs prepared via different

synthesis routes, including both natural and synthetic precursors, along with their corresponding quantum yields and applications.

Recent studies have increasingly emphasized the use of biomass waste as a renewable carbon precursor for the sustainable synthesis of carbon dots (CDs). This emerging trend reflects a shift from conventional chemical precursors toward waste valorization and circular bioeconomy practices. Researchers are now exploring diverse biomass sources including rice husk, sugarcane bagasse, corncob, sawdust, fruit peels, and oil palm empty fruit bunch (EFB) to produce CDs with tunable optical and surface properties. These biomass-derived CDs exhibit excellent photoluminescence, abundant oxygen- and nitrogen-containing surface groups, and high biocompatibility, making them suitable for environmental remediation, sensing, and photocatalytic applications (Wang & Liu, 2023). The hydrothermal such agricultural residues enable a low-energy, solvent-free route to generate functional nanomaterials while simultaneously addressing waste accumulation and greenhouse gas emissions (De Francesco et al., 2024). EFB, in particular, represents a significant lignocellulosic waste stream in Malaysia's palm oil industry and has gained attention as a viable carbon source for green nanomaterial synthesis (Wang et al., 2020). This direction underscores the growing global trend toward integrating waste-to-resource conversion with advanced nanotechnology for sustainable environmental management.

From a photocatalytic perspective, the integration of EFB-derived CDs with ZnO nanoparticles is anticipated to significantly enhance photocatalytic performance of ZnO by improving photogenerated charge separation, expanding visible-light absorption, and suppressing electron-hole recombination. This study investigates the ZnO/CDs nanocomposite as a novel, energy-efficient photocatalyst for the degradation of tetracycline in wastewater, presenting a green and sustainable strategy for environmental remediation.

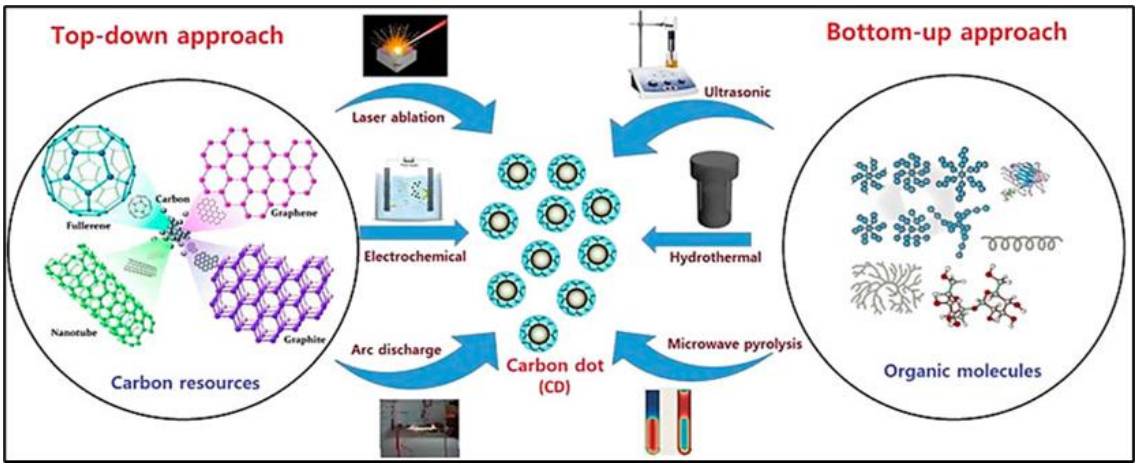

Figure 2.5 Top-Down And Bottom-Up Approach For Synthesizes Of CDs (Khairol Anuar et al., 2021)

Table 2.2 provides a comparative overview of reported carbon dots (CDs) synthesis methods, highlighting the influence of precursor type, processing technique, and reaction conditions on the resulting quantum yield and application. Both natural and synthetic carbon sources have been successfully utilized, with biomass-based precursors such as lemon juice, coffee powder, fennel seeds, peanut shells, and prawn shells demonstrating high potential for sustainable synthesis. Among the various routes, hydrothermal and microwave-assisted methods are the most frequently employed due to their operational simplicity, scalability, and ability to preserve surface functional groups that enhance photoluminescence efficiency. Reported quantum yields range from 2.3% to 28.2%, indicating that process parameters particularly temperature, duration, and precursor composition strongly influence optical performance (Nazibudin et al., 2023). This variation arises from the influence of synthesis conditions on the structural and surface properties of CDs. Temperature and reaction time govern the degree of carbonization and graphitization, where higher temperatures promote more ordered carbon structures but may reduce surface defect sites that act as emissive centers. In contrast, moderate synthesis conditions favor the formation of abundant surface functional groups and defect states, which enhance radiative recombination and increase quantum yield. Additionally, synthesis methods such as hydrothermal and microwave processes promote effective surface passivation and heteroatom incorporation, resulting in improved electron transition efficiency, whereas high-energy methods such as pyrolysis and arc discharge often produce less passivated surfaces, leading to lower quantum yield due to increased non-radiative recombination.

Hydrothermal processes, typically conducted at 180–250 °C for 3–12 hours, consistently yield CDs with superior luminescence, whereas pyrolysis and arc discharge methods often result in lower quantum yields due to partial carbonization and reduced surface passivation (Nazibudin et al., 2023). The summarized studies also reveal the diverse applicability of CDs in bioimaging, ion detection, photocatalysis, and sensing, confirming their multifunctional character and broad technological relevance.

Table 2.2
Summary of CDs Preparation Via Different Synthesis Methods

Precursor	**Synthesis Methods**	**Treatment condition**	**Quantum yield (%)**	**Application**	**References**
Lemon juices	Hydrothermal	240℃, 12h	21%	Detection ion V^{5+}	(Hoan,et al., 2019)
Carbon glassy	Laser ablation	Batch, Continuous Flow Jet	4.5%	Bioimaging	(Doñate-Buendia et al., 2018)
Coffee powder	Solvothermal	100℃, 2h	-	Photocatalyst	(Maddu et al., 2021)
Purple perilla	Microwave	500 W,3min	20%	Photocatalyst	(Zhao et al., 2019)
Fennel seeds	Pyrolysis	500℃, 3h	9.5%	Bio-sensing	(Dager et al., 2019a)
Peanut shells	Pyrolysis	400℃, 4h	7.06%	Metal ion sensing	(Ma et al., 2017)
Trapa bispinosa peel	Thermal oxidation	30℃, 2.5h	-	Bioimaging	(Mewada et al., 2013)
Apple juice	Hydrothermal method	180℃, 3h	9.21%	Carbon material	(Lou et al., 2021)
Catharanthus roseus	Hydrothermal method	200℃, 4h	28.2%	Multi ion detection and bioimaging	(Arumugham et al., 2020)
Wheat straw	Hydrothermal method	250℃, 10h	9.2%	Detection of Fe^{3+} and bioimaging	(Yuan et al., 2015)
Prawn shells	Hydrothermal method	200℃, 8h	9%	Detection of Cu^{2+}	(Gedda et al., 2016)
Rice grains	Pyrolysis	400℃, 4h	16- 24%	Bioimaging	(Kalita et al., 2016)

Precursor	Synthesis Methods	Treatment condition	Quantum yield (%)	Application	References
Kelp	Microwave	200℃, 10 min	23.5%	Detection of Co^{2+} based on fluorescence quenching	(Zhao et al., 2019)
Citric acid	Carbonization	300℃, 2 h	16.28%	-	(Wang et al., 2015)

2.3.3 Hydrothermal synthesis of carbon dots

Among various bottom-up synthesis techniques, hydrothermal method is widely recognized as the most practical and sustainable approach for the fabrication of carbon dots from green and biomass-based precursors. This method is highly favoured due to its simplicity, relatively short reaction time, moderate operating conditions, and scalability for large-scale production (Jamaludin et al., 2020). Moreover, it is regarded as an environmentally friendly method because it utilizes non-toxic reagents and minimizes secondary pollution, that is, the generation of harmful byproducts or waste effluents during synthesis.

Hydrothermal synthesis conditions are typically dependent on the type of precursor material utilized. For instance, the production of CDs from grass carp was carried out at 200 °C for 20 hours (Nazatul Akmal Nazibudin et al., 2023), whereas apple juice-derived C-Dots required only 150 °C for 12 hours (Khairol Anuar et al., 2021). The introduction of heteroatoms such as nitrogen, sulfur, or other dopants into the carbon structure is a common strategy to enhance the quantum yield and tune the physicochemical properties of CDs. Nitrogen, in particular, is widely used due to its five valence electrons, which facilitate bonding with carbon atoms and contribute to modifications in surface reactivity, optical behavior, and electronic properties (Atchudan et al., 2020).

In addition to the synthesis technique, the type of carbon precursor and specific reaction parameters play crucial roles in determining the morphology, structure, and functionality of the resultant CDs. According to Radnia et al. (2020), the selection of raw materials influences the extent of carbonization and surface passivation processes (Raina et al., 2020) . Biomass-derived precursors can generally be classified into three categories:

i. Low-molecular-weight biomass derivatives, such as glucose, sucrose, citric acid, and ascorbic acid.
ii. Biomass-based macromolecular constituents, including cellulose, hemicellulose, chitin, and lignin.
iii. Natural biomass waste, for example, rice husk, peanut shell, corn straw, empty fruit binch (EFB) and other lignocellulosic materials.

Different precursors contribute distinct structural frameworks and functional groups to the final CDs (Hossain et al., 2020; Jamaludin et al., 2020; Sevilla & Fuertes,

2009). These variations, in turn, influence the carbonization pathway and the optical and surface properties of the resulting nanomaterials. The general formation mechanism of CDs involves a sequence of chemical transformations, including dehydration, polymerization, aromatization, carbonization, and surface passivation (Cui et al., 2021).

For instance, when sucrose is employed as a precursor, it undergoes hydrolysis under hydrothermal conditions to produce glucose and fructose. In contrast, the synthesis of CDs from more complex biomass such as cellulose requires relatively higher temperatures typically above 200 °C to initiate hydrolysis (Su et al., 2020). During this process, the long polysaccharide chains are initially depolymerized into oligomeric sugars, which are further degraded into smaller molecules such as glucose. Subsequent reactions, including isomerization, dehydration, and decomposition, yield various soluble intermediates such as furfural, ketones, aldehydes, and organic acids (Sevilla & Fuertes, 2009).

These intermediate compounds promote the formation of hydronium ions, which act as catalysts for further polymerization and condensation reactions. As the reaction progresses, aromatic structures are formed via aldol condensation and cycloaddition pathways. When the concentration of these aromatic clusters surpasses a critical level, nucleation occurs, resulting in the spontaneous formation of carbon dots (Liu et al., 2020). Meanwhile, hydrophilic and oxygen-containing functional fragments remain on the surface, forming a passivation shell around the carbon-rich core. This configuration results in CDs with a hydrophobic core and a surface-rich shell bearing various functional groups (Sevilla & Fuertes, 2009; Su et al., 2020). In this study, the hydrothermal method was selected for its simplicity, scalability, and minimal environmental impact. As shown in Table 2.3, this method offers clear advantages over conventional methods such as pyrolysis or microwave-assisted synthesis. Table 2.3 highlights that hydrothermal synthesis of carbon dots from diverse biomass precursors yields a wide range of quantum efficiencies, indicating a strong dependence on precursor composition and processing conditions. In general, higher quantum yields are associated with precursors rich in proteins or nitrogen-containing compounds, such as egg white and cow milk, suggesting that in situ heteroatom incorporation enhances surface emissive states and radiative recombination. In contrast, lignocellulosic precursors such as fruit peels and agricultural residues typically exhibit moderate quantum yields, which can be attributed to variations in carbonization degree and less effective surface passivation.

The synthesis temperature also plays a critical role. Temperatures in the range of 180–220 °C tend to produce CDs with balanced graphitization and surface functionality, while excessively high temperatures may reduce surface defect density and consequently lower photoluminescence efficiency. However, this trend is not universal, indicating that precursor chemistry and reaction time must be considered concurrently.

From an application perspective, most reported CDs are utilized in bioimaging and sensing, whereas comparatively fewer studies focus on environmental remediation, particularly photocatalytic degradation of contaminants. This suggests that although biomass-derived CDs possess favourable optical properties, their photocatalytic potential remains underexplored. Furthermore, inconsistencies in reporting quantum yield and application data across studies limit direct comparison and highlight the need for standardized characterization protocols.

Overall, these observations demonstrate that optimizing the balance between carbon core formation and surface functionalization is essential for enhancing the functional performance of CDs. This provides a strong rationale for the present study, which focuses on tailoring biomass-derived CDs to improve charge transfer behaviour and photocatalytic efficiency in ZnO/CDs composite systems.

2.3.3.1 Reaction Mechanism and Parameters

The hydrothermal synthesis of carbon dots generally proceeds through a two-step mechanism: (i) carbonization of the precursor material and (ii) in situ surface passivation or functionalization. Under high-temperature and pressure conditions (typically between 150–250 °C), organic precursors undergo dehydration, condensation, and polymerization reactions, leading to the nucleation and growth of carbonaceous nanostructures (Wang & Liu, 2023). These reactions transform biomass into carbon cores while forming surface defects and functional groups that govern the photoluminescent behaviour of the resulting CDs.

The incorporation of heteroatoms such as nitrogen, sulphur, or phosphorus either inherently present in the biomass precursor or introduced via doping enhances the CDs' optical and electronic properties. These heteroatoms contribute to the formation of surface emissive states, ultimately increasing the quantum yield, a key performance parameter in photocatalytic applications (Nayak et al., 2025).

Several synthesis parameters, including temperature, reaction duration, precursor concentration, and pH, significantly influence the structural and optical characteristics of the CDs. Higher temperatures facilitate graphitization and crystallinity, which reduce surface defects that often act as fluorescence quenching centres. However, excessively long reaction times may lead to particle aggregation, increasing particle size and introducing non-radiative decay pathways, thereby reducing the quantum yield (Abinaya et al., 2021). Similarly, pH conditions can impact the ionization of functional groups on the precursor, influencing the degree of carbonization and surface passivation.

Careful optimization of these parameters is essential for producing high-performance CDs tailored to specific applications. For instance, Rodríguez-Padrón et al. (2020) successfully synthesized bifunctional CDs from orange peel waste using a hydrothermal approach, achieving notable photocatalytic activity in dye degradation (Figure 2.6) (Rodríguez-Padrón et al., 2020). The term *bifunctional* refers to the dual functionality of the synthesized CDs, which can simultaneously serve as effective photocatalysts and fluorescent probes due to their abundant surface functional groups and strong photoluminescence characteristics. This dual nature enhances their applicability in both environmental remediation and analytical sensing systems. This underscores the versatility and effectiveness of hydrothermal synthesis and reinforces its status as a preferred green method for fabricating functional, high-yield carbon dots. The hydrothermal conversion of biomass precursors into carbon dots can be represented by simplified reaction pathways involving dehydration, polymerization, and carbonization processes (Nazibudin et al., 2023). Initially, carbohydrate-based precursors undergo dehydration according to:

$$C_6H_{12}O_6 \rightarrow C_6H_6O_3 + 3H_2O \quad (2.1)$$

followed by condensation and aromatization reactions leading to the formation of carbonaceous nuclei:

$$n(C_6H_6O_3) \rightarrow C_x + \text{volatile products } (CO_2, CO, H_2O) \quad (2.2)$$

During this process, heteroatom-containing functional groups are retained or introduced on the surface:

$$C_x + –OH / –COOH / –NH_2 \rightarrow CDs \text{ (surface-passivated carbon dots)} \qquad (2.3)$$

These reaction steps are strongly influenced by synthesis parameters, which in turn determine the photocatalytic performance of the resulting CDs (Nazibudin et al., 2023). Higher temperatures promote carbonization and graphitic core formation, enhancing electron conductivity but potentially reducing surface functional groups that act as active sites for charge transfer (Nazibudin et al., 2023). Conversely, moderate temperatures and shorter reaction times favour the retention of oxygen- and nitrogen-containing functional groups, which introduce surface defect states and improve charge separation efficiency (Baruah & Dutta, 2009). Additionally, heteroatom incorporation enhances electron donor–acceptor interactions, facilitating interfacial charge transfer in semiconductor composites. Therefore, the balance between core graphitization and surface functionalization, governed by reaction conditions, plays a critical role in determining the photocatalytic efficiency of carbon dots (Josun et al., 2024).

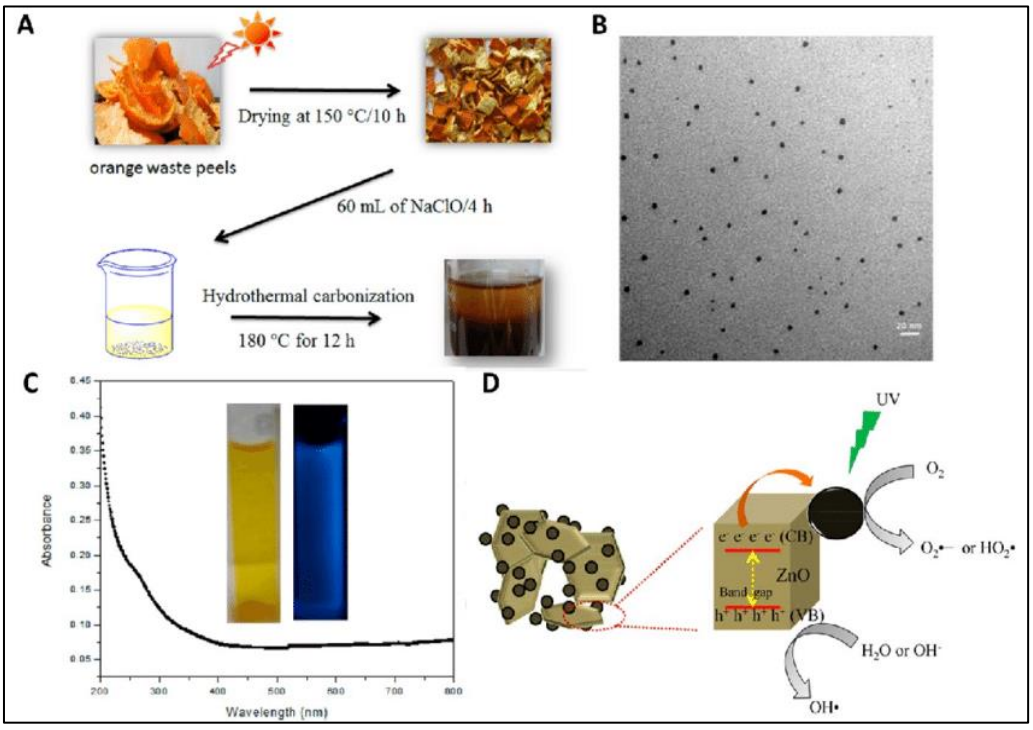

Figure 2.6 Illustration Of Formation Of CDs From Hydrothermal Treatment Of Orange (Rodríguez-Padrón et al., 2020)

2.3.3.2 Selection of biomass derived precursors

Biomass waste materials, particularly agricultural residues, are increasingly recognized as eco-friendly and cost-effective precursors for the synthesis of carbon dots. Among these, empty fruit bunches an abundant byproduct of the palm oil industry stand out due to their high carbon content, lignocellulosic structure, and natural abundance of oxygen-containing functional groups such as hydroxyl and carboxyl groups (Jamaludin et al., 2020). These functional groups not only facilitate carbonization but also contribute to the surface passivation and photoluminescent efficiency of the synthesized CDs (Jamaludin et al., 2020).

Compared to other biomass types like rice husk or sugarcane bagasse, EFB offers lower ash content and higher carbon yield, making it a superior candidate for carbon nanomaterial production (Tavan et al., 2025). Furthermore, the utilization of EFB addresses environmental concerns related to agricultural waste disposal, supporting waste valorization and aligning with the principles of green chemistry and sustainable development (Khairol Anuar et al., 2021).

Table 2.3
Hydrothermal Treatment Of Green Precursors For CDs Synthesis And Application

Precursor	Treatment condition	Quantum Yield (%)	Application	References
Sweet Potato	Hydrothermal,180℃	8.64%	Bioimaging, metal ion detection	(Shen et al., 2018)
Pamelo peel	Hydrothermal,200℃	6.9%	Metal ion detection	(J. J. Liu et al., 2018)
Cow milk	Hydrothermal,180° C	34.5%	Antimicrobial	(Sawalha et al., 2021)
Egg white	Hydrothermal, 220℃	61%	Metal ion detection, bioimaging	(Zhang et al., 2016)
Lemon Juice	Hydrothermal,120℃ to 280℃	14.86-24.89%	Optoelectronic, bioimaging	(Hoan, Tam, et al., 2019)
Sweet pepper	Hydrothermal,180℃	19.3%	Hypochlorite (ClO^-) detection	(Rowson Ali et al., 2021)
Cabbage	Hydrothermal,140° C	16.5%	In-vitro imaging	(Abinaya et al., 2021)
Larch wood	Hydrothermal,250ºC	10.2%	Modification of wood	(Rowson Ali et al., 2021)
Sugarcane bagasse	Hydrothermal,190ºC	35.7%	Removal of contaminants from wastewater	(Prasannamedha & Kumar, 2022)
Rice husk	Hydrothermal, 200ºC	57.9%	Removal of dye from wastewater	(Hossain et al., 2020)
Orange waste peel	Hydrothermal, 180ºC	11.3%	Removal of dye from wastewater	(Rodríguez-Padrón et al., 2020)
Pomelo	Hydrothermal, 90ºC	9.2%	Improves the comprehensive utilization of agricultural wastes	(Li et al., 2021)
EFB Biochar	Hydrothermal, 250ºC	55.84%	Removal of dye from wastewater	(Jamaludin et al., 2020)
Pear juice	Hydrothermal, 180ºC	10.8%	Removal of dye from wastewater	(Bhamore et al., 2018)
Durian Peel	Hydrothermal, 200ºC	12.5%	Removal of dye from wastewater	(Nazibudin et al., 2023)
Gingko leaf	Hydrothermal, 180ºC	21.7%	Removal of dye from wastewater	(Khayal et al., 2021)

2.3.4 Carbon dots as Photocatalyst

Photocatalysis is a process in which the rate of a chemical reaction is altered or initiated by ultraviolet (UV), visible (Vis), or infrared (IR) light in the presence of a photocatalyst (Wang et al., 2022). The photocatalyst absorbs light energy and participates in the chemical transformation of reactants (Ozyurt et al., 2023). Carbon dots have emerged as promising photocatalysts due to their ability to directly absorb light. Upon light absorption, electrons in CDs are excited from the highest occupied molecular orbital (HOMO) to the lowest unoccupied molecular orbital (LUMO), leaving behind a hole in the HOMO (Liu et al., 2020). The generated electron-hole pairs facilitate redox reactions, making CDs effective photocatalysts.

CDs exhibit strong absorption in the UV-Vis range due to π-π^* transitions of sp^2-hybridized C=C bonds in their core (Khairol Anuar et al., 2021). Additionally, surface functional groups such as -COOH, -OH, and $-NH_2$ contribute to light absorption in the visible region through n-π^* transitions (Cui et al., 2021). CDs also exhibit tunable photoluminescence, emitting different colors depending on their size, structure, and surface states (Figure 2.7). Their emission can be adjusted from blue to red by modifying synthesis parameters, making them valuable for photocatalysis and optoelectronic applications.

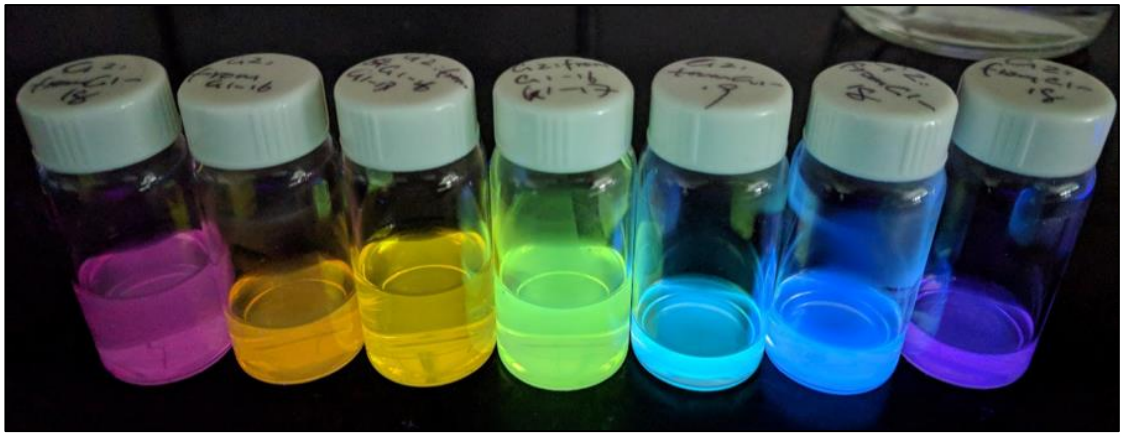

Figure 2.7 Carbon Dots Exhibiting Various Colors Under UV Light, Demonstrating Their Tunable Photoluminescence Properties (Sbacchi et al., 2023)

Similar to other carbon-based materials like graphene oxide, multilayer graphene, and carbon nanotubes, CDs possess sp^2 domains responsible for their broad optical absorption properties (De & Karak, 2017). However, unlike traditional

semiconductor quantum dots, where quantum confinement determines the bandgap and optical properties, CDs' absorption and emission characteristics are primarily governed by their surface states and functional groups (Sbacchi et al., 2023). Recent studies indicate that modifying the surface functional groups of CDs can shift their absorption towards the near-infrared (NIR) region, enabling improved light harvesting for photocatalytic applications. This tunability is particularly beneficial as a significant portion of solar energy is concentrated in the Vis-NIR range, making UV-based photocatalysis less effective in real-world applications.

The advanced oxidation process is one of the most effective treatment technologies for the removal of pharmaceutical pollutants. Unlike conventional treatment methods, AOPs facilitates complete mineralization of contaminants into non-toxic end products such as CO_2 and H_2O through highly reactive hydroxyl (•OH) and superoxide ($•O_2^-$) radicals (Sendão et al., 2023). These radicals can be generated via various methods, including Fenton-based, UV-assisted, ozone-based, and photocatalytic processes. Photocatalysis, in particular, is advantageous due to its ability to degrade pollutants rather than merely transferring them to another phase, as seen in adsorption-based methods. Moreover, it eliminates the need for hazardous oxidants such as ozone or chlorine, making it an environmentally friendly alternative (Sbacchi et al., 2023).

CDs play a crucial role in photocatalysis by serving as both electron donors and acceptors. They can be combined with other materials to form high-efficiency hybrid photocatalysts, enhancing charge separation and extending light absorption (Sbacchi et al., 2023). Their ultra-small size, water solubility, and ease of synthesis make them highly versatile. Notably, pristine CDs have demonstrated the ability to facilitate photocatalytic water splitting for hydrogen production without the need for additional modifications (Liu et al., 2020). This further underscore their potential for clean energy applications.

In conclusion, the unique optical and electronic properties of CDs make them highly promising candidates for photocatalytic applications, particularly in environmental remediation and renewable energy generation. Their tunable absorption, excellent charge transfer capabilities, and ability to be integrated into hybrid systems position them as an emerging class of sustainable photocatalysts.

2.3.5 Carbon dots Based Composite Photocatalyst

Traditional semiconductor photocatalysts primarily utilize wide-bandgap semiconductors, which can only function under ultraviolet light irradiation. However, since UV light accounts for only 4% of solar energy, this severely limits their practical applications (Ayu et al., 2023). To overcome this limitation, carbon dots have been employed to modify conventional semiconductors, enhancing their photocatalytic activity due to their superior electron transport and optical properties (Widiyandari et al., 2023). Incorporating CDs into semiconductors can extend the photo response range and improve charge separation, leading to more efficient photocatalysis. Numerous studies have shown that fabricating composite materials of CDs and other photocatalysts is a straightforward yet effective strategy to boost photocatalytic efficiency (Ayu et al., 2023; Fiszka Borzyszkowska et al., 2023). One of the most widely studied photocatalysts, TiO_2, is commonly used due to its low cost, high efficiency, excellent photostability, and resistance to photo corrosion, making it suitable for solar energy conversion and environmental remediation (Sawunyama et al., 2023). Various TiO_2-based composites have been developed to expand the light absorption range from the UV region to the visible and even near-infrared (NIR) spectrum. For example, Sharma et al. (2022) demonstrated that incorporating CDs into TiO_2 significantly enhanced its visible light absorption, resulting in a 90% degradation of tetracycline within 120 minutes 3.6 times faster than unmodified TiO_2 (Sharma et al., 2022a). Beyond TiO_2, CDs have also been successfully integrated with other metal-oxide semiconductors for environmental pollution degradation. Several studies have highlighted the remarkable electron storage capacity of CDs, which allows them to act as efficient charge transfer mediators, reducing electron-hole recombination. Akbar et al. (2021) reported that CDs facilitate electron shuttling across a semiconductor's conduction network, thereby improving charge separation efficiency (Akbar et al., 2021). Additionally, Huang et al. (2023) synthesized a CDs/$ZnFe_2O_4$ composite photocatalyst using a simple hydrothermal method, achieving an eightfold increase in transient photocurrent response compared to pristine $ZnFe_2O_4$ (Huang et al., 2023). This composite demonstrated enhanced photocatalytic activity for gaseous NO_2 degradation under visible light, with CDs functioning as electron reservoirs and efficient energy transfer components. Similarly, ZnO has attracted significant interest as a photocatalyst due to its high exciton binding energy, strong oxidizing ability, and environmental

friendliness. However, its wide bandgap (3.27 eV) limits its activity under visible light. The integration of CDs into ZnO has been explored as a promising strategy to enhance its photocatalytic efficiency.

Furthermore, CDs can act as a light-harvesting material, absorbing a broader spectrum of solar radiation and converting it into reactive electron-hole pairs. This synergy has been demonstrated in various studies, (Ayu et al., 2023; Maddu et al., 2021; Semeraro et al., 2020) where ZnO/CDs composites exhibited superior photocatalytic degradation of antibiotics like tetracycline compared to pristine ZnO. In general, the mechanism of CDs-based photocatalysis involves three major steps: (1) light absorption, which generates electron-hole pairs, (2) charge transfer and separation, which enhances the formation of reactive species, and (3) catalytic degradation, where the generated radicals facilitate the breakdown of organic pollutants (Wan Ishak, et al., 2025). The inclusion of CDs not only expands the optical response range of the photocatalyst but also increases the number of active sites due to the high surface area of CDs. Despite these advancements, challenges remain in optimizing the synthesis conditions of CDs-based photocatalysts to improve their efficiency. Future research should focus on developing scalable and environmentally friendly synthesis techniques while enhancing the functionalization of CDs to achieve targeted photocatalytic applications.

2.4 Heterogenous Photocatalysis for Environmental Remediation

Heterogeneous photocatalysis utilizes inorganic semiconductors, such as ZnO, Bi_2O_3, SnO_2, ZrO_2, MoS_2, CdS, WO_3, and TiO_2, to create electron/hole pairs (e-/h+) upon exposure to light of energy equal to or greater than the semiconductor's bandgap energy (Wang et al., 2023). This process involves exciting electrons from the valence band (VB) to the conduction band (CB) of the semiconductor, leaving positive holes in the VB (Wang et al., 2022). The generated e-/h+ pairs can migrate to the photocatalyst surface without recombination, leading to redox reactions with water and oxygen adsorbed on the surface, resulting in the degradation and mineralization of pollutants, making it an effective method for environmental remediation and wastewater treatment schematically presented in Figure 2.8 (Sendão et al., 2023).

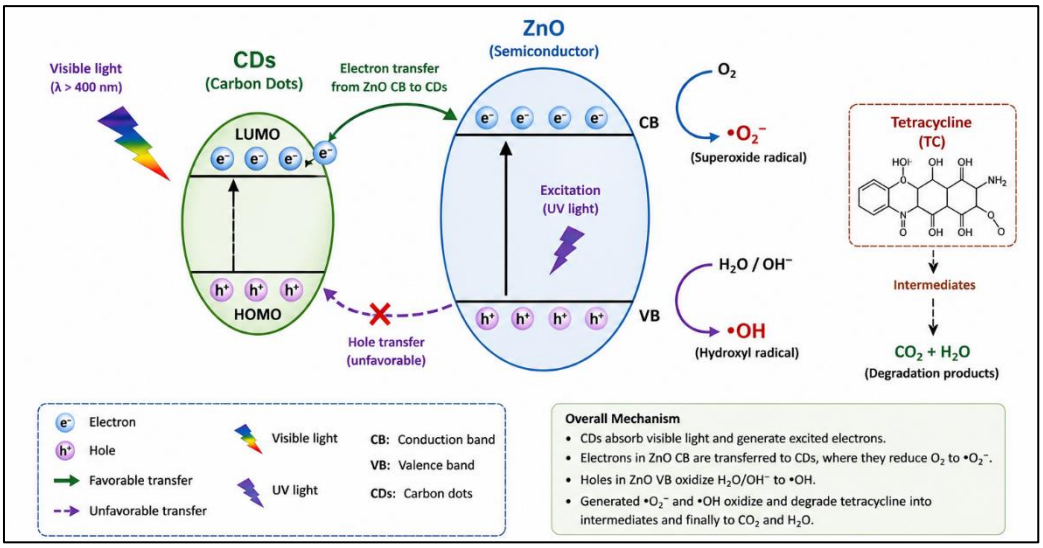

Figure 2.8 The Schematic Diagram Of A Semiconductor Photocatalytic Degradation

The heterogeneous photocatalytic process comprises four main steps: (i) light-harvesting, (ii) photogeneration of charges, (iii) charge transfer and recombination, and (iv) oxidation-reduction reactions. The efficiency of the photocatalytic process is dependent on the performance of each step (Balapure et al., 2024). Factors such as the surface morphology and porosity of the photocatalyst play a crucial role in light-harvesting and pollutant absorption (Sawunyama et al., 2023). While a smooth surface may cause higher light reflection, leading to decreased efficiency, uneven and porous photocatalysts enable multiple reflections and scattering of light within their structures, enhancing light utilization and generating more photoexcited e– /h+ pairs (Sawunyama et al., 2023). Rapid recombination of charge carriers on the photocatalyst surface is a major hindrance to efficiency. Additionally, significant agglomeration of nanostructured particles reduces the specific surface area, slowing down reduction and oxidation processes and increasing diffusion boundaries of the reagents (Adeyemi et al., 2021; Jung et al., 2022; Kouhail et al., 2020). Careful consideration of these factors is essential to enhance the overall efficiency of the photocatalytic process. For the photodegradation of organic pollutants in aqueous solutions, a porous photocatalyst with enhanced adsorption and diffusion rates can significantly improve efficiency by reducing mass-transport boundaries and increasing the activation rate of adsorbed species (Jin et al., 2023). The control of photocatalyst performance is complex and requires skilful handling of various factors. From a thermodynamic perspective, photocatalytic redox reactions rely on the photoinduced e– and h+ with reduction and oxidation potentials falling between the conduction band (CB) and valence band (VB)

potentials (Liu et al., 2020). The energy levels of E_{CB} and E_{VB} determine the potentials of photogenerated electrons and holes, respectively. Photogenerated electrons can reduce the oxidized form of a redox couple if E_{CB} is more negative than the species' potential in solution. Conversely, photogenerated holes can oxidize the reduced form of a redox couple if E_{VB} is more positive than the species' potential. Understanding the relative edge positions of the bands and the energetic levels of the redox couples is crucial in determining the thermodynamic feasibility of reactions with photogenerated species on the catalyst surface to produce reactive species for organic contaminant degradation (Jin et al., 2023).

The knowledge of the redox potentials of different species at pH = 7 as shown in Figure 2.9 is vital for the successful implementation of photocatalytic processes. The potentials of the VB and CB edges of a semiconductor can be calculated using Mulliken electronegativity theory (Ayu et al., 2023). This information enables the assessment of whether the thermodynamics allows the occurrence of reactions with the photogenerated species on the catalyst surface to generate reactive species that effectively degrade organic contaminants. By understanding and skilfully managing the factors influencing photocatalyst performance and considering the thermodynamic aspects of redox reactions, the efficiency of the photocatalytic process can be significantly enhanced, making it a promising technology for environmental remediation and wastewater treatment. Below is an equation that necessary to use for calculating the conduction and valance edges potential of nanocomposite (Ayu et al., 2023).

$$E_{CB} = X - E^{\theta} - 0.5E_g \tag{2.4}$$

$$E_{VB} = E_{CB} + E_g \tag{2.5}$$

Where, E_{VB} is the valence band edge potential, E_{CB} is the conduction band potential, Eg is the bandgap of the semiconductor, E^{θ} is the energy of free electrons on the hydrogen scale (4.5 eV) and X is the electronegativity of the semiconductor, obtained by summing the electronegativity of each atom in the semiconductor. Thus, a more negative CB positions of a photocatalyst are favourable for the reduction reactions, while a more positive VB positions of semiconductors are beneficial for

oxidation reactions (Ayu et al., 2023). Numerous semiconductors such as PbS, CdS, ZnS, WO_3, SnO_2, and ZnO have been tested for heterogeneous photocatalysis, especially for environmental remediation (Karaca et al., 2023). However, ZnO is the most widely used after titanium dioxide semiconductor due to its outstanding properties such as stability, non-toxicity, and inexpensive and inertness, and therefore, it is generally considered the best photocatalyst material (Karaca et al., 2023).

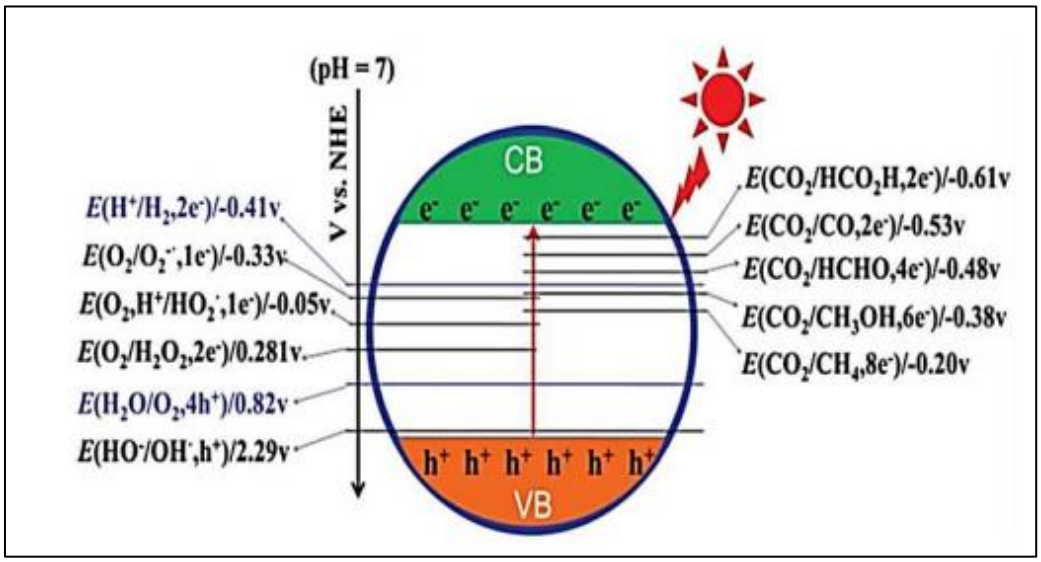

Figure 2.9 The Redox Potentials Of Different Species In Heterogeneous Photocatalysis (Liu et al., 2021)

2.4.1 ZnO as a photocatalyst

ZnO has been widely employed as an efficient semiconductor photocatalyst capable of facilitating the photodegradation of diverse organic pollutants. The ZnO is an n-type II-VI semiconductor, having a wide and direct bandgap, large exciton binding energy (of 60 meV at room temperature) making the emission process persists at room temperature, high physical and chemical stability, and high reactivity (Bozetine et al., 2016). The ZnO generally exists in three crystal structures: wurtzite, zinc blende, and rocksalt, from which hexagonal wurtzite structure is the most stable form of ZnO at room temperature (Ayu et al., 2023). Although the application of ZnO as a photocatalyst has been promising, there are shortcomings like the wide bandgap requiring UV light as the photoexcitation source, the high recombination rate of the excited electrons, and the photo corrosion that impede its industrial applications (Fiszka Borzyszkowska et al.,

2023). Therefore, despite the fact of great development and progress in this field, the major objective is to cater to the demand for a highly efficient, low-cost photocatalyst, with high reusability for large-scale industrial applications with the expected parameters such as low recombination rate and a broad range of light absorption to have maximum utilization of the solar spectrum.

2.4.2 Semiconductor oxide/carbon dots composite photocatalyst

The integration of carbon dots with semiconductor metal oxides has emerged as a promising strategy to fabricate high-performance photocatalysts for environmental and energy-related applications. This hybrid approach capitalizes on the complementary properties of both components, where CDs function as a multifunctional nanomaterial capable of enhancing the inherent photocatalytic performance of semiconductor oxides. CDs offer several advantageous features, including low toxicity, excellent dispersibility in aqueous media, outstanding biocompatibility, and cost-effective synthesis from sustainable precursors (Ozyurt et al., 2023). In particular, their unique optical and electronic properties such as tunable photoluminescence (PL), high electron mobility, and capacity to act as an electron reservoir enable effective light harvesting and charge carrier management within the composite system (Jung et al., 2022). When coupled with semiconductor oxides such as ZnO, TiO_2, or g-C_3N_4, CDs contribute to a significant enhancement in photocatalytic efficiency by extending the light absorption range into the visible region, suppressing the recombination of photo-generated electron-hole pairs, and improving charge carrier transport (Sbacchi et al., 2023). This is primarily attributed to the ability of CDs to serve as a conduit for photoinduced electron transfer, thereby promoting more efficient separation and migration of charge carriers under light irradiation (Sbacchi et al., 2023). Moreover, the surface functionalities present on CDs (e.g., –OH, –COOH, –NH_2) facilitate strong interfacial interactions with semiconductor surfaces, further boosting the overall photocatalytic activity (Jung et al., 2022). As a result, semiconductor oxide/CDs composites have shown improved performance in various photocatalytic applications, including the degradation of organic pollutants, hydrogen evolution, and antibacterial activity (Z. Zhang et al., 2016). Several studies have reported enhanced photocatalytic degradation of various organic pollutants using semiconductor oxide/carbon dots composites. These improvements are attributed to synergistic effects, such as increased visible light

absorption, reduced electron-hole recombination, and better charge carrier mobility. Table 2.4 summarizes recent advancements in carbon dot-based photocatalysts, including their synthesis methods, photocatalytic degradation efficiencies, and operational conditions.

Table 2.4
Summary Of Photocatalytic Performance Of Various Carbon Dots-Based Composite Photocatalysts

Type of photocatalyst	**Degradation Efficiency**	**Synthesis method**	**Pollutant degradation time and light source**	**Refs**
ZnO/CDs	98 % removal of Methylene Blue	Hydrothermal	90 min with a xenon lamp, γ = 425nm	(Bozetine et al., 2016; Zhao et al., 2019)
ZnO/CDs	98 % removal of Ciprofloxacin	Hydrothermal	110min with 30W γ = 365nm	(Mukherjee et al., 2021)
TiO2/CDs	98 % removal of Methylene Blue	Hydrothermal	6 min with 500W Xenon lamp γ =420 nm	(Chai et al., 2018)
ZnO/CQDs	99% removal of Methylene Blue	Wet impregnation	60 min with visible light	(Atchudan et al., 2020)
CdS/CQDs	90 % removal of RhB	CQDs: electrochemical CDs/CQDs: hydrothermal	300W xenon lamp γ =420 nm	(S. Sharma et al., 2019a)
TiO2/CDs	95% removal of CIP	Hydrothermal	30 min with 350W Xe lamp natural sunlight γ >420 nm	(S. Sharma et al., 2019a)
CDs/g-C3N4	90% removal 2,4-DCP	g-C3N4: thermal heating CDs/g-C3N4: hydrothermal	120 min with natural sunlight	(Hak et al., 2020)

Type of photocatalyst	Degradation Efficiency	Synthesis method	Pollutant degradation time and light source	Refs
ZnO/CDs	ZnO/CDs three times higher than pure ZnO	Sonochemical	150 min with 6W of visible light γ =350 nm	(Maddu et al., 2021)
CdS/CQDs/BiOCl	99.5% removal of phenol	CQDs: hydrothermal CdS/CQDs/BiOCl: region-selective deposition	105 min, 500W xenon lamp with 400 nm cut-off the filter and 500W mercury lamp	(S. Sharma et al., 2019b)
Bi/BiOCl/TiO_2/CQDs	Bi/BiOCl/TiO_2/CQDs was 10.3 and 4.8 times more than BiOCl/TiO_2	CQDs: Solvothermal, Bi/BiOCl/TiO_2/CQDs: hydrothermal	100min γ = 240nm, 500 W xenon lamp	(Dager et al., 2019)
CDs/TiO_2	100 % removal of Methylene Blue	Sol-gel method	25 min with 300W halogen lamp	(Ding et al., 2016)
CDs/ZnO foam	MB>RhB>MO	Dispersion in CDs solution	250W Xe lamp with γ ≥ 400nm	(Chu et al., 2019)

2.5 Factors influencing photodegradation

This study investigated the factor influencing the photodegradation of tetracycline which consist of the dosage of photocatalyst, the concentration of tetracycline, and the source of light.

2.5.1 Effect of photocatalyst dosage

The degradation rate of tetracycline is influenced by the dosage of the photocatalyst. Table 2.5 show the photocatalyst dosage from previous studies. Several

research has shown that initially, increasing the catalyst dosage leads to a faster degradation rate (Cao et al., 2016; Ong et al., 2016; Yan et al., 2023). However, at higher dosages, the rate decreases due to light scattering and screening effects. In addition, the higher dosage of photocatalyst lead to a greater propensity for agglomeration, caused a reduction in the available surface area for light absorption and resulting in a decline in the photocatalytic degradation rate. Although adding more catalyst increases the number of active sites for the reaction, there's a point where the excessive particle concentration compromises light penetration. Active sites represent specific locations on the catalyst surface capable of forming strong chemical bonds with adsorbed atoms/molecules (Chen et al., 2022). In the photocatalytic degradation process, pollutants initially absorb onto the photocatalyst surface and subsequently undergo reaction with hydroxyl radicals, leading to their destruction. Consequently, an augmented amount of pollutant absorbed by the photocatalyst results in higher degradation efficiency. The delicate trade-off between these opposing phenomena gives rise to an optimum catalyst loading for the photocatalytic reaction. Beyond this optimal point, further increases in photocatalyst dosage yield nonuniform light intensity distribution, leading to a reduced reaction rate.

According to Azmi et al that synthesized the PbS-CdS onto clinoptilolite nanoparticles on tetracycline degradation by varying photocatalyst dosage from 0.25 to 2.5 gL^{-1} shows the result when increased dosage to 1.5 gL^{-1}, it led to a higher degradation of tetracycline which then remain constant. Notably,1.5 gL^{-1} was used as the optimal dosage of photocatalyst in their study. In other work, the degradation of tetracycline using FeO/clinoptilolite was investigated (Nezamzadeh-Ejhieh & Shirzadi, 2014). It observed that increasing the dosage of photocatalyst to 0.25 gL^{-1} initially enhanced higher performance of degradation but then decrease. This decrease was attributed to the increased turbidity of the suspension, light scattering, and agglomeration of solid particles that occur with higher catalyst concentrations. Finally, this study found that the best degradation rate was achieved with a catalyst dosage of 0.25 gL^{-1}(Azimi & Nezamzadeh-Ejhieh, 2015).

Pouretedal et al applied Zr and Sn-doped TiO_2 for the photodegradation of tetracycline under UV light (Pouretedal & Afshari, 2016). The initial step involved the adsorption of TC molecules onto the surface of the heterogeneous catalyst. It was observed that as the amount of dosage increased, accompanied by a decrease in particle size, result in higher degradation of TC. However, beyond a catalyst dosage of 0.8 gL^{-}

^{1}, a decline in degradation efficiency was noticed. This decline attributed to the aggregation of nanoparticles and the resulting turbidity of the aqueous samples, which restricted the penetration of photons (Nezamzadeh-Ejhieh & Salimi, 2010). In other work, photodegradation of tetracycline increased by varying dosage of photocatalyst 0.25 gL^{-1}until 1.0 gL^{-1}(Safari et al., 2015). The increase in TC degradation with the density of nano sized TiO_2 can be attributed to various factors, including an increased number of active sites, higher formation of hydroxyl radicals (OH•), and more effective interaction with TC molecules. However, at very high concentrations (1.0 gL^{-1}), the degradation rate constants exhibited a slight decline. This can be attributed to the reductive influence of light, which enhances the dispersion or sedimentation and agglomeration of TiO_2 particles under higher dosages (Lazar et al., 2012),(Nosrati et al., 2012). Additionally, the accumulation and precipitation of TiO_2 particles at higher catalyst dosage will reduce the available catalyst surface for photon absorption, lead to a decrease in the degradation rate.

In the case of In_2S_3 as a catalyst for TC degradation in a batch reactor, the concentration of In_2S_3 was found to have an impact on the degradation efficiency (Ai et al., 2015). The results indicated that increasing the concentration of In_2S_3 from 1.0 to 2.5 gL^{-1} resulted in improved TC degradation efficiency. However, interestingly, concentrations above 2.5 gL^{-1} did not further enhance the degradation efficiency, exhibiting a similar phenomenon observed at concentrations below 2.5 gL^{-1}. This behaviour can be attributed to the geometry and working conditions of the reactor, as well as the specific surface area exposed to In_2S_3. Beyond a certain concentration, higher amounts of In_2S_3 particles tend to aggregate, impeding the penetration of light into the reactor.

Wang et al. synthesized an Ag-Ag_3PO_4/active carbon composite photocatalyst and evaluated its photocatalytic performance for TC degradation (Saadati et al., 2016). The photodegradation rates of TC varied with the different loading levels of the composite photocatalyst. The results indicated that the photocatalytic activity of the composite photocatalyst depended on both the loaded Ag_3PO_4 dosage and the photo-induced time. However, the photocatalyst prepared with 10 wt% Ag_3PO_4 loading and a 20-minute photo-induced time exhibited the best photocatalytic performance. This optimal performance may be attributed to the appropriate dosage of metallic Ag and Ag_3PO_4, which provided an optimal match for photoelectron transfer and action under the specific preparation conditions.

Table 2.5
Effect Of Photocatalyst Dosage On The TC Degradation (Saadati et al., 2016).

Light source	Photocatalyst	Co range (gL^{-1})	Optimum Co (gL^{-1})	Refs
UV light	FeO/clinoptilolite	0.05, 0.1, 0.2, 0.25, 0.3	0.25	(Nezamzadeh-Ejhieh & Shirzadi, 2014)
UV light	TiO_2	0.25, 0.5, 1, 1.5, 2	1	(Safari et al., 2015)
Natural solar light	In_2S_3	2, 2.5, 3	2.5	(Ai et al., 2015)
UV light	Clinoptilolite/PbS-CdS	0.25, 0.75, 1.5, 2.5	1.5	(Azimi & Nezamzadeh-Ejhieh, 2015)
UV light	Zr and Sn-doped TiO2	0.1, 0.3, 0.5, 0.8, 1	0.8	(Pouretedal & Afshari, 2016)

2.5.2 Effect of tetracycline concentration

The successful application of the photocatalytic oxidation system in various environmental remediation processes necessitates a comprehensive investigation of the dependence of the photocatalytic degradation rate on the concentration of the substrate. Different initial contaminant concentrations have been found to influence the reaction rates significantly. This important relationship was studied in a series of experiments on the photocatalytic degradation of TC (target compound) under various initial concentrations, and the results are summarized in Table 2.6. In a specific study carried out by Liu et al., they synthesized a Cl–TiO_2 imprinted photocatalyst and employed it for the degradation of TC. The influence of TC concentration was examined within a range of 10–30 mgL^{-1}. Notably, the most effective degradation rate of 72.35% within 60 minutes was observed when the TC concentration was maintained at 15 mgL^{-1}. However, it was noted that at a concentration as low as 10 mgL^{-1}, the molecular imprinted photocatalyst failed to fully interact with the target molecule, leading to reduced selectivity and performance. Conversely, concentrations higher than 15 mgL^{-1}hindered the photocatalytic process, as the amount of molecular imprinted photocatalyst became insufficient for complete reaction, resulting in lower degradation rates. Furthermore, Wang et al, (Wang et al., 2011) conducted a study on the photocatalytic activity of C–N–S tridoped TiO_2 for TC degradation. The Langmuir-Hinshelwood (L-H) reaction rate constant was quantified at 0.197 $mgl.min^{-1}$. The L-H

kinetic model was used to describe the photocatalytic degradation process as shown in specific equation (2.2):

$$r = \frac{K_r KC}{1 + KC} \tag{2.6}$$

The equation presented the reaction rate (r) is determined by various factors, including the reaction rate constant (kr), the reactant adsorption constant (K), the fraction of the catalyst's surface covered by TC, and the concentration of TC (C) at any given time. A higher reaction rate constant (kr) corresponds to a faster degradation rate (r), highlighting its significant influence on the overall process. The researchers concluded that as the initial concentration of TC increased, the degradation efficiency decreased. This observation was consistent with the findings of another study by Ai et al.,(Ai et al., 2015). The reason behind this behaviour lies in the fact that at higher initial TC concentrations, more TC molecules are adsorbed on the surface of In_2S_3 (the photocatalyst used). However, the generation of hydroxyl radicals (•OH) and superoxide radicals ($\bullet O_2^-$) on the surface of In_2S_3 remains constant. Consequently, with an increasing number of TC molecules on the catalyst's surface, the relative proportion of •OH and $\bullet O_2-$ radicals available to attack the TC molecules is reduced, leading to a decrease in degradation efficiency.

Azimi et al.(Azimi & Nezamzadeh-Ejhieh, 2015) conducted a study on the photocatalytic degradation rate of a mixture of TC and cephalexin (CPX) and found that the degradation extents of both pollutants increased significantly when the solution was diluted from 50- to 100-fold. However, beyond that point, the degradation rates started to decrease. Nezamzadeh et al.(Nezamzadeh-Ejhieh & Shirzadi, 2014) investigated the photodegradation of TC in an aqueous solution using FeO-doped nanoclinoptilolite particles and discovered that the best degradation efficiency was achieved when the solution was 100 times diluted. In a separate study, Safari et al., (Safari et al., 2015) examined the effect of TC concentration using nano-sized titanium dioxide. Their results demonstrated that the removal efficiency of TC decreased with increasing initial TC concentration. Specifically, irradiation of TC solutions with initial concentrations of 27, 55, 74, and 103 mg/l for 90 minutes led to degradation percentages of 91.4%, 82.6%, 76.4%, and 69.3%, respectively, indicating a lower removal efficiency at higher TC concentrations. In order to quantitatively investigate the degradation rate of TC,

experimental data was fitted using pseudo-first-order kinetics. The fitting results revealed TC degradation rate constants (k) of 2.49×10^{-1}, 1.63×10^{-1}, 1.33×10^{-1}, and 1.1×10^{-1} min^{-1} at initial TC concentrations of 27, 55, 74, and 103 mgL^{-1}, respectively. Pouretedal et al. also observed similar trends in their study, where they synthesized TiO_2 nanoparticles doped with Zr and Sn as a ternary nanocomposite of $Ti_{1-(x+y)}Zr_xSn_yO_2$ and applied it for photocatalytic degradation of TC (Pouretedal & Afshari, 2016). The obtained data indicated the maximum degradation rate at 20 mgL^{-1} of TC. Confirming these findings, Huo et al.,2014 demonstrated that the degradation rate increased significantly with lower TC concentrations, suggesting that lower concentrations led to higher degradation rates (Huo et al., 2014). Moreover, the results indicated that at low concentrations, the degradation process was better fitted to the first kinetic equation, while at higher concentrations, the second kinetic equation provided a better fit for the degradation process. It is generally observed that the degradation rate of TC exhibits a positive correlation with its concentration up to a certain level, beyond which further increases in TC concentration led to a decrease in its degradation rate. The degradation rate is influenced by the likelihood of hydroxyl radical (•OH) formation on the catalyst surface and their subsequent reaction with TC molecules. In more diluted solutions, the immediate collision probability between hydroxyl radicals and TC molecules decreases significantly, resulting in lower degradation extents (Azimi & Nezamzadeh-Ejhieh, 2015; Pouretedal & Afshari, 2016). Conversely, at higher initial TC concentrations, the probability of reaction between TC molecules and oxidizing species increases, leading to an enhancement in the degradation rate. However, as TC concentration rises further, the degradation efficiency decreases. This can be attributed to the reduction in •OH radical generation on the catalyst's surface due to the coverage of active sites by TC ions at high concentrations. The increasing adsorption of drug molecules on the catalyst's surface inhibits their reaction with catalytic holes or •OH radicals, as fewer semiconductor molecules can be excited,(Liu et al., 2013; Shanthi et al., 2012). Moreover, the primary degradation occurs in the region near the irradiated side (referred to as the reaction zone), where the light intensity is significantly higher compared to other areas. Consequently, at higher TC concentrations, degradation diminishes at longer distances from the light source or reaction zone due to light penetration retardation. Thus, it can be concluded that with an increase in the initial concentration of TC, the demand for catalyst surface area also rises. This shift can be attributed to the

transition from a kinetic control regime at low concentrations to mass transfer limitations at higher concentrations.

During photocatalytic oxidation, the concentration of the organic substrate over time is dependent on the photonic efficiency. However, at elevated substrate concentrations, the photonic efficiency diminishes, and the catalyst surface becomes saturated, leading to catalyst deactivation,(Araña et al., 2004; Habibi et al., 2007). Additionally, higher substrate concentrations may generate intermediates that can adsorb on the catalyst's surface. The slow diffusion of these intermediates from the catalyst surface can deactivate active sites, resulting in a reduction of the degradation rate. Furthermore, at higher concentrations, an accumulation of intermediate products can make hydroxyl radicals the limiting reactant, causing a decrease in the degradation rate constants.

Table 2.6
Effect Of TC Concentration,(Saadati et al., 2016)

Light source	**Photocatalyst**	**Co (mgL^{-1})**	**Optimum Co**	**Refs**
UV light	FeO/clinoptilolite	50,100,200,300,400	100	(Nezamzadeh-Ejhieh & Shirzadi, 2014)
Visible light	Cl-TiO_2	10,15,20,25,30	15	(X. Liu et al., 2013)
Visible light	C-N-S tridoped TiO_2	5,15,30,50	5	(P. Wang et al., 2011)
UV light	TiO_2	25,55,74,13	25	(Safari et al., 2015)
Natural solar light	ln_2S_3	10,20,30,40,50	20	(Ai et al., 2015)
UV light	Clinoptilolite/PbS–CdS	50, 100, 200	100	(Azimi & Nezamzadeh-Ejhieh, 2015)
UV light	Zr- and Sn-doped TiO_2	10, 20, 30, 40, 50	20	(Pouretedal & Afshari, 2016)
Visible light	Fe3+@TiO_2/HNTs	10, 20, 30, 40, 50	10	(Huo et al., 2014)
UV light	Clinoptilolite/PbS–CdS	3, 5, 7, 10	3	(Azimi & Nezamzadeh-Ejhieh, 2015)

Light source	Photocatalyst	Co (mgL^{-1})	Optimum Co	Refs
UV light	Zr- and Sn-doped TiO_2	2–9	3	(Pouretedal & Afshari, 2016)
Visible light	Sr–Bi_2O_3	3, 5, 7, 9, 11	9	(Saadati et al., 2016)
UV light	TiO_2	3, 7, 9	9	(Saadati et al., 2016)
Simulated solar light	TiO_2	3–10	8.7	(Saadati et al., 2016)
Simulated solar light	ZnO	3–10	11	(Saadati et al., 2016)

2.5.3 Effect source of light

Sharma et al. investigated the photodegradation of tetracycline in simulated sunlight and UV light using TiO_2 as the photocatalyst (Sharma et al., 2022). The study found that the rate of photodegradation was faster in simulated sunlight than in UV light. This is because simulated sunlight contains a wider range of wavelengths, including UV light, which can better activate the photocatalyst. Wu et al, also investigated the photodegradation of tetracycline in simulated sunlight and UV light using TiO_2 as the photocatalyst (Wu et al., 2020). The study found that the rate of photodegradation was faster in simulated sunlight than in UV light, but the difference was not as pronounced as in the study by Kim et al. This is because the photocatalyst used in this study was more active in the UV range than the photocatalyst used in the study by Kim et al (Kim et al., 2018).

Saadati et al. investigated the photodegradation of tetracycline using visible light using Nb-doped ZnO as the photocatalyst (Saadati et al., 2016). The study found that the rate of photodegradation was slower than in UV light, but it was still significant. This is because the photocatalyst used in this study was able to absorb visible light and initiate the photodegradation process. Wu et al. investigated the photodegradation of tetracycline using UV light using CdS as the photocatalyst (Wu et al., 2020). The study found that the rate of photodegradation was comparable to that of TiO_2 in UV light. This is because CdS has a good overlap with the absorption spectrum of tetracycline and can be activated by UV light. Next, Saadati et al., investigated the photodegradation of tetracycline using UV light and visible light using SnO_2 as the photocatalyst (Saadati

et al., 2016). The study found that the rate of photodegradation was faster in UV light than in visible light, but it was still significant in visible light. This is because SnO_2 has a good overlap with the absorption spectrum of tetracycline and can be activated by both UV light and visible light. et al., investigated the photodegradation of tetracycline using visible light using g-C_3N_4 as the photocatalyst (Chen et al., 2022). The study found that the rate of photodegradation was comparable to that of TiO_2 in visible light. This is because g-C_3N_4 has a good overlap with the absorption spectrum of tetracycline and can be activated by visible light.

2.5.4 Effect of dissolved oxygen

The impact of dissolved oxygen on the removal efficiency of TC by nano sized TiO_2 (P25) was evaluated by purging nitrogen and air into the suspension (Nezamzadeh-Ejhieh & Salimi, 2010). The results demonstrated that the removal efficiency of TC increased as the concentration of dissolved oxygen rose. Several factors contributed to this phenomenon. Firstly, the recombination of photogenerated electron-hole pairs (e^-/h^+) was inhibited due to the trapping of conduction band electrons by dissolved oxygen molecules. This mechanism prevented the loss of photoinduced charge carriers, promoting more efficient photocatalysis. Additionally, higher concentrations of dissolved oxygen led to an increased generation rate of reactive oxygen species (ROS). These ROS, including hydroxyl radicals and singlet oxygen, played a crucial role in the degradation process, leading to enhanced removal efficiency of TC in the presence of dissolved oxygen (Pelaez et al., 2011).

2.5.5 Effect of additives and oxidants

The photocatalytic process for TC degradation involves various active species, including hole ($h^{+)}$, superoxide anion radical ($\bullet O_2^-$), and hydroxyl-free radical (•OH). Trapping experiments were conducted using different scavengers, such as three ethanolamine (TEOA) and ammonium oxalate (AO) for h^+ scavengers, ethanol and $AgNO_3$ for e^- scavengers, benzoquinone (BQ) for $\bullet O_2^-$ scavenger, and isopropyl alcohol (IPA), isopropanol (IP), and methanol (MO) for •OH scavengers. Hong et al.(Saadati et al., 2016) synthesized magnetically separable, visible-light-driven $Ni_{(1x)}$ Cu $_{(x)}$ Fe_2O_4 (Cu–Ni ferrite) photocatalysts and tested them for TC photodegradation (Tsay et al.,

2023). The addition of TEOA significantly decreased the TC degradation rate, indicating that the photo-generated holes were the major oxidative species responsible for TC degradation. When IP was added, the TC photodegradation was slightly inhibited, suggesting that although the photocatalysts could not directly generate •OH from surface hydroxyl groups or water, excited electrons can react with adsorbed molecular oxygen to produce $\bullet O_2^-$ and further combine with h^+ to generate •OH. The addition of $AgNO_3$ slightly reduced the TC degradation rate, further confirming the importance of photogenerated holes and •OH in TC degradation.

In another study, TC photocatalytic degradation using multiwall carbon nanotubes–Bi_2WO_6 microspheres was examined. $AgNO_3$ had no significant effect on TC degradation, while the presence of methanol depressed the degradation, with the inhibition increasing with methanol concentration (S. Liang et al., 2012). IPA showed similar results to methanol, suggesting that •OH might play a significant role in the photodegradation process (Li et al., 2015). Addition of AO led to a decrease in TC removal rate, indicating that the contribution of h^+ cannot be neglected, and both •OH and h^+ likely played pivotal roles in TC degradation. This conclusion was further supported by the results obtained with the addition of KI at different concentrations.

2.6 Kinetic studies of photocatalytic of tetracycline

Photocatalytic degradation (PCD) has emerged as a promising advanced oxidation process for eliminating persistent organic pollutants, including antibiotics, from aqueous systems. Understanding the kinetics of these reactions is essential for optimizing both photocatalyst design and process parameters. Since PCD primarily occurs at the interface between the photocatalyst surface and the pollutant in solution, the overall reaction rate is governed by a combination of adsorption behavior and surface reaction dynamics. Among the models commonly employed to describe such processes, the pseudo-order kinetic models and the Langmuir–Hinshelwood (L–H) model are most widely utilized in heterogeneous photocatalysis. Pseudo-order models offer a simplified representation of the reaction rate as a function of pollutant concentration, while the L–H model more comprehensively integrates adsorption equilibrium with surface reaction kinetics. This section critically examines the theoretical foundations, assumptions, and applicability of both models, with particular emphasis on their relevance to the degradation of tetracycline. By synthesizing findings

from prior studies, a robust framework is developed for interpreting experimental data and guiding the advancement of photocatalytic systems for wastewater treatment.

2.6.1 The Langmuir–Hinshelwood model

The Langmuir–Hinshelwood (L–H) mechanism is widely applied to model heterogeneous catalytic reactions, including photocatalytic degradation (PCD) of organic pollutants. It describes a multi-step process comprising: (i) adsorption of reactant molecules onto the catalyst surface, (ii) surface reaction between adsorbed species, (iii) formation of products, and (iv) desorption of the products from the surface. This mechanism is particularly relevant in heterogeneous systems, where both adsorption equilibrium and surface reaction kinetics govern the overall reaction rate (Ernawati et al., 2021; Syahin et al., 2019).

Numerous studies have validated the applicability of the L-H model in photocatalysis. For example, Irani et al. observed that the degradation of methylene blue using ZnO nanoparticles was best described by the L–H model, showing better correlation than first-order kinetics (Irani et al., 2017). Similarly, the photocatalytic degradation of 2-chlorophenol by TiO_2 exhibited excellent agreement with the L–H model, achieving a high correlation coefficient ($R^2 = 0.987$). Shaik Basha et al. evaluated the PCD of amoxicillin using activated carbon-supported TiO_2 nanocomposites, reporting that the L–H model yielded a more accurate fit than the pseudo-first-order model (Basha et al., 2011). Lin et al. also emphasized the relevance of the L–H model in describing the kinetics of acid orange 7 degradation using ordered mesoporous TiO_2 supported on carbon fiber substrate (Lin et al., 2015).

Despite its wide applicability, the L–H model has limitations in capturing the complete dynamics of photocatalytic systems, particularly those involving synergistic effects. Two critical considerations arise regarding its use in photocatalysis: (i) The L–H model is predicated on the Langmuir adsorption theory, which assumes dynamic equilibrium between adsorption and desorption processes. However, photocatalytic mechanisms often exceed this simplification. Specifically, when surface reactions occur at a significantly faster rate than adsorption–desorption, the equilibrium assumption underlying the model becomes invalid. (ii) The L–H model assumes a constant number of active sites on the catalyst surface. In reality, the number of photo-excited active sites is influenced by the intensity of incident radiation, which varies throughout the reaction

due to changes in pollutant concentration and solution absorbance. As the PCD process progresses, especially in systems involving coloured organic contaminants, the solution's optical properties evolve, subsequently altering light penetration and the effective number of excited sites.

Therefore, while the L–H model remains a valuable tool for interpreting photocatalytic reaction kinetics, its assumptions must be carefully evaluated within the context of dynamic and light-sensitive heterogeneous systems.

2.6.2 The pseudo-order kinetic model

To elucidate the kinetic mechanism governing the degradation of organic pollutants in aqueous media, the pseudo-order kinetic model is often employed to evaluate the photocatalytic degradation rate. In general, when only the variation of the pollutant concentration with respect to time is considered, the PCD rate can be expressed as:

$$\ln C_t = -kt + \ln C_o \tag{2.7}$$

$$\ln\left(\frac{C_o}{C_t}\right) = kt \tag{2.8}$$

where Co and Ct are the pollutant concentrations at time zero and time t, respectively, and k is the apparent rate constant. A linear plot of ln (Co/Ct) versus time confirms PFO behavior, typically observed at low initial concentrations and in systems with an excess of active sites.

In many photocatalytic studies, the pseudo-first order (PFO) model has provided excellent fits. For instance, Peters et al. achieved a high correlation coefficient (R^2 = 0.9923) for Rhodamine B degradation using TiO_2 immobilized on ceramic supports, while Liu et al. and Gharbani et al. reported similarly strong fits for ofloxacin and methylene blue degradation, respectively (De Mello Peters et al., 2018; Gharbani et al., 2022;Liu et al., 2018). The model has also been validated in tetracycline degradation, as seen in systems involving Cu_3P-loaded carbon nitride and photo-Fenton catalysts based on g-C_3N_4.

However, pseudo-second order (PSO) models have also proven effective in certain cases, particularly when chemisorption dominates. For example, Ernawati et al. demonstrated a strong PSO fit for methylene blue degradation using $CaTiO_3$ photocatalysts, where valence bonding and electron exchange mechanisms were dominant (Ernawati et al., 2021).

2.6.3 Linking L-H and Pseudo-Order Models

To bridge mechanistic interpretation with empirical data, the L–H rate expression can be linearized and expressed in a pseudo-first-order form under low pollutant concentrations. Furthermore, the initial degradation rate r_o can be described by the L-H rate expression (Dong et al., 2021):

$$r_o = -\frac{dC}{dt} = \frac{K_R K_{LH} C_O}{1 + K_{LH} C_o} = k_{app} C_o \tag{2.9}$$

Here, K_R represents the intrinsic reaction rate constant, K_{LH} is the Langmuir equilibrium constant associated with monolayer adsorption, and k_{app} is the apparent rate constant under specific experimental conditions. Linearization of this model is achieved by plotting $1/k_{app}$ against Co, yielding:

$$\frac{1}{k_{app}} = \frac{1}{K_R K_{LH}} + \frac{C_o}{K_R} \tag{2.10}$$

This relationship allows for the estimation of both K_{LH} and K_R, offering insight into whether the reaction is primarily surface-mediated or influenced by mass transport or bulk-phase interactions. The PFO model has been reported as a suitable fit for kinetic data in numerous photocatalytic studies. For instance, Peters et al., demonstrated the degradation of rhodamine B using TiO_2 immobilized on a ceramic matrix, achieving a high correlation coefficient (R^2 = 0.9923) (De Mello Peters et al., 2018). Similarly, Liu et al. reported that the PCD of ofloxacin using Mn-doped CuO photocatalysts conformed well to the PFO model (R^2 = 0.9813) (Liu et al., 2021). Gharbani et al. observed a similar trend for methylene blue degradation using CdSe nanoparticles (Gharbani et al., 2022).

Furthermore, Kumar et al. demonstrated the applicability of the PFO model in UV-assisted degradation of methylene blue under three different systems (UV/TiO_2, UV/H_2O_2, and UV/TiO_2/H_2O_2) (Kumar et al., 2022). In the case of tetracycline, the PFO model has been found compatible for describing degradation kinetics on Cu_3P nanoparticles supported on hollow tubular carbon nitride and for photo-Fenton reactions utilizing ultrathin porous g-C_3N_4. However, it is also susceptible to various operational parameters such as initial pollutant concentration, catalyst loading, particle size, and light intensity. For instance, Mahmoud et al. demonstrated that the presence of surface-deposited particles on SiO_2 nanoparticles influenced the degradation rate of methyl red, highlighting the importance of catalyst surface modifications (Mahmoud et al., 2020).

While fewer studies adopt the PSO model, it has shown suitability in certain systems. For example, Ernawati et al. reported strong agreement between experimental data and the PSO model for methylene blue degradation using $CaTiO_3$ photocatalysts (Ernawati et al., 2021). The applicability of the PSO model often implies chemisorption between adsorbent and adsorbate, characterized by valence interactions and electron exchange mechanisms. In conclusion, the Langmuir-Hinshelwood model serves as a robust and widely accepted framework for describing the kinetics of photocatalytic tetracycline degradation. Its ability to couple adsorption phenomena with surface reaction kinetics makes it especially suitable for modeling complex heterogeneous systems involving semiconductor photocatalysts. Nonetheless, deviations from this model may arise at high pollutant concentrations or in the presence of competitive adsorption, necessitating further investigation into multi-site and advanced kinetic models.

2.7 Mechanism of photocatalytic degradation

Photocatalytic degradation, also known as photodegradation, is a process that uses ultraviolet (UV), visible (Vis), or infrared (IR) light to convert an environmental pollutant into a harmless or less damaging product on a solid surface known as a photocatalyst. A typical semiconductor photocatalyst absorbs the radiation that drives an electron (e-) from its valence band (VB) to its conduction band (CB), leaving a hole (h+) in VB during a light-absorbing event as depicted in Figure 2.9. Based on the redox potential of the process and the electronic band structure of the photocatalyst, generated electrons and holes can drive a variety of redox reactions. The conversion of dissolved

oxygen and OH ions into their respective radicals is another example of a redox process. Transferring an electron (reduction) to molecular oxygen produces reactive superoxide anion (•O_2-), while transferring a hole (oxidation) to OH- produces reactive •OH radical. These reactive radical species can degrade organic contaminants by converting them to inert CO_2 and H_2O (S. Sharma et al., 2019). Thus, light acts as a reagent in the photodegradation process, converting an environmental contaminant into innocuous or benign chemicals. Rapid recombination of electron-hole pairs without producing reactive radical species inhibits photodegradation activity in numerous ways. Recombination can occur by the release of heat or radiation. The basic mechanism of photocatalyst activation can be shown as follows in (Mukherjee et al., 2021).In his study, ZnO will absorb the light of energy which greater than its band gap to produce photoexcited electron and holes in conduction and valence respectively .The photocatalytic degradation based on reactive oxygen species generation is depends on the ability of the photocatalyst to inhibit recombination of the excitons so they can transit alternately to produce reactive oxygen species. CDs will play at least two important roles. Firstly, it assists in absorbing visible light in addition to the long UV light for producing free excitons. Second, the CDs will act as excellent electrons and hole acceptors. The CDs that coupling with ZnO could trap the photoexcited electrons and holes. Due to this, the lifetime of the photoexcited electrons is enhanced which provided ample time to the electrons and holes to carry out specific photochemical reactions which leading to faster photocatalytic degradation of the pollutant molecule. For example, the separated electrons can easily reduce molecular O_2 adsorbed on the surface of the photocatalyst to generate superoxide radicals $(.O_2^-)$.Similarly, the hole accepting property of the CDs can lead the generation of hydroxyl radicals (. OH), (Mukherjee et al., 2021). This summary of photocatalytic process has been shown in Figure 2.10.

Photoexcitation:

$$\text{Photocatalyst} + hv \longrightarrow h_{VB}^{+} + e_{CB}^{-} \quad (2.11)$$

$$h_{VB}^{+} + e_{CB}^{-} \longrightarrow \text{energy (heat)} \quad (2.12)$$

Reductive reaction:

$$H_2O + h_{VB}^{+} \cdot \longrightarrow OH \text{ (hydroxyl radical)} + H^{+} \quad (2.13)$$

Oxidative reaction:

$$O_2 + e_{CB}^{-} \cdot \longrightarrow O_2^{-} \text{ (superoxide radical)} \quad (2.14)$$

Photodegradation:

$$\cdot OH + \text{pollutant} \longrightarrow H_2O + CO_2 \quad (2.15)$$

$$O_2^{-} + \text{pollutant} \longrightarrow H_2O + CO_2 \quad (2.16)$$

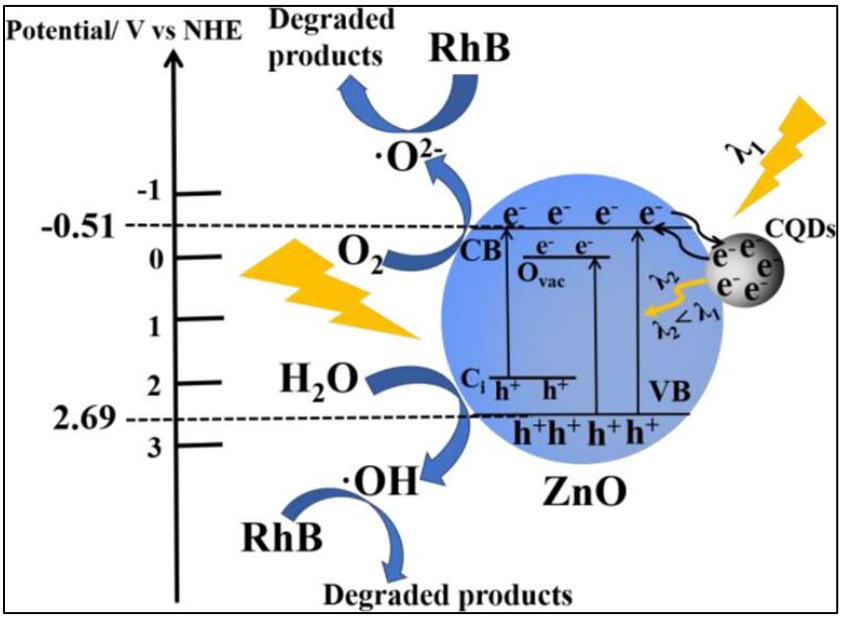

Figure 2.10 Ilustration Mechanism Of Photocatalyst ZnO/CDs (Ayu et al., 2023)

2.7.1 CDs in Enhancing Photodegradation of Antibiotic and Drugs

Antibiotics are widely used in many treatments especially in medical treatment due to their potential in eliminating bacteria. However, most antibiotics turn out in aqueducts and conventional wastewater treatment is unable to decompose them. This gives ample time for harmful bacteria to develop resistance to these antibiotics. As a result, these antibiotics no longer work when humans get infected with a disease. Therefore, a quick technique is needed before these antibiotics enter an aqueduct. Given the pervasiveness of sunshine, photodegradation provides a one-of-a-kind answer.

There is no record of the use of bare carbon dots for the photodegradation of antibiotics in the published literature. Carbon dots are a promising active light-harvesting material, however, there are only a few numbers of published accounts of its use in this capacity (Ye et al., 2022).For instance, under visible light irradiation, the photodegradation of malachite green dye and ampicillin antibiotic were evaluated using hybrids of trimetallic La/Cu/Zr C-dots synthesized by Sharma et al. To improve the composite's photocatalytic characteristics, researchers developed a hybrid production method using trimetallic nanoparticles that reduced the bandgap of bare C-dots from 2.55 to 1.56 eV, allowing them to better absorb visible light (Sharma et al., 2022). Following 4 hours of photodegradation, the La/Cu/Zr C-dots hybrid was able to remove 96% of the ampicillin antibiotic and 75% of the malachite green. However, before 4 hours of photodegradation, adsorption alone was able to remove 88% of ampicillin and 48% of dye, showing the significant significance of these materials in reducing the antibiotic/dye concentration in the wastewater (Sharma et al., 2022).

2.8 Rationale for Electrochemical Diagnostics in Wastewater Applications

The application of CQDs based photocatalysts in wastewater is hindered by the complexity of contaminant mixtures. Evaluating their charge transfer properties and catalytic activity requires robust diagnostic tools. Electrochemical techniques, such as cyclic voltammetry, impedance spectroscopy, and photocurrent measurements, provide direct insights into electron–hole dynamics, charge transfer resistance, and long-term stability (Rocco et al., 2023).

Electrochemical diagnostics are particularly valuable in distinguishing between photocatalyst deactivation caused by intrinsic material limitations versus those induced by environmental fouling in wastewater (Mintz et al., 2019; Sun et al., 2025). For example, electrochemical impedance spectroscopy (EIS) allows quantification of interfacial charge transfer resistance, which is directly correlated with catalytic efficiency under varied pH and pollutant concentrations (Rocco et al., 2023). Similarly, Mott–Schottky analysis provides information on flat-band potentials, which helps predict pollutant degradation pathways. Applying these techniques to CQDs modified photocatalysts not only accelerates the optimization of hybrid designs but also strengthens the mechanistic understanding of how pollutant classes (e.g.,

pharmaceuticals vs. dyes) influence catalytic pathways (Abd Rani et al., 2022). This diagnostic rationale is crucial for scaling laboratory results to field applications.

Wan et al., (2025) demonstrated that the ZnO/CQDs heterostructure significantly lowered charge-transfer resistance, as shown by EIS and produced a transient photocurrent three times greater than that of bare ZnO (Velumani et al., 2020). Such findings directly link CQDs to improved interfacial charge migration. However, application of these methods across the literature remains inconsistent. In some cases, potentials are reported without conversion to the reversible hydrogen electrode (RHE), making cross-study comparisons difficult. Mott–Schottky analyses are often performed at a single frequency, which may distort flat-band potential values due to surface state effects (Rocco et al., 2023). Similarly, EIS results are sometimes shown without quantitative equivalent-circuit fitting, and photocurrent densities are reported without normalization to electrode area or light intensity (Rocco et al., 2023). These methodological shortcomings undermine mechanistic interpretation and perpetuate speculative assignments. Although several reviews have summarized CQDs synthesis, optical properties, and photocatalytic applications including recent efforts on biomass-derived CQDs for sustainable synthesis none has systematically interrogated electrochemical diagnostics as mechanistic probes. This omission is critical because electrochemical analysis provide quantitative evidence that directly distinguishes type-II, Z-scheme, and S-scheme pathways (Xu et al., 2018; Zhao, Chen, et al., 2022). Without rigorous application of these methods, mechanism assignments often remain speculative, leading to misinterpretation of charge-transfer dynamics and limiting the rational design of advanced photocatalysts. By addressing this overlooked dimension, the present section moves beyond descriptive summaries and establishes electrochemical characterization as a central diagnostic framework, enabling more reliable mechanistic validation and guiding the development of next-generation CQDs-based photocatalysts for sustainable wastewater remediation.

The objectives of this section are fourfold: (i) to quantify the adoption of electrochemical methods in CQDs photocatalysis research, (ii) to synthesize correlations between electrochemical signatures and photocatalytic performance, (iii) to assess the robustness of type-I, type-II, Z-scheme, and S-scheme assignments, and (iv) to propose a diagnostic framework for reliable mechanistic validation. By bridging photocatalysis and electrochemistry, this review positions CQDs not only as performance enhancers but as mechanistic modulators, establishing best practices for

the rational design of next generation photocatalysts for sustainable wastewater remediation. By bridging photocatalysis and electrochemistry, this review uniquely reframes CQDs not as mere performance enhancers but as mechanistic modulators, establishing a diagnostic framework that enables reliable mechanism identification and accelerates the rational design of next generation photocatalysts for sustainable wastewater remediation.

2.8.1 Types of heterojunctions-based charge transfer mechanism

To prolong the lifetime of photoinduced excitons and suppress rapid electron–hole recombination, heterogeneous coupling strategies are commonly employed. These involve integrating two dissimilar semiconductors or combining a semiconductor with either a metal or a carbon-based material. Such hybridization results in the formation of a new electronic configuration, arising from the alignment and interaction of their respective energy bands. At the interface of the coupled materials, band bending typically occurs, giving rise to a built-in potential difference. This potential gradient facilitates the formation of an internal electric field across the space charge region, thereby promoting effective spatial separation of charge carriers. This interfacial phenomenon is known as a *heterojunction*.

In organic semiconductors, the inherently low dielectric constant limits efficient charge separation, often resulting in strongly bound excitons due to Coulombic attraction. To overcome this limitation, various types of heterojunction architectures have been developed to enhance exciton dissociation and charge transfer efficiency. Similarly, heterojunction engineering in inorganic semiconductor systems has also proven effective in improving not only charge separation but also light harvesting capabilities, thereby augmenting the overall photocatalytic performance (Balapure et al., 2024). Based on the CB and VB there are two major types of heterojunctions: type I (straddling gap) and type II (staggering) as shown on Figure 2.11.

2.8.2 Type I

In a type I heterojunction, a semiconductor with a narrower bandgap is coupled with another semiconductor possessing a wider bandgap, such that the conduction band and valence band edges of the narrower bandgap material lie within the bandgap of the

wider bandgap semiconductor. This arrangement results in a straddling band alignment. Upon photoexcitation with appropriate photon energy, charge carriers generated in the wider bandgap semiconductor transfer to the narrower bandgap component, leading to the accumulation of both electrons and holes within the latter. Consequently, charge separation efficiency in type I heterojunctions is generally considered to be limited, as spatial separation of electrons and holes is restricted due to their co-localization in the same component (Low et al., 2017; Ong et al., 2016).

However, the judicious selection of semiconductor materials can significantly enhance the performance of type I heterojunction systems beyond that of their individual constituents. For instance, Zhao et al. reported the fabrication of ZnS@$ZnIn_2S_4$ core–shell nanostructures exhibiting a type I heterojunction configuration. This system demonstrated improved photon absorption and efficient exciton separation, resulting in enhanced photocatalytic activity for CO_2 reduction (Y. Zhao, Chen, et al., 2022). Similarly, the CuO/$BaTiO_3$ heterojunction, characterized by a compatible type I p–n interface, exhibited superior photocatalytic degradation of methyl orange and enhanced CO_2 sensing performance (Joshi et al., 2018). The observed improvements were attributed to the effective built-in potential established at the nanoscale interface of the heterojunction.

2.8.3 Type II

The type II heterojunction is widely regarded as more effective than the type I counterpart due to its staggered band edge alignment, which facilitates directional flow of charge carriers in opposite directions. This spatial separation of electrons and holes significantly reduces their recombination rate, thereby enhancing charge separation efficiency (Low et al., 2017; Ong et al., 2016). Consequently, numerous studies have reported type II heterojunctions demonstrating superior photocatalytic performance compared to single-component systems.

For example, L.Zhang et al. synthesized a SnS_2/In_2S_3 type II heterojunction via a one-pot hydrothermal method. The staggered band alignment at the interface of SnS_2 and In_2S_3 enabled efficient separation of photogenerated excitons, resulting in photodegradation activities for Rhodamine B that were 99.2 and 15.3 times higher than those of the individual SnS_2 and In_2S_3 components, respectively (Zhang et al., 2022). Moreover, this heterojunction exhibited a remarkable enhancement in the degradation

of tetracycline, achieving activity improvements of 118.8 and 12.8 times relative to SnS_2 and In_2S_3 alone. Liu et al. synthesized a $BiVO_4/Bi_{25}VO_{40}$ composite via an alkali-mediated dissolution–recrystallization approach, which enabled the formation of an intimate type-II heterojunction with strong interfacial contact (Liu et al., 2022). This structural configuration promoted efficient charge transfer and spatial separation of photogenerated carriers, thereby enhancing the photocatalytic degradation efficiency toward tetracycline. Similarly, Huang et al., fabricated a type-II heterostructure by integrating a zirconium-based metal–organic framework (UiO-66-NH_2) with tungsten oxide (WO_3) on a carbon cloth substrate. The resulting UiO-66-NH_2@WO_3 composite achieved complete removal of tetracycline within 60 minutes under visible-light irradiation (Huang et al., 2022). More recently, Li et al., developed a ferroelectric $Ag_{10}Si_4O_{13}/TiO_2$ type-II heterojunction that demonstrated superior photocatalytic performance in methylene blue degradation under visible light (Li et al., 2022). Ong et al., further summarized numerous g-C_3N_4-based type-II heterojunctions coupled with various semiconductor systems, highlighting their broad adaptability in photocatalytic applications (Ong et al., 2016).

Despite these advances, type-II heterojunctions inherently suffer from a thermodynamic limitation. Although the spatial separation of electrons and holes is effectively achieved, it occurs at the expense of redox potential. Specifically, the migration of electrons from a higher conduction band to a lower one weakens their reduction capability, while the corresponding transfer of holes to a higher valence band diminishes their oxidation strength. This trade-off restricts the overall redox driving force, thereby limiting the photocatalytic efficiency of conventional type-II systems.

2.8.4 Z-scheme and S-scheme heterojunction

The concept of the Z-scheme photocatalytic system was initially introduced by Bard in 1979, inspired by the natural photosynthetic Z-scheme in green plants (Bard, 1979). In biological photosynthesis, photons at wavelengths of 700 nm and 680 nm are absorbed by photosystems I and II (type I and II), respectively, enabling the photolysis of water to molecular oxygen with a quantum yield approaching unity. Translating this principle to artificial systems, the Z-scheme photocatalytic system comprises two distinct semiconductors connected through a redox mediator or solid-state interface, designed to facilitate efficient charge separation and utilization. In such systems,

photogenerated electrons in the conduction band (CB) of one semiconductor recombine with holes in the valence band (VB) of the other at an energetically intermediate level. This configuration ensures that only the high-energy electrons in the CB of the reduction photocatalyst and the high-energy holes in the VB of the oxidation photocatalyst are retained, thereby preserving their strong reduction and oxidation capabilities, respectively. Compared to conventional type II heterojunctions which often compromise redox potential due to energy band alignment the Z-scheme mechanism is advantageous as it allows for enhanced redox reactions while effectively suppressing bulk recombination (Li et al., 2021). A notable demonstration of this concept is the Z-scheme system developed by Xing et al., which integrated vanadium-substituted phosphomolybdic acid clusters with g-C_3N_4 nanosheets for the upcycling of polyethylene an innovative approach addressing plastic waste remediation (Xing et al., 2022). This application exemplifies the versatility and real-world relevance of Z-scheme heterojunctions. Z-scheme systems are generally classified into two types:

- The indirect Z-scheme, where charge transfer is mediated by electron shuttle materials (e.g., I^-/IO_3^-, Fe^{3+}/Fe^{2+}, or noble metals).
- The direct Z-scheme, in which two semiconductors are coupled via strong interfacial coupling or solid-state interfaces without external mediators, allowing direct recombination at the interface (Li et al., 2021).

Significant progress has been reported in understanding and optimizing Z-scheme photocatalysts. For example:

- Low et al. proposed a developmental roadmap outlining the evolution of Z-scheme photocatalytic systems across three generations (Low et al., 2017).
- Li et al. elaborated on the underlying mechanisms of direct Z-scheme systems, including internal electric field-driven charge transfer, interfacial defect states, and facet-induced separation (Xu et al., 2018).

Despite these developments, a persistent issue in some Z-scheme systems is the unintended recombination of charge carriers at intermediate CB and VB levels, which diminishes overall quantum efficiency. To address this limitation, a refined model known as the S-scheme heterojunction has been proposed. This configuration couples an oxidation-type photocatalyst (characterized by a high VB potential) with a reduction-type photocatalyst (exhibiting a high CB potential), facilitating an interfacial band bending that promotes directional charge transfer and efficient charge separation. From a macroscopic perspective, the energy band configuration resembles a "step" structure,

while microscopically, the electron flow pathway traces a shape akin to the letter "N". For instance, Fu et al. reported the synthesis of an ultrathin 2D/2D WO_3/g-C_3N_4 S-scheme photocatalyst, with the charge transfer mechanism elucidated through ex situ and in situ irradiated X-ray photoelectron spectroscopy (XPS), electron paramagnetic resonance (EPR), and atomic force microscopy (AFM) in potential mode (Fu et al., 2019) Similarly, Xia et al. fabricated a CeO_2 quantum dot/polymeric carbon nitride (PCN) heterojunction, confirming the S-scheme charge migration using XPS, EPR, and DFT simulations. The improved interfacial charge transfer translated into superior antibacterial activity against *Staphylococcus aureus* under light irradiation (Xia et al., 2020). Recent studies have further validated the effectiveness of S-scheme systems. For instance:

- Li et al. synthesized a TaON/Bi_2MoO_6 core–shell heterojunction, demonstrating enhanced removal of levofloxacin and Cr(VI) due to efficient S-scheme charge separation (Goodarzi et al., 2023).
- Xu et al. developed a TiO_2/$CsPbBr_3$ hybrid for CO_2 photoreduction, where DFT calculations and in situ XPS revealed the presence of an internal electric field (IEF) from $CsPbBr_3$ to TiO_2. Upon irradiation, electron flow reversed from TiO_2 back to $CsPbBr_3$, confirming S-scheme operation (Balapure et al., 2024).

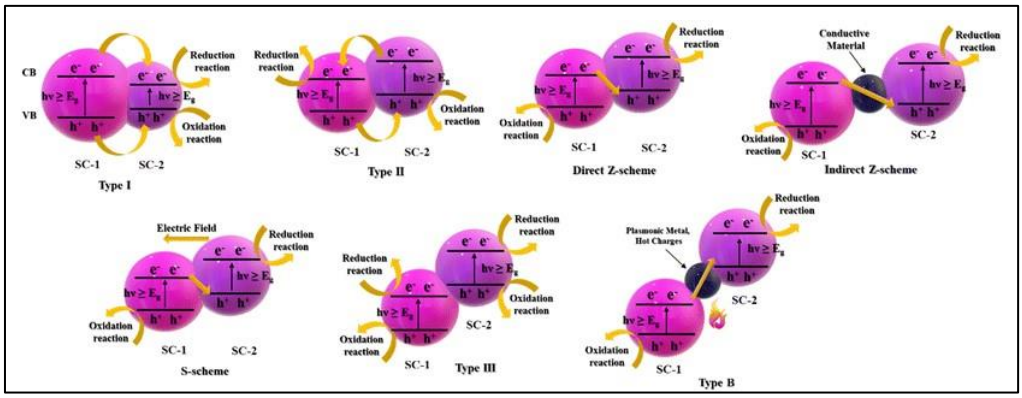

Figure 2.11 A Composite Schematic Diagram Depicting Different Types Of Heterojunctions Classified Based On The Charge Transfer Mechanism (Balapure et al., 2024)

A direct comparison of band alignment mechanisms reveals that each heterojunction configuration presents distinct advantages and limitations in photocatalytic applications. Type I heterojunctions generally suffer from poor charge separation due to the accumulation of electrons and holes in the same semiconductor,

leading to rapid recombination. Type II systems improve charge separation by spatially separating charge carriers; however, this occurs at the expense of redox potential, as electrons and holes migrate to lower energy band positions. In contrast, Z-scheme and S-scheme heterojunctions overcome this limitation by preserving high-energy electrons and holes, thereby maintaining strong reduction and oxidation capabilities. The Z-scheme achieves this through interfacial recombination of low-energy carriers, while the S-scheme further enhances this process via internal electric field-driven band bending and selective charge recombination. Consequently, Z-scheme and S-scheme configurations are more suitable for photocatalytic degradation of persistent pollutants such as tetracycline, where both efficient charge separation and strong redox potential are required.

2.8.5 Electronic Conditions Governing Different Heterojunction Schemes

The formation of a specific heterojunction scheme Type I, Type II, direct Z-scheme, or S-scheme is governed by the electronic conditions at the interface between two semiconductors asa summarized in Table 2.7. These conditions are dictated by the relative positions of the conduction band (CB), valence band (VB), and Fermi levels (E_xf) after contact (Balapure et al., 2024). When two semiconductors are coupled, electrons flow from the material with the higher Fermi level to that with the lower one until equilibrium is established, producing band bending and an internal electric field at the interface. The resulting potential gradient determines the direction of electron and hole migration and defines the photocatalytic mechanism of the heterojunction (Wan Ishak, Tan, Abu Bakar, Radacsi, et al., 2025).

2.8.5.1 Type I (Straddling-gap) Heterojunction

In a Type I configuration, both the CB and VB of one semiconductor lie within the band gap of the other (Balapure et al., 2024). Consequently, the photogenerated electrons and holes from the wider-band-gap semiconductor migrate into the narrower-band-gap semiconductor. This leads to the accumulation of both charge carriers in the same region, which favors radiative recombination and is useful for applications such as light emission but generally unfavorable for photocatalytic reactions where charge separation is essential (Nguyen et al., 2023). Type I systems are usually formed when

the band edges of the narrow-gap material are fully enclosed by those of the wide-gap material for example, CdSe/ZnS and CdS/TiO_2 core–shell structures.

2.8.5.2 Type II (Staggered gap) Heterojunction

In Type II systems, the CB and VB edges of one semiconductor are both higher in energy than those of the other. Electrons transfer from the higher CB to the lower CB, while holes migrate in the opposite direction ($VB_2 \rightarrow VB_1$) (Balapure et al., 2024). This configuration promotes spatial charge separation and prolongs carrier lifetime; however, it reduces redox potential since the transferred carriers occupy less energetic bands. Typical examples include TiO_2/CdS and g-C_3N_4/$BiVO_4$ composites(C. Zhao et al., 2023).

2.8.5.3 Direct Z-Scheme Heterojunction

The direct Z-scheme maintains band alignment similar to Type II but exhibits opposite charge migration behavior. Electrons in the CB of the less-reductive semiconductor recombine directly with holes in the VB of the less-oxidative semiconductor at the interface (Balapure et al., 2024). The remaining high-energy electrons and holes retain strong redox potentials comparable to the pristine semiconductors. Such systems require strong interfacial coupling and an internal electric field oriented to facilitate this direct recombination.

2.8.5.4 S-Scheme Heterojunction

The S-scheme represents a more recent model describing systems composed mainly of two n-type semiconductors with staggered band structures and different Fermi levels (Balapure et al., 2024). Upon contact, electrons migrate from the semiconductor with the higher Fermi level to that with the lower one, producing band bending and a strong built-in field. The internal field selectively recombines low-energy carriers while preserving high-energy electrons and holes on opposite sides, thus maintaining superior redox capability and enhanced photocatalytic efficiency.

Table 2.7
Comparison Of Type I, Type II, Z-Scheme, And S-Scheme Heterojunctions In Terms Of Band Alignment, Charge Transfer Mechanism, Charge Separation Efficiency, And Redox Capability For Photocatalytic Applications

Heterojunction type	**Band alignment**	**Charge transfer behaviour**	**Charge separation**	**Redox ability**	**Main limitation**	**Typical application**
Type I (straddling gap)	CB and VB of one semiconductor lie within the band gap of the other	Electrons and holes migrate to the same semiconductor	Poor	Weak	High recombination rate	LEDs, quantum wells, light emission
Type II (staggered gap)	CB of one semiconductor is lower and VB of the other is higher	Electrons and holes separate into different semiconductors	Moderate to good	Weakened	Loss of oxidation and reduction power	Photocatalysis with emphasis on separation
Z scheme	Two semiconductors with staggered bands linked by recombination pathway	Low energy electrons recombine with low energy holes	Good	Strong	Requires controlled interfacial recombination	Overall water splitting, redox reactions
S scheme (step scheme)	Band bending induced by Fermi level alignment at interface	Low energy carriers recombine, high energy carriers preserved	Excellent	Strong	Requires proper Fermi level mismatch and interface contact	Advanced photocatalysis, heterojunction catalysts

2.8.6 Photoelectrochemical Characterization of Photocatalysts

Electrochemical diagnostics provide a mechanistic foundation for evaluating the photoactivity of semiconductor catalysts used in wastewater remediation. Photocatalytic degradation of organic contaminants in wastewater such as antibiotics, dyes, and pharmaceuticals depends critically on the generation and transport of photogenerated charge carriers capable of initiating oxidative and reductive reactions at the catalyst surface. However, in complex aqueous environments containing multiple ions, dissolved oxygen, and organic matter, these charge carriers are prone to rapid recombination, surface trapping, and competitive side reactions. Electrochemical

techniques thus serve as quantitative diagnostic tools to assess how effectively a photocatalyst can maintain charge separation and sustain redox activity under simulated wastewater conditions.

Cyclic voltammetry (CV) provides insight into the redox potentials of the photocatalyst relative to pollutant degradation reactions such as $O_2/\bullet O_2^-$ or $H_2O/\bullet OH$ formation (Rocco et al., 2023). These redox potentials confirm whether the band positions are thermodynamically adequate to generate reactive oxygen species (ROS) required for contaminant mineralization (Prieto et al., 2024). Electrochemical impedance spectroscopy (EIS) quantifies interfacial charge transfer resistance (Rct) between the photocatalyst and the electrolyte, reflecting the ease with which electrons migrate through the solid–liquid interface a critical factor governing pollutant degradation kinetics (Wan Ishak, et al., 2025). A smaller semicircular arc in the Nyquist plot signifies lower resistance and more efficient electron transfer pathways, which correlate strongly with faster pollutant removal rates (Wan Ishak, Tan, Abu Bakar, Radacsi, et al., 2025).

Mott–Schottky (M–S) analysis determines the flat-band potential and semiconductor type, providing essential parameters for constructing energy band diagrams that predict the feasibility of electron–hole participation in redox reactions within aqueous systems (Wang et al., 2023). This information allows the evaluation of whether photogenerated electrons possess sufficient reducing power to activate dissolved oxygen and whether holes can oxidize organic pollutants effectively (Y. Wang et al., 2023). Transient photocurrent response measurements, meanwhile, assess the stability and intensity of photogenerated carrier flow under periodic illumination, serving as a proxy for catalyst durability and charge utilization efficiency during continuous wastewater treatment (Zhang et al., 2024).

Collectively, these electrochemical diagnostics bridge the gap between material properties and real-world photocatalytic performance, enabling rational interpretation of pollutant degradation data. By correlating electrochemical parameters such as Rct, photocurrent density, and flat-band potential with degradation efficiency, it becomes possible to identify the dominant charge-transfer processes and optimize the design of ZnO/CDs and other heterojunction photocatalysts for sustainable wastewater purification.

2.8.6.1 Cyclic Voltammetry

Cyclic voltammetry (CV) is widely employed to investigate the redox behavior and electrochemical activity of photocatalysts. This technique enables the determination of oxidation and reduction potentials, which are closely associated with the positions of the conduction band and valence band. These parameters are fundamental for predicting the thermodynamic feasibility of redox reactions during photocatalysis, such as the formation of reactive oxygen species (ROS) or the degradation of organic pollutants. Additionally, the shape, intensity, and symmetry of the redox peaks, as well as peak-to-peak separation and onset potentials, provide valuable information about the reversibility of redox processes, interfacial charge transfer kinetics, and the overall electron mobility of the material (X. Wang et al., 2023) . In semiconductor systems modified with conductive carbonaceous materials such as carbon dots, the CV profiles often display more defined redox peaks and increased current densities (Patil et al., 2025). These features are typically indicative of enhanced electrical conductivity, improved charge separation efficiency, and stronger interfacial synergy between the CDs and the base semiconductor (Tang et al., 2020). Such modifications are known to facilitate faster electron transport and reduce recombination losses, which are critical for improving photocatalytic performance.

For instance, Wang et al. (2023) reported that a 2.5 wt% ZnO/g-C_3N_4 heterojunction exhibited the highest oxygen reduction reaction (ORR) peak among the tested samples when evaluated in a 0.1 M Na_2SO_4 electrolyte at a scan rate of 50 mV/s (M. Wang & Liu, 2023). The pronounced cathodic peak, coupled with a 2.3-fold increase in peak current density and a 120 mV cathodic shift in ORR onset potential, signified enhanced electron transfer kinetics and superior interfacial contact, as shown in Figure 2.12 (a) and (b). Similarly, Xu et al. (2022) demonstrated that a 1.5 wt% Ag_2ZrO_3/TiO_2 composite exhibited favorable electron mobility, evidenced by intensified redox currents in the CV profile, which facilitated more efficient electron injection during Rhodamine B (RhB) photodegradation (H. Xu et al., 2020). These results underscore the utility of CV as a diagnostic tool for evaluating redox activity and confirming the enhanced charge carrier dynamics induced by compositional or interfacial engineering.

Moreover, the position and intensity of the redox peaks derived from CV analysis not only reflect the material's intrinsic conductivity and band edge positions

but also help validate whether the photogenerated electrons possess sufficient potential to initiate key reduction reactions, such as O_2 to $\bullet O_2^-$, which is crucial in the degradation of antibiotics and other persistent pollutants.

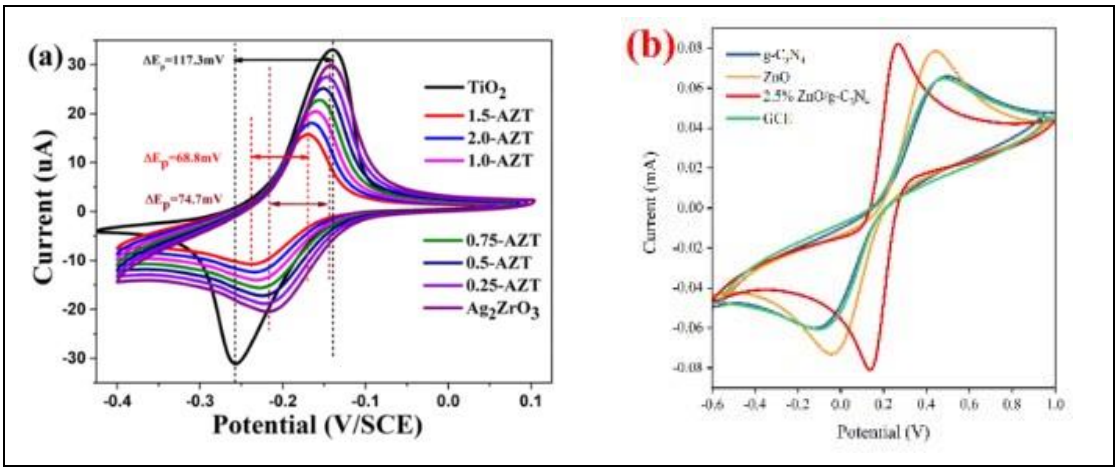

Figure 2.12 Cyclic Voltammogram Of Photocatalytic (Wang et al., 2023; Xu et al., 2020).

2.8.6.2 Electrochemical Impedance Spectroscopy

Electrochemical impedance spectroscopy (EIS) is a widely employed diagnostic technique for evaluating the interfacial charge transfer resistance (Rct) and electron transport characteristics of photocatalysts. In a typical Nyquist plot, the high-frequency semicircular arc represents Rct, where a smaller arc radius indicates lower resistance and more efficient charge transfer across the electrode–electrolyte interface (Wang et al., 2023). A reduced Rct value is generally associated with improved electrical conductivity, accelerated interfacial electron movement, and decreased recombination losses all of which are essential for enhancing photocatalytic activity (Patil et al., 2025).

The decrease in arc radius typically stems from factors such as better interfacial contact, improved crystallinity, and the formation of heterojunctions or conductive pathways that promote charge separation and migration (Zandipak et al., 2024). These structural and electronic modifications enable more rapid extraction of photogenerated electrons from the photocatalyst surface to the electrolyte, thereby sustaining redox reactions involved in pollutant degradation.

For instance, Wang et al. (2023) demonstrated that a 2.5 wt% ZnO/g-C_3N_4 nanocomposite exhibited the smallest semicircular arc among the tested samples,

indicating a markedly reduced charge transfer resistance and enhanced interfacial conductivity, as shown in Figure 2.13 (a) and (b). This improvement was attributed to the synergistic effect of the heterojunction structure, which promoted effective charge separation and electron mobility.

Compared to techniques such as cyclic voltammetry (CV), which reveals redox activity and potential window behavior, EIS offers frequency-dependent insights into interfacial kinetics, capacitive behavior, and the efficiency of electron migration. When interpreted alongside other techniques such as transient photocurrent or Mott-Schottky analysis, EIS provides a more comprehensive understanding of charge dynamics within photocatalytic systems.

Inspired by these findings, the present study utilizes EIS to investigate the ZnO/CDs heterojunction system, focusing on the Nyquist semicircular arc diameter as a key indicator of interfacial charge transfer efficiency. The incorporation of carbon dots is hypothesized to introduce additional conductive pathways and interfacial sites, thereby lowering Rct and enhancing the overall electron transport capability of the nanocomposite. This diagnostic approach enables a deeper understanding of the role of CDs in modulating the interfacial properties and improving the photocatalytic performance of ZnO-based materials.

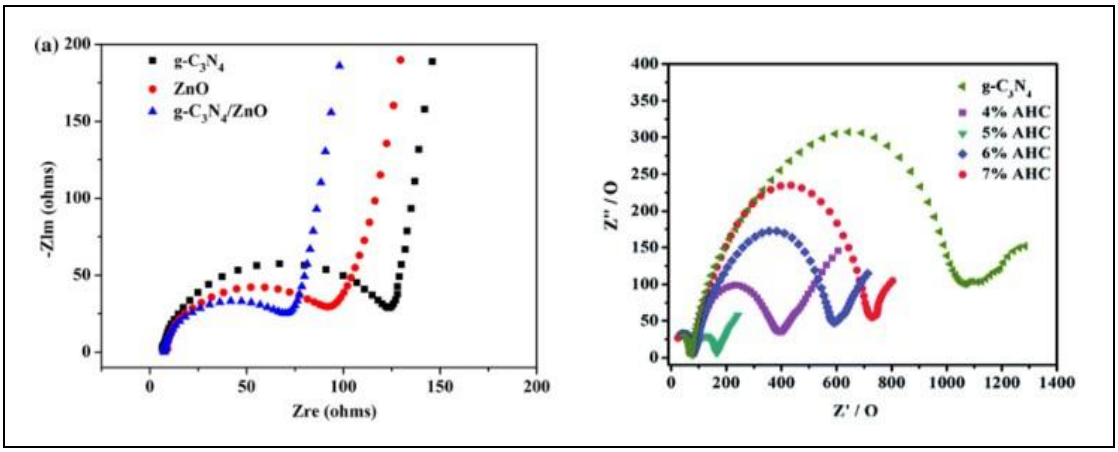

Figure 2.13 EIS Analysis (M. Li et al., 2022; Parida et al., 2023)

2.8.6.3 Transient photocurrent

Transient photocurrent response measurements are widely used to evaluate the efficiency of charge carrier separation and transport in semiconductor photocatalysts

under periodic light irradiation. The technique involves illuminating a photoelectrode with chopped light and recording the resulting current, where higher and more stable photocurrent intensities are indicative of improved photogenerated electron–hole separation, faster charge transfer kinetics, and suppressed recombination as shown in Figure 2.14 (Li et al., 2022; Parida et al., 2023). These improvements are directly correlated with enhanced photocatalytic performance, particularly in systems engineered to facilitate directional charge migration through heterojunction or surface modification strategies.

Recent studies have shown that the incorporation of carbon-based nanostructures, such as carbon dots, into wide-bandgap semiconductors like ZnO markedly enhances transient photocurrent responses. This enhancement is primarily attributed to the excellent electron-accepting and -shuttling properties of CDs, which function as electron reservoirs and interfacial mediators, thereby facilitating more efficient charge extraction and migration across the ZnO/CDs heterojunction (Fiszka Borzyszkowska et al., 2023; Li et al., 2013). Moreover, the abundance of oxygen- and nitrogen-containing surface functional groups on CDs enables strong chemical interactions with the semiconductor matrix, forming intimate contact that prolongs charge carrier lifetimes and minimizes recombination losses (Liu et al., 2020).

Notably, the increased photocurrent observed in such hybrid systems is also reflective of improved interfacial band alignment and enhanced electrical conductivity, which contribute to rapid and sustained electron flow during illumination cycles (Yan et al., 2023). These observations reinforce the potential of ZnO/CDs nanocomposites for high-performance photocatalysis and photoelectrochemical applications, especially in visible-light-driven pollutant degradation. In this context, transient photocurrent analysis serves as a critical tool for correlating structural modifications with functional performance in advanced photocatalytic systems.

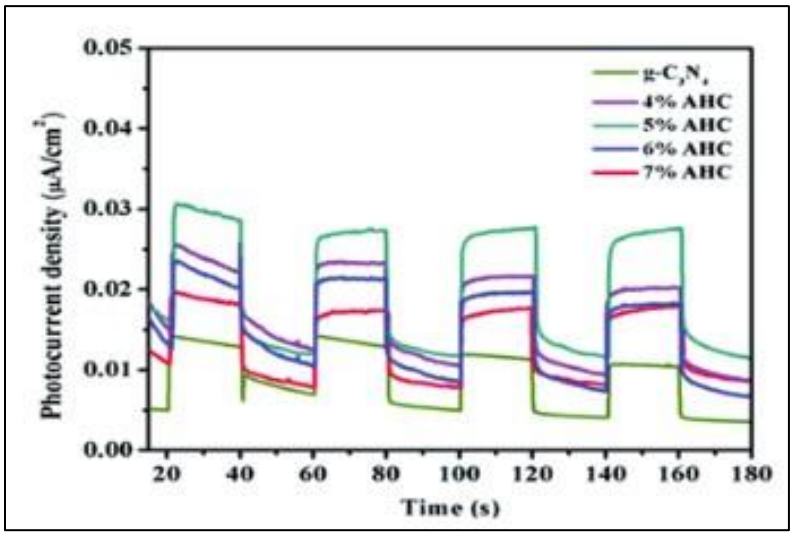

Figure 2.14 Transient Photocurrent Of Photocatalyst (Li et al., 2022).

2.8.6.4 Mott Schottky

Mott–Schottky (MS) analysis is a widely employed electrochemical technique for evaluating the flat band potential and charge carrier density of semiconductor materials. It involves measuring the capacitance of the semiconductor–electrolyte interface as a function of applied potential, typically in the dark (Wang et al., 2023). By plotting the reciprocal square of the capacitance ($1/C^2$) versus the applied potential, a linear relationship is obtained in the depletion region. The slope of this linear segment reveals the type of semiconductor: a positive slope indicates an n-type semiconductor (electron-majority carriers), whereas a negative slope corresponds to a p-type material (hole-majority carriers). The x-intercept of the extrapolated linear region corresponds to the flat band potential, which provides insight into the energy band alignment relative to standard references such as the normal hydrogen electrode (NHE) (Tang et al., 2020). For example, Tang et al. (2020) reported that graphitic carbon nitride (g-C_3N_4) exhibited a positive MS slope (Figure 2.15), confirming its n-type nature dominated by electron conduction. When such a semiconductor is coupled with carbon dots (CDs), a shift in the flat band potential is frequently observed, typically toward more negative values. This shift suggests the formation of a favorable heterojunction interface and efficient band alignment, which facilitate directional charge transfer. Such band bending and interfacial interactions are critical for constructing Z-scheme or S-scheme heterojunctions, wherein electrons and holes are spatially separated across the junction, resulting in stronger redox potentials and enhanced photocatalytic activity.

In the context of the ZnO/CDs system, MS analysis serves as a vital tool to confirm the n-type behavior of ZnO and to monitor any flat band potential shifts induced by CD incorporation. These shifts provide direct evidence of electronic interaction at the interface and help elucidate the band structure evolution responsible for improved charge separation and pollutant degradation efficiency.

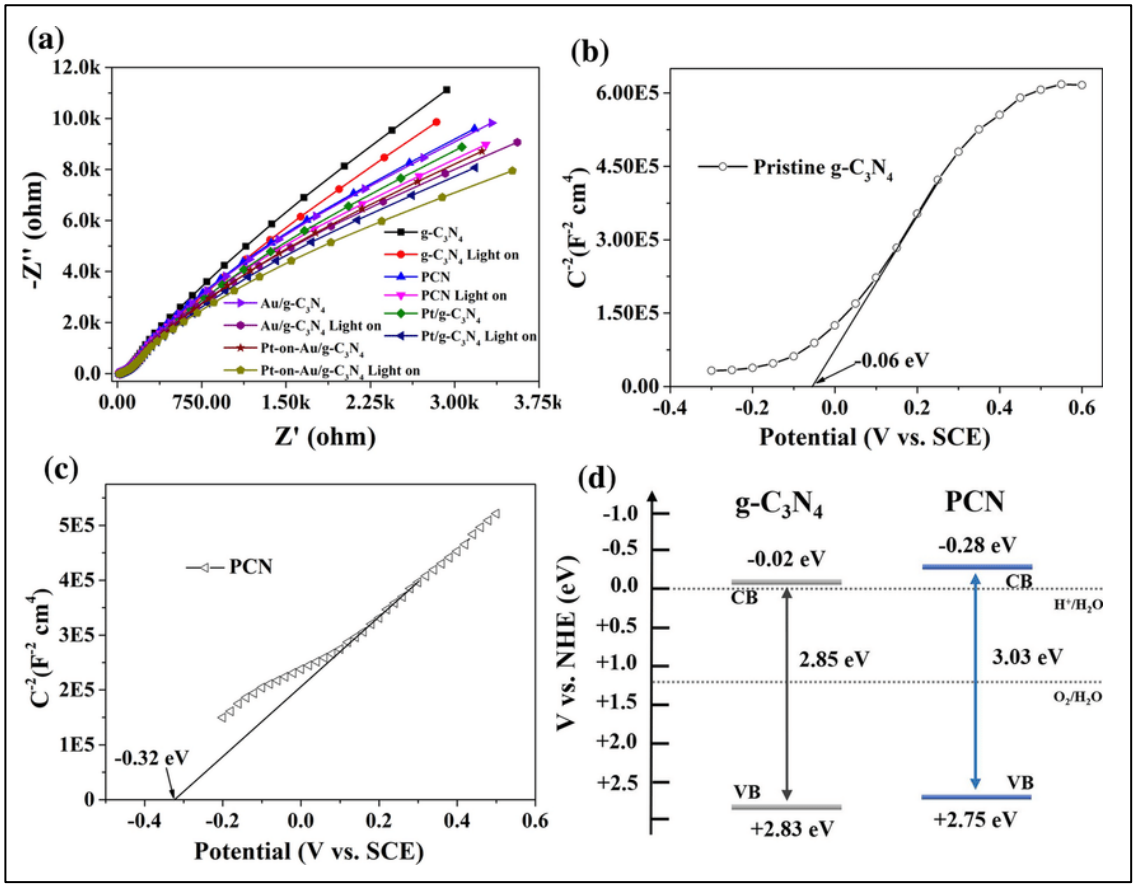

Figure 2.15 Mott-Schottky (Tang et al., 2020)

2.9 Closing remarks

In summary, this chapter has provided a comprehensive overview of the fundamental principles and recent advancements relevant to the development of carbon dot-based photocatalysts. Key emphasis was placed on the synthesis strategies of carbon dots from sustainable biomass precursors, particularly via hydrothermal methods, due to their simplicity, scalability, and environmental compatibility. The integration of carbon dots with semiconductor oxides such as ZnO has been widely explored to enhance photocatalytic activity through improved light absorption, charge separation,

and surface reactivity. Additionally, the evolution of heterojunction architectures ranging from conventional type II to advanced Z-scheme and S-scheme systems was critically reviewed to highlight their role in enhancing photocatalytic efficiency. These emerging heterojunction systems offer a promising pathway for overcoming the limitations of traditional photocatalysts by retaining high redox potentials and minimizing electron–hole recombination. The insights presented in this chapter lay the theoretical foundation for the experimental work that follows. They support the rationale for developing a novel ZnO/carbon dots nanocomposite synthesized via hydrothermal methods and evaluated for its photocatalytic performance in tetracycline degradation. The next chapter will describe the materials, synthesis procedures, and characterization techniques employed in this study.

CHAPTER 3
RESEARCH METHODOLOGY

3.1 Introduction

This chapter outlines the experimental methodologies employed for the synthesis, characterization, and evaluation of ZnO nanoparticles and biomass-derived carbon dots for the photocatalytic degradation of tetracycline, as illustrated in Figure 3.1. The study involves the hydrothermal synthesis of carbon dots from oil palm empty fruit bunches, preparation of ZnO nanoparticles, and fabrication of ZnO/CDs nanocomposites. The experimental design was structured to ensure reproducibility and systematic evaluation of material performance.

The synthesized materials were characterized using a range of techniques to investigate their structural, morphological, optical, surface, and electrochemical properties. Photocatalytic performance was evaluated through tetracycline degradation under controlled conditions, with key parameters such as catalyst dosage, pollutant concentration, and light irradiation systematically examined. The methodologies presented in this chapter establish the framework for correlating material properties with photocatalytic performance. The methodologies presented in this chapter establish the framework for correlating material properties with photocatalytic performance. A clear overview of the experimental facilities used throughout the study is provided in Table 3.1, which summarizes the major instruments and equipment involved in synthesis, characterization, photoelectrochemical analysis, photocatalytic degradation, and degradation pathway identification.

Table 3.1
Summary Of Equipment And Instruments Used In This Study

Category	**Equipment / Item**	**Model / Specification**	**Purpose**
Major equipment and analytical instruments	Hydrothermal autoclave reactor	Teflon lined autoclave	Synthesis of carbon dots, zinc oxide nanoparticles, and ZnO/CDs nanocomposites
	Grinder and sieve	0.25 mm sieve	Preparation and size reduction of empty fruit bunch powder

Category	Equipment / Item	Model / Specification	Purpose
	Centrifuge	5000 rpm and 10,000 rpm	Separation, washing, purification, photocatalyst recovery, and LC MS sample preparation
	Freeze dryer	Not specified	Drying of purified carbon dots solution
	Drying oven	60 to 70 °C	Drying of zinc oxide, ZnO/CDs nanocomposites, and recovered photocatalyst
	UV lamp	Kintons KT6 UVC, 2 × 15 W	UV irradiation for photocatalytic tetracycline degradation
	FTIR spectrometer	Perkin Elmer Spectrum 400	Identification of surface functional groups and interaction between CDs and ZnO
	X ray diffractometer	Rigaku Ultima IV XRD	Determination of crystalline phase, crystallinity, and crystallite size
	FESEM EDX	JSM 7600F, JEOL	Surface morphology, elemental composition, and elemental mapping
	HRTEM	JEOL JEM 2100F	Nanostructure, particle size, lattice fringes, d spacing, and CDs anchoring on ZnO
	XPS	Axis Ultra DLD, Kratos, UK	Surface elemental composition, chemical states, and interfacial interaction
	BET surface area analyzer	Micromeritics ASAP 2020	Specific surface area, pore volume, and pore size distribution
	UV Vis spectrophotometer	Agilent Cary 60	Tetracycline absorbance measurement, concentration monitoring, and degradation efficiency

Category	Equipment / Item	Model / Specification	Purpose
	UV Vis DRS system	Agilent Cary 60 with $BaSO_4$ reference	Optical absorption and band gap estimation using Tauc plot
	PL / TRPL spectrometer	Edinburgh Instruments FLS920	Photoluminescence behaviour, charge recombination, and carrier lifetime
	Potentiostat	Autolab PGSTAT302N	CV, EIS, Mott Schottky, and transient photocurrent analysis
	LC MS system	Agilent G2449A Q TOF MS	Identification of tetracycline degradation intermediates
Consumables and supporting items	Nylon syringe filter	0.22 µm	Filtration of carbon dots solution
	PTFE syringe filter	0.22 µm	Filtration of photocatalytic samples before LC MS analysis
	Screen printed electrodes	Metrohm DropSens DRP 110 and DRP 220AT	Working electrode platform for photoelectrochemical measurements
	Magnetic stirrer	Not specified	Continuous mixing during synthesis and photocatalytic degradation

3.2 Methodology Flowchart

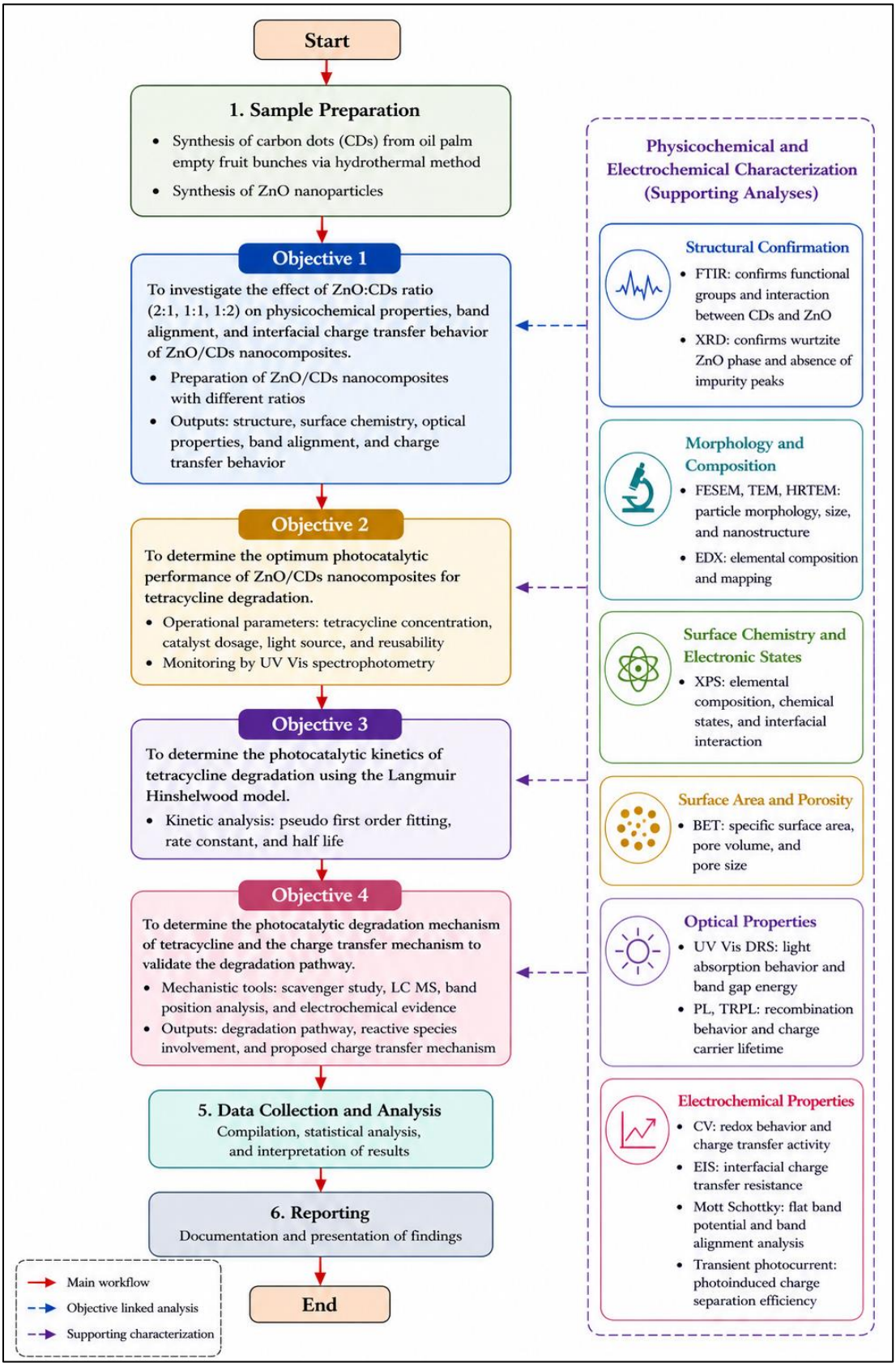

Figure 3.1 Methodology Flowchart

3.3 Materials and chemicals

Carbon dots (CDs) were synthesized from Empty Fruit Bunches (EFB), a lignocellulosic biomass sourced from a Malaysian oil palm plantation in Kedah. All chemicals and reagents were used without further purification. Zinc (II) acetate dihydrate Zn $(CH_3COO)_2.2H_2O$, > 98%, ethanol (CH_3CH_2OH, > 99.8%), and sodium hydroxide (NaOH, > 98%) were supplied by Sigma-Aldrich. Tetracycline (TC > 98%) antibiotics were supplied by Merck Millipore. All chemicals were in analytic purity, and all solutions were prepared in deionized (DI) water. UV lamps, Kintons KT6-UVC, (2 units x 15 W) were supplied from a local supplier in Malaysia. All reagents were of analytical grade and used without further purification to minimize impurity driven variability and ensure experimental reproducibility across synthesis and photocatalytic tests.

3.4 Synthesis of photocatalysts

3.4.1 Synthesis of carbon dots

Initially, the EFB was washed several times under running tap water to remove impurities and dried under sunlight prior to grinding. A grinding machine was used to cut the EFB into smaller pieces and sieved with 0.25 mm sieve before mixing it with DI water. CDs were synthesized by using a hydrothermal method according to previously reported works (Egorova et al., 2018; Mahat & Shamsudin, 2020), as shown in Figure 3.2a. 6g of EFB powder was mixed with 150 mL of DI water and put into a Teflon-lined autoclave reactor. Then, the hydrothermal reactor was heated at 200 ℃ for 3 hours, followed by cooling down overnight (Mukherjee et al., 2021). The hydrothermal condition of 200 °C for 3 hours was selected as it provides sufficient energy for effective carbonization and formation of carbon dots while preserving surface functional groups (Josun et al., 2024). Lower temperatures may lead to incomplete carbonization, whereas higher temperatures or prolonged duration can reduce surface functionality and promote aggregation (Nazibudin et al., 2023). These conditions are consistent with commonly reported optimal ranges for biomass-derived carbon dots synthesis The brown solution was centrifuged at 5000 rpm for 15 minutes and filtered with a nylon syringe (0.22 μm) to remove precipitates and large particles.

The final solution was freeze-dried and stored for further characterization and application. The hydrothermal method was selected due to its ability to produce uniformly dispersed carbon dots with abundant surface functional groups under relatively mild conditions (Rowson Ali et al., 2021). The selected temperature range was chosen to balance carbonization and surface passivation, as excessively low temperatures lead to incomplete carbonization while higher temperatures promote particle aggregation and reduced photoluminescence efficiency (Nazibudin et al., 2023).

3.4.2 Synthesis of zinc oxide

ZnO nanoparticles were synthesized using a one-step hydrothermal method according to previously reported works (Mukherjee et al., 2021), as shown in Figure 3.2b. 0.3 g of zinc acetate dissolved in 15 mL of deionized water and the solution was adjusted until alkali (pH 11) by adding 8M of NaOH solution dropwise while stirring vigorously. Then, the mixture was transferred into a 150 mL Teflon-lined autoclave, where it was kept at 80 ℃ for 3 hours. The hydrothermal temperature of 80 °C was selected to enable controlled nucleation and formation of ZnO nanoparticles with smaller particle size and higher surface area (Semeraro et al., 2020). Lower temperature synthesis can also promote the formation of surface defects and hydroxyl groups, which are beneficial for photocatalytic activity and interfacial interaction with carbon dots (Mukherjee et al., 2021). Although higher temperatures typically improve crystallinity, several studies have reported that ZnO synthesized at lower temperatures can exhibit enhanced photocatalytic performance due to increased active sites and defect-mediated charge transfer (Tegenaw et al., 2023). After that, the mixture was centrifuged at 5000 rpm for 15 minutes. The precipitate was washed with ethanol and DI water to remove the impurities, followed by drying at 60 ℃ and then grinding in a mortar.

3.4.3 Fabrication of ZnO/CDs nanocomposites

0.3 g of ZnO nanoparticles were mixed with 0.3 g of CDs in a 1:1 ratio, followed by the addition of 30 mL of deionized water and stirring for 1 hour to form a homogenous solution. Then, the mixture was transferred into a 150 mL Teflon-lined autoclave, and it was kept at 80 °C for 3 hours, followed by centrifugation at 5000 rpm

for 15 minutes (Ayu et al., 2023; Mukherjee et al., 2021). The brown precipitate was washed 4 times with ethanol and DI water with a ratio of 1:3. The obtained ZnO/CDs nanocomposites were dried at 60 °C and then ground to a fine powder with an agate pestle and mortar. The synthesized ZnO/CDs nanocomposite catalyst is schematically depicted in Figure 3.2c. This process was repeated to obtain ZnO/ CDs nanocomposites with ratios of 1:2 and 2:1. The ZnO/CDs mass ratios (1:1, 1:2, and 2:1) were selected to systematically evaluate the effect of carbon dots loading on interfacial charge transfer and photocatalytic performance (Ayu et al., 2023; Mukherjee et al., 2021). A lower CDs content (2:1) provides limited electron trapping and visible-light sensitization, whereas a higher CDs content (1:2) enhances light absorption and electron mediation but may induce light shielding and surface coverage that reduce active sites (Wan Ishak, Tan, Abu Bakar, Radacsi, et al., 2025). The intermediate ratio (1:1) serves as a balance between these effects. Therefore, these ratios were chosen to identify the optimal composition that maximizes charge separation while avoiding excessive CDs loading, as commonly reported for semiconductor/CDs composites. The ZnO to carbon dots ratios were systematically varied to investigate the threshold at which charge transfer enhancement outweighs potential light shielding and recombination effects caused by excessive carbon loading (Ayu et al., 2023; Wan Ishak, et al., 2025).

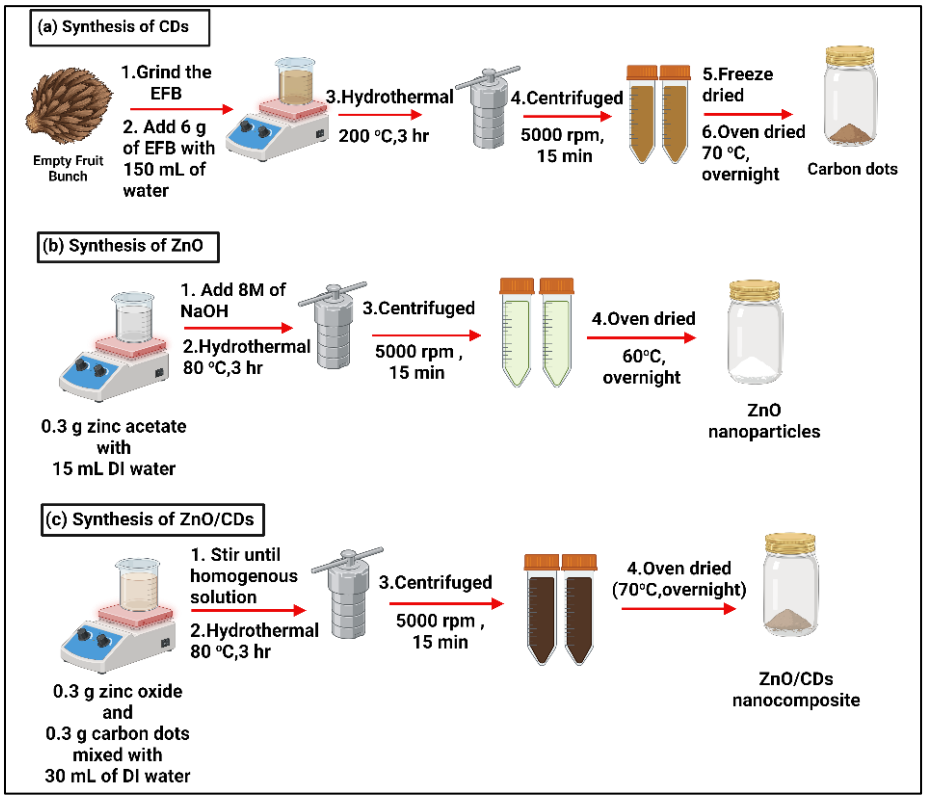

Figure 3.2 Schematic Illustration Of The Hydrothermal Synthesis Of Zno/Cds Composites: (a) CDs From EFB, (b) ZnO Nanoparticles, (c) ZnO/CDs Composites (2:1,1:1,1:2).

3.5 Characterization techniques

To comprehensively evaluate the structural, morphological, optical, electronic, and surface properties of the synthesized ZnO/CDs nanocomposites, various advanced characterization techniques were employed. These analyses provide critical insights into the material properties that influence photocatalytic performance.

3.5.1 Structural and Morphological Characterization

3.5.1.1 Fourier transform infrared spectroscopy (FTIR)

FTIR (Perkin Elmer Spectrum 400) was employed to analyze the surface properties and functional groups present in CDs, ZnO, and ZnO/CDs nanocomposites. The FTIR spectra were recorded in the wavenumber range of 4000–500 cm^{-1} using an attenuated total reflectance (ATR) mode to ensure accurate measurement (ASTM International, 2021). A thin layer of finely ground photocatalyst powder was carefully

placed onto the FTIR crystal plate, ensuring uniform contact with the infrared beam. The spectra were analyzed to identify characteristic functional groups, particularly hydroxyl (O–H), carbonyl (C=O), and Zn–O bonds, which provide insights into the structural modifications and interactions between ZnO and CDs. The presence of carbohydrates on the surface of CDs was also confirmed, likely originating from the stabilizing and capping agents involved in the hydrothermal synthesis. The observed spectral shifts and intensity variations were examined to understand the role of surface chemistry in enhancing photocatalytic performance.

3.5.1.2 X-ray Diffraction (XRD) Analysis

XRD (Rigaku Ultima IV XRD) was conducted to determine the crystallinity XRD analysis was conducted to determine the crystallinity, phase composition, and structural properties of the synthesized ZnO/CDs nanocomposites. The diffraction patterns were recorded using Cu Kα radiation (λ = 1.5406 Å) in the 2θ range of 10°–80°. The observed peaks were indexed based on the JCPDS reference database, and the crystallite size (DDD) was estimated using the Scherrer equation:

$$D = \frac{K\lambda}{\beta cos\theta} \tag{3.1}$$

where K is the shape factor (0.9), λ is the X-ray wavelength, β is the full width at half maximum (FWHM), and θ is the Bragg angle. The effect of carbon dots incorporation on ZnO crystallinity was examined, particularly regarding peak broadening and shifts indicating potential lattice distortions.

3.5.1.3 Field Emission Scanning Electron Microscopy (FESEM) and Energy Dispersive X-ray Spectroscopy (EDX)

Field Emission Scanning Electron Microscopy (FESEM) analysis was performed using a JSM-7600F, Jeol instrument to examine the surface morphology and nanostructure of the synthesized nanocomposites. Images were obtained at various magnifications (ranging from 10× to 300,000×) to evaluate particle size, agglomeration

behavior, and the distribution of carbon dots (CDs) within the ZnO matrix. The high resolution and extended depth of field enabled detailed visualization of the sample's topographical features. In addition, Energy Dispersive X-ray (EDX) spectroscopy was employed for elemental mapping, confirming the presence of Zn, O, and C, which verified the successful incorporation of CDs into the ZnO structure.

3.5.1.4 High-Resolution Transmission Electron Microscopy (HRTEM)

High-Resolution Transmission Electron Microscopy (HRTEM) analysis was carried out using a JEOL JEM-2100F microscope to examine the detailed nanostructure of the ZnO/CDs nanocomposite. This advanced imaging technique provides direct visualization of materials at the atomic scale, enabling precise analysis of particle size, lattice fringes, and interfacial interactions between ZnO and carbon dots (CDs). The Fast Fourier Transform (FFT) function was utilized to calculate the lattice spacing (d-spacing), allowing for the identification of specific crystalline planes of ZnO and the evaluation of its crystallinity. Furthermore, the HRTEM images revealed the distribution and dispersion of CDs across the ZnO matrix, offering insight into their integration and potential role in enhancing charge separation and transfer at the interface. These structural features are essential in understanding the photocatalytic behavior of the nanocomposite. In addition, Selected Area Electron Diffraction (SAED) patterns were acquired to further confirm the crystalline nature of ZnO and to distinguish between the polycrystalline and amorphous regions within the composite. The presence of distinct diffraction rings or spots in the SAED patterns corresponded to the indexed planes of ZnO, verifying its hexagonal wurtzite structure. The HRTEM images also revealed a relatively uniform dispersion of CDs across the ZnO surface, indicating strong interfacial contact, which is expected to facilitate enhanced charge separation and transfer a critical factor for improving photocatalytic efficiency.

3.5.2 Optical, Surface, and Electronic Characterization

3.5.2.1 X-ray Photoelectron Spectroscopy (XPS)

XPS (Axis Ultra DLD , Kratos, UK) analysis was conducted to determine the elemental composition, oxidation states, and chemical bonding in ZnO/CDs

nanocomposites. High-resolution spectra of Zn 2p, O 1s, and C 1s were analyzed to confirm the chemical states of Zn^{2+}, the presence of oxygen vacancies, and the functional groups introduced by CDs. Deconvolution of the O 1s peak was used to differentiate between lattice oxygen, hydroxyl groups, and surface-adsorbed oxygen species, which influence charge transfer and photocatalytic efficiency.

3.5.2.2 Brunauer-Emmett-Teller (BET) Surface Area and Porosity Analysis

BET analysis was conducted using nitrogen (N_2) adsorption-desorption isotherms at 77 K with a Micromeritics ASAP 2020 surface area and porosity analyzer to evaluate the specific surface area, pore size distribution, and total pore volume. The Brunauer–Emmett–Teller (BET) equation was employed to determine the surface area (SBET), while the Barrett–Joyner–Halenda (BJH) method was used for analyzing pore size distribution. The relationship between surface area, porosity, and photocatalytic performance was investigated to understand the impact of carbon dots (CDs) on the textural characteristics of ZnO. The samples were degassed at 200 °C for 8 hours under vacuum prior to BET analysis to remove moisture and physically adsorbed gases, ensuring accurate surface area and porosity measurements.

3.5.2.3 UV−vis spectrophotometer

The UV-Vis absorption spectra of the samples, which include CDs, ZnO, and ZnO/CDs, were recorded using an Agilent Cary 60 Spectrophotometer. $BaSO_4$ was used as the reference material. The purpose of the UV-Vis spectroscopy was to examine the linearity of the optical absorption behaviour of the samples. Additionally, the absorbance of a TC solution was recorded every 30 minutes using UV-Vis spectroscopy for a photocatalytic reaction. The wavelength of each sample was also recorded to determine the bandgap of each sample.

3.5.2.4 UV-Vis Diffuse Reflectance Spectroscopy (UV-DRS)

UV-DRS (Agilent Cary 60 Spectrophotometer) was employed to evaluate the optical properties and bandgap energy of ZnO/CDs nanocomposites. The absorption

spectra were recorded in the 200–800 nm range, and the bandgap energy (Eg) was estimated using Tauc's plot, given by:

$$(\alpha hv)^2 = A\left(hv - E_g\right) \tag{3.2}$$

where α is the absorption coefficient, hν is the photon energy, and A is a constant. The absorption coefficient was calculated from the absorbance data using the constant conversion factor 2.303, which converts logarithmic absorbance into absorption coefficient form. The value of n=½ for ZnO (direct bandgap semiconductor) was used. The bandgap narrowing due to CDs was analyzed to understand its impact on visible-light absorption.

3.5.2.5 Photoluminescence (PL) Spectroscopy

PL spectroscopy was performed to investigate the recombination behaviour of charge carriers in the ZnO/CDs nanocomposites. Since the emission characteristics varied among the samples and were not distinctly observable at a single excitation wavelength, measurements were conducted at multiple excitation wavelengths to capture the full range of photoluminescence responses. The emission spectra were analyzed to identify oxygen vacancies, defect states, and charge transfer dynamics within the nanocomposites. A decrease in PL intensity indicated improved charge separation, correlating with enhanced photocatalytic performance. Photoluminescence (PL) spectroscopy was conducted using an Edinburgh Instruments FLS920 spectrometer to investigate the optical properties and charge carrier dynamics of the synthesized samples. Photoluminescence is a light-emitting phenomenon that occurs when a material absorbs electromagnetic radiation and subsequently releases excess energy in the form of emitted light. This process begins with photoexcitation, where electrons are excited to higher energy states. As they relax back to their ground states, the energy released can manifest as either radiative emission (luminescence) or be dissipated through non-radiative pathways.

The energy of the emitted light corresponds to the energy difference between the excited and ground electronic states, providing insights into the band structure, defect states, and electron–hole recombination behavior of the material. PL is broadly

classified into fluorescence (with lifetimes typically around 10 nanoseconds) and phosphorescence (with lifetimes ranging from milliseconds to seconds), depending on the nature of the excited state.

In this study, the FLS920 system was also employed to perform fluorescence lifetime measurements using the Time-Correlated Single Photon Counting (TCSPC) technique, which offers high temporal resolution for analyzing excited-state dynamics.

3.5.2.6 Time-Resolved Photoluminescence (TRPL) Spectroscopy

Time-resolved photoluminescence (TRPL) measurements were performed to investigate the charge carrier dynamics and recombination behaviour of the ZnO/CDs nanocomposites. The decay curves were analyzed using a multi-exponential fitting model, expressed as:

$$I(t) = A_1 e^{-t/\tau 1} + A_2 e^{-t/\tau 2} + A_3 e^{-t/\tau 3} \quad (3.3)$$

where I(t) is the PL intensity at time t, A_1, A_2, and A_3 are the amplitude coefficients, and τ_1, τ_2, and τ_3 are the decay lifetimes corresponding to different recombination processes. The average lifetime (τavg) was calculated using:

$$\tau_{avg} = \frac{\sum A_i \tau_i^2}{\sum A_i \tau_i} \quad (3.4)$$

The results revealed that the ZnO/CDs nanocomposite exhibited a shorter τ_{avg} compared to pristine ZnO, confirming that the introduction of carbon dots effectively suppressed charge carrier recombination by facilitating rapid electron transfer. The shorter lifetime correlates with enhanced photocatalytic activity, as it indicates a higher separation efficiency of photogenerated charge carriers, reducing energy losses due to recombination. This behaviour is attributed to the role of CDs as electron acceptors and transport mediators, where photogenerated electrons are rapidly transferred from ZnO to the CDs surface states, thereby suppressing radiative recombination and prolonging the availability of charge carriers for photocatalytic reactions (Karaca et al., 2023).

3.6 Photoelectrochemical Characterization

Electrochemical measurements were conducted using an Autolab PGSTAT302N potentiostat in a three-electrode configuration with screen printed electrodes. Two types of screen-printed electrodes from Metrohm DropSens were used depending on the sample type. The DRP 110 SPE, consisting of a carbon working electrode, carbon counter electrode, and Ag/AgCl reference electrode, was used for ZnO and ZnO/CDs composites as shown in Figure 3.3. Meanwhile, the DRP 220AT SPE, consisting of a gold working electrode, carbon counter electrode, and Ag/AgCl reference electrode, was specifically used for carbon dots.

Prior to electrochemical measurement, the working electrode surface was modified by drop casting the photocatalyst ink onto the electrode surface and drying it at room temperature. The photocatalyst modified screen-printed electrode was prepared by drop casting 250 µL of 1 mM photocatalyst ink onto the working electrode surface. The photocatalyst loading was controlled by maintaining the same photocatalyst ink concentration and drop casting volume for all samples. After coating, the electrode was dried at room temperature to allow solvent evaporation and stable film formation. Although the actual film thickness was not directly measured, the film thickness was indirectly controlled by using a fixed photocatalyst ink concentration of 1 mM, a fixed ink volume of 250 µL, the same working electrode area, and identical drying conditions for all electrodes.

The electrochemical analyses included cyclic voltammetry, electrochemical impedance spectroscopy, Mott Schottky analysis, and transient photocurrent response. These measurements were used to evaluate the redox behaviour, interfacial charge transfer resistance, semiconductor band characteristics, and photoinduced charge separation behaviour of the synthesized photocatalysts.

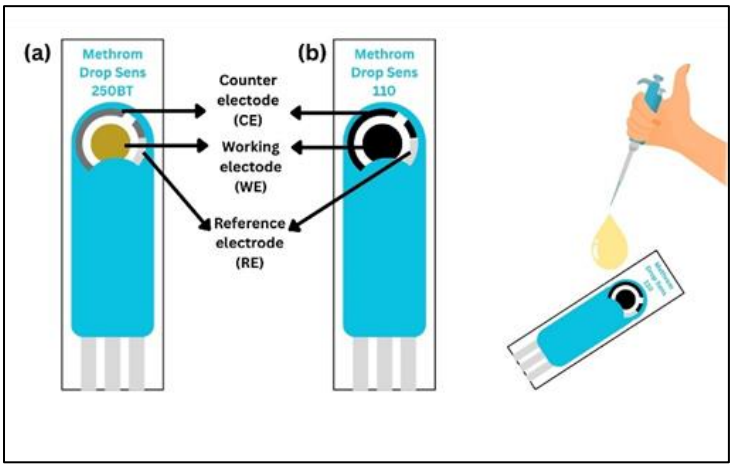

Figure 3.3 Screen Printed Electrode Use For Electrochemical Analysis

3.6.1 Cyclic Voltammetry (CV)

Cyclic voltammetry (CV) was performed to analyze the redox behaviour of ZnO/CDs nanocomposites. The potential was scanned from -1.5 V to +1.5 V vs. Ag/AgCl at a scan rate of 50 mV/s. The oxidation and reduction peaks were examined to determine the conduction band (CB) and valence band (VB) positions. The incorporation of CDs into ZnO was expected to shift the redox peaks, indicating improved electron transfer and band alignment. A 0.1 mol·L^{-1} KCl solution containing 5 mmol·L^{-1} $K_3[Fe(CN)_6]/K_4[Fe(CN)_6]$ (1:1) was used as the electrolyte for the CV measurements.

3.6.2 Electrochemical Impedance Spectroscopy (EIS)

EIS was conducted under both dark and UV light illumination to study charge transfer resistance (R_{ct}) and interfacial charge dynamics. Measurements were performed in the frequency range of 0.1 Hz to 100 kHz with an AC perturbation amplitude of 5 mV. The Nyquist plots were fitted using an equivalent circuit model to extract Rct values. A lower Rct for ZnO/CDs compared to pure ZnO confirmed enhanced charge transfer efficiency, suggesting reduced recombination losses.

3.6.3 Transient photocurrent response

The transient photocurrent response was measured under chopped UV light illumination to assess the efficiency of photogenerated charge carrier separation. The applied bias voltage was set to 0.5 V vs. Ag pseudo-reference, and the photocurrent was recorded over multiple on/off cycles. ZnO/CDs exhibited a higher and more stable photocurrent response compared to pristine ZnO, indicating enhanced charge carrier separation and prolonged electron lifetime.

3.6.4 Mott-Schottky

The Mott-Schottky curves and the instantaneous photocurrent density were measured in the 0.1 $mol \cdot L^{-1}$ Na_2SO_4 electrolyte. Mott-Schottky plots were obtained at 1 kHz, 5 kHz, and 10 kHz to determine the flat-band potential (Efb) and carrier density (Nd) of the photocatalysts. The capacitance (C) was measured as a function of applied potential (V), and the data were plotted using the Mott–Schottky relationship. The flat-band potential (Efb) was determined from the intercept of the linear region of the $1/C^2$ versus potential plot, while the carrier density (ND) was calculated from the slope of the same plot.

3.7 Photocatalytic degradation under UV light

The photocatalytic degradation of TC under UV light irradiation was used to evaluate the photocatalytic performance of the samples. Initially, 0.05 g of ZnO/CDs photocatalyst was mixed with 50 mL TC solution of 15 ppm. The suspension was put under the UV lamp, which was positioned 15 cm away from the top of the suspension. The mixture was continuously stirred in the dark for 30 minutes to achieve adsorption-desorption equilibrium, allowing photocatalytic degradation to be distinguished from physical adsorption. After that, the UV light was activated to initiate the photocatalytic degradation of TC over a period of 180 minutes. 5 mL of the solution was withdrawn at 30-minute intervals and filtered using a syringe filter 0.22µm prior to absorbance reading using a UV-Vis spectrophotometer running at 357 nm. The concentration of the solution was measured and determined using the standard curve. For comparison with UV-induced degradation, additional photocatalytic tests were conducted under natural

sunlight (10,000-30,000 lux intensity, clear sky, 12:00-2:00 PM) and visible light using an 80 W lamp with an emission peak at 400 nm. Control experiments were also conducted to evaluate photolysis and adsorption. For photolysis, the TCs solution was exposed to UV light without the addition of CDs, while for adsorption, the TCs solution was mixed with CDs and kept in the dark for 30 minutes. The TC degradation efficiency was calculated using Equation 1 (Karaca et al., 2023), where C_0 is the initial concentration of TC while Ct is the final concentration of TC. The reproducibility experiment was conducted using 10 repeated runs under identical operating conditions. The degradation efficiencies obtained were compared to assess the repeatability and reliability of the photocatalytic performance.

$$\text{Degradation efficiency} = \frac{C_o - C_t}{C_o} \times 100\% \quad (3.5)$$

Where:

C_o = Initial concentration of TC

Ct = Final concentration of TC

3.7.1 Influence of process parameters on photocatalytic activity

Photocatalytic performance was optimized by systematically varying key operational parameters based on commonly reported conditions in photocatalytic degradation studies(Saadati et al., 2016):

3.7.1.1 Effect of Catalyst Dosage

The impact of catalyst loading was investigated by varying the amount of ZnO/CDs nanocomposite in the reaction mixture. Catalyst dosages ranging from 0.5 to 1.5 gL^{-1} were tested to determine the optimal amount that maximizes degradation efficiency without excessive particle agglomeration or light scattering

3.7.1.2 Effect of initial TC concentration

Different initial concentrations of TC (5–25 mg/L) were used to evaluate the degradation kinetics and determine the effect of pollutant concentration on the

photocatalytic rate. Higher concentrations may lead to increased photon absorption competition, while lower concentrations can limit degradation efficiency due to reduced availability of TC molecules.

3.7.1.3 Effect source of light

Photocatalytic activity was evaluated under UV (365 nm), visible (400–700 nm), and solar irradiation to assess the light response of the ZnO/CDs system. This comparison enables evaluation of band gap excitation in ZnO and photosensitization effects contributed by CDs under visible light.

3.7.2 Photostability and Reusability

The photostability and reusability of the ZnO/CDs nanocomposite photocatalyst were systematically assessed across five consecutive cycles of tetracycline degradation. After each cycle, the photocatalyst was recovered by centrifugation using a 3:2 (v/v) ethanol-water mixture, followed by thorough washing to remove residual contaminants. Subsequently, the recovered photocatalyst was dried overnight at 70 °C to restore its activity for the subsequent degradation cycle. This process was repeated for five cycles to assess the consistency of its photocatalytic performance. This process was repeated for five cycles to assess the consistency of its photocatalytic performance. Following these cycles, the structural integrity and crystallinity of the regenerated photocatalyst were examined using X-ray diffraction (XRD) and High transmission electron microscopy (HRTEM) to investigate any potential alterations induced by repeated use.

3.8 Mechanistic Insights into Photocatalytic Degradation

3.8.1 Reactive species trapping experiment

The identification of the dominant reactive oxygen species (ROS) involved in tetracycline degradation was achieved by subjecting the reaction mixture to UV irradiation and subsequently introducing specific scavengers. To identify the respective roles of these ROS, 1 mM of various scavengers were then introduced to the mixture. Tert-butanol (BuOH) selectively quenched hydroxyl radicals (•OH), while

ethylenediaminetetraacetic acid disodium salt (EDTA-2Na) scavenged positively charged holes (h^+). Silver nitrate ($AgNO_3$) functioned as an electron scavenger (e^-), and finally, p-benzoquinone (PBQ) was used to trap superoxide anion radicals ($\bullet O_2^-$).

3.8.2 Liquid Chromatography-Mass Spectrometry (LC-MS) Analysis

LC-MS (Agilent G2449A) analysis was conducted to identify the degradation intermediates of tetracycline (TC) after photocatalytic treatment using ZnO/CDs nanocomposites. A high-performance liquid chromatography (HPLC) system coupled with a quadrupole time-of-flight mass spectrometer (Q-TOF MS) was used in positive electrospray ionization (ESI^+) mode to detect molecular fragments. Chromatographic separation was achieved using a C18 column with a mobile phase of 0.1% formic acid in water and acetonitrile under a gradient elution program. The mass spectra were recorded in the m/z range of 50–1000, with fragmentation energy set at 20, 40, and 60 eV. Prior to analysis, the photocatalytic samples were centrifuged at 10,000 rpm, filtered through a 0.22 μm PTFE membrane, and diluted if necessary. The disappearance of the TC parent peak (m/z = 445.16) and the emergence of lower molecular weight species indicated sequential degradation through hydroxylation, deamination, demethylation, and ring cleavage, leading toward mineralization. The kinetic profile of intermediate formation and decomposition was analyzed to determine dominant degradation routes. LC-MS confirmed the efficiency of ZnO/CDs nanocomposites by providing molecular-level insights into the photocatalytic transformation, supporting UV-Vis and electrochemical analyses in elucidating the degradation mechanism.

3.9 Kinetic study

In this study, the photocatalytic degradation of tetracycline (TC) is explored using the Langmuir-Hinshelwood (LH) model, which is commonly observed in heterogeneous photocatalytic reactions. Based on the LH model, the rate equation is expressed as $\ln(C_o/C_t) = -kt$, where C_o represents the initial concentration of tetracycline, Ct denotes the concentration at time t, k is the rate constant, and t is the reaction time. The experimental data of the photocatalytic degradation of TC is analyzed

through a pseudo first-order reaction, yielding a straight line when $\ln(C_0/C_t)$ is plotted against time.

$$\ln C_t = -kt + \ln C_o \tag{3.6}$$

$$\ln\left(\frac{C_o}{C_t}\right) = kt \tag{3.7}$$

The ln (C_o/C_t) slope provides the apparent first-order rate, with the equation involving r_0 as the initial degradation rate, k_R interpreted as a pseudo first-order Langmuir-Hinshelwood rate coefficient, and k_{LH} as a pseudo-equilibrium constant associated with monolayer adsorption. From the equation, graph 1/kapp vs C_O is plot and the relationship between k_{LH} and k_R is compared to determine whether the reaction take place at the surface of the catalyst or in the bulk of solution.

$$r_o = -\frac{dC}{dt} = \frac{K_R K_{LH} C_o}{1 + K_{LH} C_o} = k_{app} C_o \tag{3.8}$$

$$\frac{1}{k_{app}} = \frac{1}{K_R K_{LH}} + \frac{C_o}{K_R} \tag{3.9}$$

3.10 Replication, Error Analysis and Statistical Treatment

The reproducibility experiment was conducted using 10 repeated runs under identical operating conditions. The obtained degradation efficiencies were compared to assess the repeatability and reliability of the photocatalytic performance. Where applicable, repeated measurements were expressed as mean values with standard deviation. Error bars were used in the relevant graphs to represent experimental variation between repeated measurements. The kinetic fitting was evaluated using the coefficient of determination, R^2, while the apparent rate constant and half-life were calculated based on the pseudo first order Langmuir Hinshelwood kinetic model. This statistical treatment was applied to ensure that the reported photocatalytic trends were reproducible and not based on single measurement variation.

3.11 Closing remarks

This chapter has presented a comprehensive description of the materials, chemicals, and experimental procedures employed in the synthesis and characterization of ZnO/CDs nanocomposites for photocatalytic degradation of tetracycline. The methodologies included the hydrothermal synthesis of carbon dots derived from oil palm Empty Fruit Bunch (EFB), the preparation of ZnO nanoparticles, and the subsequent formation of ZnO/CDs nanocomposites. A series of advanced characterization techniques, namely FTIR, XRD, FESEM-EDX, HRTEM, UV-Vis, UV-DRS, PL, TRPL, BET, and XPS, along with electrochemical analyses such as CV, EIS, Mott-Schottky, and photocurrent response, were employed to investigate the structural, morphological, optical, and electronic properties of the synthesized materials. The novelty of the methodology lies in the sustainable approach to carbon dot synthesis using agricultural biomass waste and the strategic coupling with ZnO to enhance photocatalytic activity under visible light irradiation. This study is among the first to utilize EFB-derived carbon dots as a green additive for tuning the photocatalytic behaviour of ZnO. The integration of experimental and electrochemical analyses provided valuable insights into the charge transfer dynamics and degradation mechanisms, laying a solid foundation for the development of efficient and environmentally friendly photocatalysts for wastewater treatment.

CHAPTER 4
RESULTS AND DISCUSSION

4.1 Introduction

This chapter presents and discusses the experimental findings on the synthesized ZnO nanoparticles, carbon dots, and ZnO/CDs nanocomposites with different ZnO:CDs ratios of 2:1, 1:1, and 1:2. The discussion focuses on the relationship between material properties, charge transfer behaviour, and photocatalytic degradation performance toward tetracycline.

The results are organized into physicochemical characterization, optical and electrochemical properties, photocatalytic performance, kinetic analysis, reactive species identification, and proposed degradation mechanism. The findings are compared with previous studies where relevant to support the interpretation and highlight the role of biomass derived carbon dots in improving the photocatalytic activity of ZnO.

4.2 Morphology of photocatalysts

4.2.1 X-ray diffraction (XRD) analysis

Figure 4.1 displays the X-ray diffraction (XRD) patterns of pristine ZnO, CDs, and ZnO/CDs nanocomposites prepared at various weight ratios (2:1, 1:1, and 1:2). The observed diffraction peaks, corresponding to the (100), (002), (101), (102), (110), (103), (200), (112), (201), (004), and (202) lattice planes align well with the standard hexagonal wurtzite structure of ZnO, as referenced in JCPDS card no. 36-1451. No additional impurity peaks were observed, indicating that the ZnO phase was successfully formed and retained after CDs incorporation.

The XRD patterns of the ZnO/CDs nanocomposites closely resemble that of pristine ZnO, suggesting that the incorporation of CDs did not significantly alter the main crystalline structure of ZnO. The absence of distinct CDs diffraction peaks can be attributed to their relatively low content, amorphous nature, and high dispersion on the ZnO surface. Similar observations have been reported in ZnO/CDs based systems,

where the amorphous carbon phase is not clearly detected by XRD due to weak crystallinity and low diffraction intensity compared with crystalline ZnO (Ayu et al., 2023; Xu et al., 2023). Since amorphous phases generally lack long range order, the presence of CDs was further supported by HRTEM analysis, as shown in Figure 4.10e. The HRTEM image revealed faint lattice fringes with an interplanar spacing of approximately 0.32 nm, which can be assigned to the disordered graphitic carbon domain of CDs. This confirms the presence of localized graphitic regions within the carbon dots, although their overall structure remains largely amorphous. Despite the structural similarity, the crystallite size of ZnO/CDs composites exhibits a decreasing trend with increasing CDs content. The average crystallite size (D) was determined using the Debye-Scherrer in Equation 4.0:

$$D = \frac{0.9\lambda}{\beta cos\theta} \tag{4.1}$$

where λ represents the X-ray wavelength (1.54 Å), β is the full width at half maximum (FWHM), and θ is the diffraction angle of the most intense peak, corresponding to the (101) plane. The calculated crystallite sizes for ZnO nanoparticles, ZnO/CDs (2:1), ZnO/CDs (1:1), and ZnO/CDs (1:2) nanocomposites were 26.62, 24.24, 14.57, and 11.34 nm, respectively. The reduction in crystallite size is consistent with previous ZnO/CDs studies, where CDs were reported to influence ZnO nucleation and crystal growth (Ayu et al., 2023; Bozetine et al., 2016). The oxygen containing functional groups on the CDs surface, such as hydroxyl, carbonyl, and carboxyl groups, may interact with Zn^{2+} species and provide additional nucleation sites during hydrothermal treatment (Maddu et al., 2021). This can promote the formation of smaller ZnO crystallites. At higher CDs loading, partial surface coverage by CDs may further limit ZnO grain growth, resulting in smaller crystallite size and broader diffraction peaks (Karaca et al., 2023).

The broadening of ZnO diffraction peaks after CDs incorporation may be attributed to the reduction in crystallite size and the formation of local structural disorder at the ZnO/CDs interface (Ayu et al., 2023; Bozetine et al., 2016). Interfacial interaction between ZnO and CDs may generate defect sites, oxygen vacancies, and possible lattice strain without changing the primary wurtzite phase of ZnO (Ayu et al.,

2023; Bozetine et al., 2016). Similar peak broadening and crystallite size reduction have been reported for ZnO/CDs and carbon modified ZnO composites, where carbon-based species influenced ZnO crystallization and introduced defect related structural distortion (Mukherjee et al., 2021). To further evaluate the impact of CDs on ZnO's unit cell structure, the lattice parameters (a, b, and c) were calculated using the interplanar spacing (d) and Miller indices (h, k, l) from the dominant (101) plane, as given by equation 4.1:

$$\frac{1}{d^2} = \frac{4}{3}\left(\frac{h^2 + hk + l^2}{a^2}\right) + \frac{l^2}{c^2} \qquad (4.2)$$

The obtained lattice parameters for ZnO/CDs (1:2) were a=b 3.250 Å and c =6.6702 Å, which are marginally higher than those of pristine ZnO (a=b=3.249 Å and c =5.2066 Å). The calculated lattice parameters for pristine ZnO and ZnO/CDs nanocomposites showed only minor variation in a parameter, while no obvious peak shift was observed in the ZnO diffraction peaks. This indicates that the hexagonal wurtzite structure of ZnO was retained after CDs incorporation. Therefore, significant lattice strain or bulk lattice distortion is unlikely. Any slight variation in the calculated lattice parameters may arise from fitting uncertainty, crystallite size variation, or local interfacial effects rather than true lattice expansion. Thus, CDs incorporation is more appropriately interpreted as surface attachment or interfacial coupling with ZnO rather than substitution into the ZnO crystal lattice. Overall, the XRD results confirm the successful formation of ZnO/CDs nanocomposites while retaining the hexagonal wurtzite structure of ZnO. The decrease in crystallite size and slight peak broadening suggest that CDs affected ZnO crystal growth by restricting crystallite development and introducing local interfacial disorder. These structural changes may contribute to improved photocatalytic performance by increasing surface active sites, enhancing interfacial charge transfer, and reducing charge recombination (Ayu et al., 2023; Mukherjee et al., 2021).

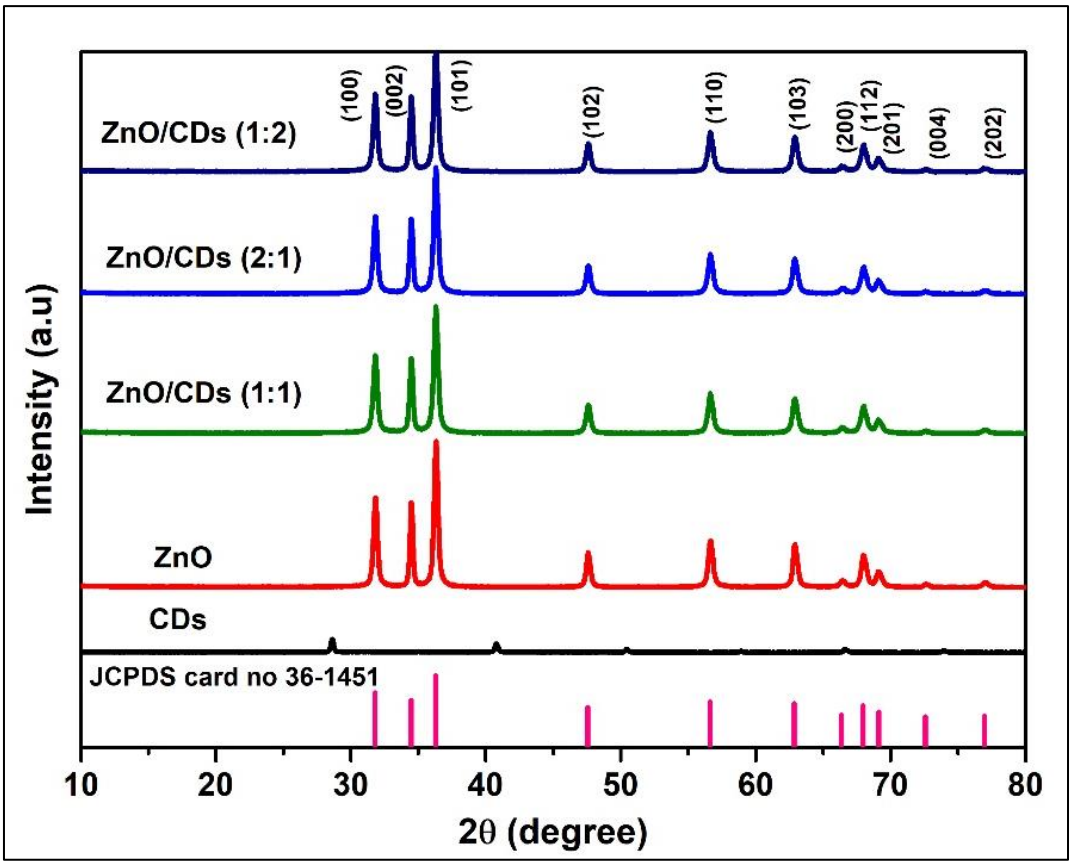

Figure 4.1 XRD Pattern Of The Samples

4.2.2 Fourier Transform Infrared Spectroscopy (FTIR)

The FTIR spectra of CDs, ZnO nanoparticles, and ZnO/CDs nanocomposites (2:1,1:1 and 1:2) are presented in Figure 4.2 to identify surface functional groups and examine the chemical interactions between components. For pristine ZnO nanoparticles, a distinct absorption band around 455 cm^{-1} is attributed to the stretching vibration of the Zn–O bond, confirming the presence of ZnO (Mukherjee et al., 2021). In addition, a peak at 1639 cm^{-1} corresponds to the bending vibration of hydroxyl (O–H) groups, while the broad absorption band observed around 3415 cm^{-1} is associated with O–H stretching vibrations from adsorbed water molecules on the nanoparticle surface (Bozetine et al., 2016). These functional groups are commonly found on metal oxide surfaces and are known to play a significant role in photocatalytic activity by serving as active sites for the generation of reactive oxygen species. For the CDs sample, distinct absorption bands were observed at 1520 cm^{-1} and 649 cm^{-1}, which are assigned to the stretching vibrations of C−O−C and C=C functional groups, respectively (Josun et al., 2024). These stretching are also detected in the ZnO/CDs composites,

suggesting that the essential functional moieties of CDs are retained following composite formation. Notably, the intensity of the C=C band increases with the CDs content, indicating the successful incorporation of CDs into the ZnO matrix (Xu et al., 2023), (Aljaafari et al., 2020). This enhancement could also suggest the formation of π–π interactions or other interfacial interactions between ZnO and the graphitic domains of the CDs (Jamaludin et al., 2018). The presence of abundant hydroxyl and oxygen-containing functional groups in both ZnO and CDs can facilitate enhanced photocatalytic performance. These groups not only increase surface hydrophilicity, promoting better dispersion in aqueous media, but also contribute to pollutant adsorption and the formation of hydroxyl radicals under light irradiation (Xie et al., 2018). Furthermore, the potential interaction between the ZnO surface and the CDs evident from the preserved and slightly intensified Zn–O and C=C bands may result in improved charge transfer and suppressed electron-hole recombination (Hussein Abdurahman et al., 2022).

In conclusion, FTIR analysis confirms the presence of functional groups characteristic of both ZnO and CDs in the ZnO/CDs nanocomposites, supporting the formation of a stable and interactive heterostructure. The successful integration of CDs, as evidenced by the emergence and intensification of specific bands, plays a critical role in modulating the surface chemistry and enhancing the photocatalytic performance of the hybrid materials.

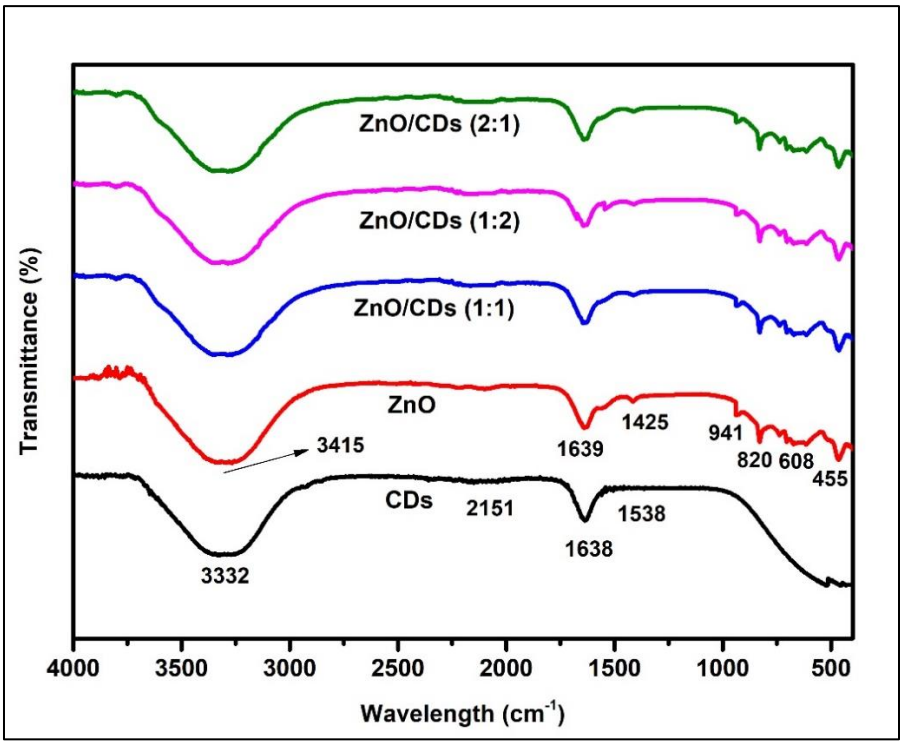

Figure 4.2 FTIR Spectra of CDs, ZnO and ZnO/CDs Nanocomposites

4.2.3 Brunauer-Emmett-Teller analysis

The porous characteristics of the synthesized CDs, ZnO nanoparticles and ZnO/CDs composites each ratio (2:1,1:1 and 1:2) were analysed using N_2 adsorption-desorption isotherms. As illustrated in Figure 4.3 shows the isotherm for synthesized photocatalyst exhibited typical type IV isotherms with a distinct hysteresis loop at a high relative pressure (P/P_0) range of 0.85-1.0 (Wang et al., 2023). Correspondingly, the data in Table 4.1 confirm the presence of mesopores with diameters below 50 nm in ZnO/CDs composites, a critical factor in enhancing wastewater pollutant degradation (Di et al., 2016; Hu et al., 2021). The incorporation of CDs into the ZnO matrix produced a loading dependent effect on the BET surface area. At low CDs loading, represented by ZnO/CDs (2:1), the surface area increased compared with pristine ZnO. This may be attributed to the improved dispersion of ZnO particles and the presence of CDs on the ZnO surface, which can reduce particle aggregation and create additional accessible surface sites. Therefore, at low loading, CDs may enhance the accessible surface area rather than block the pores. However, as the CDs content increased in ZnO/CDs (1:1) and ZnO/CDs (1:2), the surface area decreased. This reduction may be due to partial pore blockage, surface coverage, and aggregation of excess CDs, which

can form a denser layer on ZnO and restrict access to the mesoporous structure. Therefore, the effect of CDs on surface area depends strongly on CDs loading, where low CDs content improves surface accessibility, while excessive CDs loading can reduce surface area and porosity. Although the measured BET surface areas were relatively low, with values below 15 m^2/g, they are still within the range reported for several ZnO and ZnO/CD based photocatalysts. For example, Ayu et al. reported BET surface areas of 3.827 m^2/g for N doped ZnO and 3.757 m^2/g for N ZnO/CD nanocomposites, while the materials still showed photocatalytic activity under light irradiation (Ayu et al., 2023). Similarly, ZnO based photocatalysts with surface areas in the range of approximately 5 to 14 m^2/g have also been reported for pollutant degradation applications (Ayu et al., 2023). Therefore, the low surface area in the present study may reduce adsorption driven photocatalysis to some extent, but it does not fully determine the overall degradation efficiency. In ZnO/CDs systems, photocatalytic activity is also strongly governed by light absorption, band gap modification, interfacial charge transfer, recombination suppression, and reactive oxygen species generation (Maddu et al., 2021). The incorporation of CDs into the ZnO matrix did not produce a uniform decrease in surface area but showed a loading dependent trend. This reduction in surface area could be attributed to the partial obstruction or blockage of ZnO's porous network by the incorporated CDs (Z. Wang et al., 2024). At higher CDs loadings, aggregation leads to the formation of a dense layer on the surface of ZnO nanoparticles, as confirmed by a significant reduction in surface area from BET analysis, which indicates the obstruction of active sites and limited accessibility for adsorption (Velumani et al., 2020). Furthermore, CDs could occupy or block the mesopores present within the ZnO nanoparticles, which further contributes to a decrease in the overall porosity of the composite material. The aggregation of CDs at higher loadings can also impede the effective dispersion of ZnO nanoparticles, further restricting the accessible surface area. Despite this reduction in surface area and adsorption sites, the mesoporous structure still promotes efficient mass transfer and molecular diffusion, enabling reactant accessibility to active sites (Chang & Hsu, 2020). More importantly, the incorporation of CDs significantly improves visible light absorption and enhances photogenerated charge separation by facilitating electron transfer, which collectively outweighs the drawback of reduced surface area. These synergistic effects result in a superior photocatalytic performance for tetracycline degradation.

Therefore, although increasing CDs content compromises surface area and porosity, the overall photocatalytic efficiency of the ZnO/CDs composites is substantially enhanced, highlighting a performance trade-off that ultimately favors photocatalytic activity due to improved charge dynamics and light utilization (Ayu et al., 2023). In summary, the nitrogen adsorption-desorption isotherm analysis confirmed that all synthesized materials, including ZnO nanoparticles, CDs, and ZnO/CDs composites, possess mesoporous structures, beneficial for pollutant diffusion and reaction kinetics. While the incorporation of CDs into ZnO resulted in a noticeable reduction in surface area particularly at higher loading ratios due to pore blockage and CDs aggregation the overall photocatalytic efficiency was not hindered. Instead, the enhanced light absorption and improved charge separation facilitated by the CDs compensated for the loss in surface area. This trade-off underscores the crucial role of structural and optical synergy in photocatalytic systems. The subsequent UV-DRS analysis will further elucidate the impact of CDs on the optical absorption properties of the composites, particularly in the visible light region.

Table 4.1
Results of CDs, ZnO Nanoparticles and ZnO/CDs Nanocomposites

Sample	**S_{BET} ($m^2.g$-1)**	**Average pore volume ($cm^3.g^{-1}$)**	**Average pore size (nm)**
CDs	0.36 ± 0.1	0.002 ± 0.001	28.51± 0.11
ZnO	6.14 ± 0.12	0.032± 0.0012	18.82± 0.19
ZnO/CDs (2:1)	14.70 ± 0.2	0.085± 0.0044	22.09± 0.13
ZnO/CDs (1:1)	11.12 ± 0.13	0.086± 0.0024	31.96± 0.24
ZnO/CDs (1:2)	7.92 ± 0.11	0.052± 0.0026	23.57± 0.22

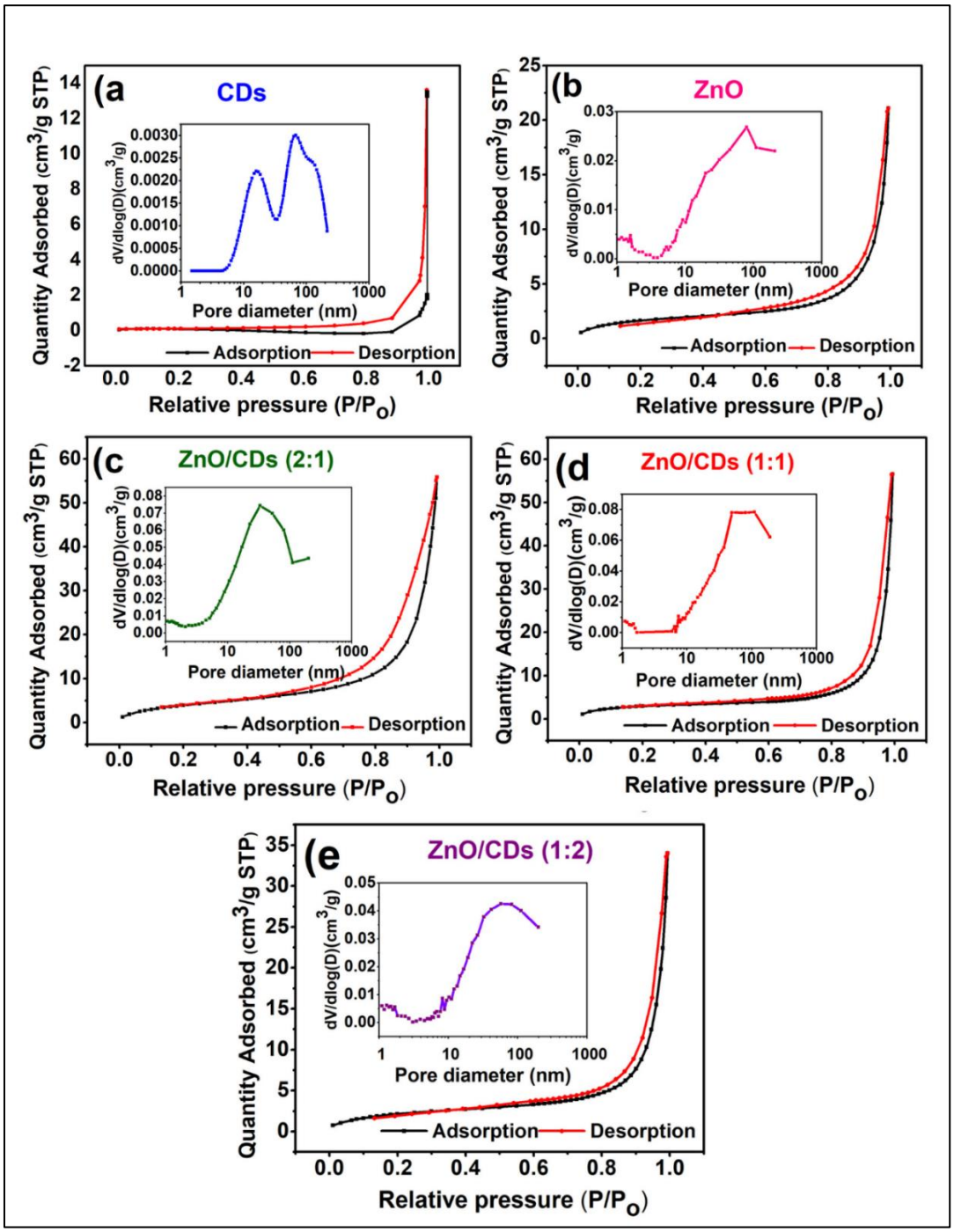

Figure 4.3 N_2 Adsorption−Desorption Isotherms And The Pore Size Distribution (inset) of CDs (a), ZnO (b), ZnO/CDs (2:1) (c), ZnO/CDs (1:1) (d) and ZnO/CDs (1:2) (e).

4.2.4 Optical Properties

4.2.4.1 UV-Vis spectroscopy

The photocatalytic activity of semiconductor materials is strongly influenced by their light-harvesting capabilities and the efficiency of photogenerated charge carrier separation. To assess the optical properties of the synthesized carbon dots , pristine ZnO nanoparticles, and ZnO/CDs nanocomposites with varying ratios (2:1, 1:1, and 1:2), UV–visible diffuse reflectance spectroscopy (UV-DRS) was employed, as illustrated in Figure 4.4.The UV-DRS spectrum of CDs (Figure 4.4a) reveals distinct absorption peaks at 241 nm and 287 nm, attributed to π–π* transitions of aromatic C=C bonds and n–π* transitions of C=O groups, respectively (Edakkaparamban et al., 2023). For pristine ZnO nanoparticles, the absorption edge appears at approximately 383 nm, consistent with its intrinsic wide bandgap. However, with increasing CDs content in the ZnO/CDs composites. Specifically, the absorption edges for ZnO/CDs (2:1), ZnO/CDs (1:1), and ZnO/CDs (1:2) are observed at 390 nm, 398 nm, and 440 nm, respectively (Figure 4.4c), indicating enhanced visible light absorption as a result of carbon dots integration.

This signifies a progressive narrowing of the optical band gap, thereby enabling the composite to absorb a broader range of visible light. The enhanced light-harvesting ability is ascribed to the synergistic effect between ZnO and CDs, where the latter introduce surface states and interfacial charge-transfer pathways that suppress electron-hole recombination (Liang et al., 2020). Moreover, the surface state modification and up-conversion photoluminescence properties of CDs enhance the light-harvesting capability of the composite under visible light irradiation (Xu et al., 2023). The ZnO/CDs (1:2) composite demonstrated the highest light absorption capacity. The data obtained from UV-DRS was used to investigate the bandgap for each of the composite material (Xu et al., 2023). The ZnO/CDs (1:2) composite demonstrated the highest light absorption capacity. The data obtained from UV-DRS was used to investigate the bandgap for each composite using Tauc equation as given in Equation (4.3):

$$(\alpha h\nu)^2 = A\left(h\nu - E_g\right) \tag{4.3}$$

Where α is the absorption coefficient, A is the proportionality constant, hv is the frequency of the incident light, and E_g is the band gap of the samples. E_g was determined by extrapolation of the $(\alpha hv)^2$ versus E. The intercept of the E axis where $(\alpha hv)^2 = 0$ gives the E_g value of each sample. The estimated bandgap energies for CDs, ZnO, ZnO/CDs (2:1), ZnO/CDs (1:1), and ZnO/CDs (1:2) were 4.50 eV, 3.27 eV, 3.17 eV, 3.10 eV, and 2.99 eV, respectively (Figure 4.4b and 4.4c). The observed band gap narrowing with increasing CDs content confirms the role of CDs in modulating the electronic structure of ZnO to improve solar energy utilization.

Despite the intrinsically wide band gap (4.5 eV) of CDs, which limits their absorption to the UV region, their surface is rich in defect states and functional groups. These surface features introduce mid-gap energy levels that facilitate sub-bandgap transitions, allowing CDs to absorb visible light (Ateia et al., 2024; Mintz et al., 2019). This behavior supports the extended absorption observed in the ZnO/CDs composites and underscores the critical role of quantum confinement and surface passivation.

Furthermore, this visible-light activity is further evidenced by the optical behavior of the ZnO/CDs composites, where a reduced band gap of 2.99 eV is observed in Figure 4.4d. This narrowing of the band gap is indicative of strong electronic coupling and synergistic interactions between ZnO and CDs, facilitating improved charge delocalization and extended light absorption into the visible range (Ateia et al., 2024; J. Liu et al., 2020). Such effects are characteristic of quantum confinement-induced band structure tailoring in CDs.

The UV–vis absorption spectrum of the synthesized carbon dots reveals a relatively high optical band gap of approximately 4.5 eV, corresponding to an absorption edge in the ultraviolet (UV) region. This large band gap indicates limited π-conjugation within the carbon core, attributed to quantum confinement effects and extensive surface passivation (Ateia et al., 2024; Mintz et al., 2019). However, CDs are known to exhibit abundant surface states and defect sites, which can introduce mid-gap energy levels (Prieto et al., 2024). These surface-related states facilitate sub-bandgap transitions, enabling visible-light absorption despite the intrinsic wide band gap of the carbon core.

The photocatalytic efficiency enhancement in the ZnO/CDs composites is further supported by time-resolved photoluminescence (TRPL) analysis (Figure 4.6b and Table 4.3). The ZnO/CDs (1:2) composite exhibits a significantly reduced average photocarrier lifetime (τ_{avg} = 2.084 ns) compared to pristine ZnO (τ_{avg} = 4.198 ns) and

CDs (τ_{avg} = 2.013 ns). This shortened lifetime implies accelerated non-radiative recombination (Berends et al., 2016; J. Wang et al., 2022), suggesting that the photoexcited electrons originating from visible-light absorption by CDs via surface states are efficiently transferred to ZnO, thus avoiding radiative recombination and instead participating in redox reactions (Kshirsagar et al., 2006; van Dam et al., 2017).

In summary, the integration of CDs into ZnO significantly narrows the bandgap and extends the light absorption range into the visible region. These modifications are pivotal for promoting efficient utilization of solar energy, particularly under sunlight, thereby enhancing the overall photocatalytic efficiency of the composite system (K. Jia et al., 2022). The observed narrowing of the bandgap particularly for the ZnO/CDs (1:2) composite, indicates a substantial improvement in the material's capacity to harvest solar energy. However, efficient photocatalysis not only relies on enhanced light absorption but also critically depends on the ability to convert absorbed photons into reactive charge carriers. To gain deeper insight into the photo-response behaviour and assess the potential of the synthesized materials under practical conditions, fluorescence quantum yield (QY) analysis was performed. Quantum yield serves as a vital parameter that quantitatively evaluates the efficiency of photon utilization during the excitation and emission processes, thereby providing an indirect indication of charge carrier recombination dynamics (Yadav et al., 2023). Hence, quantum yield analysis complements the UV-DRS findings and offers a more comprehensive understanding of the photocatalytic capability of the ZnO/CDs composites.

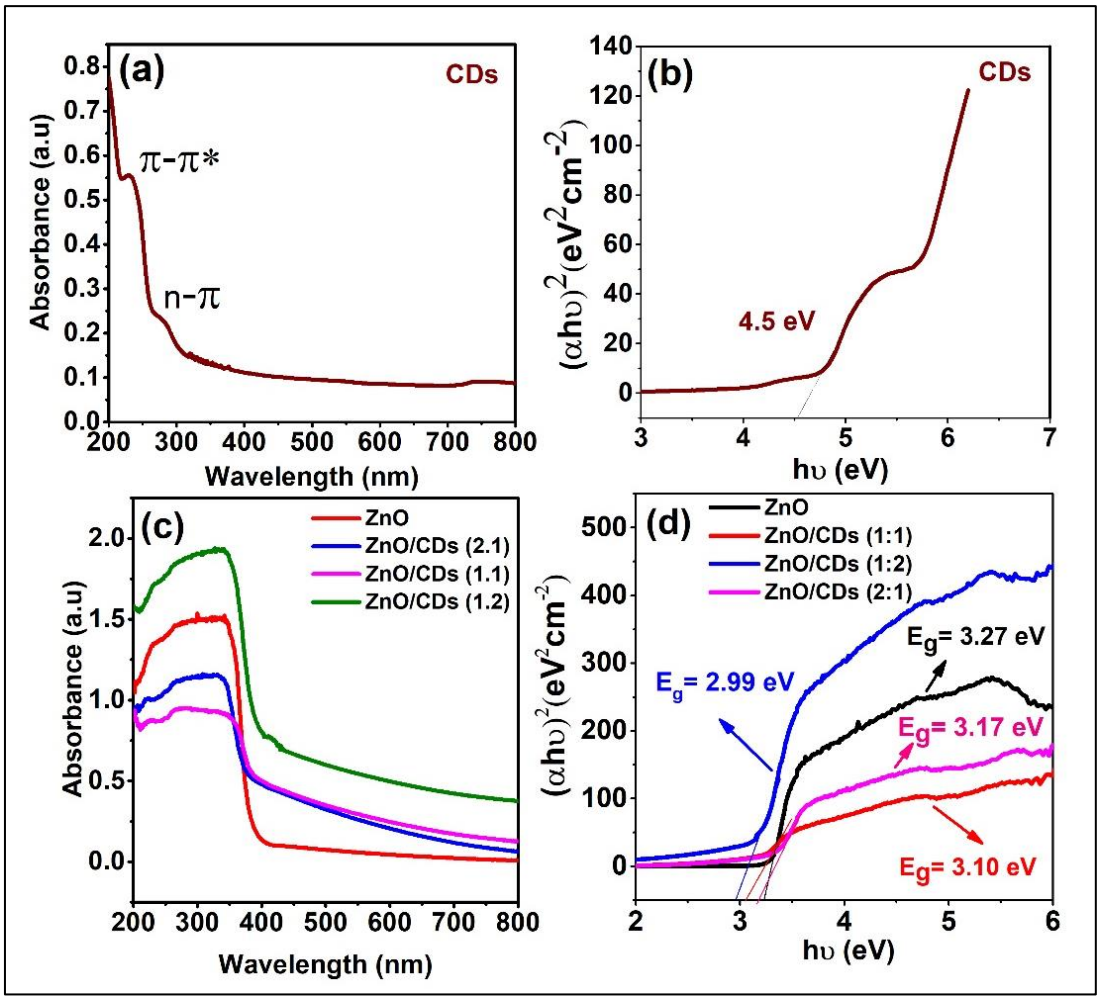

Figure 4.4 UV-DRS And Plot Of $(Ahv)^2$ Versus Photon Energy Of The Of (a), (b) CDs And (c), (d) ZnO/CDs.

4.2.4.2 Quantum yield

The fluorescence quantum yield, defined as the ratio of emitted photons to absorbed photons, was determined using the well-established comparative method. This method involves comparing the wavelength-integrated fluorescence intensities of the test sample with a suitable standard exhibiting an overlapping excitation wavelength range (Ayu et al., 2023). To enhance the accuracy of quantum yield determination, the influence of absorbance on the integrated fluorescence intensity was considered for both the test sample and the standard as shown in Figure 4.5. The quantum yield of CDs was determined by comparing the optical properties of CDs to the standard quinine sulfate solution 0.1 M H_2SO_4, which has a quantum yield of 54.6 % at an excitation wavelength

of 350 nm (Ayu et al., 2023). The quantum yield of the CD samples was calculated by using the following Equation 4.4.

$$Q_{YS} = Q_{YR}\left(\frac{I_S}{I_R}\right) \times \left(\frac{A_R}{A_S}\right) \times \left(\frac{n_s}{n_r}\right)^2 \quad (4.4)$$

where *R* and *S* are the reference (quinine sulphate) and sample (carbon dots) Q_y is the quatum yield, *I* is PL area under the graph, (Figure 4.5) and n_r is the refractive index where n of the sample and reference are 1.294 and 1.33, respectively (Jamaludin et al., 2020). The quantum yield of CDs obtained in this study was compared with the quantum yield of CDs derived from other natural precursors, and their quantum yields are listed in Table 4.2. This significant improvement in quantum yield can be attributed to the abundant oxygen-containing surface functional groups and efficient surface passivation inherent in the EFB-derived CDs. Such characteristics not only enhance fluorescence emission but also play a crucial role in facilitating photoinduced charge carrier separation during photocatalysis (Jamaludin et al., 2020). Moreover, the high QY observed in this study provides further evidence of the superior photo-response behaviour of the ZnO/CDs composites, as previously discussed in the UV-DRS section. The enhanced QY is indicative of efficient photon utilization, making EFB-derived CDs highly promising for visible-light-driven photocatalytic applications. This underscores the viability of EFB as a green and sustainable carbon source for the development of advanced nanomaterials in environmental remediation.

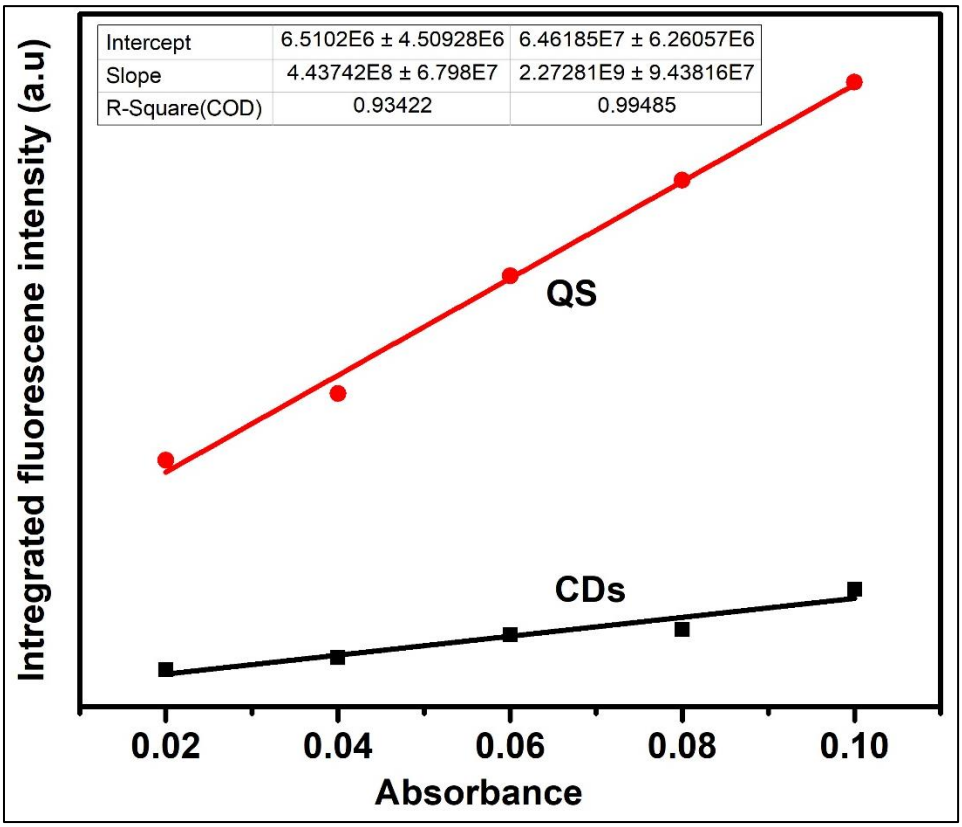

Figure 4.5 The Variation Of The Integrated Fluorescence With Absorbance Of Carbon Dots And Quinine Sulphate.

Table 4.2
Comparison of Fluorescence Quantum Yields of Carbon Dots Synthesized from Different Precursors

Carbon Precursors from waste	**Excitation wavelength (nm)**	**Synthesis Condition**	**Quantum Yield (%)**	**References**
Soybean	340	Hydrothermal treatment at 180 °C for 8 h	25	(Ayu et al., 2023)
Magnolia flower	400	Hydrothermal treatment at 200 °C for 8 h	8.13	(C. Wang et al., 2020)
Onion waste	300 to 425	Acid free hydrothermal extraction method at 250 °C for 6 h	28	(Jamaludin et al., 2020)

Carbon Precursors from waste	Excitation wavelength (nm)	Synthesis Condition	Quantum Yield (%)	References
Dried lemon peels	350	Hydrothermal treatment at 300 °C for 2 h	22.3	(Jayakumar et al., 2024)
Waster carbon paper	360	Hydrothermal treatment at 200 °C for 6 h	8.5	(Jiao et al., 2019)
Orange waste peels	330	Hydrothermal treatment at 200 °C for 6 h	11.37	(Surendran et al., 2020)
Lemon juice	400 to 480 nm	Hydrothermal treatment at 120, 150, 200, 240, and 280 °C for 1-12 h	14.86	(Hoan, Tam, et al., 2019)
Empty Fruit Bunch	370 to 500	Hydrothermal treatment at 200 °C for 2 h	30	This study

4.2.4.3 Photoluminescence spectroscopy

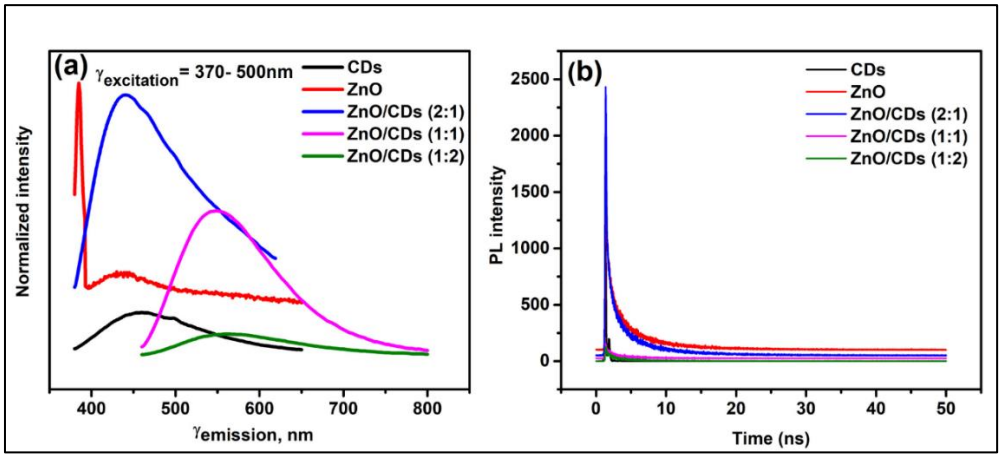

Figure 4.6 (a) The PL Spectra Of ZnO/CDs Composites At Different Excitation Wavelength and (b) TRPL of ZnO Nanoparticles and ZnO/CDs Nanocomposites

Figure 4.6 presents the photoluminescence and time resolved photoluminescence analyses of ZnO, CDs, and ZnO/CDs nanocomposites. These

analyses were performed to evaluate the recombination behaviour and charge carrier lifetime of the synthesized photocatalysts. The PL spectra provide information on radiative recombination and defect related emission, while the TRPL decay profiles provide further insight into the lifetime and transfer behaviour of photogenerated charge carriers. Therefore, PL and TRPL analyses are important to clarify the role of CDs in suppressing recombination, facilitating interfacial electron transfer, and enhancing the photocatalytic performance of ZnO/CDs nanocomposites. Figure 4.6 presents the PL spectra of ZnO, CDs, and ZnO/CDs composites under excitation wavelengths ranging from 370 to 500 nm, with each sample optimized to capture its most prominent emission peaks. Pristine ZnO exhibits a broad PL emission, primarily due to excitonic recombination and defect-related emissions, particularly oxygen vacancies, which promote electron-hole recombination (Shao et al., 2020). Upon incorporating CDs, the PL intensity of ZnO/CDs composites undergoes significant modulation, reflecting changes in surface states and charge carrier dynamics. The ZnO/CDs (2:1) composite exhibits the highest PL intensity, indicating enhanced radiative recombination pathways, likely due to the passivation of ZnO surface defects by CDs. In contrast, the ZnO/CDs (1:2) composite displays the lowest PL intensity, suggesting efficient charge separation and suppressed recombination, which aligns with the electron-trapping role of CDs (Xu et al., 2023). This suppression indicates that CDs facilitate charge transfer, minimizing electron-hole pair recombination and enhancing photocatalytic performance.

A distinct trend in PL intensity is observed across the different ZnO/CDs nanocomposites ratios. The initial increase in PL intensity for ZnO/CDs (2:1) nanocomposites is attributed to defect passivation, which enhances radiative recombination (Li et al., 2017). However, as the CDs content increases (ZnO/CDs 1:1 and ZnO/CDs 1:2), PL intensity decreases, suggesting the introduction of non-radiative recombination pathways. This behavior, widely reported in literature, confirms that excess CDs act as electron-trapping sites, leading to fluorescence quenching in ZnO due to efficient charge transfer (Kshirsagar et al., 2006; J. J. Xu et al., 2023).Furthermore, the observed shifts in emission peaks reinforce the hypothesis that CDs modify the electronic states of ZnO, thereby influencing its optical and charge recombination properties. The shift in PL maxima between pristine ZnO and ZnO/CDs composites suggests strong electronic interactions, altering the charge carrier recombination dynamics (Wan Ishak, et al., 2025). These findings highlight the role of CDs in tailoring

ZnO's optical behavior and charge carrier kinetics, which are critical for enhancing its photocatalytic efficiency. The optimized ZnO/CDs ratio balances charge separation and recombination, making it a promising material for photocatalytic applications. To further elucidate the recombination dynamics of photoinduced charge carriers, time-resolved photoluminescence (TRPL) measurements were conducted on ZnO nanoparticles and ZnO/CDs (1:2) composites, as depicted in Figure 4.6b. The TRPL decay profiles were accurately fitted using a triexponential function (Samanta et al., 2019). The emission lifetimes (τ) were determined as τ_1, τ_2, and τ_3, corresponding to radiative recombination of electron-hole pairs and nonradiative recombination via electron trapping and transfer processes, respectively. The calculated average lifetime, τavg, decreased from 4.198 ns for pristine ZnO to 2.084 ns for ZnO/CDs (1:2). This lifetime reduction indicates that the photogenerated charge carriers in ZnO/CDs (1:2) undergo faster interfacial electron transfer compared with pristine ZnO. In pristine ZnO, the longer lifetime is mainly related to radiative recombination of electron hole pairs and defect mediated relaxation within ZnO. After the incorporation of CDs, the CDs act as electron accepting and electron mediating sites, allowing photogenerated electrons from ZnO to be rapidly extracted and transferred to the CDs surface states.

Therefore, the shorter lifetime of ZnO/CDs (1:2) does not indicate poorer photocatalytic behaviour. Instead, it suggests that non radiative charge transfer pathways become more dominant due to the interfacial interaction between ZnO and CDs. This rapid electron transfer reduces the probability of radiative electron hole recombination in ZnO, which is consistent with the lower PL intensity observed for ZnO/CDs (1:2). The combined PL quenching and shorter TRPL lifetime confirm that CDs facilitate charge separation and increase the availability of photogenerated electrons and holes for reactive oxygen species generation, thereby enhancing tetracycline degradation performance. According to Xu et al., the shortened fluorescence lifetime of ZnO/CDs (1:2) compared to ZnO nanoparticles signifies suppressed charge recombination, attributable to efficient electron transfer facilitated by CDs modification, which is beneficial for charge separation (Jiang et al., 2017; Zeng et al., 2018).

Table 4.3
TRPL Decay Rate Of Zno Nanoparticles and ZnO/CDs Composites

Sample	τ_1 (ns)	B_1 (%)	τ_2 (ns)	B_2 (%)	τ_3 (ns)	B_3 (%)	τ_{avg} (ns)
CDs	0.0456	0.096	1.142	0.002	4.416	0.001	2.013
ZnO	0.149	0.009	1.657	0.002	6.370	0.001	4.198
ZnO/CDs (2:1)	0.0931	0.020	1.367	0.003	5.999	0.001	3.492
ZnO/CDs (1:1)	0.146	0.072	2.467	0.007	9.209	0.001	3.485
ZnO/CDs (1:2)	0.177	0.017	3.317	0.491	3.3176	0.489	2.084

4.2.5 X-ray Photoelectron Spectroscopy (XPS)

To further investigate the surface chemical composition and confirm the presence of functional groups responsible for the enhanced quantum yield, X-ray Photoelectron Spectroscopy (XPS) analysis was performed. The XPS spectra of the CDs (Figure 4.7a) revealed prominent peaks corresponding to carbon (C 1s) and oxygen (O 1s), indicating the presence of abundant oxygen-containing functional groups on the surface. The deconvoluted C 1s spectrum exhibited peaks assigned to C–C/C=C, C–O, and C=O bonds, while the O 1s spectrum displayed peaks related to C=O and C–OH functionalities (Saheeda et al., 2019). These findings validate the existence of diverse surface oxygen species, which are known to facilitate effective surface passivation and contribute to the improved photoluminescence and quantum yield of the CDs. Survey spectra (Figure 4.7(a)) confirmed the presence of expected elements: C, O, and N in CDs; Zn and O in ZnO; and all four elements in the composite, validating the successful incorporation of CDs into the ZnO matrix (Mukherjee et al., 2021). The quantitative atomic concentration obtained from the XPS survey spectrum of ZnO/CDs (1:2) is summarized in Table 4.4. The composite surface consisted mainly of C, O, Zn, and N with atomic concentrations of 69.20%, 24.95%, 3.38%, and 2.47%, respectively. The high carbon content confirms the surface contribution of CDs in the ZnO/CDs composite, while the presence of Zn and O verifies the ZnO component. The detection of N further indicates the presence of nitrogen containing surface functional groups originating from the biomass derived CDs. These atomic concentration results provide additional evidence for the successful incorporation of CDs into the ZnO matrix and support the role of CDs in modifying the surface chemistry of the nanocomposite.

Table 4.4
XPS Atomic Concentration of ZnO/CDs (1:2) Nanocomposite

Element	Peak	Binding energy (eV)	Atomic concentration (%)	Mass concentration (%)
Zn	Zn 2p	1020.149	3.38	24.88
O	O 1s	532.149	24.95	26.86
N	N 1s	399.149	2.47	2.33
C	C 1s	286.149	69.20	55.94

The presence of nitrogen (N) in the CDs is particularly noteworthy, as it plays a crucial role in modulating the electronic structure and emission properties. The nitrogen-related bonding states introduce surface defects and mid-gap states that facilitate radiative recombination, contributing to the observed green fluorescence of the CDs as shown in Figure 4.8(b) (Du et al., 2018; Khan et al., 2017). This green emission is attributed to surface passivation by nitrogen-containing groups, which can enhance quantum yield by reducing non-radiative recombination pathways (Du et al., 2018; Khan et al., 2017).

The Zn 2p region (Figure 4.7(b)) for ZnO nanoparticles exhibits characteristic spin-orbit split peaks at 1021.6 eV (Zn 2p3/2) and 1044.7 eV (Zn 2p1/2), consistent with Zn^{2+} in ZnO (Ayu et al., 2023) . The energy separation of 23.1 eV between these peaks confirms the +2 oxidation state of zinc (Xu et al., 2023). Upon CDs incorporation, these peaks shift to 1020.79 eV (Zn 2p3/2) and 1043.82 eV (Zn 2p1/2) in the composite, a shift of approximately 0.8 eV toward lower binding energies, suggesting a change in the electronic environment of Zn^{2+} due to interaction with the CDs, potentially indicating charge transfer or the formation of Zn-O-C bonds at the interface. In the high-resolution of C 1s spectra (Figure 4.7(c)), there are four peaks observed at 284, 286, 288 and 289 eV for CDs which are corresponding to C=C/C-C, C-N, C=O and O-C=O respectively (Ayu et al., 2023). In the ZnO/CDs (1:2) composite, a new peak at 286.1 eV further confirms the successful incorporation of CDs into the ZnO matrix. For the O 1s spectra of ZnO and ZnO/CDs (1:2) nanocomposites, distinct peaks represent various oxygen species and defects (Figure 4.7(d)). In pristine ZnO, the peak at 531.5 eV corresponds to surface oxygen vacancies (Ovac), while the peaks at 533.7 eV and 530.1 eV are attributed to oxygen in hydroxyl groups (O–H) and lattice oxygen, respectively. In the ZnO/CDs (1:2) composite, shifts in binding energies and variations in peak intensities are observed, reflecting the strong interface interaction between ZnO

and CDs. The peak for oxygen vacancies shifts to 531.8 eV in the composite and shows increased intensity, indicating that the addition of CDs promotes the formation of more oxygen vacancies during the synthesis process (Xu et al., 2023). Oxygen vacancies are known to play a crucial role in photocatalysis by trapping photogenerated electrons and facilitating charge separation (Xu et al., 2023). Additionally, the peaks at 533.1 eV and 532.2 eV in the composite are assigned to hydroxyl oxygen and adsorbed oxygen species, respectively. The higher concentration of oxygen vacancies in ZnO/CDs enhances surface activity, facilitates reactant adsorption, and narrows the band gap, thereby improving light absorption and photocatalytic performance (Xu et al., 2023). These results demonstrate the significant role of CDs in optimizing the structural and surface properties of ZnO. The overall changes in the characteristic's peaks of C 1s, O 1s high-resolution spectra further provides evidence supporting the successful preparation of ZnO/CDs.

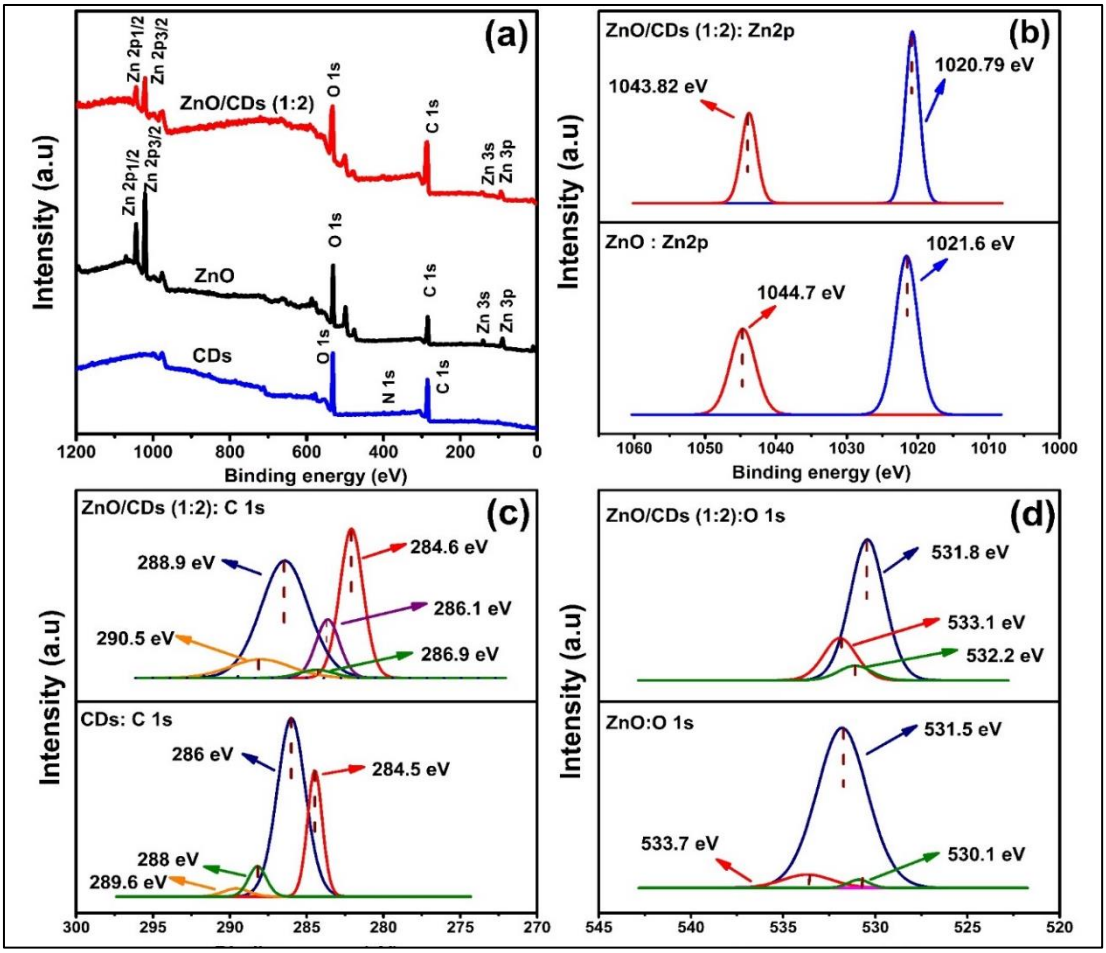

Figure 4.7 XPS Spectra of (a) Survey Scans, (b) Zn 2p Core Level Spectra, (c) C 1s Core Level Spectra, and (d) O 1s Core Level Spectra For ZnO, CDs, and the ZnO/CDs (1:2) composite.

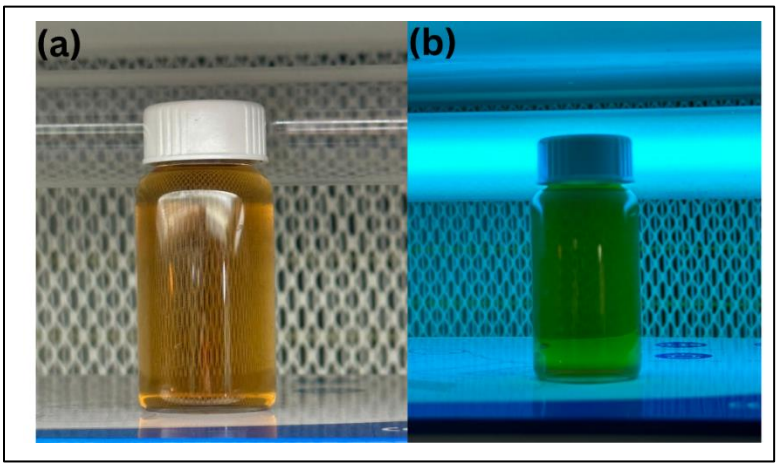

Figure 4.8 Carbon Dots Under (a) Daylight and (b) UV Light

4.2.6 High resolution Transmission Electron Microscopy (HRTEM) and Scanning Electron Microscopy Energy Dispersive (SEM-EDX)

The ZnO/CDs (1:2) nanocomposite was specifically selected for HRTEM analysis based on its superior photocatalytic performance and favorable physicochemical properties. This ratio exhibited the highest degradation efficiency of tetracycline among all tested formulations, suggesting enhanced interfacial charge transfer and reduced recombination. High-Resolution Transmission Electron Microscopy (HRTEM) was employed to investigate the morphology, particle dimensions, lattice structures, and interfacial characteristics of the synthesized ZnO nanoparticles, CDs, and ZnO/CDs (1:2) nanocomposite. The HRTEM analysis revealed that the synthesized ZnO nanoparticles exhibited an irregular needle-like morphology, with widths ranging from 20 to 50 nm and lengths between 100 and 200 nm (Figure 4.10(c)). The observed lattice fringe with a d-spacing of 0.26 nm in the HRTEM image corresponds to the (002) crystallographic plane of hexagonal wurtzite ZnO. This observation is in good agreement with the XRD pattern, which also exhibits a prominent diffraction peak at $2\theta \approx 26.62°$, corresponding to the (002) plane, as indexed by the JCPDS card no. 36-1451. (Figure 4.1).

Meanwhile, CDs exhibited an irregular spherical morphology with particle sizes ranging from 2 to 10 nm, with an average diameter of 4.5 ± 1.1 nm, as shown in Figure 4.9. The presence of CDs was further supported by lattice fringes with a d-spacing of 0.32 nm (Figure 4.10(e)), which is consistent with previous studies. HRTEM images of

the ZnO/CDs (1:2) composite (Figure 4.10(e)) showed that ZnO retained its needle-like morphology, with CDs successfully anchored onto its surface (Figure 4.10 a and b) (Xu et al., 2023). . Additionally, SEM-EDX analysis confirmed the presence of Zn, O, C, and K, indicating the successful integration of ZnO and CDs within the composite (Figure 4.11). The detected carbon (C) originated from the CDs, while zinc (Zn) and oxygen (O) validated the ZnO phase. The trace presence of potassium (K) likely resulted from the biomass precursor, further supporting the sustainability of the synthesis approach. Furthermore, the Selected area electron diffraction (SAED) pattern (Figure 4.10(d)) displayed concentric diffraction rings, indicating the polycrystalline nature of the ZnO/CDs nanocomposite (Mukherjee et al., 2021). The indexed diffraction rings corresponded to the hexagonal wurtzite structure of ZnO, consistent with JCPDS card no. 36-1451. These HRTEM findings provide direct structural evidence supporting the improved photocatalytic performance of the ZnO/CDs (1:2) nanocomposite. The retention of ZnO needle like morphology provides an elongated structure that can facilitate charge transport and expose reactive surface sites for tetracycline degradation (Mukherjee et al., 2021). The successful anchoring of CDs on the ZnO surface creates intimate interfacial contact between both components, which is essential for electron transfer from photoexcited ZnO to CDs (Xu et al., 2023). This interfacial coupling can suppress electron hole recombination and increase the availability of photogenerated charge carriers for reactive oxygen species generation (Jamaludin et al., 2020) . In addition, the small size and good dispersion of CDs on ZnO improve surface interaction and light harvesting, while the graphitic domains indicated by the 0.32 nm lattice spacing can act as electron accepting or electron mediating sites (Jamaludin et al., 2020). Therefore, the HRTEM results support the proposed role of CDs in enhancing charge separation, improving interfacial electron transport, and increasing photocatalytic tetracycline degradation efficiency.

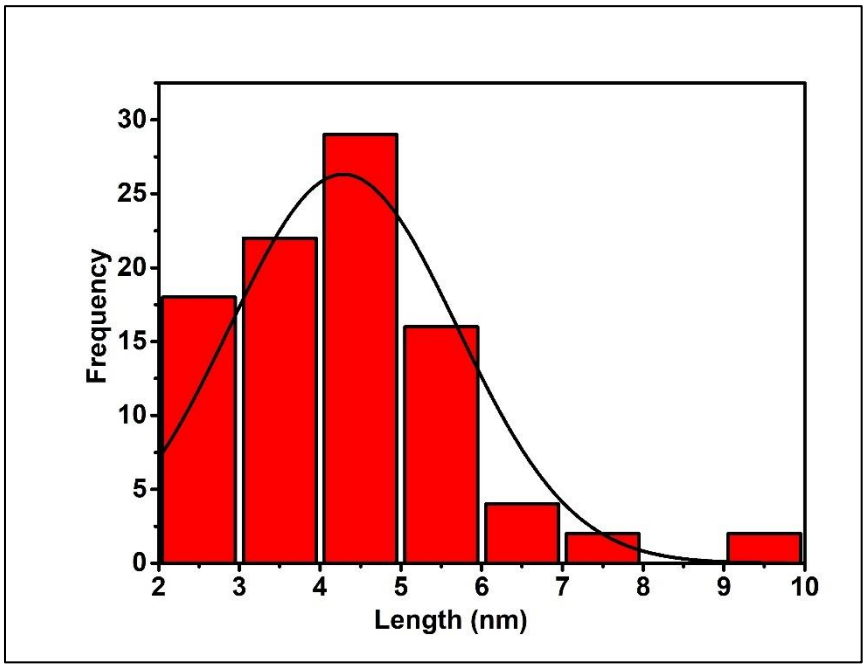

Figure 4.9 Particle Distribution Of Carbon Dots

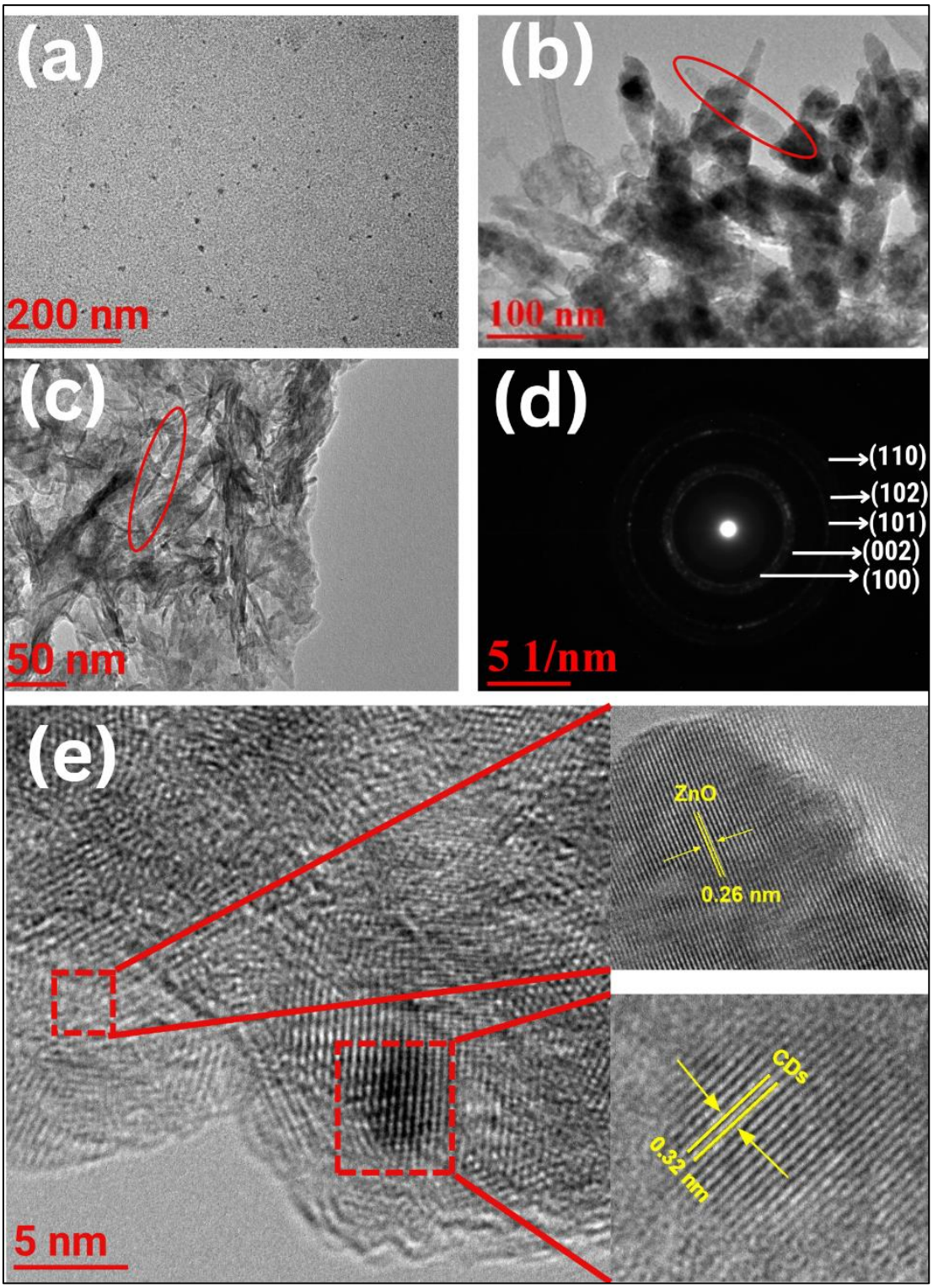

Figure 4.10 HRTEM Images (a) CDs, (b) ZnO, (c) ZnO/CDs (1:2); (d) SAED Patterns Of ZnO/CDs and (e) Lattice Fringes From HRTEM Analysis Of ZnO/CDs Nanocomposite

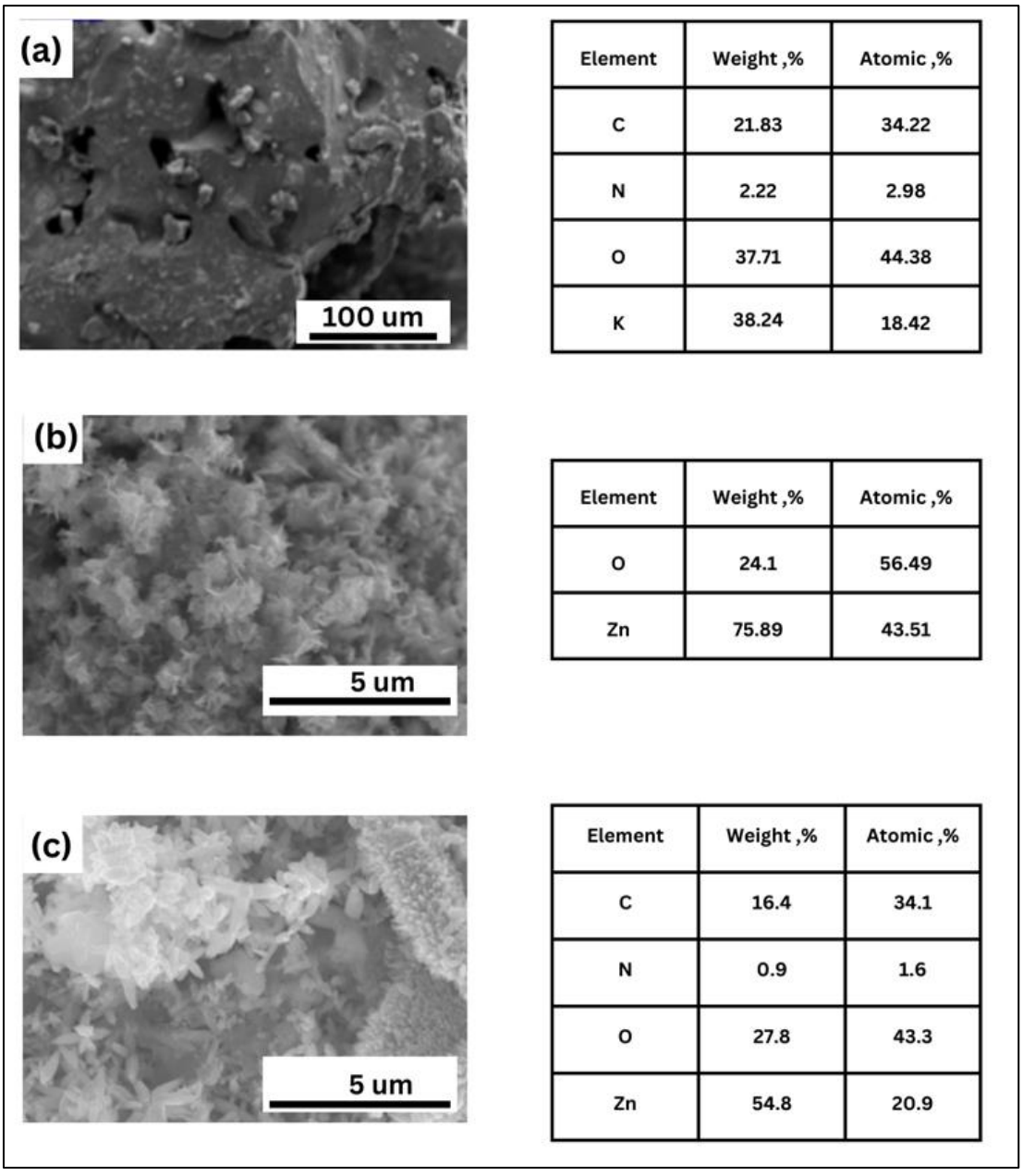

Element	Weight ,%	Atomic ,%
C	21.83	34.22
N	2.22	2.98
O	37.71	44.38
K	38.24	18.42

Element	Weight ,%	Atomic ,%
O	24.1	56.49
Zn	75.89	43.51

Element	Weight ,%	Atomic ,%
C	16.4	34.1
N	0.9	1.6
O	27.8	43.3
Zn	54.8	20.9

Figure 4.11 SEM Images And Elemental Analysis Results of (a) CDs, (b) ZnO Nanoparticles, and (c) ZnO/CDs Nanocomposites

The possible chemical interaction between ZnO and CDs was further supported by FTIR and XPS analyses. FTIR showed the presence of oxygen containing functional groups, such as O–H, C=O, and C–O, on the CDs surface, which can interact with ZnO through surface coordination or interfacial bonding. In the ZnO/CDs nanocomposite, the interaction between ZnO and CDs is likely formed through Zn–O–C interfacial linkages or coordination between Zn^{2+} sites and oxygenated functional groups on CDs. However, since no direct structural evidence of substitution into the ZnO lattice was

observed from XRD, the interaction is more appropriately interpreted as surface chemical coupling or interfacial coordination rather than bulk lattice incorporation.

4.3 Photoelectrochemical studies

Cyclic voltammetry (CV) and electrochemical impedance spectroscopy (EIS) were employed to investigate the charge transfer behavior of the synthesized catalysts. CV measurements were conducted using a UV lamp as the light source and a scan rate of 100 mV/s. A higher oxidation-reduction reaction (ORR) peak current in the CV spectrum generally indicates a higher charge transfer efficiency (Figure 4.12a). The CDs exhibited minimal current response, consistent with their role as charge mediators rather than active redox participants. ZnO displayed moderate redox activity with broad peaks, reflecting limited electron transfer kinetics due to charge carrier recombination (Nugroho et al., 2024). In contrast, the ZnO/CDs nanocomposites exhibited significantly enhanced current densities and well-defined redox peaks, attributed to the synergistic interaction between ZnO and CDs, where the latter facilitated efficient charge separation and suppressed recombination. At 0.2 V, the current density of the ZnO/CDs (1:2) composite is approximately 2.5 times higher than that of pristine ZnO. This significant increase in current density suggests that the ZnO/CDs (1:2) composite possesses a higher electron transfer efficiency compared to the other ratios (Figure 4.12a).

This enhanced efficiency could be attributed to the optimal distribution of CDs within the ZnO matrix at this specific ratio, facilitating efficient electron transport. Meanwhile, for EIS, the Nyquist plots (Figure 4.12b) reveal that pristine ZnO exhibits the highest impedance, evidenced by the largest semicircle, which is consistent with its known poor electrical conductivity (Xu et al., 2023). The incorporation of CDs into the ZnO matrix leads to a significant reduction in charge transfer resistance, indicating an improvement in electrical conductivity and a facilitation of efficient charge separation. Notably, the ZnO/CDs (1:2) composite demonstrates the smallest semicircle among all the tested materials, signifying the lowest resistance and, consequently, the most efficient charge transport properties. This observed enhancement in charge transport is attributed to the synergistic effect of the incorporated CDs. The CDs introduce highly conductive pathways within the composite structure, effectively enhancing electron mobility and reducing the overall resistance to charge transfer. This improvement in

conductivity and charge transport aligns with the findings from the CV analysis and further supports the conclusion that the ZnO/CDs (1:2) composite possesses superior photocatalysis performance. To further investigate the photoresponse behavior of ZnO, CDs, and ZnO/CDs composites with different ratios, transient photocurrent response (I-t) were conducted under periodic light on/off cycles, as shown in Figure 4.12c. Pristine ZnO exhibits the lowest photocurrent response due to rapid charge carrier recombination and limited light absorption (Fu et al., 2018). The incorporation of CDs significantly enhances the photocurrent, indicating improved charge separation and transport. Among the composites, ZnO/CDs (1:2) demonstrates the highest and most stable photocurrent response, suggesting superior photogenerated charge carrier dynamics facilitated by CDs, which act as electron acceptors and promote efficient charge transfer (Xu et al., 2023). The repetitive and consistent photocurrent cycles confirm the excellent photostability of the materials.

4.3.1 Energy band structure

The Mott-Schottky analysis confirmed the n-type semiconducting behavior of all materials, with ZnO exhibiting the highest carrier concentration, followed by the ZnO/CDs composite and CDs, as shown in Figure 4.12d-f. The flat band potentials (Efb) were determined as 0.3 V (CDs), -1.52 V (ZnO), and -1.2 V (ZnO/CDs) (vs. Ag/AgCl). After conversion to the NHE scale, the corresponding conduction band (CB) edge positions were 0.497 V (CDs), -1.323 V (ZnO), and -1.003 V (ZnO/CDs), while the valence band (VB) positions were 4.997 V, 1.947 V, and 1.987 V (vs. NHE), respectively. The significant shift in E_{fb} for ZnO/CDs suggests a Z-scheme charge transfer mechanism, where electrons from the CDs CB recombine with holes from the ZnO VB, preserving the highly reduced electrons in ZnO CB and the strongly oxidizing holes in CDs VB. This charge separation facilitates the generation of superoxide radicals (O_2^-) and hydroxyl radicals (•OH), as confirmed by scavenger experiments, which showed reduced photocatalytic activity upon radical inhibition. Further validation was obtained from photoluminescence (PL) quenching, extended carrier lifetime (TRPL), lower charge transfer resistance (EIS), and enhanced photocurrent response, all of which indicate suppressed charge recombination and improved charge mobility. These findings collectively confirm an efficient Z-scheme mechanism,

enabling superior photocatalytic activity for the ZnO/CDs composite in environmental remediation applications.

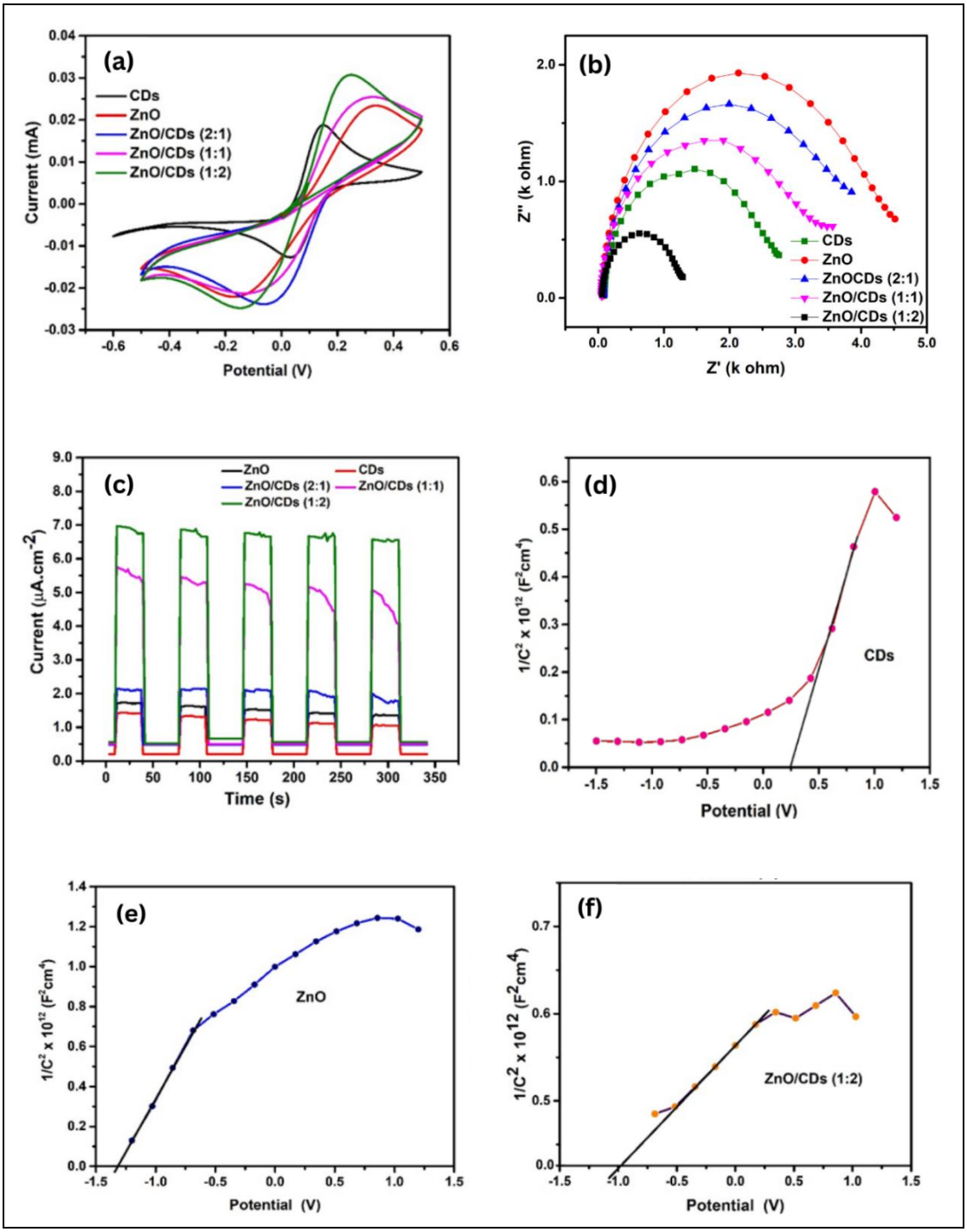

Figure 4.12 Electrochemical Characterization Of ZnO, CDs, and ZnO/CDs Composites (2:1, 1:1, 1:2) (a) Cyclic Voltammetry. (b) Nyquist Plots. (c) Photocurrent Response. (d-f) Mott-Schottky Plots For (d) CDs, (e) ZnO, and (f) ZnO/CD Composites

4.4 Trapping experiment

Radical quenching experiments were conducted to investigate the predominant active species in ZnO/CDs nanocomposites. Compounds Ethylenediamine tetraacetic acid disodium salt (EDTA-2Na), silver nitrate ($AgNO_3$), p-benzoquinone (PBQ), and tert-butanol (BuOH) were introduced to TC solution as a scavenger for protons (h+), electrons (e−), superoxide radicals ($\bullet O_2^-$), and for hydroxyl radicals (•OH) respectively (Ramezanalizadeh & Rafiee, 2021). As displayed in Figure 4.13, BuOH exhibited the strongest restraint effect, which was followed by PBQ. The addition of $AgNO_3$ gives subtle changes in the degradation efficiency of TC, which means only a small portion of the electrons participated in the photodegradation processes. However, the use of n-BuOH or PBQ as scavengers for •OH or ($\bullet O^{2-}$), respectively, clearly hampered the rate of degradation, which indicates that •OH and ($\bullet O^{2-}$) are the main active species in the photodegradation system when irradiated with light. This charge separation facilitates the generation of superoxide radicals (O_2^-) and hydroxyl radicals (•OH), as confirmed by scavenger experiments, which showed reduced photocatalytic activity upon radical inhibition. These findings collectively confirm an efficient Z-scheme mechanism (Figure 4.14), enabling superior photocatalytic activity for the ZnO/CDs composite in environmental remediation applications.

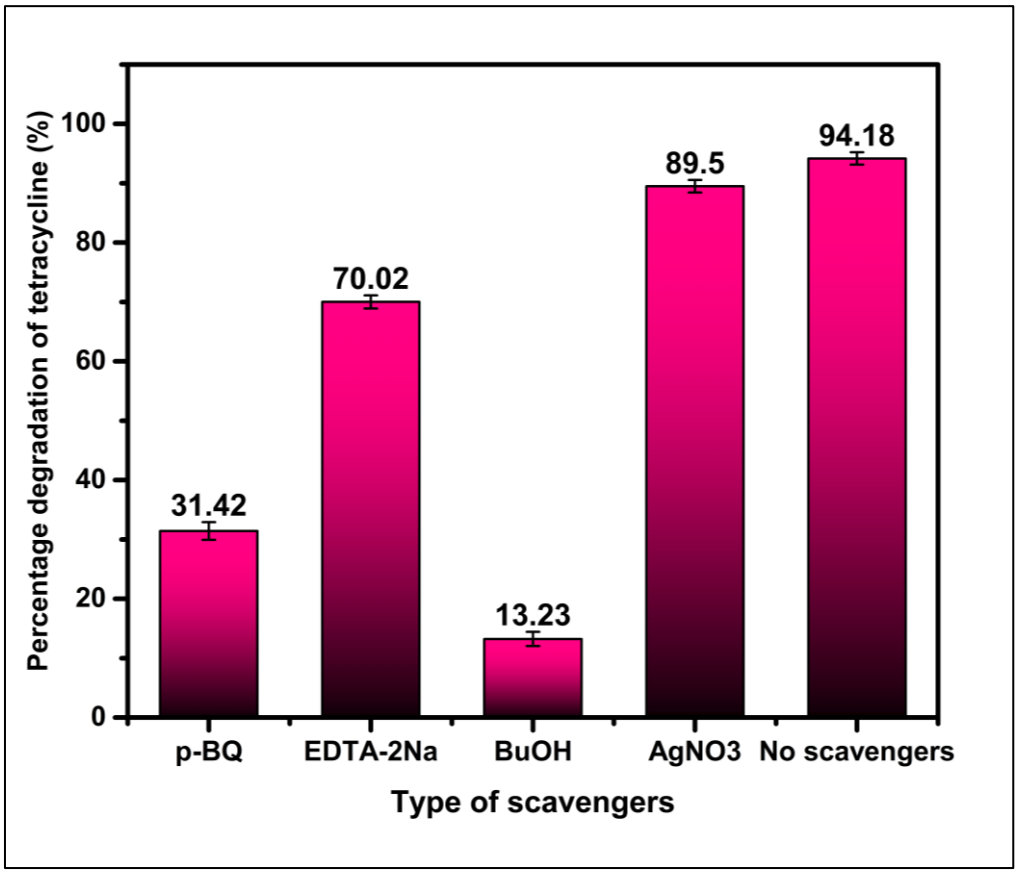

Figure 4.13 Scavenger Effects On TC degradation

4.4.1 Possible Insights into the Photocatalytic Mechanism of ZnO/CDs Nanocomposites

Upon illumination, both ZnO and carbon dots absorb photons, leading to the excitation of electrons from the valence band (VB) to the conduction band (CB), generating electron-hole pairs in both semiconductors. The Z-scheme charge transfer mechanism facilitates the recombination of photogenerated electrons in the CB of CDs with holes in the VB of ZnO. This selective recombination process ensures that the ZnO CB retains highly energetic electrons with strong reducing capability, while the CDs of VB preserves holes with potent oxidative power. Consequently, this spatial charge separation minimizes charge carrier recombination losses and enhances redox reactions, thereby improving the photocatalytic efficiency of the composite. The preserved electrons in the CB of ZnO possess sufficient reducing power to react with adsorbed oxygen molecules, generating superoxide radicals ($\cdot O_2^-$). These radicals further undergo secondary reactions to form hydroxyl radicals (·OH), which exhibit strong oxidation

potential and play a critical role in the degradation of organic pollutants. Meanwhile, the holes retained in the VB of CDs participate in the oxidation of hydroxyl groups or water molecules, generating additional hydroxyl radicals that further contribute to the degradation process. This dual-pathway generation of reactive oxygen species (ROS) enhances the degradation efficiency, leading to the effective breakdown of contaminants into harmless mineralized products. The synergistic charge transfer and ROS generation within the ZnO/CDs composite contribute to its superior photocatalytic activity compared to pristine ZnO. The efficient utilization of charge carriers not only facilitates rapid redox reactions but also ensures sustained photocatalytic performance. The Z-scheme heterojunction plays a pivotal role in extending the charge carrier lifetime, suppressing electron-hole recombination, and promoting the selective participation of charge carriers in oxidation-reduction reactions. The overall mechanism is governed by the following reactions:

$$\mathrm{CD_s} + h\nu \rightarrow \mathrm{e^-_{CB,CDs}} + \mathrm{h^+_{VB,CDs}} \tag{4.5}$$

$$\mathrm{ZnO} + h\nu \rightarrow \mathrm{e^-_{CB,ZnO}} + \mathrm{h^+_{VB,ZnO}} \tag{4.6}$$

$$\mathrm{e^-_{CB,CDs}} + \mathrm{h^+_{VB,CDs}} \rightarrow \mathrm{recombination} \tag{4.7}$$

$$\mathrm{H_2O} + \mathrm{h^+_{VB,CDs}} \rightarrow \cdot\mathrm{OH} + \mathrm{H^+} \tag{4.8}$$

$$\mathrm{OH^-} + \mathrm{h^+_{VB,CDs}} \rightarrow \cdot\mathrm{OH} \tag{4.9}$$

By leveraging this Z-scheme mechanism, the ZnO/CDs composite efficiently facilitates charge separation and enhances ROS generation, ultimately leading to improved photocatalytic degradation of organic contaminants.

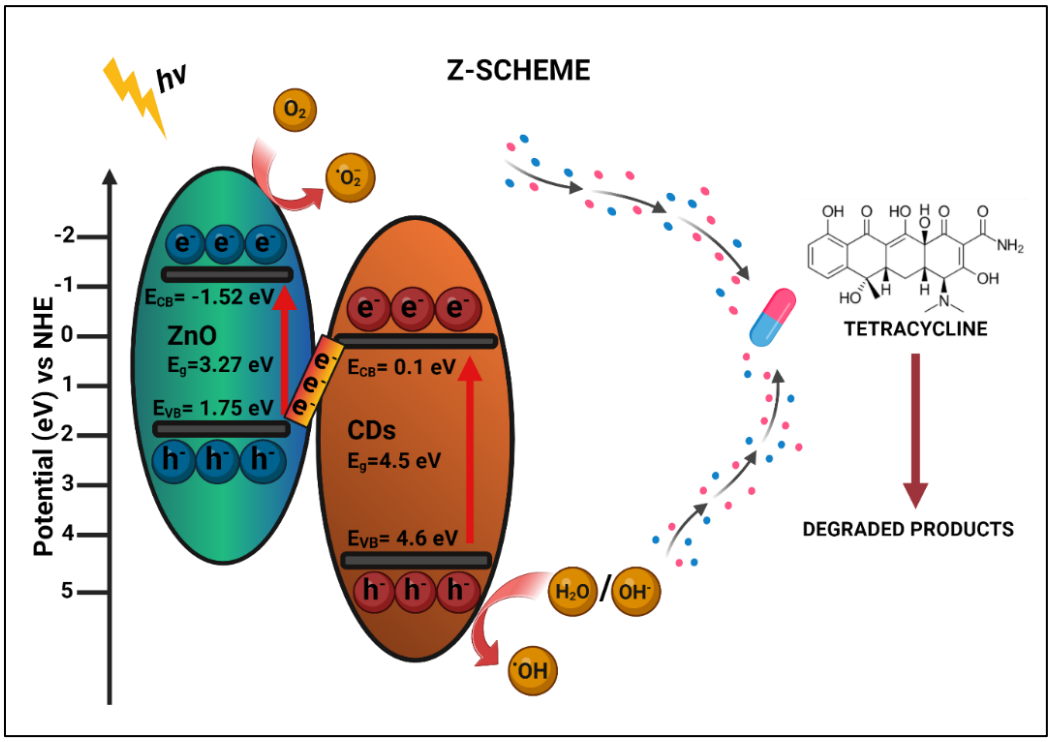

Figure 4.14 Z-Scheme Charge Transfer Mechanism Of ZnO/CDs Nanocomposite For Tetracycline Photodegradation.

4.4.2 TC degradation pathways

Table 4.5
Structural Information Of Possible Intermediate Products Identified By LCMS

Formula	m/z	Proposed structures	Refs
$C_{22}H_{24}N_2O_8$	445	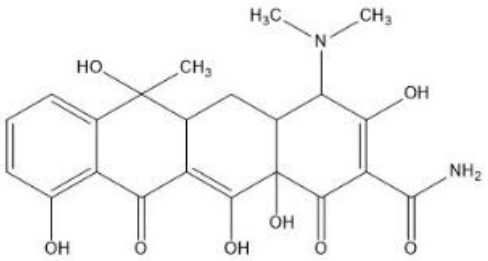	(Fernández et al., 2019)
$C_{22}H_{26}N_2O_9$	461	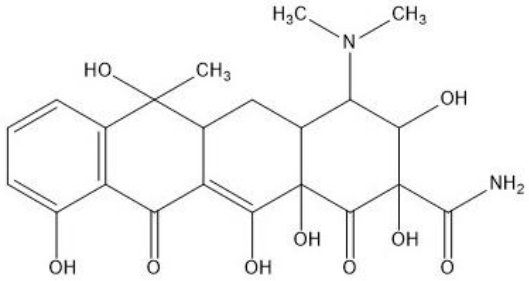	(Jia et al., 2023)

Formula	m/z	Proposed structures	Refs
$C_{23}H_{25}NO_8$	442	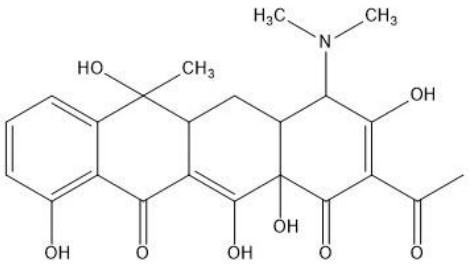	(Guo et al., 2020)
$C_{21}H_{22}N_2O_8$	430	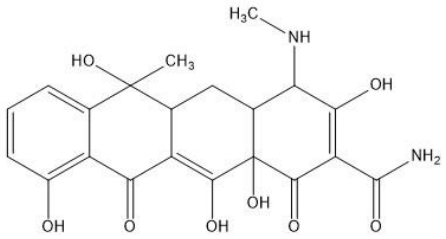	(Fernández et al., 2019)
$C_{15}H_{18}O_5$	278	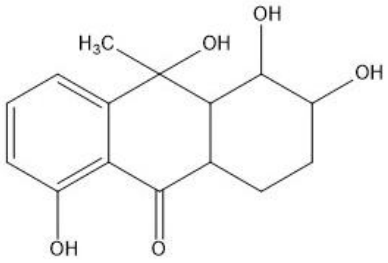	(Okab & Alwared, 2023)
$C_{14}H_{14}O_3$	230	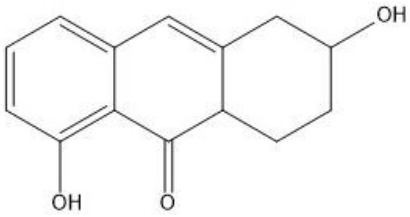	(Niu et al., 2013)
$C_9H_{10}O_2$	150	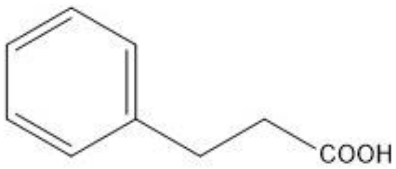	(Hussein Abdurahman et al., 2022)

The proposed photocatalytic degradation pathway of TC (Table 4.5 and Table 4.6) over the ZnO/Carbon Dots nanocomposite was developed based on LC-MS analysis of degradation intermediates and theoretical predictions of reactive molecular sites (Figure 4.15). The photocatalytic process is initiated by the conversion of the parent TC molecule (TC, *m/z* 445) into two primary intermediates. The first intermediate (*m/z* 430) is presumed to originate from demethylation or oxidative decarboxylation, reflecting the loss of a methylene group ($–CH_2$) (Xie et al., 2018). The second intermediate (*m/z* 461) likely results from the incorporation of an oxygen atom, possibly due to hydroxylation or epoxidation reactions facilitated by reactive oxygen species (ROS), particularly hydroxyl radicals (•OH) and superoxide ions ($O_2•^-$) generated during the photocatalytic process. These initial transformations are followed by the emergence of a new intermediate (*m/z* 442), which may result from concurrent demethylation and oxidation, likely involving the removal of a methyl group ($–CH_3$) and the formation of a carbonyl functional group (C=O) (Jia et al., 2023). Subsequently, the intermediate at m/z 430 undergoes further degradation to form m/z 395, which is attributed to the cleavage of the amide bond ($–CONH_2$) alongside additional demethylation, a degradation route commonly associated with advanced oxidation processes. Deeper fragmentation is evident with the detection of *m/z 278*, which points to the breakdown of aromatic rings likely initiated by hydroxyl radical attack, leading to ring-opening reactions (Guo et al., 2020). The subsequent formation of m/z 230 indicates continued oxidative disintegration of the molecular backbone. A smaller fragment at m/z 150, tentatively identified as a benzoic acid derivative, appears at later stages of the reaction and is presumed to be produced through combined hydroxylation and decarboxylation reactions. With extended irradiation, these intermediates are expected to be further decomposed into mineral end-products such as CO_2 and H_2O (Hussein Abdurahman et al., 2022). This mechanistic pathway provides insight into the stepwise degradation of TC and demonstrates the capability of the ZnO/CDs nanocomposite to facilitate deep oxidation, effectively converting complex antibiotic molecules into simpler and less harmful species. Such findings support its potential application in advanced photocatalytic treatment of pharmaceutical-contaminated wastewater.

Table 4.6
Summary Of Tetracycline Photocatalytic Degradation Intermediates And Pathways

m/z Value	Proposed Reaction(s)	Transformation Description
445	–	Parent compound (Tetracycline)
430	Oxidative decarboxylation / demethylation	Loss of $–CH_2$ group
461	Hydroxylation / epoxidation	Addition of oxygen atom
442	Demethylation + oxidation	Loss of $–CH_3$ and keto group formation
395	Amide cleavage + demethylation	Loss of $–CH_3$ and $–CONH_2$
278	Hydroxyl radical attack / ring opening	Major structural fragmentation
230	Oxidative bond scission	Core skeleton breakdown
150	Hydroxylation + decarboxylation	Formation of benzoic acid derivative
-	Final mineralization	CO_2 and H_2O generation

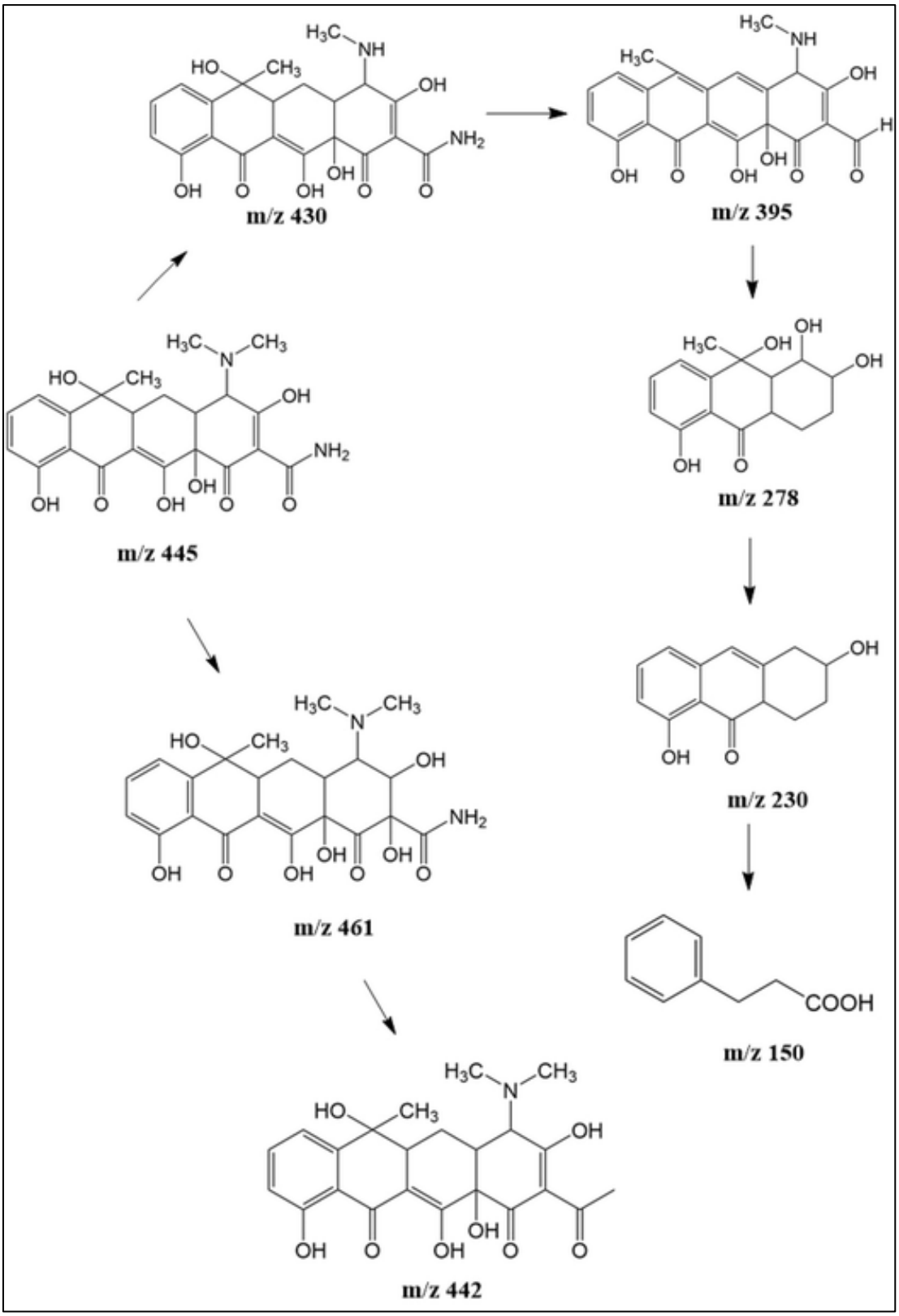

Figure 4.15 The Intermediates Product Of TC Degradation

4.5 Photodegradation of tetracycline

4.5.1 Effect dosage of photocatalyst

The effect of photocatalyst dosage on the photocatalytic degradation of ZnO/CDs (1 g/L) was investigated at pH 7 with varying dosages as shown in Figure 4.16. Among the different ZnO/CDs ratios, the 1:2 ratio exhibited the highest photodegradation performance under UV light irradiation, achieving an 82.87% removal rate at the optimal dosage of 1 g/L (Figure 4.16a). This optimal dosage ensures enough active sites available for the photocatalytic reaction, which is crucial for effective contaminant degradation. At the 1:2 ratio, the CDs enhance the photocatalytic activity by improving light absorption and facilitating the separation of electron-hole pairs in ZnO/CDs, supported by PL analysis in Figure 4.11a showing low recombination rates (Sheikh et al., 2024). Lower dosages may not provide sufficient active sites, thus reduced photocatalytic efficiency. Conversely, higher dosages can cause particle aggregation, which decreases the effective surface area and disrupts the availability of active sites, thus impairing light penetration and overall photocatalytic activity (Karaca et al., 2023). Thus, the optimal dosage maximizes photocatalytic efficiency by providing a balanced concentration of the photocatalyst that maintains an adequate number of active sites while avoiding issues related to insufficient or excessive amounts.

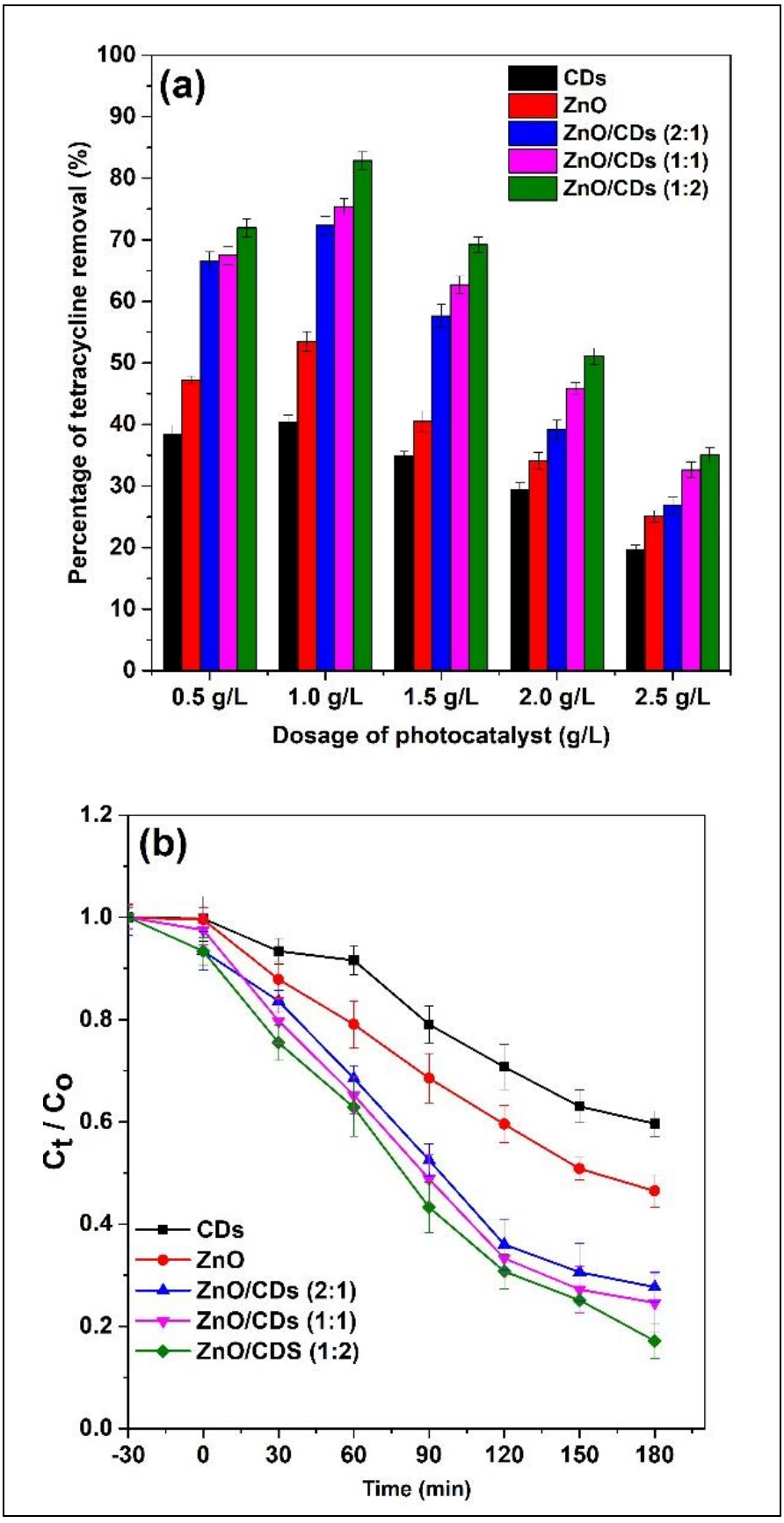

Figure 4.16 Effect Of Photocatalysts Dosage Under UV Light Irradiation Over 180 min At 15 ppm Of TC

4.5.2 Effect concentration of tetracycline

The ZnO/CDs (1:2) composite demonstrated superior photocatalytic degradation of TC, particularly at lower concentrations (5 ppm), achieving a 96.17% removal rate as shown in Figure 4.17a and b. This enhanced performance is attributed to efficient hydroxyl radicals (•OH) generation(Tegenaw et al., 2023). At lower TC concentrations, the available hydroxyl radicals are sufficient to effectively oxidize and degrade TC molecules. However, as the concentration increases (more than 5ppm), the demand for hydroxyl radicals outstrips their supply, resulting in a decrease in degradation efficiency. Time-dependent studies confirmed the significant role of light in activating the ZnO/CDs photocatalyst and generating hydroxyl radicals. The ZnO/CDs (1:2) composite's optimal composition facilitates efficient light absorption and charge separation, ensuring a steady supply of hydroxyl radicals for effective TC degradation. These findings corroborate previous work by Tegenaw et al., who reported a 98.4% higher removal rate of dye at lower concentrations using ZnO/CDs nanocomposites as photocatalysts (Tegenaw et al., 2023).

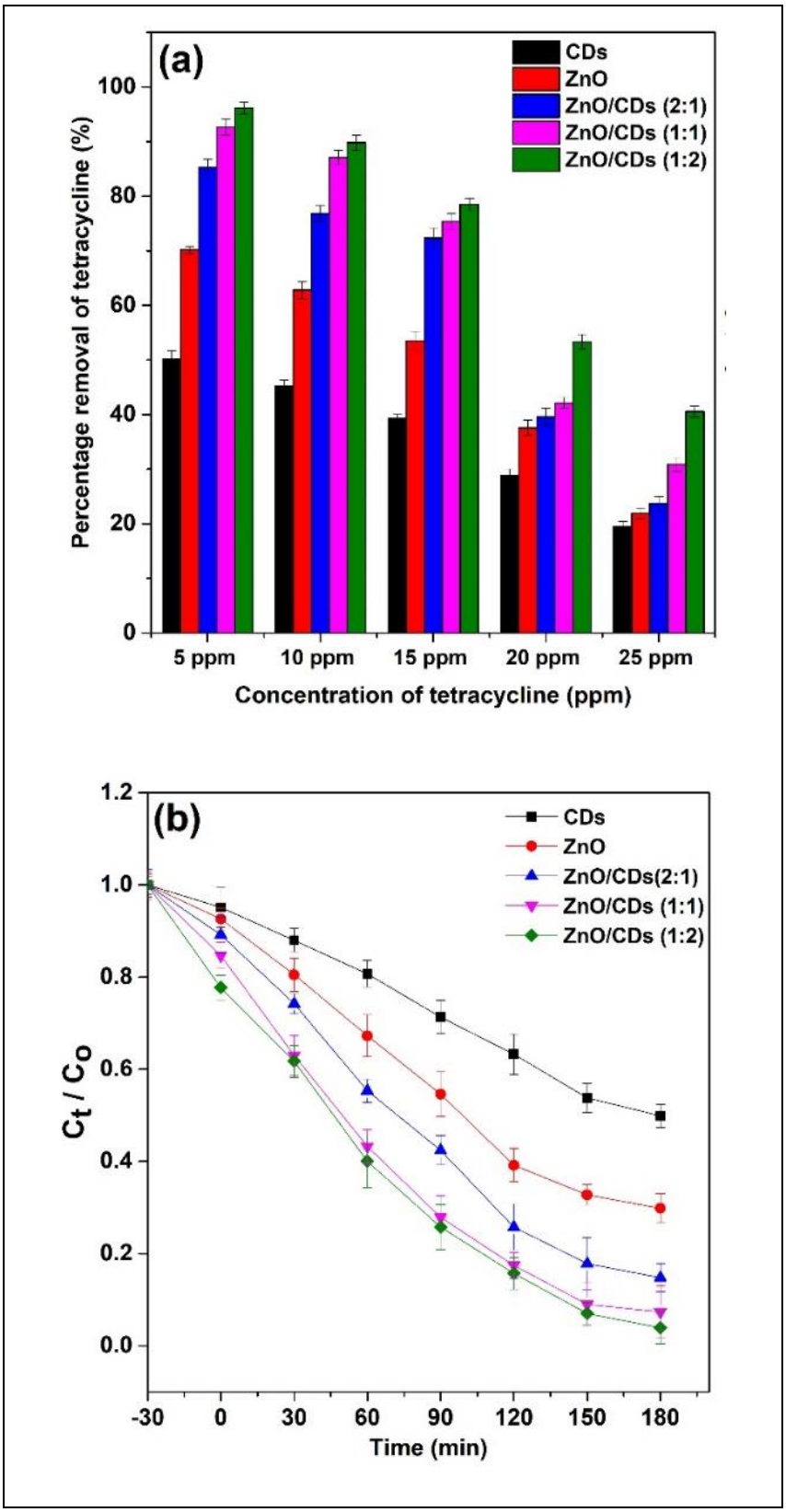

Figure 4.17 Effect of TC Concentration Under UV Light Irradiation Over 180 min at 1 g/L Of Photocatalyst

4.5.3 Effect of different source of light

The varying photocatalytic performance of ZnO/CDs nanocomposites under different light sources such as UV, visible, and sunlight can be attributed to the light absorption properties and charge separation efficiency of the materials. Under UV light, ZnO, with its wide bandgap (~3.27 eV), absorbs efficiently, generating electron-hole pairs that contribute to high degradation efficiency (Figure 4.18a). A higher ratio of CDs to ZnO enhances this process by acting as electron sinks, preventing recombination and leading to better performance. However, under visible light, where ZnO has limited absorption, CDs play a more critical role by absorbing visible light and transferring the resulting photoinduced electrons to ZnO, significantly boosting photocatalytic activity, as seen with the 86.87% efficiency for the ZnO/CDs (1:2) ratio. In contrast, a lower CDs to ZnO content reduces visible light absorption and hinders charge separation, resulting in lower performance of 31.55% as illustrated in Figure 4.18a. The performance under sunlight, which contains both UV and visible light components, is influenced by the interplay between ZnO's UV absorption and the visible light contribution of carbon dots', achieving an efficiency of 58.74% for 2:1 ratio. These findings are consistent with studies by Zhang et al. (2015) and Liu et al. (2016), which highlight the synergistic effects of ZnO and CDs across different wavelengths. Optimal ZnO/CDs ratios were shown to enhance the photocatalytic performance under both solar and visible light conditions. The photocatalytic efficiency of ZnO/CDs nanocomposites varies under different illumination conditions UV, visible, and sunlight due to their distinct light-harvesting capabilities and charge carrier dynamics. Under UV irradiation, ZnO (bandgap ~3.27 eV) exhibits strong photon absorption, generating electron-hole pairs that drive photocatalysis. The incorporation of CDs enhances this process by serving as electron acceptors, promoting charge separation, and suppressing recombination, thereby augmenting the overall degradation efficiency. The increasing CDs content further improves charge carrier dynamics, with the ZnO/CDs (1:2) exhibiting the highest photocatalytic activity. Under visible light, ZnO alone demonstrates minimal activity due to its wide bandgap, which limits direct excitation. However, CDs function as visible-light sensitizers, effectively absorbing photons and facilitating charge transfer processes. Given that the conduction band edge of CDs is positioned more positively than that of ZnO, direct electron injection into ZnO is unlikely. Instead, CDs promote photocatalysis through alternative mechanisms, such as

facilitating interfacial charge transfer or generating reactive oxygen species (ROS). The superior photocatalytic performance observed for the 1:2 ZnO/CDs ratio (86.87% degradation) underscores the pivotal role of CDs in extending light absorption and enhancing charge dynamics. Conversely, a lower CDs content diminishes visible-light absorption, leading to a significant reduction in photocatalytic efficiency (31.55%).Under natural sunlight, which comprises both UV and visible components, a synergistic enhancement is observed. ZnO primarily absorbs the UV fraction, generating electron-hole pairs, while CDs harness the visible spectrum, facilitating additional charge separation and ROS formation. The optimal 1:2 ZnO/CDs composite achieves the highest degradation efficiency by leveraging both ZnO's intrinsic UV activity and CDs' extended visible-light response. In contrast, an excessive ZnO content ZnO/CDs (2:1) results in a lower degradation rate (58.74%), likely due to limited visible-light absorption and suboptimal charge transfer. These findings align with prior studies (Zhang et al., 2015; Liu et al., 2016), which highlight the role of CDs in extending the optical response of ZnO and mitigating charge recombination. Complementary analyses, including electrochemical impedance spectroscopy (EIS), photoluminescence (PL), and time-resolved photoluminescence (TRPL), further substantiate these observations, revealing reduced charge transfer resistance, prolonged carrier lifetimes, and suppressed recombination kinetics in ZnO/CDs composites.The superior light-harvesting capability and enhanced charge carrier dynamics of the optimized ZnO/CDs nanocomposites underscore their potential as highly efficient, solar-driven photocatalysts for environmental remediation (Wan Ishak, Tan, Abu Bakar, Radacsi, et al., 2025).

4.6 Recycling and reusability

"These findings emphasize the excellent stability and reusability of the ZnO/CDs (1:2) photocatalyst, which retained a high degradation efficiency of 88% even after five consecutive cycles (Figure 4.18b). Although a slight decrease from the initial 96% efficiency was observed, the photocatalyst demonstrated remarkable durability with minimal structural changes. XRD analysis (Figure 4.18c) revealed only minor modifications in the catalyst's structure following repeated recycling, likely attributed to surface alterations or slight degradation due to prolonged exposure to the reaction environment. Additionally, HRTEM analysis confirmed the preservation of the

ZnO/CDs heterostructure after multiple cycles, further demonstrating the material's structural integrity (Figure 4.18c). Morphological analysis also showed that the overall structure of the ZnO/CDs catalyst remained unchanged after the reusability test, reinforcing its robustness in long-term applications. These results align with previous studies, which have also reported negligible structural changes in photocatalysts after multiple degradation cycle(J. J. Xu et al., 2023)(Mukherjee et al., 2021). Collectively, these observations highlight the significant potential of ZnO/CDs (1:2) as a highly stable and recyclable photocatalyst for sustainable wastewater treatment.

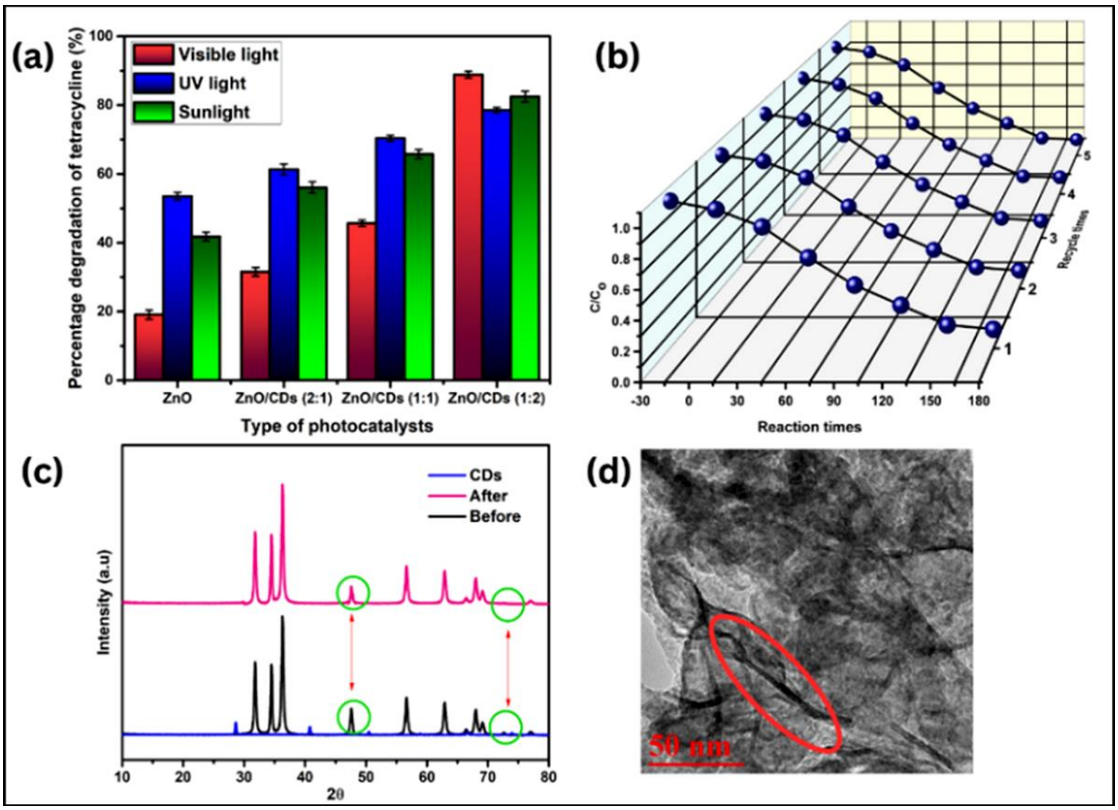

Figure 4.18 (a) Effect Source of Light on TC Degradation; (b) Reusability Test; (c) XRD Pattern and (d) HRTEM Image Of the Recycled ZnO/CDs (1:2)

4.7 Kinetic study for photodegradation of TC

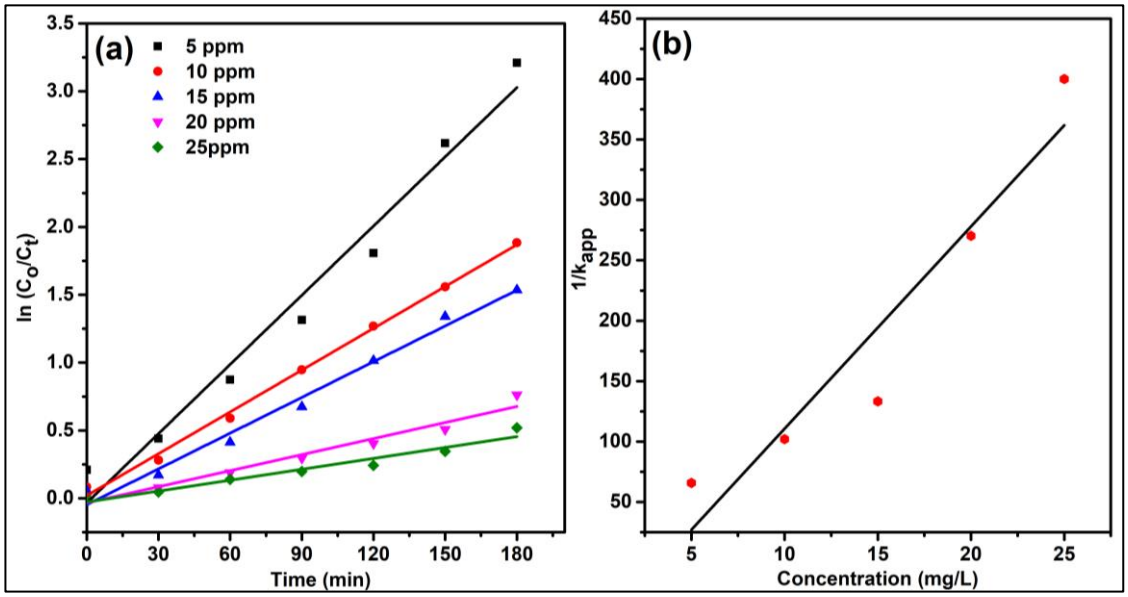

Figure 4.19 Photocatalytic Degradation of Tetracycline (TC) By ZnO/CDs: (a) Pseudo-First-Order Kinetic Plots At Varying Initial TC Concentrations; (b) Dependence Of The Apparent Rate Constant (kapp) On Initial TC Concentration.

Figure 4.19 demonstrates an inverse correlation between the reaction rate constant and initial concentration, indicating that the reaction rate decreases with increasing concentration. At lower concentrations, the reaction proceeds more rapidly, as evidenced by the higher rate constants. However, with the increase in initial TC concentration, the rate constant decreases, which indicates a decrease in the catalytic efficiency of the system (Table 4.7). This may be because of active site saturation or mass transfer limitations (Mukherjee et al., 2021). On the other hand, the half-life, the period of time for the concentration of the reactant to decrease by one half, increased with increasing initial concentration. This observation is in agreement with first order kinetic behaviour, according to which the half-life is inversely proportional to the rate constant. These results indicate that higher pollutant concentrations decrease degradation efficiency, potentially due to system limitations in pollutant utilization,(Mukherjee et al., 2021).

Table 4.7
The Kinetic Parameters at Different TC Concentration

Initial TC concentration (mgL^{-1})	Rate constant k (min^{-1})	Half-life (min)	R^2
5	0.017	40.77	0.9873
10	0.010	69.31	0.9983
15	0.007	99.02	0.9931
20	0.004	173.29	0.9821
25	0.003	231.05	0.9761

The photocatalytic activity of the ZnO/CDs nanocomposite with a reaction rate constant (K_R) of 0.018 mg L^{-1} min^{-1}, exhibits an intermediate rate of pollutant removal, which is attributed to the photocatalytic activity of ZnO and the adsorption enhancement of the CDs, as illustrated in Figure 4.19b. The presence of CDs improves the surface contact and offers additional number of active sites for the reaction, however, other factors like charge transport and photon capture may be suboptimal. The adsorption equilibrium constant (K_{LH}) of 3.399 mg L^{-1} obtained from the Langmuir isotherm indicates an average interaction between the photocatalyst and the pollutant, suggesting that the adsorption is a monolayer adsorption on a homogeneous surface. This effective but reversible adsorption makes it possible to release the degraded products. Furthermore, the equilibrium data obtained using the Langmuir equation and the moderate adsorption and reaction rate indicate that the photocatalytic reaction occurs both at the ZnO/CDs composite surface and within the bulk solution (Syahin et al., 2019). The size of the nanocomposite and the reactive species formed on the catalyst surface generated contribute to pollutant degradation at both the interface and in solution, confirming a synergistic effect between adsorption and photocatalysis. This dual mechanism enhances the performance of the ZnO/CDs nanocomposite, demonstrating its potential for environmental remediation. Notably, ZnO/CDs achieved a 96.12% TC degradation efficiency within 180 min, comparable to or exceeding that of other reported photocatalysts (Table 4.8).

Table 4.8
Performance Evaluation Of Zno/Cds and Other Photocatalytic Materials In The Degradation Of Tetracycline

Photocatalyst	Source of light	Dosage (mg/L)	Concentration (mg/L)	Efficiency (%)	Refs
UiO-66-NDC/P−C_3N_4	500 W of Xe lamp	1000	20	95 in 120 min	(X. Jia et al., 2023)
CQDs/TiO_2	350 W of Xe lamp	300	20	91.5 in 120 min	(Choi et al., 2024)
CN/CQD/ $BiOCl_xBr_{1-x}$	500 W of Xe lamp	100	10	84.5 in 180 min	(Hussein Abdurahman et al., 2022)
CDs-ZSO	300 W Xe lamp	250	10	81.76 in 60 min	(Guo et al., 2020)
MoO_3/g-C_3N_4	350 W Xe lamp	2000	20	88.4 in 240 min	(Xie et al., 2018)
ZnO/CDs	15 W of UVB light	1000	5	96.17 in 180 min	This study

4.8 Economic and Environmental Feasibility of ZnO/CDs Photocatalysis

This study assesses the economic viability of a novel photocatalytic method for the degradation of tetracycline in wastewater using ultraviolet light irradiation in conjunction with recyclable zinc oxide/carbon dots nanocomposites at a 1:2 ratio. The economic feasibility of the proposed pilot-scale photocatalytic process was evaluated (Table 4.9), revealing a total treatment cost of \$7.09/m³ a reduction compared to the \$7.34/m³ reported in a previous study (Demarema et al., 2024). This cost reduction is attributed to process optimization and the incorporation of biomass-derived carbon dots as a sustainable co-catalyst, reducing reliance on expensive precursors. Additionally, the enhanced photocatalytic efficiency of the ZnO/CDs composite lowers operational costs by improving degradation performance. Overall, these findings highlight the scalability and cost-effectiveness of the developed system for the treatment of antibiotic-contaminated wastewater.

Table 4.9
Detailed Cost Analysis Of The Pilot-Scale ZnO/CDs Photocatalytic System For Antibiotic Degradation

Cost Component	**Cost ($)/m^3[a]**
Capital Costs over 10 years	
Photocatalytic Reaction Tank and System[b]	$0.60
UV Light Source	$0.50
Ultrafiltration Unit[b] (McGraw-Hill, 1984)	$0.30
Feed Pump[b]	$0.069
Recycling System	$0.20
Hydrothermal Unit (Carbon dots Synthesis Unit)	$0.27
Total Capital Cost	$1.99
Operational Costs	
Energy Consumption (UV light source: 5 kW, feed pump: 2 kW, filtration: 2 kW, recycling system: 1 kW; $0.10/kWh)[c]	$0.70
Raw Material Cost for Zinc Oxide and Carbon dots [f]	$0.08
Labor Cost [e]	$2.50
Maintenance Cost [d]	$1.20
Waste Disposal Cost	$0.87
Utility Costs	$0.45
Total Operational Cost	$5.10
Total Cost (per m^3)	$7.09

[a]The estimated annual cost of tetracycline (TC) removal is based on a batch wastewater treatment process that operated 10 hr/day, 6 days/week and 50 weeks/year.

[b]The estimated data of equipment is calculated based on data established by Perry of Chemical Engineering Book, (Perry, 2008)

[c]The estimated cost is calculated using the Malaysian tariff rate established by Tenaga Nasional Berhad, (Tenaga Nasional Berhad, 2024)

[d]Based on cost for installation of TC removal using filtration

[e]The estimated cost incorporates 2024 Malaysian labour rates, (Indeed, 2024)

[f]The estimated cost of precursor material for ZnO synthesis is based on prices listed on the Sigma-Aldrich website, (Merck, 2024)

CHAPTER 5
CONCLUSION

5.1 Conclusion

This chapter presents a comprehensive summary of the key findings derived from the synthesis, characterization, and photocatalytic performance evaluation of ZnO nanoparticles decorated with biomass-derived carbon dots. The overarching objective of this study was to develop a green, sustainable, and efficient photocatalyst for the degradation of tetracycline in wastewater, thereby addressing the growing global concern surrounding emerging pharmaceutical contaminants.

Through the successful integration of CDs synthesized via a hydrothermal method from oil palm empty fruit bunch into ZnO, significant enhancements in the photoelectrochemical, optical, structural, and photocatalytic properties of the material were achieved. These results offer valuable insights into the synergistic effects of carbon-based modification on semiconductor photocatalysts and underscore the potential of biomass-derived nanomaterials for sustainable environmental remediation applications.

5.2 Summary of Findings

This study successfully demonstrated the development of a sustainable, high-performance photocatalyst by integrating zinc oxide nanoparticles with biomass-derived carbon dots, synthesized via a simple, low-cost, and environmentally friendly hydrothermal method using empty fruit bunch as the carbon precursor. The key objective was to enhance the photocatalytic degradation efficiency of tetracycline, a representative emerging pharmaceutical contaminant, under UV irradiation, sunlight and visible light conditions.

The synthesized ZnO/CDs nanocomposites were extensively characterized using XRD, FTIR, UV–DRS, FESEM, HRTEM, and electrochemical techniques to understand their structural, optical, and surface properties. The optimal photocatalyst formulation with a ZnO:CDs ratio of 1:2 exhibited outstanding photocatalytic performance, achieving 96.17% degradation of 5 ppm tetracycline under UV light

within 180 minutes. The kinetics followed a pseudo-first-order reaction model, with an apparent rate constant of 0.017 min^{-1} substantially higher than that of pristine ZnO, indicating an effective enhancement in degradation efficiency.

The superior performance of the ZnO/CDs composite is attributed to the formation of a direct Z-scheme heterojunction, wherein the CDs serve dual roles as both visible-light sensitizers and electron mediators. This configuration facilitates spatial separation of photogenerated electrons and holes, thereby suppressing recombination losses. Photoluminescence (PL) analysis supported this mechanism by showing reduced recombination intensity, while photoelectrochemical measurements including cyclic voltammetry (CV), electrochemical impedance spectroscopy (EIS), Mott-Schottky analysis, and transient photocurrent response confirmed improved interfacial conductivity, increased carrier density, and enhanced photocurrent generation.

Further validation of the degradation pathway was achieved through reactive species scavenger studies, which revealed that hydroxyl radicals (•OH) and superoxide anions ($•O_2^-$) played dominant roles in the photodegradation of tetracycline. The incorporation of CDs not only extended the light absorption of ZnO toward the visible region and narrowed its bandgap but also enabled more efficient utilization of solar energy. Band structure analysis indicated that the conduction and valence band positions of ZnO and CDs were suitably aligned to support a Z-scheme electron transfer, thus confirming the proposed mechanism.

In addition to its high efficiency, the ZnO/CDs photocatalyst exhibited excellent recyclability and stability, retaining over 88 % of its activity after five consecutive cycles, with minimal structural deterioration. These outcomes underscore the long-term durability and practical viability of the composite in wastewater treatment applications.

This study not only fulfils the objectives outlined at the beginning of the research but also contributes to the broader field of environmental nanotechnology by offering a scalable, low-cost, and green strategy for water purification. Importantly, it leverages biomass waste an abundant agricultural by-product to produce high-value nanomaterials, supporting the principles of circular economy and contributing directly to Sustainable Development Goal 6 (Clean Water and Sanitation).

5.3 Key Scientific Contributions

i. Successfully synthesized a ZnO/CDs nanocomposite using waste-derived CDs from EFB via a green hydrothermal method.
ii. Demonstrated significant improvement in photocatalytic degradation efficiency of tetracycline under both UV and visible light.
iii. Validated a Z-scheme charge transfer mechanism through comprehensive electrochemical, optical, and band structure analysis.
iv. Provided mechanistic insight into reactive species participation using scavenger experiments.
v. Proved the reusability and long-term stability of the photocatalyst for practical application.
vi. Contributed a novel, sustainable solution for antibiotic removal in wastewater treatment.

5.4 Recommendations for Future Work

Building upon the promising outcomes of this study, several future research directions are proposed to advance both the scientific understanding and practical deployment of the developed ZnO/CDs photocatalyst system. These recommendations are intended to address current limitations, explore wider applications, and move towards scalable and sustainable solutions for wastewater treatment.

Firstly, it is recommended that the photocatalytic performance of the ZnO/CDs nanocomposite be further evaluated using real wastewater samples. While synthetic tetracycline solutions provide a controlled and reproducible environment for performance assessment, they fail to replicate the complexity of actual wastewater matrices, which may contain a wide range of organic and inorganic contaminants, fluctuating pH levels, and competing species. Testing the photocatalyst under such realistic conditions will offer a more accurate evaluation of its efficiency, stability, and adaptability for field applications.

Secondly, expanding the scope of pollutants targeted by the ZnO/CDs system will enhance its environmental relevance and versatility. Future studies should consider the degradation of other common antibiotics such as ciprofloxacin, amoxicillin, or sulfamethoxazole. Additionally, exploring the photocatalyst's performance in treating

multi-component systems comprising various pharmaceuticals, dyes, and heavy metals can provide valuable insights into its selectivity, synergistic effects, and robustness under complex environmental scenarios.

To facilitate industrial-scale application, the design and testing of continuous-flow photoreactor systems are highly recommended. Unlike batch reactors commonly used in laboratory-scale studies, continuous-flow systems better simulate operational conditions in wastewater treatment facilities. Such systems allow for improved control over hydraulic retention time, catalyst reusability, and overall treatment capacity. Moreover, to enhance catalyst stability and ease of recovery, the incorporation of ZnO/CDs into a photocatalytic membrane should be investigated. Embedding the nanocomposite into polymeric or ceramic membrane matrices may enable simultaneous pollutant filtration and photodegradation, reduce catalyst leaching, and support long-term operation through mechanical durability and reusability.

Furthermore, additional strategies to improve photocatalytic performance should be considered. Surface modification through elemental doping (e.g., nitrogen, sulfur, silver) or surface functionalization can promote better charge separation, extend light absorption into the visible region, and improve the photocatalyst's interaction with target pollutants. Such modifications are known to enhance photocatalytic efficiency, stability, and light-harvesting capabilities, which are critical for real-world application under solar or low-energy visible-light irradiation.

In conclusion, these proposed future directions provide a comprehensive roadmap for advancing the ZnO/CDs photocatalytic system from a laboratory-scale innovation to a practical, sustainable solution for wastewater remediation. By addressing performance under realistic conditions, exploring new contaminant classes, integrating advanced reactor or membrane systems, and applying rational material design strategies, future research can significantly contribute to the development of next generation photocatalysts aligned with environmental and industrial needs.

REFERENCES

Abd Rani, U., Ng, L. Y., Ng, Y. S., Ng, C. Y., Ong, Y. H., & Lim, Y. P. (2022). Photocatalytic Degradation Of Methyl Green Dye By Nitrogen-Doped Carbon Quantum Dots: Optimisation Study By Taguchi Approach. *Materials Science And Engineering: B*, *283*. Https://Doi.Org/10.1016/J.Mseb.2022.115820

Abinaya, K., Rajkishore, S. K., Lakshmanan, A., Anandham, R., Dhananchezhiyan, P., & Praghadeesh, M. (2021). Synthesis And Characterization Of Carbon Dots From Coconut Shell By Optimizing The Hydrothermal Carbonization Process. *Journal Of Applied And Natural Science*, *13*(4), 1151–1157. Https://Doi.Org/10.31018/Jans.V13i4.2916

Adeyemi, J. O., Ajiboye, T., & Onwudiwe, D. C. (2021). Mineralization Of Antibiotics In Wastewater Via Photocatalysis. *Water, Air, & Soil Pollution*, *232*(5), 219. Https://Doi.Org/10.1007/S11270-021-05167-3

Ai, C., Zhou, D., Wang, Q., Shao, X., & Lei, Y. (2015). Optimization Of Operating Parameters For Photocatalytic Degradation Of Tetracycline Using In2s3 Under Natural Solar Radiation. *Solar Energy*, *113*, 34–42. Https://Doi.Org/10.1016/J.Solener.2014.12.022

Akbar, K., Moretti, E., & Vomiero, A. (2021). Carbon Dots For Photocatalytic Degradation Of Aqueous Pollutants: Recent Advancements. In *Advanced Optical Materials* (Vol. 9, Issue 17). John Wiley And Sons Inc. Https://Doi.Org/10.1002/Adom.202100532

Aljaafari, A., Ahmed, F., Awada, C., & Shaalan, N. M. (2020). Flower-Like Zno Nanorods Synthesized By Microwave-Assisted One-Pot Method For Detecting Reducing Gases: Structural Properties And Sensing Reversibility. *Frontiers In Chemistry*, *8*. Https://Doi.Org/10.3389/Fchem.2020.00456

Araña, J., Martínez Nieto, J. L., Herrera Melián, J. A., Doña Rodríguez, J. M., González Díaz, O., Pérez Peña, J., Bergasa, O., Alvarez, C., & Méndez, J. (2004). Photocatalytic Degradation Of Formaldehyde Containing Wastewater From Veterinarian Laboratories. *Chemosphere*, *55*(6), 893–904. Https://Doi.Org/10.1016/J.Chemosphere.2003.11.060

Arumugham, T., Alagumuthu, M., Amimodu, R. G., Munusamy, S., & Iyer, S. K. (2020). A Sustainable Synthesis Of Green Carbon Quantum Dot (Cqd) From Catharanthus Roseus (White Flowering Plant) Leaves And Investigation Of Its

Dual Fluorescence Responsive Behavior In Multi-Ion Detection And Biological Applications. *Sustainable Materials And Technologies*, *23*, E00138. Https://Doi.Org/10.1016/J.Susmat.2019.E00138

Atchudan, R., Edison, T. N. J. I., Mani, S., Perumal, S., Vinodh, R., Thirunavukkarasu, S., & Lee, Y. R. (2020). Facile Synthesis Of A Novel Nitrogen-Doped Carbon Dot Adorned Zinc Oxide Composite For Photodegradation Of Methylene Blue. *Dalton Transactions*, *49*(48), 17725–17736. Https://Doi.Org/10.1039/D0dt02756a

Ateia, E. E., Rabie, O., & Mohamed, A. T. (2024). Assessment Of The Correlation Between Optical Properties And Cqd Preparation Approaches. *European Physical Journal Plus*, *139*(1). Https://Doi.Org/10.1140/Epjp/S13360-023-04811-7

Ayu, D. G., Gea, S., Andriayani, N., Telaumbanua, D. J., Piliang, A. F. R., Harahap, M., Yen, Z., Goei, R., & Tok, A. I. Y. (2023). Photocatalytic Degradation Of Methylene Blue Using N-Doped Zno/Carbon Dot (N-Zno/Cd) Nanocomposites Derived From Organic Soybean. *Acs Omega*, *8*(17), 14965–14984. Https://Doi.Org/10.1021/Acsomega.2c07546

Azimi, S., & Nezamzadeh-Ejhieh, A. (2015). Enhanced Activity Of Clinoptilolite-Supported Hybridized Pbs-Cds Semiconductors For The Photocatalytic Degradation Of A Mixture Of Tetracycline And Cephalexin Aqueous Solution. *Journal Of Molecular Catalysis A: Chemical*, *408*, 152–160. Https://Doi.Org/10.1016/J.Molcata.2015.07.017

Bai, X., Chen, W., Wang, B., Sun, T., Wu, B., & Wang, Y. (2022). Photocatalytic Degradation Of Some Typical Antibiotics: Recent Advances And Future Outlooks. In *International Journal Of Molecular Sciences* (Vol. 23, Issue 15). Mdpi. Https://Doi.Org/10.3390/Ijms23158130

Balapure, A., Ray Dutta, J., & Ganesan, R. (2024). Recent Advances In Semiconductor Heterojunctions: A Detailed Review Of The Fundamentals Of Photocatalysis, Charge Transfer Mechanism And Materials. *Rsc Applied Interfaces*, *1*(1), 43–69. Https://Doi.Org/10.1039/D3lf00126a

Bard, A. J. (1979). Photoelectrochemistry And Heterogeneous Photo-Catalysis At Semiconductors. *Journal Of Photochemistry*, *10*(1), 59–75. Https://Doi.Org/10.1016/0047-2670(79)80037-4

Basha, S., Barr, C., Keane, D., Nolan, K., Morrissey, A., Oelgemöller, M., & Tobin, J. M. (2011). On The Adsorption/Photodegradation Of Amoxicillin In Aqueous Solutions By An Integrated Photocatalytic Adsorbent (Ipca): Experimental Studies And Kinetics Analysis. *Photochemical & Photobiological Sciences*, *10*(6), 1014–1022. Https://Doi.Org/10.1039/C0pp00368a

Berdimurodov, E., Berdimuradov, K., Bahodir, K., Kholikov, A., Akbarov, K., Dagdag, O., Rbaa, M., El Ibrahimi, B., Kumar Verma, D., Haldhar, R., & Kumar Mahish, P. (2023). Chapter 1 Recent Trends And Developments In Carbon Dots. In *Carbon Dots In Biology* (Pp. 1–14). De Gruyter. Https://Doi.Org/10.1515/9783110799958-001

Berends, A. C., Rabouw, F. T., Spoor, F. C. M., Bladt, E., Grozema, F. C., Houtepen, A. J., Siebbeles, L. D. A., & De Mello Donegá, C. (2016). Radiative And Nonradiative Recombination In Cuins2 Nanocrystals And Cuins2-Based Core/Shell Nanocrystals. *Journal Of Physical Chemistry Letters*, *7*(17), 3503–3509. Https://Doi.Org/10.1021/Acs.Jpclett.6b01668

Bhamore, J. R., Jha, S., Singhal, R. K., Park, T. J., & Kailasa, S. K. (2018). Facile Green Synthesis Of Carbon Dots From Pyrus Pyrifolia Fruit For Assaying Of Al3+ Ion Via Chelation Enhanced Fluorescence Mechanism. *Journal Of Molecular Liquids*, *264*, 9–16. Https://Doi.Org/10.1016/J.Molliq.2018.05.041

Bhuin, A., Udayakumar, S., Gopalarethinam, J., Mukherjee, D., Girigoswami, K., Ponraj, C., & Sarkar, S. (2024). Photocatalytic Degradation Of Antibiotics And Antimicrobial And Anticancer Activities Of Two-Dimensional Zno Nanosheets. *Scientific Reports*, *14*(1), 10406. Https://Doi.Org/10.1038/S41598-024-59842-6

Bozetine, H., Wang, Q., Barras, A., Li, M., Hadjersi, T., Szunerits, S., & Boukherroub, R. (2016). Green Chemistry Approach For The Synthesis Of Zno-Carbon Dots Nanocomposites With Good Photocatalytic Properties Under Visible Light. *Journal Of Colloid And Interface Science*, *465*, 286–294. Https://Doi.Org/10.1016/J.Jcis.2015.12.001

Cao, M., Wang, P., Ao, Y., Wang, C., Hou, J., & Qian, J. (2016). *Visible Light Activated Photocatalytic Degradation Of Tetracycline By A Magnetically Separable Composite Photocatalyst: Graphene Oxide/Magnetite/Cerium-Doped Titania*.

Chai, Y. Y., Qu, D. P., Ma, D. K., Chen, W., & Huang, S. (2018). Carbon Quantum Dots/Zn 2+ Ions Doped-Cds Nanowires With Enhanced Photocatalytic Activity

For Reduction Of 4-Nitroaniline To P-Phenylenediamine. *Applied Surface Science*, *450*, 1–8. Https://Doi.Org/10.1016/J.Apsusc.2018.04.121

Chang, Y. C., & Hsu, C. C. (2020). Synergetic Effect Of Carbon Black As Co-Catalyst For Enhanced Visible-Light Photocatalytic Activity And Stability On Zno Nanoparticles. *Solid State Sciences*, *107*. Https://Doi.Org/10.1016/J.Solidstatesciences.2020.106366

Chaudhary, N., Gupta, P. K., Eremin, S., & Solanki, P. R. (2020). One-Step Green Approach To Synthesize Highly Fluorescent Carbon Quantum Dots From Banana Juice For Selective Detection Of Copper Ions. *Journal Of Environmental Chemical Engineering*, *8*(3), 103720. Https://Doi.Org/10.1016/J.Jece.2020.103720

Chen, R., Wang, X., & Zhu, L. (2022). *Adsorption And Photocatalytic Degradation Of Tetracycline By Porous G-C3n4/Tio2*. Https://Doi.Org/10.21203/Rs.3.Rs-1172368/V1

Choi, N., Tang, C., Park, Y., Du, A., Ayoko, G. A., Hwang, Y., & Chae, S. (2024). Visible-Light-Driven Photocatalytic Degradation Of Tetracycline Using Citric Acid And Lemon Juice-Derived Carbon Quantum Dots Incorporated Tio2 Nanocomposites. *Separation And Purification Technology*, *350*, 127836. Https://Doi.Org/10.1016/J.Seppur.2024.127836

Chopra, I., & Roberts, M. (2001). Tetracycline Antibiotics: Mode Of Action, Applications, Molecular Biology, And Epidemiology Of Bacterial Resistance. *Microbiology And Molecular Biology Reviews*, *65*(2), 232–260. Https://Doi.Org/10.1128/Mmbr.65.2.232-260.2001

Chu, K. W., Lee, S. L., Chang, C. J., & Liu, L. (2019). Recent Progress Of Carbon Dot Precursors And Photocatalysis Applications. In *Polymers* (Vol. 11, Issue 4). Mdpi Ag. Https://Doi.Org/10.3390/Polym11040689

Cui, L., Ren, X., Sun, M., Liu, H., & Xia, L. (2021). Carbon Dots: Synthesis, Properties And Applications. In *Nanomaterials* (Vol. 11, Issue 12). Mdpi. Https://Doi.Org/10.3390/Nano11123419

Dager, A., Uchida, T., Maekawa, T., & Tachibana, M. (2019a). Synthesis And Characterization Of Mono-Disperse Carbon Quantum Dots From Fennel Seeds: Photoluminescence Analysis Using Machine Learning. *Scientific Reports*, *9*(1). Https://Doi.Org/10.1038/S41598-019-50397-5

Dager, A., Uchida, T., Maekawa, T., & Tachibana, M. (2019b). Synthesis And Characterization Of Mono-Disperse Carbon Quantum Dots From Fennel Seeds: Photoluminescence Analysis Using Machine Learning. *Scientific Reports*, *9*(1). Https://Doi.Org/10.1038/S41598-019-50397-5

De, B., & Karak, N. (2017). Recent Progress In Carbon Dot-Metal Based Nanohybrids For Photochemical And Electrochemical Applications. *Journal Of Materials Chemistry A*, *5*(5), 1826–1859. Https://Doi.Org/10.1039/C6ta10220d

De Francesco, C., Gasperini, T., Duca, D., Toscano, G., & Ilari, A. (2024). Hydrothermal Carbonization Of Residual Biomass From Agricultural And Agro-Industrial Sector. *Processes*, *12*(8), 1673. Https://Doi.Org/10.3390/Pr12081673

De Mello Peters, R. F., Mantey Dos Santos, P. A., Machado, T. C., Rodriguez Lopez, D. A., Machado, Ê. L., & Lawisch Rodriguez, A. D. A. (2018). Photocatalytic Degradation Of Methylene Blue Using Tio2 Supported In Ceramic Material. *Eclética Química Journal*, *43*(1), 26. Https://Doi.Org/10.26850/1678-4618eqj.V43.1.2018.P26-32

Demarema, S., Nasr, M., Ookawara, S., & Abdelhaleem, A. (2024). New Insights Into Green Synthesis Of Metal Oxide Based Photocatalysts For Photodegradation Of Organic Pollutants: A Bibliometric Analysis And Techno-Economic Evaluation. *Journal Of Cleaner Production*, *463*, 142679. Https://Doi.Org/10.1016/J.Jclepro.2024.142679

Di, J., Xia, J., Ji, M., Xu, L., Yin, S., Chen, Z., & Li, H. (2016). Bidirectional Acceleration Of Carrier Separation Spatially Via N-Cqds/Atomically-Thin Bioi Nanosheets Nanojunctions For Manipulating Active Species In A Photocatalytic Process. *Journal Of Materials Chemistry A*, *4*(14), 5051–5061. Https://Doi.Org/10.1039/C6ta00284f

Ding, D., Lan, W., Yang, Z., Zhao, X., Chen, Y., Wang, J., Zhang, X., Zhang, Y., Su, Q., & Xie, E. (2016). A Simple Method For Preparing Zno Foam/Carbon Quantum Dots Nanocomposite And Their Photocatalytic Applications. *Materials Science In Semiconductor Processing*, *47*, 25–31. Https://Doi.Org/10.1016/J.Mssp.2016.02.004

Doñate-Buendia, C., Torres-Mendieta, R., Pyatenko, A., Falomir, E., Fernández-Alonso, M., & Mínguez-Vega, G. (2018). Fabrication By Laser Irradiation In A

Continuous Flow Jet Of Carbon Quantum Dots For Fluorescence Imaging. *Acs Omega*, *3*(3), 2735–2742. Https://Doi.Org/10.1021/Acsomega.7b02082

Dong, S., Lian, X., Chen, S., Li, H., Liu, E., & Xu, K. (2021). Kinetic Analysis And Mechanism Study On The Photocatalytic Degradation Of 2,4-Dinitrophenylhydrazine Over Surface Plasmonic Ag/Cu/Tio2 Composite. *Reaction Kinetics, Mechanisms And Catalysis*, *134*(1), 485–499. Https://Doi.Org/10.1007/S11144-021-02054-0

Du, Q., Zheng, J., Wang, J., Yang, Y., & Liu, X. (2018). The Synthesis Of Green Fluorescent Carbon Dots For Warm White Leds. *Rsc Advances*, *8*(35), 19585–19595. Https://Doi.Org/10.1039/C8ra02226g

Edakkaparamban, S., Kitamura, M., Ide, Y., Umemura, K., & Ishizawa, A. (2023). Photocatalytic Degradation Study Of Methylene Blue Using Carbon Quantum Dots Synthesized From Coconut Husk. *Materials Letters*, *345*, 134508. Https://Doi.Org/10.1016/J.Matlet.2023.134508

Egorova, M. N., Tomskaya, A. E., Kapitonov, A. N., Alekseev, A. A., & Smagulova, S. A. (2018). Hydrothermal Synthesis Of Luminescent Carbon Dots From Glucose And Birch Bark Soot. *Journal Of Structural Chemistry*, *59*(4), 780–785. Https://Doi.Org/10.1134/S0022476618040054

Ernawati, L., Yusariarta, A. W., Laksono, A. D., Wahyuono, R. A., Widiyandari, H., Rebeka, R., & Sitompul, V. (2021). Kinetic Studies Of Methylene Blue Degradation Using Catio 3 Photocatalyst From Chicken Eggshells. *Journal Of Physics: Conference Series*, *1726*(1), 012017. Https://Doi.Org/10.1088/1742-6596/1726/1/012017

Fang, J., Xie, K., Kang, Q., & Gou, Y. (2022). Facile Fabrication Of G-C3n4/Cds Heterojunctions With Enhanced Visible-Light Photocatalytic Degradation Performances. *Journal Of Science: Advanced Materials And Devices*, *7*(1). Https://Doi.Org/10.1016/J.Jsamd.2021.100409

Fernández, L., Gamallo, M., González-Gómez, M. A., Vázquez-Vázquez, C., Rivas, J., Pintado, M., & Moreira, M. T. (2019). Insight Into Antibiotics Removal: Exploring The Photocatalytic Performance Of A Fe_3O_4/Zno Nanocomposite In A Novel Magnetic Sequential Batch Reactor. *Journal Of Environmental Management*, *237*, 595–608. Https://Doi.Org/10.1016/J.Jenvman.2019.02.089

Fiaz, A., Zhu, D., & Sun, J. (2021). Environmental Fate Of Tetracycline Antibiotics: Degradation Pathway Mechanisms, Challenges, And Perspectives. In

Environmental Sciences Europe (Vol. 33, Issue 1). Springer Science And Business Media Deutschland Gmbh. Https://Doi.Org/10.1186/S12302-021-00505-Y

Fiszka Borzyszkowska, A., Sulowska, A., Czaja, P., Bielicka-Giełdoń, A., Zekker, I., & Zielińska-Jurek, A. (2023). Zno-Decorated Green-Synthesized Multi-Doped Carbon Dots From Chlorella Pyrenoidosa For Sustainable Photocatalytic Carbamazepine Degradation. *Rsc Advances*, *13*(36), 25529–25551. Https://Doi.Org/10.1039/D3ra04188c

Fu, J., Xu, Q., Low, J., Jiang, C., & Yu, J. (2019). Ultrathin 2d/2d Wo3/G-C3n4 Step-Scheme H2-Production Photocatalyst. *Applied Catalysis B: Environmental*, *243*, 556–565. Https://Doi.Org/10.1016/J.Apcatb.2018.11.011

Fu, L. X., Guo, Y., Yang, X. C., Huang, J., & Wang, L. J. (2018). Carbon Dots Modifier For Highly Active Photocatalysts Based On Zno Porous Microspheres. *Journal Of Materials Science: Materials In Electronics*, *29*(23), 19994–20002. Https://Doi.Org/10.1007/S10854-018-0129-3

Gedda, G., Lee, C.-Y., Lin, Y.-C., & Wu, H. (2016). Green Synthesis Of Carbon Dots From Prawn Shells For Highly Selective And Sensitive Detection Of Copper Ions. *Sensors And Actuators B: Chemical*, *224*, 396–403. Https://Doi.Org/10.1016/J.Snb.2015.09.065

Gharbani, P., Mehrizad, A., & Mosavi, S. A. (2022). Optimization, Kinetics And Thermodynamics Studies For Photocatalytic Degradation Of Methylene Blue Using Cadmium Selenide Nanoparticles. *Npj Clean Water*, *5*(1), 34. Https://Doi.Org/10.1038/S41545-022-00178-X

Gong, D., Guo, J., Wang, F., Zhang, J., Song, S., Feng, B., Zhang, X., & Zhang, W. (2023). Green Construction Of Metal- And Additive-Free Citrus Peel-Derived Carbon Dot/G-C3n4 Photocatalysts For The High-Performance Photocatalytic Decomposition Of Sunset Yellow. *Food Chemistry*, *425*. Https://Doi.Org/10.1016/J.Foodchem.2023.136470

Goodarzi, N., Ashrafi-Peyman, Z., Khani, E., & Moshfegh, A. Z. (2023). Recent Progress On Semiconductor Heterogeneous Photocatalysts In Clean Energy Production And Environmental Remediation. *Catalysts*, *13*(7), 1102. Https://Doi.Org/10.3390/Catal13071102

Gopal, G., Alex, S. A., Chandrasekaran, N., & Mukherjee, A. (2020). A Review On Tetracycline Removal From Aqueous Systems By Advanced Treatment

Techniques. In *Rsc Advances* (Vol. 10, Issue 45, Pp. 27081–27095). Royal Society Of Chemistry. Https://Doi.Org/10.1039/D0ra04264a

Gunjyal, N., Ojha, C. S. P., & Tygai, V. K. (2023). Prevalence Of Antibiotics And Antibiotic Resistance Genes In Landfill Leachate. In *Landfill Leachate Management* (Pp. 393–410). Iwa Publishing. Https://Doi.Org/10.2166/9781789063318_0393

Guo, F., Huang, X., Chen, Z., Sun, H., & Shi, W. (2020). Investigation Of Visible-Light-Driven Photocatalytic Tetracycline Degradation Via Carbon Dots Modified Porous Znsno3 Cubes: Mechanism And Degradation Pathway. *Separation And Purification Technology*, *253*, 117518. Https://Doi.Org/10.1016/J.Seppur.2020.117518

Habibi, M. H., Talebian, N., & Choi, J. H. (2007). The Effect Of Annealing On Photocatalytic Properties Of Nanostructured Titanium Dioxide Thin Films. *Dyes And Pigments*, *73*(1), 103–110. Https://Doi.Org/10.1016/J.Dyepig.2005.10.016

Hak, C. H., Leong, K. H., Chin, Y. H., Saravanan, P., Tan, S. T., Chong, W. C., & Sim, L. C. (2020). Water Hyacinth Derived Carbon Quantum Dots And G-C3n4 Composites For Sunlight Driven Photodegradation Of 2,4-Dichlorophenol. *Sn Applied Sciences*, *2*(6). Https://Doi.Org/10.1007/S42452-020-2840-Y

Hoan, B. T., Tam, P. D., & Pham, V.-H. (2019). Green Synthesis Of Highly Luminescent Carbon Quantum Dots From Lemon Juice. *Journal Of Nanotechnology*, *2019*, 1–9. Https://Doi.Org/10.1155/2019/2852816

Hoan, B. T., Thanh, T. T., Tam, P. D., Trung, N. N., Cho, S., & Pham, V. H. (2019). A Green Luminescence Of Lemon Derived Carbon Quantum Dots And Their Applications For Sensing Of V5+ Ions. *Materials Science And Engineering B: Solid-State Materials For Advanced Technology*, *251*. Https://Doi.Org/10.1016/J.Mseb.2019.114455

Hosny, M., Fawzy, M., & Eltaweil, A. S. (2022). Green Synthesis Of Bimetallic Ag/Zno@Biohar Nanocomposite For Photocatalytic Degradation Of Tetracycline, Antibacterial And Antioxidant Activities. *Scientific Reports*, *12*(1), 7316. Https://Doi.Org/10.1038/S41598-022-11014-0

Hossain, N., Nizamuddin, S., Griffin, G., Selvakannan, P., Mubarak, N. M., & Mahlia, T. M. I. (2020). Synthesis And Characterization Of Rice Husk Biochar Via Hydrothermal Carbonization For Wastewater Treatment And Biofuel

Production. *Scientific Reports*, *10*(1). Https://Doi.Org/10.1038/S41598-020-75936-3

Hu, C., Liu, Z.-T., Yang, P.-C., Ding, Y.-X., Lin, K.-Y. A., & Nguyen, B.-S. (2021). Self-Assembly L-Cysteine Based 2d G-C3n4 Nanoflakes For Light-Dependent Degradation Of Rhodamine B And Tetracycline Through Photocatalysis. *Journal Of The Taiwan Institute Of Chemical Engineers*, *123*, 219–227. Https://Doi.Org/10.1016/J.Jtice.2021.04.064

Huang, F., Tan, D., Li, D., Guo, S., Yan, Y., & Zhang, W. (2023). Synthesis Of Broad Spectrum-Driven Photocatalysts Waste Biomass-Derived Carbon Quantum Dots/G-C3n4 With Superior Energy Bands For Ppcps Restoration. *Journal Of Alloys And Compounds*, *947*. Https://Doi.Org/10.1016/J.Jallcom.2023.169487

Huang, J., Xue, P., Wang, S., Han, S., Lin, L., Chen, X., & Wang, Z. (2022). Fabrication Of Zirconium-Based Metal-Organic Frameworks@Tungsten Trioxide (Uio-66-Nh2@Wo3) Heterostructure On Carbon Cloth For Efficient Photocatalytic Removal Of Tetracycline Antibiotic Under Visible Light. *Journal Of Colloid And Interface Science*, *606*, 1509–1523. Https://Doi.Org/10.1016/J.Jcis.2021.08.108

Huo, P., Gao, X., Lu, Z., Liu, X., Luo, Y., Xing, W., Li, J., & Yan, Y. (2014). Photocatalytic Degradation Of Antibiotics In Water Using Metal Ion@Tio_2/Hnts Under Visible Light. *Desalination And Water Treatment*, *52*(37–39), 6985–6995. Https://Doi.Org/10.1080/19443994.2013.822327

Hussein Abdurahman, M., Zuhairi Abdullah, A., Da Oh, W., Fazliani Shopware, N., Faisal Gasim, M., Okoye, P., Ul-Hamid, A., & Rahman Mohamed, A. (2022). Tunable Band Structure Of Synthesized Carbon Dots Modified Graphitic Carbon Nitride/Bismuth Oxychlorobromide Heterojunction For Photocatalytic Degradation Of Tetracycline In Water. *Journal Of Colloid And Interface Science*. Https://Doi.Org/10.1016/J.Jcis.2022.08.172

Indeed. (2024, July 8). *Operators Salary In Malaysia*. Https://Malaysia.Indeed.Com/Career/Operator/Salaries

Irani, M., Mohammadi, T., & Mohebbi, S. (2017). Photocatalytic Degradation Of Methylene Blue With Zno Nanoparticles; A Joint Experimental And Theoretical Study. *Journal Of The Mexican Chemical Society*, *60*(4). Https://Doi.Org/10.29356/Jmcs.V60i4.115

Jamaludin, N., Rashid, S. A., & Tan, T. (2018). Natural Biomass As Carbon Sources For The Synthesis Of Photoluminescent Carbon Dots. In *Synthesis, Technology And Applications Of Carbon Nanomaterials* (Pp. 109–134). Elsevier. Https://Doi.Org/10.1016/B978-0-12-815757-2.00005-X

Jamaludin, N., Tan, T. L., Zaman, A. S. K., Sadrolhosseini, A. R., & Rashid, S. A. (2020). Acid-Free Hydrothermal-Extraction And Molecular Structure Of Carbon Quantum Dots Derived From Empty Fruit Bunch Biochar. *Materials*, *13*(15). Https://Doi.Org/10.3390/Ma13153356

Javan, H., Asghari, E., & Ashassi-Sorkhabi, H. (2019). Fabrication And Electrochemical Kinetics Studies Of Reduced Carbon Quantum Dots-Supported Palladium Nanoparticles As Bifunctional Catalysts In Methanol Oxidation And Hydrogen Evolution Reactions. *Synthetic Metals*, *254*, 153–163. Https://Doi.Org/10.1016/J.Synthmet.2019.06.006

Jayakumar, A., Radoor, S., Shin, G. H., & Kim, J. T. (2024). Lemon Peel-Based Fluorescent Carbon Quantum Dots As A Functional Filler In Polyvinyl Alcohol-Based Films For Active Packaging Applications. *Industrial Crops And Products*, *209*, 117968. Https://Doi.Org/10.1016/J.Indcrop.2023.117968

Jia, K., Liu, G., Lang, D.-N., Chen, S.-F., Yang, C., Wu, R.-L., Wang, W., & Wang, J.-D. (2022). Degradation Of Tetracycline By Visible Light Over Zno Nanophotocatalyst. *Journal Of The Taiwan Institute Of Chemical Engineers*, *136*, 104422. Https://Doi.Org/10.1016/J.Jtice.2022.104422

Jia, X., Wang, F., Xu, X., Liu, C., Zhang, L., Jiao, S., Zhu, G., Wang, X., & Yu, G. (2023). Highly Efficient Photocatalytic Degradation Of Tetracycline By Modifying Uio-66 Via Different Regulation Strategies. *Acs Omega*, *8*(30), 27375–27385. Https://Doi.Org/10.1021/Acsomega.3c02762

Jiang, J., Cao, S., Hu, C., & Chen, C. (2017). A Comparison Study Of Alkali Metal-Doped G-C3n4 For Visible-Light Photocatalytic Hydrogen Evolution. *Chinese Journal Of Catalysis*, *38*(12), 1981–1989. Https://Doi.Org/10.1016/S1872-2067(17)62936-X

Jiao, X.-Y., Li, L., Qin, S., Zhang, Y., Huang, K., & Xu, L. (2019). The Synthesis Of Fluorescent Carbon Dots From Mango Peel And Their Multiple Applications. *Colloids And Surfaces A: Physicochemical And Engineering Aspects*, *577*, 306–314. Https://Doi.Org/10.1016/J.Colsurfa.2019.05.073

Jin, X.-Y., Ying, W.-Y., Che, R.-J., Xiao, P., Zhou, Y.-Q., Liu, Y., Liu, M.-Y., & Chen, S.-P. (2022). Cqds/Zno Composites Based On Waste Rice Noodles: Preparation And Photocatalytic Capability. *Rsc Advances*, *12*(36), 23692–23703. Https://Doi.Org/10.1039/D2ra03709b

Jin, Y., Tang, W., Wang, J., Ren, F., Chen, Z., Sun, Z., & Ren, P.-G. (2023). Construction Of Biomass Derived Carbon Quantum Dots Modified TiO_2 Photocatalysts With Superior Photocatalytic Activity For Methylene Blue Degradation. *Journal Of Alloys And Compounds*, *932*, 167627. Https://Doi.Org/10.1016/J.Jallcom.2022.167627

Joshi, S., Canjeevaram Balasubramanyam, R. K., Ippolito, S. J., Sabri, Y. M., Kandjani, A. E., Bhargava, S. K., & Sunkara, M. V. (2018). Straddled Band Aligned Cuo/$Batio_3$ Heterostructures: Role Of Energetics At Nanointerface In Improving Photocatalytic And Co 2 Sensing Performance. *Acs Applied Nano Materials*, *1*(7), 3375–3388. Https://Doi.Org/10.1021/Acsanm.8b00583

Josun, J., Sharma, P., & Kumar Garg, V. (2024). Optical And Structural Behavior Of Hydrothermally Synthesized Zno Nanoparticles At Various Temperatures With Naoh Molar Ratios. *Results In Optics*, *14*. Https://Doi.Org/10.1016/J.Rio.2023.100601

Jung, H., Sapner, V. S., Adhikari, A., Sathe, B. R., & Patel, R. (2022). Recent Progress On Carbon Quantum Dots Based Photocatalysis. In *Frontiers In Chemistry* (Vol. 10). Frontiers Media S.A. Https://Doi.Org/10.3389/Fchem.2022.881495

Kalita, H., Mohapatra, J., Pradhan, L., Mitra, A., Bahadur, D., & Aslam, M. (2016). Efficient Synthesis Of Rice Based Graphene Quantum Dots And Their Fluorescent Properties. *Rsc Advances*, *6*(28), 23518–23524. Https://Doi.Org/10.1039/C5ra25706a

Karaca, M., Eroğlu, Z., Açışlı, Ö., Metin, Ö., & Karaca, S. (2023). Boosting Tetracycline Degradation With An S-Scheme Heterojunction Of N-Doped Carbon Quantum Dots-Decorated Tio2. *Acs Omega*. Https://Doi.Org/10.1021/Acsomega.3c03532

Khairol Anuar, N. K., Tan, H. L., Lim, Y. P., So'aib, M. S., & Abu Bakar, N. F. (2021). A Review On Multifunctional Carbon-Dots Synthesized From Biomass Waste: Design/ Fabrication, Characterization And Applications. In *Frontiers In Energy Research* (Vol. 9). Frontiers Media S.A. Https://Doi.Org/10.3389/Fenrg.2021.626549

Khan, W. U., Wang, D., Zhang, W., Tang, Z., Ma, X., Ding, X., Du, S., & Wang, Y. (2017). High Quantum Yield Green-Emitting Carbon Dots For Fe(Iii) Detection, Biocompatible Fluorescent Ink And Cellular Imaging. *Scientific Reports*, *7*(1). Https://Doi.Org/10.1038/S41598-017-15054-9

Khayal, A., Dawane, V., Amin, M. A., Tirth, V., Yadav, V. K., Algahtani, A., Khan, S. H., Islam, S., Yadav, K. K., & Jeon, B. H. (2021). Advances In The Methods For The Synthesis Of Carbon Dots And Their Emerging Applications. In *Polymers* (Vol. 13, Issue 18). Mdpi. Https://Doi.Org/10.3390/Polym13183190

Kim, C., Ryu, H. D., Chung, E. G., Kim, Y., & Lee, J. Kwan. (2018). A Review Of Analytical Procedures For The Simultaneous Determination Of Medically Important Veterinary Antibiotics In Environmental Water: Sample Preparation, Liquid Chromatography, And Mass Spectrometry. In *Journal Of Environmental Management* (Vol. 217, Pp. 629–645). Academic Press. Https://Doi.Org/10.1016/J.Jenvman.2018.04.006

Kouhail, M., Elberouhi, K., Elahmadi, Z., Benayada, A., & Gmouh, S. (2020). A Comparative Study Between Tio2 And Zno Photocatalysis: Photocatalytic Degradation Of Textile Dye. *Iop Conference Series: Materials Science And Engineering*, *827*(1). Https://Doi.Org/10.1088/1757-899x/827/1/012009

Kraemer, S. A., Ramachandran, A., & Perron, G. G. (2019). Antibiotic Pollution In The Environment: From Microbial Ecology To Public Policy. In *Microorganisms* (Vol. 7, Issue 6). Mdpi Ag. Https://Doi.Org/10.3390/Microorganisms7060180

Kshirsagar, S. D., Nikesh, V. V., & Mahamuni, S. (2006). Exciton Structure In Sodium Doped Zinc Oxide Quantum Dots. *Applied Physics Letters*, *89*(5). Https://Doi.Org/10.1063/1.2222334

Kumar, R., Singh, A. K., & Mondal, P. S. (2022). Study Of Uv Assisted Photocatalytic Degradation Of Organic Dye. *Materials Today: Proceedings*, *66*, 3244–3249. Https://Doi.Org/10.1016/J.Matpr.2022.06.257

Lazar, M. A., Varghese, S., & Nair, S. S. (2012). Photocatalytic Water Treatment By Titanium Dioxide: Recent Updates. In *Catalysts* (Vol. 2, Issue 4, Pp. 572–601). Mdpi Ag. Https://Doi.Org/10.3390/Catal2040572

Li, C., Ding, L., Liang, C., Zhang, J., Zhang, C., Mei, H., Wang, C., Wu, W., Zhang, J., & Xu, W. (2017). Photon-Induced Light Emission From Foamed Gold With Micro/Nanohollow Sphere Structures. *Acs Omega*, *2*(9), 5759–5765. Https://Doi.Org/10.1021/Acsomega.7b00798

Li, C., Sun, H., Jin, H., Li, W., Liu, J. L., & Bashir, S. (2022). Performance Of Ferroelectric Visible Light Type Ii Ag10si4o13/Tio2 Heterojunction Photocatalyst. *Catalysis Today*, *400–401*, 146–158. Https://Doi.Org/10.1016/J.Cattod.2022.03.009

Li, D., Huang, J., Huang, L., Tan, S., & Liu, T. (2021). High-Performance Three-Dimensional Aerogel Based On Hydrothermal Pomelo Peel And Reduced Graphene Oxide As An Efficient Adsorbent For Water/Oil Separation. *Langmuir*, *37*(4), 1521–1530. Https://Doi.Org/10.1021/Acs.Langmuir.0c03062

Li, F. T., Zhao, Y., Wang, Q., Wang, X. J., Hao, Y. J., Liu, R. H., & Zhao, D. (2015). Enhanced Visible-Light Photocatalytic Activity Of Active Al2o3/G-C3n4 Heterojunctions Synthesized Via Surface Hydroxyl Modification. *Journal Of Hazardous Materials*, *283*, 371–381. Https://Doi.Org/10.1016/J.Jhazmat.2014.09.035

Li, M., Dong, B., Chang, Z., Dang, H., Ma, S., & Li, W. (2022). Synthesis Of Tio2/G-C3n4 Photocatalyst With Recovered Tio2 From Spent Scr Catalyst For Photodegrading Rhodamine B. *Waste And Biomass Valorization*. Https://Doi.Org/10.1007/S12649-022-01917-4

Li, X., Garlisi, C., Guan, Q., Anwer, S., Al-Ali, K., Palmisano, G., & Zheng, L. (2021). A Review Of Material Aspects In Developing Direct Z-Scheme Photocatalysts. *Materials Today*, *47*, 75–107. Https://Doi.Org/10.1016/J.Mattod.2021.02.017

Li, Y., Zhang, B. P., Zhao, J. X., Ge, Z. H., Zhao, X. K., & Zou, L. (2013). Zno/Carbon Quantum Dots Heterostructure With Enhanced Photocatalytic Properties. *Applied Surface Science*, *279*, 367–373. Https://Doi.Org/10.1016/J.Apsusc.2013.04.114

Li, Z., Tang, J., Wang, X., Yuan, H., Ma, X., & Wan, J. (2025). *The Fate Of Antibiotics And Resistance Genes In Advanced Wastewater Treatment* (Pp. 251–257). Https://Doi.Org/10.1007/978-3-031-86829-0_30

Liang, H., Tai, X., Du, Z., & Yin, Y. (2020). Enhanced Photocatalytic Activity Of Zno Sensitized By Carbon Quantum Dots And Application In Phenol Wastewater. *Optical Materials*, *100*. Https://Doi.Org/10.1016/J.Optmat.2020.109674

Liang, S., Liang, R., Wen, L., Yuan, R., Wu, L., & Fu, X. (2012). Molecular Recognitive Photocatalytic Degradation Of Various Cationic Pollutants By The Selective Adsorption On Visible Light-Driven Snnb 2o 6 Nanosheet

Photocatalyst. *Applied Catalysis B: Environmental*, *125*, 103–110. Https://Doi.Org/10.1016/J.Apcatb.2012.05.017

Lin, X., Li, M., Li, Y., & Chen, W. (2015). Enhancement Of The Catalytic Activity Of Ordered Mesoporous Tio 2 By Using Carbon Fiber Support And Appropriate Evaluation Of Synergy Between Surface Adsorption And Photocatalysis By Langmuir–Hinshelwood (L–H) Integration Equation. *Rsc Advances*, *5*(127), 105227–105238. Https://Doi.Org/10.1039/C5ra21083f

Liu, B., Li, Y., Wu, Y., & Xing, S. (2021). Enhanced Degradation Of Ofloxacin By Persulfate Activation With Mn Doped Cuo: Synergetic Effect Between Adsorption And Non-Radical Activation. *Chemical Engineering Journal*, *417*, 127972. Https://Doi.Org/10.1016/J.Cej.2020.127972

Liu, J. J., Li, D., Zhang, K., Yang, M., Sun, H., & Yang, B. (2018). One-Step Hydrothermal Synthesis Of Nitrogen-Doped Conjugated Carbonized Polymer Dots With 31% Efficient Red Emission For In Vivo Imaging. *Small*, *14*(15). Https://Doi.Org/10.1002/Smll.201703919

Liu, J., Li, R., & Yang, B. (2020). Carbon Dots: A New Type Of Carbon-Based Nanomaterial With Wide Applications. *Acs Central Science*, *6*(12), 2179–2195. Https://Doi.Org/10.1021/Acscentsci.0c01306

Liu, X., Liu, Y., Liu, T., Jia, Y., Deng, H., Wang, W., & Zhang, F. (2022). Alkali-Mediated Dissolution-Recrystallization Strategy For In Situ Construction Of A Bivo4/Bi25vo40 Heterojunction With Promoted Interfacial Charge Transfer: Formation Mechanism And Photocatalytic Tetracycline Degradation Studies. *Chemical Engineering Journal*, *431*, 134181. Https://Doi.Org/10.1016/J.Cej.2021.134181

Liu, X., Lv, P., Yao, G., Ma, C., Huo, P., & Yan, Y. (2013). Microwave-Assisted Synthesis Of Selective Degradation Photocatalyst By Surface Molecular Imprinting Method For The Degradation Of Tetracycline Onto Cltio2. *Chemical Engineering Journal*, *217*, 398–406. Https://Doi.Org/10.1016/J.Cej.2012.12.007

Liu, X., Zheng, J., Yang, Y., Chen, Y., & Liu, X. (2018). Preparation Of N-Doped Carbon Dots Based On Starch And Their Application In White Led. *Optical Materials*, *86*, 530–536. Https://Doi.Org/10.1016/J.Optmat.2018.10.057

Liu, Y.-Y., Yu, N.-Y., Fang, W.-D., Tan, Q.-G., Ji, R., Yang, L.-Y., Wei, S., Zhang, X.-W., & Miao, A.-J. (2021). Photodegradation Of Carbon Dots Cause

Cytotoxicity. *Nature Communications*, *12*(1), 812. Https://Doi.Org/10.1038/S41467-021-21080-Z

Lou, Y., Hao, X., Liao, L., Zhang, K., Chen, S., Li, Z., Ou, J., Qin, A., & Li, Z. (2021). Recent Advances Of Biomass Carbon Dots On Syntheses, Characterization, Luminescence Mechanism, And Sensing Applications. *Nano Select*, *2*(6), 1117–1145. Https://Doi.Org/10.1002/Nano.202000232

Louros, V. L., Ferreira, L. M., Silva, V. G., Silva, C. P., Martins, M. A., Otero, M., Esteves, V. I., & Lima, D. L. D. (2021). *Toxics Photodegradation Of Aquaculture Antibiotics Using Carbon Dots-Tio 2 Nanocomposites*. Https://Doi.Org/10.3390/Toxics

Low, J., Yu, J., Jaroniec, M., Wageh, S., & Al-Ghamdi, A. A. (2017). Heterojunction Photocatalysts. *Advanced Materials*, *29*(20). Https://Doi.Org/10.1002/Adma.201601694

Lu, Y.-X., Yuan, H., Shao, Y., Chand, H., Wu, Y., Yang, Y.-L., & Song, H.-L. (2023). Shedding Light On The Transfer Of Tetracycline In Forward Osmosis Through Experimental Investigation And Machine Learning Modeling. *Chemosphere*, *319*, 137959. Https://Doi.Org/10.1016/J.Chemosphere.2023.137959

Ma, X., Dong, Y., Sun, H., & Chen, N. (2017). Highly Fluorescent Carbon Dots From Peanut Shells As Potential Probes For Copper Ion: The Optimization And Analysis Of The Synthetic Process. *Materials Today Chemistry*, *5*, 1–10. Https://Doi.Org/10.1016/J.Mtchem.2017.04.004

Maddu, A., Meliafatmah, R., & Rustami, E. (2021). Enhancing Photocatalytic Degradation Of Methylene Blue Using Zno/Carbon Dots Nanocomposite Derived From Coffee Grounds. *Polish Journal Of Environmental Studies*, *30*(1), 273–282. Https://Doi.Org/10.15244/Pjoes/120156

Mahat, N. A., & Shamsudin, S. A. (2020). Blue Luminescence Carbon Quantum Dots Derived From Oil Palm Empty Fruit Bunch Biomass. *Iop Conference Series: Materials Science And Engineering*, *736*(5). Https://Doi.Org/10.1088/1757-899x/736/5/052001

Mahmoud, M. E., Fekry, N. A., & Abdelfattah, A. M. (2020). Removal Of Uranium (Vi) From Water By The Action Of Microwave-Rapid Green Synthesized Carbon Quantum Dots From Starch-Water System And Supported Onto Polymeric Matrix. *Journal Of Hazardous Materials*, *397*, 122770. Https://Doi.Org/10.1016/J.Jhazmat.2020.122770

Mcgraw-Hill. (1984). *Perry's Chemical Engineers' Handbook*.

Merck. (2024). *Sigma*. Https://Www.Sigmaaldrich.Com/My/En

Mewada, A., Pandey, S., Shinde, S., Mishra, N., Oza, G., Thakur, M., Sharon, M., & Sharon, M. (2013). Green Synthesis Of Biocompatible Carbon Dots Using Aqueous Extract Of Trapa Bispinosa Peel. *Materials Science And Engineering C*, *33*(5), 2914–2917. Https://Doi.Org/10.1016/J.Msec.2013.03.018

Mintz, K. J., Zhou, Y., & Leblanc, R. M. (2019). Recent Development Of Carbon Quantum Dots Regarding Their Optical Properties, Photoluminescence Mechanism, And Core Structure. In *Nanoscale* (Vol. 11, Issue 11, Pp. 4634–4652). Royal Society Of Chemistry. Https://Doi.Org/10.1039/C8nr10059d

Mukherjee, I., Cilamkoti, V., & Dutta, R. K. (2021). Sunlight-Driven Photocatalytic Degradation Of Ciprofloxacin By Carbon Dots Embedded In Zno Nanostructures. *Acs Applied Nano Materials*, *4*(8), 7686–7697. Https://Doi.Org/10.1021/Acsanm.1c00883

Murillo-Sierra, J. C., Hernández-Ramírez, A., Hinojosa-Reyes, L., & Guzmán-Mar, J. L. (2021). A Review On The Development Of Visible Light-Responsive Wo3-Based Photocatalysts For Environmental Applications. *Chemical Engineering Journal Advances*, *5*, 100070. Https://Doi.Org/10.1016/J.Ceja.2020.100070

Nammahachak, N., Aup-Ngoen, K. K., Asanithi, P., Horpratum, M., Chuangchote, S., Ratanaphan, S., & Surareungchai, W. (2022). Hydrothermal Synthesis Of Carbon Quantum Dots With Size Tunability *Via* Heterogeneous Nucleation. *Rsc Advances*, *12*(49), 31729–31733. Https://Doi.Org/10.1039/D2ra05989d

Nayak, R. R., Khairun S., H., Parveen, G., Garg, A., Chumachenko, Y. A., Shu, R., & Gupta, N. K. (2025). A Review On Biomass-Derived Carbon Quantum Dots: Emerging Catalysts For Hydrogenation Catalysis. *Chemistry – An Asian Journal*, *20*(6). Https://Doi.Org/10.1002/Asia.202401005

Nazatul Akmal Nazibudin, Mohammad Faiz Zainuddin, & Che Azurahanim Che Abdullah. (2023). Hydrothermal Synthesis Of Carbon Quantum Dots: An Updated Review. *Journal Of Advanced Research In Fluid Mechanics And Thermal Sciences*, *101*(1), 192–206. Https://Doi.Org/10.37934/Arfmts.101.1.192206

Nazibudin, N. A., Zainuddin, M. F., & Abdullah, C. A. C. (2023). Hydrothermal Synthesis Of Carbon Quantum Dots: An Updated Review. *Journal Of Advanced*

Research In Fluid Mechanics And Thermal Sciences, *101*(1), 192–206. Https://Doi.Org/10.37934/Arfmts.101.1.192206

Nezamzadeh-Ejhieh, A., & Salimi, Z. (2010). Heterogeneous Photodegradation Catalysis Of O-Phenylenediamine Using Cuo/X Zeolite. *Applied Catalysis A: General*, *390*(1–2), 110–118. Https://Doi.Org/10.1016/J.Apcata.2010.09.038

Nezamzadeh-Ejhieh, A., & Shirzadi, A. (2014). Enhancement Of The Photocatalytic Activity Of Ferrous Oxide By Doping Onto The Nano-Clinoptilolite Particles Towards Photodegradation Of Tetracycline. *Chemosphere*, *107*, 136–144. Https://Doi.Org/10.1016/J.Chemosphere.2014.02.015

Nguyen, M. B., Lan, P. T., Anh, N. T., Tung, N. N., Guan, S., Ting, V. P., Nguyen, T. T. B., Doan, H. V., Tung, M. T., & Lam, T. D. (2023). Ternary Heterogeneous Z-Scheme Photocatalyst Tio2/Cuins2/Ocn Incorporated With Carbon Quantum Dots (Cqds) For Enhanced Photocatalytic Degradation Efficiency Of Reactive Yellow 145 Dye In Water. *Rsc Advances*, *13*(50), 35339–35348. Https://Doi.Org/10.1039/D3ra07546j

Nikzad, M., Mousavi, S. Y., Heydarian, M., Rahmani, S., Shabanian, S. R., & Hejazi, F. (2024). A Review On Recent Advances In Photodegradation Of Tetracycline In Aqueous Media. In *Journal Of The Iranian Chemical Society* (Vol. 21, Issue 4, Pp. 887–902). Springer Science And Business Media Deutschland Gmbh. Https://Doi.Org/10.1007/S13738-024-02982-3

Niu, J., Ding, S., Zhang, L., Zhao, J., & Feng, C. (2013). Visible-Light-Mediated Sr-Bi2o3 Photocatalysis Of Tetracycline: Kinetics, Mechanisms And Toxicity Assessment. *Chemosphere*, *93*(1), 1–8. Https://Doi.Org/10.1016/J.Chemosphere.2013.04.043

Nosrati, R., Olad, A., & Maramifar, R. (2012). Degradation Of Ampicillin Antibiotic In Aqueous Solution By Zno/Polyaniline Nanocomposite As Photocatalyst Under Sunlight Irradiation. *Environmental Science And Pollution Research*, *19*(6), 2291–2299. Https://Doi.Org/10.1007/S11356-011-0736-5

Nugroho, D., Wannakan, K., Nanan, S., & Benchawattananon, R. (2024). The Synthesis Of Carbon Dots//Zincoxide (Cds/Zno-H400) By Using Hydrothermal Methods For Degradation Of Ofloxacin Antibiotics And Reactive Red Azo Dye (Rr141). *Scientific Reports*, *14*(1). Https://Doi.Org/10.1038/S41598-024-53083-3

Nyaaba, B. A., Gyesi, J. N., Darko, G., & Borquaye, L. S. (2023). Occurrence And Ecological Risk Assessment Of Pharmaceutical Residues In Effluents From

Pharmaceutical Manufacturing Facilities In Kumasi, Ghana. *Chemistry Africa*, *6*(6), 3131–3143. Https://Doi.Org/10.1007/S42250-023-00703-6

Okab, A. A., & Alwared, A. I. (2023). Photodegradation Of Tetracycline Antibiotic By Ternary Recyclable Z-Scheme G-C3n4/Fe3o4/Bi2wo6/Bi2s3 Photocatalyst With Improved Charge Separation Efficiency: Characterization And Mechanism Studies. *Environmental Nanotechnology, Monitoring And Management*, *19*. Https://Doi.Org/10.1016/J.Enmm.2022.100767

Oluwole, A. O., & Olatunji, O. S. (2022). Photocatalytic Degradation Of Tetracycline In Aqueous Systems Under Visible Light Irridiation Using Needle-Like Sno2 Nanoparticles Anchored On Exfoliated G-C3n4. *Environmental Sciences Europe*, *34*(1). Https://Doi.Org/10.1186/S12302-021-00588-7

Ong, W.-J., Tan, L.-L., Ng, Y. H., Yong, S.-T., & Chai, S.-P. (2016). Graphitic Carbon Nitride (G-C 3 N 4)-Based Photocatalysts For Artificial Photosynthesis And Environmental Remediation: Are We A Step Closer To Achieving Sustainability? *Chemical Reviews*, *116*(12), 7159–7329. Https://Doi.Org/10.1021/Acs.Chemrev.6b00075

Ozyurt, D., Kobaisi, M. Al, Hocking, R. K., & Fox, B. (2023). Properties, Synthesis, And Applications Of Carbon Dots: A Review. In *Carbon Trends* (Vol. 12). Elsevier Ltd. Https://Doi.Org/10.1016/J.Cartre.2023.100276

Papaioannou, N., Titirici, M.-M., & Sapelkin, A. (2019). Investigating The Effect Of Reaction Time On Carbon Dot Formation, Structure, And Optical Properties. *Acs Omega*, *4*(26), 21658–21665. Https://Doi.Org/10.1021/Acsomega.9b01798

Parida, V. K., Srivastava, S. K., Gupta, A. K., & Rawat, A. (2023). A Review On Nanomaterial-Based Heterogeneous Photocatalysts For Removal Of Contaminants From Water. *Materials Express*, *13*(1), 1–38. Https://Doi.Org/10.1166/Mex.2023.2319

Patil, A. V., Sawant, P. N., Suryawanshi, V. R., Bhoite, S. D., Shinde, N. S., & Vhatkar, R. S. (2025). Influence Of Carbonization Time On Electrochemical Properties Of Sugarcane Juice Derived Carbon Aerogel Electrodes. *Journal Of Analytical And Applied Pyrolysis*, *186*, 106957. Https://Doi.Org/10.1016/J.Jaap.2025.106957

Pelaez, M., De La Cruz, A. A., O'shea, K., Falaras, P., & Dionysiou, D. D. (2011). Effects Of Water Parameters On The Degradation Of Microcystin-Lr Under

Visible Light-Activated Tio2 Photocatalyst. *Water Research*, *45*(12), 3787–3796. Https://Doi.Org/10.1016/J.Watres.2011.04.036

Perry, R. H. , & G. D. W. (2008). *Perry's Chemical Engineers' Handbook. Mcgraw-Hill Education.*

Pouretedal, H. R., & Afshari, B. (2016). Preparation And Characterization Of Zr And Sn Doped Tio2 Nanocomposite And Photocatalytic Activity In Degradation Of Tetracycline. *Desalination And Water Treatment*, *57*(23), 10941–10947. Https://Doi.Org/10.1080/19443994.2015.1041056

Prasannamedha, G., & Kumar, P. S. (2022). Hydrothermal Carbonization Of Waste Sugarcane Bagasse For The Effective Removal Of Emerging Contaminants From Aqueous Solution. *Adsorption Science And Technology*, *2022*. Https://Doi.Org/10.1155/2022/8684737

Prieto, M., Yue, H., Brun, N., Ellis, G. J., Naffakh, M., & Shuttleworth, P. S. (2024). Hydrothermal Carbonization Of Biomass For Electrochemical Energy Storage: Parameters, Mechanisms, Electrochemical Performance, And The Incorporation Of Transition Metal Dichalcogenide Nanoparticles. *Polymers*, *16*(18), 2633. Https://Doi.Org/10.3390/Polym16182633

Raina, S., Thakur, A., Sharma, A., Pooja, D., & Minhas, A. P. (2020). Bactericidal Activity Of Cannabis Sativa Phytochemicals From Leaf Extract And Their Derived Carbon Dots And Ag@Carbon Dots. *Materials Letters*, *262*, 127122. Https://Doi.Org/10.1016/J.Matlet.2019.127122

Ramezanalizadeh, H., & Rafiee, E. (2021). Very Fast Photodegradation Of Tetracycline By A Novel Ternary Nanocomposite As A Visible Light Driven Photocatalyst. *Materials Chemistry And Physics*, *261*. Https://Doi.Org/10.1016/J.Matchemphys.2021.124242

Rocco, D., Moldoveanu, V. G., Feroci, M., Bortolami, M., & Vetica, F. (2023). Electrochemical Synthesis Of Carbon Quantum Dots. In *Chemelectrochem* (Vol. 10, Issue 3). John Wiley And Sons Inc. Https://Doi.Org/10.1002/Celc.202201104

Rodríguez-Padrón, D., Luque, R., & Muñoz-Batista, M. J. (2020). Waste-Derived Materials: Opportunities In Photocatalysis. In *Topics In Current Chemistry* (Vol. 378, Issue 1). Springer. Https://Doi.Org/10.1007/S41061-019-0264-1

Rowson Ali, M. D., Abdullah, U. H., Ashaari, Z., Hamid, N. H., & Hua, L. S. (2021). Hydrothermal Modification Of Wood: A Review. *Polymers*, *13*(16). Https://Doi.Org/10.3390/Polym13162612

Saadati, F., Keramati, N., & Ghazi, M. M. (2016). Influence Of Parameters On The Photocatalytic Degradation Of Tetracycline In Wastewater: A Review. In *Critical Reviews In Environmental Science And Technology* (Vol. 46, Issue 8, Pp. 757–782). Taylor And Francis Inc. Https://Doi.Org/10.1080/10643389.2016.1159093

Safari, G. H., Hoseini, M., Seyedsalehi, M., Kamani, H., Jaafari, J., & Mahvi, A. H. (2015). Photocatalytic Degradation Of Tetracycline Using Nanosized Titanium Dioxide In Aqueous Solution. *International Journal Of Environmental Science And Technology*, *12*(2), 603–616. Https://Doi.Org/10.1007/S13762-014-0706-9

Saheeda, P., Sabira, K., Joseph, J., & Jayaleksmi, S. (2019). Green Chemistry Route To Realize, High Quantum Yield Carbon Quantum Dots For Cellular Imaging Applications. *Materials Research Express*, *6*(7), 075025. Https://Doi.Org/10.1088/2053-1591/Ab1450

Samanta, S., Satpati, B., & Srivastava, R. (2019). Unraveling The Impact Of The Pd Nanoparticle@Bivo 4 /S-Cn Heterostructure On The Photo-Physical &Amp; Opto-Electronic Properties For Enhanced Catalytic Activity In Water Splitting And One-Pot Three-Step Tandem Reaction. *Nanoscale Advances*, *1*(4), 1395–1412. Https://Doi.Org/10.1039/C8na00372f

Sawalha, S., Azzam, H., Bin Ali, R., Dweikat, H., & Anaya, K. (2021). *Photodegradation Of Methylene Blue By Carbon Nanodots Synthesized From Olive Solid Wastes*.

Sawunyama, L., Oyewo, O., Onwudiwe, D. C., & Makgato, S. S. (2023). Photocatalytic Degradation Of Tetracycline Using Surface Defective Black Tio2–Zno Heterojunction Photocatalyst Under Visible Light. *Heliyon*, *9*(11), E21423. Https://Doi.Org/10.1016/J.Heliyon.2023.E21423

Sbacchi, M., Mamone, M., Morbiato, L., Gobbo, P., Filippini, G., & Prato, M. (2023). Shining Light On Carbon Dots: New Opportunities In Photocatalysis. *Chemcatchem*, *15*(16). Https://Doi.Org/10.1002/Cctc.202300667

Selvakumar, P., Gande, R. K., Jaweria, R., Das, A., & Bhattacharya, S. (2025). *Biological Treatment Methods For Pharmaceutical Wastewater* (Pp. 337–366). Https://Doi.Org/10.4018/979-8-3693-8487-9.Ch011

Semeraro, P., Bettini, S., Sawalha, S., Pal, S., Licciulli, A., Marzo, F., Lovergine, N., Valli, L., & Giancane, G. (2020). Photocatalytic Degradation Of Tetracycline By Zno/Γ-Fe2o3 Paramagnetic Nanocomposite Material. *Nanomaterials*, *10*(8), 1458. Https://Doi.Org/10.3390/Nano10081458

Sendão, R. M. S., Esteves Da Silva, J. C. G., & Pinto Da Silva, L. (2023). Applications Of Fluorescent Carbon Dots As Photocatalysts: A Review. In *Catalysts* (Vol. 13, Issue 1). Mdpi. Https://Doi.Org/10.3390/Catal13010179

Sevilla, M., & Fuertes, A. B. (2009). The Production Of Carbon Materials By Hydrothermal Carbonization Of Cellulose. *Carbon*, *47*(9), 2281–2289. Https://Doi.Org/10.1016/J.Carbon.2009.04.026

Shanthi, M., Ginish, E., & Rajamanickam, D. (2012). Optimization Of The Heterogeneous Photo Fenton Degradation Of A Model Pollutant, Benzyl Alcohol Using Uv/Zno Process. In *Usak University Journal Of Material Sciences* (Vol. 2). Http://Uujms.Usak.Edu.Tr

Shao, Z., Jia, H., Zhang, Y., Yang, X., Zhong, M., & Chang, C. (2020). Oxygen Vacancy-Mediated Interfacial Charge Transfer Of Au/Zno Schottky Heterojunctions For Enhanced Uv Photodegradation. *International Journal Of Photoenergy*, *2020*, 1–17. Https://Doi.Org/10.1155/2020/2456968

Sharma, M., Mandal, M. K., Pandey, S., Kumar, R., & Dubey, K. K. (2022a). Visible-Light-Driven Photocatalytic Degradation Of Tetracycline Using Heterostructured Cu2o-Tio2nanotubes, Kinetics, And Toxicity Evaluation Of Degraded Products On Cell Lines. *Acs Omega*, *7*(37), 33572–33586. Https://Doi.Org/10.1021/Acsomega.2c04576

Sharma, M., Mandal, M. K., Pandey, S., Kumar, R., & Dubey, K. K. (2022b). Visible-Light-Driven Photocatalytic Degradation Of Tetracycline Using Heterostructured Cu2o-Tio2nanotubes, Kinetics, And Toxicity Evaluation Of Degraded Products On Cell Lines. *Acs Omega*, *7*(37), 33572–33586. Https://Doi.Org/10.1021/Acsomega.2c04576

Sharma, N., Sharma, I., & Bera, M. K. (2022). Microwave-Assisted Green Synthesis Of Carbon Quantum Dots Derived From Calotropis Gigantea As A Fluorescent Probe For Bioimaging. *Journal Of Fluorescence*, *32*(3), 1039–1049. Https://Doi.Org/10.1007/S10895-022-02923-4

Sharma, S., Dutta, V., Singh, P., Raizada, P., Rahmani-Sani, A., Hosseini-Bandegharaei, A., & Thakur, V. K. (2019a). Carbon Quantum Dot Supported

Semiconductor Photocatalysts For Efficient Degradation Of Organic Pollutants In Water: A Review. In *Journal Of Cleaner Production* (Vol. 228, Pp. 755–769). Elsevier Ltd. Https://Doi.Org/10.1016/J.Jclepro.2019.04.292

Sharma, S., Dutta, V., Singh, P., Raizada, P., Rahmani-Sani, A., Hosseini-Bandegharaei, A., & Thakur, V. K. (2019b). Carbon Quantum Dot Supported Semiconductor Photocatalysts For Efficient Degradation Of Organic Pollutants In Water: A Review. In *Journal Of Cleaner Production* (Vol. 228, Pp. 755–769). Elsevier Ltd. Https://Doi.Org/10.1016/J.Jclepro.2019.04.292

Sheikh, M. A., Chandok, R. S., & Abida, K. (2024). Green Perspective Of N-Cds Towards Energy Crisis And Photodegradation Of Toxic Dyes. *Discover Materials* , *4*(1). Https://Doi.Org/10.1007/S43939-024-00079-5

Shen, T., Wang, Q., Guo, Z., Kuang, J., & Cao, W. (2018). Hydrothermal Synthesis Of Carbon Quantum Dots Using Different Precursors And Their Combination With Tio2 For Enhanced Photocatalytic Activity. *Ceramics International*, *44*(10), 11828–11834. Https://Doi.Org/10.1016/J.Ceramint.2018.03.271

Sonkar, V., Venu, V., Nishil, B., & Thatikonda, S. (2024). Review On Antibiotic Pollution Dynamics: Insights To Occurrence, Environmental Behaviour, Ecotoxicity, And Management Strategies. In *Environmental Science And Pollution Research* (Vol. 31, Issue 39, Pp. 51164–51196). Springer. Https://Doi.Org/10.1007/S11356-024-34567-1

Su, Q., Gan, L., Liu, J., & Yang, X. (2020). Carbon Dots Derived From Pea For Specifically Binding With Cryptococcus Neoformans. *Analytical Biochemistry*, *589*, 113476. Https://Doi.Org/10.1016/J.Ab.2019.113476

Sun, A., & Wang, W.-X. (2023). Photodegradation Of Microplastics By Zno Nanoparticles With Resulting Cellular And Subcellular Responses. *Environmental Science & Technology*, *57*(21), 8118–8129. Https://Doi.Org/10.1021/Acs.Est.3c01307

Sun, W., He, Z., Chen, Q., Yang, X., Chen, L., Duan, J., Ji, H., & Liu, W. (2025). Carbon Quantum Dots Decoration Induced Spin Polarization Of Potassium Titanate Nanotubes For Enhanced Photocatalytic Degradation Of Naproxen. *Applied Catalysis B: Environmental*, *371*. Https://Doi.Org/10.1016/J.Apcatb.2025.125247

Surendran, P., Lakshmanan, A., Vinitha, G., Ramalingam, G., & Rameshkumar, P. (2020). Facile Preparation Of High Fluorescent Carbon Quantum Dots From

Orange Waste Peels For Nonlinear Optical Applications. *Luminescence*, *35*(2), 196–202. Https://Doi.Org/10.1002/Bio.3713

Syahin, M., Zamri, F. A., & Sapawe, N. (2019). Kinetic Study On Photocatalytic Degradation Of Phenol Using Green Electrosynthesized Tio 2 Nanoparticles. In *Materials Today: Proceedings* (Vol. 19). Www.Sciencedirect.Comwww.Materialstoday.Com/Proceedings2214-7853

Tang, Y., Huang, J., Jiang, M., Yu, J., Wang, Q., Zhao, J., Li, J., Yu, X., & Zhao, J. (2020). Photo-Induced Synthesis Of Nanostructured Pt-On-Au/G-C3n4 Composites For Visible Light Photocatalytic Hydrogen Production. *Journal Of Materials Science*, *55*(32), 15574–15587. Https://Doi.Org/10.1007/S10853-020-05120-5

Tavan, M., Yousefian, Z., Bakhtiar, Z., Rahmandoust, M., & Mirjalili, M. H. (2025). Carbon Quantum Dots: Multifunctional Fluorescent Nanomaterials For Sustainable Advances In Biomedicine And Agriculture. *Industrial Crops And Products*, *231*, 121207. Https://Doi.Org/10.1016/J.Indcrop.2025.121207

Tegenaw, A. B., Yimer, A. A., & Beyene, T. T. (2023). Boosting The Photocatalytic Activity Of Zno-Nps Through The Incorporation Of C-Dot And Preparation Of Nanocomposite Materials. *Heliyon*, *9*(10). Https://Doi.Org/10.1016/J.Heliyon.2023.E20717

Tenaga Nasional, I. T. (2024, July 14). *Tenaga Nasional, Industrial Tariffs*. Https://Www.Tnb.Com.My/Commercial-Industrial/Pricing-Tariffs1

Tsay, C. Y., Chung, C. Y., Chen, C. Y., Chang, Y. C., Chang, C. J., & Wu, J. J. (2023). Enhanced Photocatalytic Performance Of Visible-Light-Driven Bivo4 Nanoparticles Through W And Mo Substituting. *Catalysts*, *13*(3). Https://Doi.Org/10.3390/Catal13030475

Van Dam, B., Nie, H., Ju, B., Marino, E., Paulusse, J. M. J., Schall, P., Li, M., & Dohnalová, K. (2017). Excitation-Dependent Photoluminescence From Single-Carbon Dots. *Small*, *13*(48). Https://Doi.Org/10.1002/Smll.201702098

Velumani, A., Sengodan, P., Arumugam, P., Rajendran, R., Santhanam, S., & Palanisamy, M. (2020). Carbon Quantum Dots Supported Zno Sphere Based Photocatalyst For Dye Degradation Application. *Current Applied Physics*, *20*(10), 1176–1184. Https://Doi.Org/10.1016/J.Cap.2020.07.016

Wakjira, T. L., Gemta, A. B., Kassahun, G. B., Andoshe, D. M., & Tadele, K. (2024). Bismuth-Based Z-Scheme Heterojunction Photocatalysts For Remediation Of

Contaminated Water. *Acs Omega*, *9*(8), 8709–8729. Https://Doi.Org/10.1021/Acsomega.3c08939

Wan Ishak, W. N., Tan, H. L., Abu Bakar, N. F., Radacsi, N., & Lim, Y. P. (2025). Electrochemical Characterization Of Z-Scheme Charge Transfer In Biomass-Derived Zno/Carbon Dots For Efficient Tetracycline Degradation. *Rsc Advances*, *15*(30), 24726–24738. Https://Doi.Org/10.1039/D5ra02606g

Wang, C., Shi, H., Yang, M., Yan, Y., Liu, E., Ji, Z., & Fan, J. (2020). Facile Synthesis Of Novel Carbon Quantum Dots From Biomass Waste For Highly Sensitive Detection Of Iron Ions. *Materials Research Bulletin*, *124*, 110730. Https://Doi.Org/10.1016/J.Materresbull.2019.110730

Wang, J., Huang, J., Li, Y., Ding, K., Jiang, D., Dou, X., & Sun, B. (2022). Radiative And Non-Radiative Exciton Recombination Processes In A Chemical Vapor Deposition-Grown Mose2film. *Journal Of Physical Chemistry C*, *126*(36), 15319–15326. Https://Doi.Org/10.1021/Acs.Jpcc.2c04550

Wang, J., Wei, J., Su, S., & Qiu, J. (2015). Novel Fluorescence Resonance Energy Transfer Optical Sensors For Vitamin B12 Detection Using Thermally Reduced Carbon Dots. *New Journal Of Chemistry*, *39*(1), 501–507. Https://Doi.Org/10.1039/C4nj00538d

Wang, M., & Liu, Z. (2023). Enhanced Catalytic Levofloxacin Degradation Via Persulfate Activation Over Amorphous Potassium Ferricyanide@Zif-67 Nanocages. *Water And Environment Journal*, *37*(4), 804–818. Https://Doi.Org/10.1111/Wej.12887

Wang, P., Yap, P. S., & Lim, T. T. (2011). C-N-S Tridoped Tio2 For Photocatalytic Degradation Of Tetracycline Under Visible-Light Irradiation. *Applied Catalysis A: General*, *399*(1–2), 252–261. Https://Doi.Org/10.1016/J.Apcata.2011.04.008

Wang, S., Chen, X., Fang, L., Gao, H., Han, M., Chen, X., Xia, Y., Xie, L., & Yang, H. (2022). Double Heterojunction Cqds/Ceo2/Bafe12o19 Magnetic Separation Photocatalysts: Construction, Structural Characterization, Dye And Pops Removal, And The Interrelationships Between Magnetism And Photocatalysis. *Nuclear Analysis*, *1*(3), 100026. Https://Doi.Org/10.1016/J.Nucana.2022.100026

Wang, X., Yang, S., Jin, P., Peng, A., Zhao, X., Yang, K., & He, J. (2023). Highly Efficient Photocatalytic Degradation Of Microcystin-Lr With Permonosulfate Activated By Visible-Light Over Z-Scheme Zno/G-C3n4: Degradation

Pathways And Mechanism. *Journal Of Environmental Chemical Engineering*, *11*(5). Https://Doi.Org/10.1016/J.Jece.2023.111088

Wang, Y., Bai, Y., Han, C., Li, Z., Lun, X., & Zhang, C. (2023). Photocatalysis-Pms Oxidation System Based On Cqds-Doped Carbon Nitride Nanosheets For Degradation Of Residual Drugs In Water. *Environmental Science And Pollution Research*, *30*(50), 108538–108552. Https://Doi.Org/10.1007/S11356-023-30005-W

Wang, Y., Hu, Y.-J., Hao, X., Peng, P., Shi, J.-Y., Peng, F., & Sun, R.-C. (2020). Hydrothermal Synthesis And Applications Of Advanced Carbonaceous Materials From Biomass: A Review. *Advanced Composites And Hybrid Materials*, *3*(3), 267–284. Https://Doi.Org/10.1007/S42114-020-00158-0

Wang, Z., Yin, H., Guo, Y., Gao, Y., Liu, J., Han, J., & Huang, M. (2024). Synergetic Enhancement Effect Of Mof-Derived Porous Zno/ Co3o4 Cage Z-Scheme Heterostructure For High-Performance Photodegradation. *Journal Of Alloys And Compounds*, *1005*. Https://Doi.Org/10.1016/J.Jallcom.2024.176092

Widiyandari, H., Prilita, O., Al Ja'farawy, M. S., Nurosyid, F., Arutanti, O., Astuti, Y., & Mufti, N. (2023). Nitrogen-Doped Carbon Quantum Dots Supported Zinc Oxide (Zno/N-Cqd) Nanoflower Photocatalyst For Methylene Blue Photodegradation. *Results In Engineering*, *17*. Https://Doi.Org/10.1016/J.Rineng.2022.100814

World Health Organization. (2024, September). *New Global Guidance Aims To Curb Antibiotic Pollution From Manufacturing*. World Health Organization. Https://Www.Who.Int/News/Item/03-09-2024-New-Global-Guidance-Aims-To-Curb-Antibiotic-Pollution-From-Manufacturing

Wu, S., Hu, H., Lin, Y., Zhang, J., & Hu, Y. H. (2020). Visible Light Photocatalytic Degradation Of Tetracycline Over Tio2. *Chemical Engineering Journal*, *382*. Https://Doi.Org/10.1016/J.Cej.2019.122842

Xia, P., Cao, S., Zhu, B., Liu, M., Shi, M., Yu, J., & Zhang, Y. (2020). Designing A 0d/2d S-Scheme Heterojunction Over Polymeric Carbon Nitride For Visible-Light Photocatalytic Inactivation Of Bacteria. *Angewandte Chemie International Edition*, *59*(13), 5218–5225. Https://Doi.Org/10.1002/Anie.201916012

Xie, Z., Feng, Y., Wang, F., Chen, D., Zhang, Q., Zeng, Y., Lv, W., & Liu, G. (2018). Construction Of Carbon Dots Modified Moo3/G-C3n4 Z-Scheme Photocatalyst

With Enhanced Visible-Light Photocatalytic Activity For The Degradation Of Tetracycline. *Applied Catalysis B: Environmental*, *229*, 96–104. Https://Doi.Org/10.1016/J.Apcatb.2018.02.011

Xing, C., Yu, G., Zhou, J., Liu, Q., Chen, T., Liu, H., & Li, X. (2022). Solar Energy-Driven Upcycling Of Plastic Waste On Direct Z-Scheme Heterostructure Of V-Substituted Phosphomolybdic Acid/G-C3n4 Nanosheets. *Applied Catalysis B: Environmental*, *315*, 121496. Https://Doi.Org/10.1016/J.Apcatb.2022.121496

Xu, H., Shen, X., Khan, M. A., Wang, F., Lei, W., & Xia, M. (2020). Facile Synthesis Of Rock-Like Ag2zro3 Decorated With Tio2 Nanoparticles Heterostructures With Highly Enhanced Visible-Light Photocatalytic Properties. *Journal Of Nanoparticle Research*, *22*(3), 60. Https://Doi.Org/10.1007/S11051-020-4768-Y

Xu, J. J., Lu, Y. N., Tao, F. F., Liang, P. F., & Zhang, P. A. (2023). Zno Nanoparticles Modified By Carbon Quantum Dots For The Photocatalytic Removal Of Synthetic Pigment Pollutants. *Acs Omega*, *8*(8), 7845–7857. Https://Doi.Org/10.1021/Acsomega.2c07591

Xu, L., Zhang, H., Xiong, P., Zhu, Q., Liao, C., & Jiang, G. (2021). Occurrence, Fate, And Risk Assessment Of Typical Tetracycline Antibiotics In The Aquatic Environment: A Review. In *Science Of The Total Environment* (Vol. 753). Elsevier B.V. Https://Doi.Org/10.1016/J.Scitotenv.2020.141975

Xu, Q., Zhang, L., Yu, J., Wageh, S., Al-Ghamdi, A. A., & Jaroniec, M. (2018). Direct Z-Scheme Photocatalysts: Principles, Synthesis, And Applications. *Materials Today*, *21*(10), 1042–1063. Https://Doi.Org/10.1016/J.Mattod.2018.04.008

Yadav, S., Kumar, A., & Kumar, D. (2023). Photo Degradation Of Methylene Blue Onto Boron/Phosphorous Modified Carbons Dots Prepared By Hydrothermal And Microwave Assisted Methods. *Materials Science For Energy Technologies*, *6*, 260–266. Https://Doi.Org/10.1016/J.Mset.2023.01.003

Yan, C., Zhao, Z., Jin, W., Yu, Q., Yu, J., Ran, J., Bi, S., Cheng, D., Li, D., Cai, G., & Wang, X. (2023). Carbon Quantum Dots-Doped G-C3n4 Nanocomposites With Enhanced Piezoelectric Catalytic Performance. *Composites Communications*, *37*, 101466. Https://Doi.Org/10.1016/J.Coco.2022.101466

Yan, H., Li, P., Wen, F., Xu, Q., Guo, Q., & Su, W. (2023). Green Synthesis Of Carbon Quantum Dots From Plant Turmeric Holds Promise As Novel Photosensitizer For In Vitro Photodynamic Antimicrobial Activity. *Journal Of Materials*

Research And Technology, *22*, 17–34. Https://Doi.Org/10.1016/J.Jmrt.2022.11.090

Ye, H., Liu, B., Wang, J., Zhou, C., Xiong, Z., & Zhao, L. (2022). A Hydrothermal Method To Generate Carbon Quantum Dots From Waste Bones And Their Detection Of Laundry Powder. *Molecules*, *27*(19). Https://Doi.Org/10.3390/Molecules27196479

Yuan, M., Zhong, R., Gao, H., Li, W., Yun, X., Liu, J., Zhao, X., Zhao, G., & Zhang, F. (2015). One-Step, Green, And Economic Synthesis Of Water-Soluble Photoluminescent Carbon Dots By Hydrothermal Treatment Of Wheat Straw, And Their Bio-Applications In Labeling, Imaging, And Sensing. *Applied Surface Science*, *355*, 1136–1144. Https://Doi.Org/10.1016/J.Apsusc.2015.07.095

Zaman, F. Uz, Iqbal, S., Saeed, A., Muhammad, F., Ghani, U., Sammed, K. A., Ali, A. M., Khandy, S. A., & Boakye, F. O. (2024). Rational Construction Of Carbon Quantum Dots-Zinc Cobalt Oxide Heterostructure As Bifunctional Catalyst For Oxygen Evolution Reaction And Wastewater Treatment. *International Journal Of Hydrogen Energy*, *73*, 351–361. Https://Doi.Org/10.1016/J.Ijhydene.2024.06.066

Zandipak, R., Bahramifar, N., Younesi, H., & Zolfigol, M. A. (2024). Electro-Photocatalyst Effect Of N-S-Doped Carbon Dots And Covalent Organic Triazine Framework Heterostructures For Boosting Photocatalytic Degradation Of Phenanthrene In Water. *Chemosphere*, *364*. Https://Doi.Org/10.1016/J.Chemosphere.2024.142980

Zeng, Y., Liu, X., Liu, C., Wang, L., Xia, Y., Zhang, S., Luo, S., & Pei, Y. (2018). Scalable One-Step Production Of Porous Oxygen-Doped G-C3n4 Nanorods With Effective Electron Separation For Excellent Visible-Light Photocatalytic Activity. *Applied Catalysis B: Environmental*, *224*, 1–9. Https://Doi.Org/10.1016/J.Apcatb.2017.10.042

Zhang, L., Dong, X., Wang, Y., Zheng, N., Ma, H., & Zhang, X. (2022). One-Pot Synthesis Of Sns_2/In_2s_3 Heterostructures For Efficient Photocatalysis. *Applied Surface Science*, *579*, 152088. Https://Doi.Org/10.1016/J.Apsusc.2021.152088

Zhang, X., He, G., Sun, H., Cui, W., Song, H., Li, J., & Zheng, J. (2024). Preparation And Electrochemical Performance Of Cellulose-Based Biomass-Derived

Carbon Materials. *International Journal Of Electrochemical Science*, *19*(7), 100617. Https://Doi.Org/10.1016/J.Ijoes.2024.100617

Zhang, Z., Zheng, T., Li, X., Xu, J., & Zeng, H. (2016). Progress Of Carbon Quantum Dots In Photocatalysis Applications. In *Particle And Particle Systems Characterization* (Vol. 33, Issue 8, Pp. 457–472). Wiley-Vch Verlag. Https://Doi.Org/10.1002/Ppsc.201500243

Zhao, C., Li, X., Cheng, C., & Yang, Y. (2019). Green And Microwave-Assisted Synthesis Of Carbon Dots And Application For Visual Detection Of Cobalt(Ii) Ions And Ph Sensing. *Microchemical Journal*, *147*, 183–190. Https://Doi.Org/10.1016/J.Microc.2019.03.029

Zhao, C., Zhao, Z., Liang, Y., & Fu, J. (2023). Bi/Bioi/Carbon Quantum Dots Nano-Sheets With Superior Photocatalysis. *Rsc Advances*, *13*(43), 30520–30527. Https://Doi.Org/10.1039/D3ra05145e

Zhao, X., Liao, S., Wang, L., Liu, Q., & Chen, X. (2019). Facile Green And One-Pot Synthesis Of Purple Perilla Derived Carbon Quantum Dot As A Fluorescent Sensor For Silver Ion. *Talanta*, *201*, 1–8. Https://Doi.Org/10.1016/J.Talanta.2019.03.095

Zhao, Y., Chen, Y., Du, L., Wang, Q., Liu, X., Li, L., & Tian, G. (2022). Fabrication Of Size-Controlled Hierarchical Zns@Znin2s4 Heterostructured Cages For Enhanced Gas-Phase Co2 Photoreduction. *Journal Of Colloid And Interface Science*, *605*, 253–262. Https://Doi.Org/10.1016/J.Jcis.2021.07.093

Zhao, Y., Li, Z., Wei, J., Li, X., Shi, H., Cao, B., & Fan, J. (2022). Efficient Photodegradation Of Cefixime Catalyzed By A Direct Z-Scheme Cqds-Biobr/Cn Composite: Performance, Toxicity Evaluation And Photocatalytic Mechanism. *Chemosphere*, *292*, 133430. Https://Doi.Org/10.1016/J.Chemosphere.2021.133430

APPENDICES

APPENDIX 1

Standard curve of tetracycline

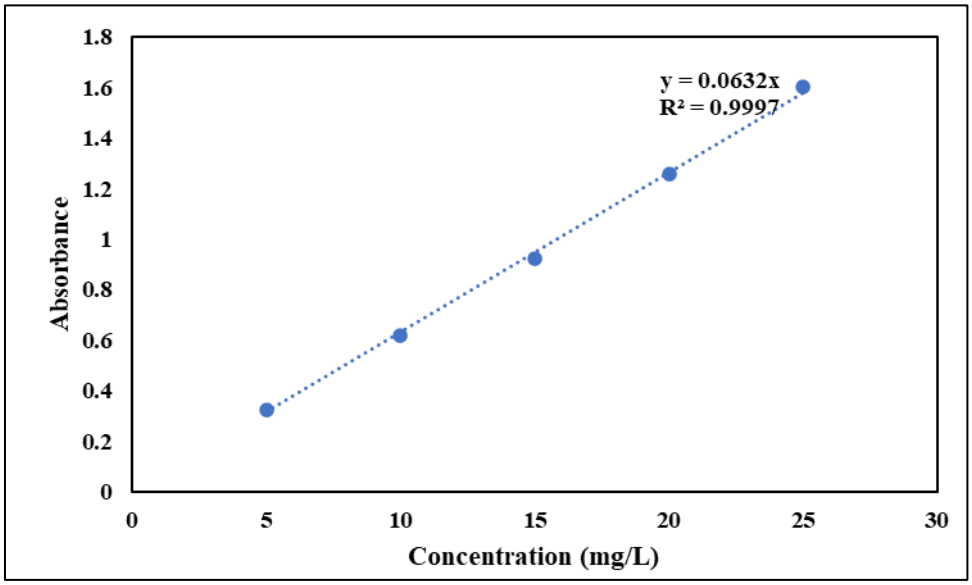

APPENDIX 2

Synthesis Of Carbon Dots, Zinc Oxide and Zinc Oxide/Carbon Dots Composite

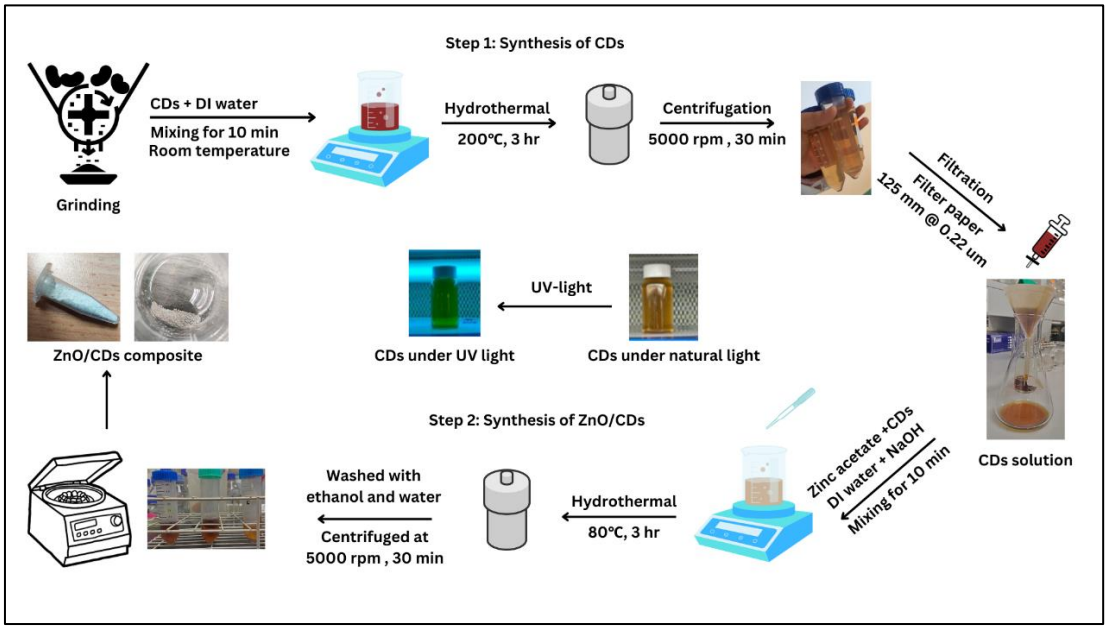

Experiment Set Up For Photocatalytic of Tetracycline Under UV light

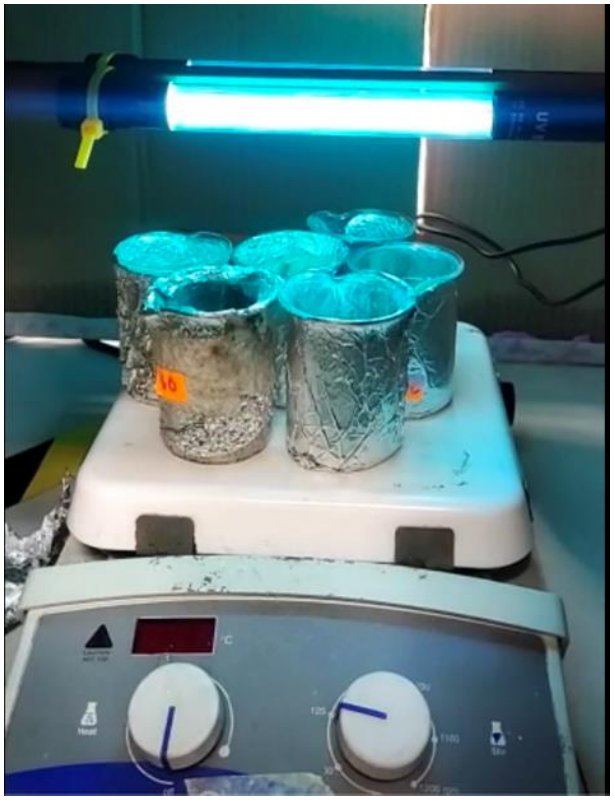

Experiment Set Up For Photocatalytic of Tetracycline Under sunlight

Experiment set up for photocatalytic of tetracycline under visible light

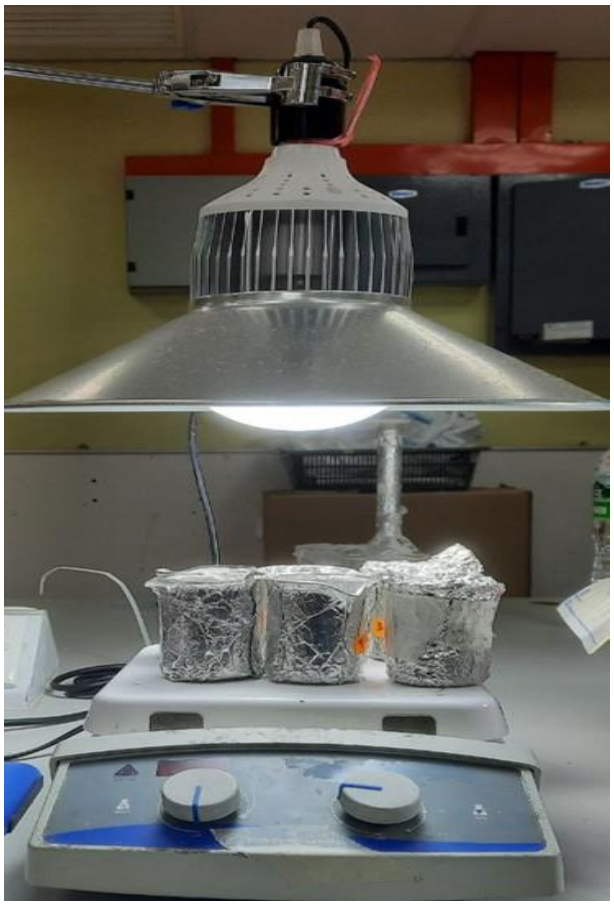

Photocatalytic of tetracycline after 180 minutes

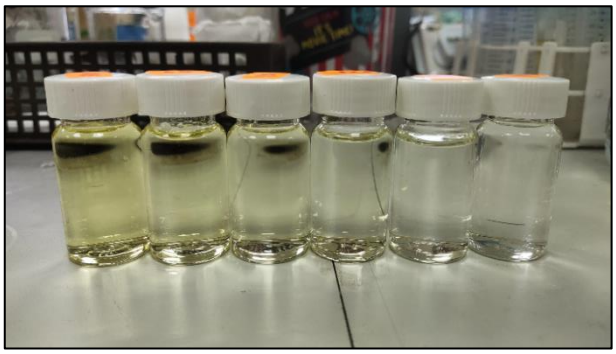

Experiment Set Up of Photoelectrochemical

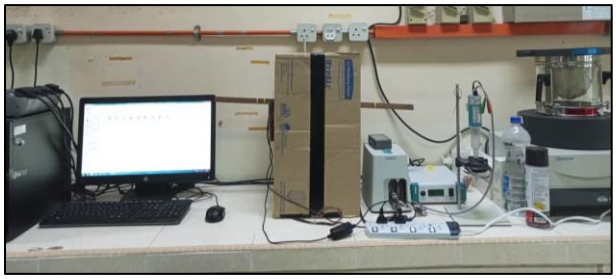

Experiment Set Up of Photoelectrochemical

AUTHOR'S PROFILE

Wan Nuraishah Binti Wan Ishak obtained her Bachelor of Chemical Engineering (Hons.) in 2022 from Universiti Teknologi MARA (UiTM), Malaysia. She is currently pursuing a PhD in Chemical Engineering at the same institution. Her PhD research focuses on the synthesis and application of biomass-derived carbon dots, particularly from oil palm empty fruit bunch, for the photocatalytic degradation of emerging contaminants in wastewater. Her work involves various characterization and analysis techniques, including electrochemical analysis, BET surface area, UV-Vis DRS, FTIR, and HRTEM. She is currently working on the development of green and energy-efficient photocatalysts based on ZnO/carbon dots nanocomposites, aligned with SDG 6 and the 10-10 MySTIE framework.

LIST OF PUBLICATION:

Wan Ishak, W. N., Tan, H. L., Abu Bakar, N. F., Lim, Y. P., Ng, L. Y., & Chun, Y. Y. (2025). Hydrothermal ZnO Photocatalysis for Efficient Removal of Tetracycline from Wastewater. ***ASEAN Journal of Chemical Engineering***, *25*(1), 184-197. https://doi.org/10.22146/ajche.16598

Wan Ishak, W. N., Tan, H. L. ., Abu Bakar, N. F. ., & Lim, Y. P. (2024). Sustainable Carbon Dots Production from Oil Palm Empty Fruit Bunch for the Photodegradation of Methylene Blue. ***Journal of Sustainable Materials Processing and Management*** , *4*(2), 31-41. https://penerbit.uthm.edu.my/ojs/index.php/jsmpm/article/view/18425

Wan Ishak, W. N., Tan, H. L., Abu Bakar, N. F., Radacsi, N., & Lim, Y. P. (2025). Electrochemical characterization of Z-scheme charge transfer in biomass-derived ZnO/carbon dots for efficient tetracycline degradation. **RSC Advances**, 15(30), 24726–24738. https://doi.org/10.1039/D5RA02606G

W. N. Wan Ishak, Y. P. Lim, N. F. Abu Bakar, L. Y. Ng, and H. L. Tan, "Carbon quantum dots for photocatalytic wastewater treatment: Mechanistic insights and economic feasibility," ***J. Environ. Manage.***, vol. 402, p. 129134, Mar. 2026, doi: 10.1016/j.jenvman.2026.129134.

W. N. Wan Ishak, N. S. Mohd Sabri, Y. P. Lim, and H. L. Tan, "HF-free dry gel synthesis of MIL-100(Fe) for adsorptive removal of salicylic acid in wastewater treatment**,"** ***Malaysian Journal of Chemical Engineering and Technology***, vol. 8, no. 2, pp. 168–179, Dec. 2025, doi: 10.24191/mjcet.v8i2.5013

W. N. W. Ishak, H. L. Tan, C.-Y. Yin, and Y. P. Lim, "Carbon quantum dot hybrid photocatalysts: Linking electrochemical diagnostics to charge transfer mechanisms in wastewater treatment," **J. Environ. Chem. Eng.**, vol. 14, no. 3, p. 122214, Jun. 2026, doi: 10.1016/j.jece.2026.122214.

Wan Nuraishah Wan Ishak, Ying Pei Lim, Huey Ling Tan, Noor Fitrah Abu Bakar, Ng Law Yong and Chun Yang Yin Green Synthesis of Carbon Dots from Empty Fruit Bunch using Hydrothermal for Tetracycline Removal, **Journal Science and Technology Pertanika** (Accepted)

Magnetic Biochar Synthesized from Tea Waste Hydrothermal Carbonization for Tetracycline Removal: Influence of Temperature, Residence Time, and Solid-to-Liquid Ratio (Under progress)

Waste-Derived Carbon Dots as Interfacial Defect Modulators in ZnO for Robust UV Photocatalytic Antibiotic Degradation (Under review)